

# A DETERMINISTIC ALGORITHM FOR GLOBAL MAXIMUM POWER POINT CALCULATION OF A SOLAR FARM

Mr. Nhan Tong Thanh

A Dissertation Submitted in Partial Fulfillment of the Requirements for  
the Degree of Doctor of Philosophy Program in Electrical Engineering

Department of Electrical Engineering

Faculty of Engineering

Chulalongkorn University

Academic Year 2015

Copyright of Chulalongkorn University

บทคัดย่อและแฟ้มข้อมูลฉบับเต็มของวิทยานิพนธ์ตั้งแต่ปีการศึกษา 2554 ที่ให้บริการในคลังปัญญาจุฬาฯ (CUIR)

เป็นแฟ้มข้อมูลของนิสิตเจ้าของวิทยานิพนธ์ที่ส่งผ่านทางบัณฑิตวิทยาลัย

The abstract and full text of theses from the academic year 2011 in Chulalongkorn University Intellectual Repository (CUIR)

are the thesis authors' files submitted through the Graduate School.

Thesis title             A DETERMINISTIC ALGORITHM FOR GLOBAL  
                              MAXIMUM POWER POINT CALCULATION OF A  
                              SOLAR FARM  
  
By                         Mr. Nhan Tong Thanh  
  
Field of study          Electronic Engineering  
  
Thesis advisor         Assistant Professor Wanchalerm Pora, Ph.D.

---

Accepted by the Faculty of Engineering, Chulalongkorn University in  
Partial Fulfillment of the Requirements for the Doctoral Degree

..... Dean of the Faculty of Engineering  
(Professor Bundhit Eua-Arporn, Ph.D.)

#### THESIS COMMITTEE

..... Chairman  
(Associate Professor Ekachai Leelarasmee, Ph.D.)

..... Thesis Advisor  
(Assistant Professor Wanchalerm Pora, Ph.D.)

..... Examiner  
(Assistant Professor Suree Pumrin, Ph.D.)

..... Examiner  
(Assistant Professor Manop Wongsaisuwan, Ph.D.)

..... Examiner  
(Assistant Professor Kittiphon Techakittiroj, Ph.D.)

ทาน ตอง ทานห์ : ขั้นตอนวิธีเชิงกำหนดสำหรับการคำนวณจุดกำลังสูงสุดโดยรวมของโซลาร์ฟาร์ม (A DETERMINISTIC ALGORITHM FOR GLOBAL MAXIMUM POWER POINT CALCULATION OF A SOLAR FARM) อ. ที่ปริกษาวิทยานิพนธ์หลัก : ผศ. ดร. วันเฉลิม โปธา, 139 หน้า.

การหาค่าที่ให้ประสิทธิภาพสูงมีบทบาทสำคัญอย่างมากในการเก็บเกี่ยวพลังงานแสงอาทิตย์ด้วยระบบโฟโตวอลเทอิก (Photovoltaic) หรือพีวี (PV) วิทยานิพนธ์ฉบับนี้ นำเสนอวิธีการในการประมาณค่าจุดกำลังสูงสุด (maximum power points) แบบเฉพาะถิ่นและแบบภาพรวมของระบบพีวีภายในระยะเวลาอันสั้น การประมาณใช้ค่าที่ได้จากการวัดขณะระบบทำงานอยู่เพียงไม่กี่ค่า ระบบพีวีสามารถพุ่งไปสู่จุดกำลังสูงสุดแบบภาพรวมได้โดยตรงไม่ต้องใช้การค้นหากำลังงาน ส่งผลให้เวลาที่ใช้ในการค้นหาจุดกำลังสูงสุดทำงานของระบบที่ลดลงจึงทำให้ระบบมีประสิทธิภาพสูงขึ้น เซลล์แสงอาทิตย์ในวิทยานิพนธ์ฉบับนี้ใช้แบบจำลองที่มีไดโอดตัวเดียว ความสัมพันธ์ระหว่างแรงดันและกระแสที่จุดกำลังสูงสุดเฉพาะถิ่นถูกนำมาใช้ประโยชน์ ซึ่งเป็นสาเหตุของความแตกต่างของวิธีการที่เสนอกับวิธีการอื่นๆ ต่างๆ พารามิเตอร์ของแบบจำลองเซลล์แสงอาทิตย์ไม่ได้ถูกจัดหาไว้แล้วโดยผู้ผลิตจึงจำเป็นต้องมีการสกัดพารามิเตอร์ดังกล่าว วิธีการใหม่ซึ่งมีความเรียบง่ายโดยอาศัยเพียงข้อมูลบางส่วนจากแผ่นข้อมูล (datasheet) ที่ได้จากผู้ผลิต แต่ให้ผลลัพธ์ที่ถูกต้องแม่นยำสูงได้ถูกนำเสนอในวิทยานิพนธ์ฉบับนี้ด้วย การจำลองและทดลองถูกนำมาใช้เพื่อทดสอบความถูกต้อง ความสภาพทนทาน และความเชื่อถือได้ของวิธีการที่นำเสนอ ผลลัพธ์ที่ได้ถูกนำไปเปรียบเทียบกับแหล่งอ้างอิงซึ่งใช้วิธีการอื่นๆ แบบจำลอง Simulink สองแบบจำลองได้รับการพัฒนาขึ้นโดยอาศัยพื้นฐานตามขั้นตอนวิธีที่นำเสนอ แบบจำลองแรกสำหรับสกัดพารามิเตอร์เซลล์แสงอาทิตย์โดยอาศัยเพียงข้อมูลจากแผ่นข้อมูล และแบบจำลองที่สองสำหรับจำลองและคำนวณหาจุดกำลังงานสูงสุดของระบบพีวีแบบจำลองนี้มีความยืดหยุ่นในการปรับแต่งแผงเซลล์แสงอาทิตย์รูปแบบการต่อเชื่อมแผงโดยผู้ใช้งาน

ภาควิชา : วิศวกรรมไฟฟ้า

ลายมือชื่อนิสิต.....

สาขาวิชา : วิศวกรรมไฟฟ้า

ลายมือชื่อ อ.ที่ปริกษาหลัก.....

ปีการศึกษา ..2558

# # 5671445221 : MAJOR ELECTRONIC ENGINEERING

KEYWORDS : SOLAR ENERGY, MAXIMUM POWER POINT, TRACKING,  
EXTRACTION

NHAN THANH TONG : A DETERMINISTIC ALGORITHM FOR GLOBAL  
MAXIMUM POWER POINT CALCULATION OF A SOLAR FARM

THESIS ADVISOR : ASSIS. PROF. WANCHALERM PORA, Ph.D., 139 pp.

Optimizing the efficiency plays a very important role in harvesting solar energy by PV systems. This dissertation proposes a few methods which estimate all local maximum power points (MPP) and the global maximum power point of a PV system in short time. They require only a few online measured values. PV systems may be driven directly to global MPP without power searching. Consequently, the time for tracking is reduced, the efficiency of PV systems is, hence, increased. In this dissertation, the solar cell is represented by the single diode model. The relation of voltage and current at (MPPs) is exploited and this differentiates the proposed method from the others. Solar cell parameters for the model are not provided by solar cell panel manufacturers. So parameter extraction is a requirement. A new simple method which uses only given data in product datasheet but yields high accurate results is also proposed. Some experiments and simulations evaluate the correctness, robustness and reliability of the proposed techniques. The results obtained are compared with those of other referenced methods. Two programs are written basing on the proposed algorithms. First one is for solar cell parameters extraction using only information in product datasheet. The second is used for simulation and calculation the MPPs of the PV system which may be configured flexibly by the users.

Department: Electrical Engineering

Student's Signature.....

Field of study: Electronic Engineering

Advisor's Signature.....

Academic Year: 2015

## Acknowledgements

*This dissertation would never have been able to finish without the guidance of my committee members, help from friends and very kind support from my advisor.*

*I would like to express my deepest gratitude to my advisor, Assist. Prof. Doctor Wanchalerm Pora, for his supports, excellent guidances. He shows me the fantastic atmosphere of scientific research and gives me the best conditions for doing my works.*

*I would like to especially thank Assoc. Prof. Doctor Ekachai Leelarasmee, who gives me very useful advices and encourage me to overcome the challenges.*

*I greatly appreciate and deeply thank committee members (Assist. Prof. Dr. Suree Pumrin, Assist. Prof. Dr. Manop Wongsaisuwan and Assist. Prof. Dr. Kittiphan Techakittiroj) for their valuable guidances which help me to solve the troubles in this dissertation.*

*I would like to express my thankfulness to staffs and my friends in ESID Lab for their very kind helps.*

*I would like to thank CU-ASEAN Scholarship 2013 and the coordinators of this program, who have supported to me to study at Chulalongkorn University since 2013.*

*Finally, I deeply thank my wife who sacrificed a lot of her time and effort so that I can focus on my study absolutely.*

# Contents

Abstract in Thai . . . . .	iv
Abstract in English . . . . .	v
Acknowledgements . . . . .	vi
Contents . . . . .	vii
List of Tables . . . . .	x
List of Figures . . . . .	xiii
Abbreviations . . . . .	xviii
Physical Constants . . . . .	xix
Symbols . . . . .	xx
<b>CHAPTER</b>	
<b>I MOTIVATION</b>	<b>1</b>
1.1 Solar PV - A Promising Electricity Source . . . . .	1
1.2 Optimizing the Efficiency of PV System . . . . .	3
1.2.1 Sun Tracking . . . . .	4
1.2.1.1 Sun Tracking Based on Photo Sensor . . . . .	4
1.2.1.2 Sun Tracking Basing on Real Time Clock, Panel Location and Tilt Angle Sensor . . . . .	5
1.2.2 Maximum Power Point Tracking . . . . .	6
1.2.3 Problems of Existing MPPT Techniques . . . . .	8
1.2.3.1 Gaps of Offline Tracking Methods . . . . .	8
1.2.3.2 Gap in Online Tracking . . . . .	8
1.2.3.3 Mismatch the GMPP in Partial Shading Condition . . . . .	9
1.3 The Target and Scope . . . . .	9
<b>II LITERATURE REVIEW</b>	<b>11</b>
2.1 Solar Cell . . . . .	11
2.1.1 Structure . . . . .	11
2.1.2 I-V Relation . . . . .	12
2.2 Maximum Power Point Tracking . . . . .	13
2.2.1 Offline Tracking . . . . .	13
2.2.2 Online Tracking . . . . .	14
2.2.2.1 Single String Tracking . . . . .	15
2.2.2.2 Multi-Strings Tracking . . . . .	20
2.3 Introducing The Proposed Tracking Method . . . . .	22
2.4 Extraction Parameters of Solar Cell . . . . .	23

2.5	Proposed Extraction Method . . . . .	28
<b>III</b>	<b>NEW EXTRACTION METHOD FOR SINGLE DIODE SOLAR CELL MODEL</b>	<b>30</b>
3.1	Introduction . . . . .	30
3.2	Equations for Proposed Method . . . . .	31
3.3	Searching Strategy . . . . .	34
3.3.1	Searching the Series Resistor $R_s$ Bases on a Given Value of $n$ . .	35
3.3.2	Determine $R_p$ , $I_S$ and $I_{ph}$ Based on Given $n$ and Calculated $R_s$	38
3.3.2.1	Parallel Resistor $R_p$ . . . . .	38
3.3.2.2	Saturation Current $I_S$ . . . . .	39
3.3.2.3	Calculating for Photo-generated Current $I_{ph}$ . . . . .	39
3.3.3	Verifying by Cost Function $\varepsilon(n, R_s, R_p, I_S, I_{ph})$ . . . . .	40
<b>IV</b>	<b>PROPOSED METHOD FOR CALCULATION THE GLOBAL MAXIMUM POWER POINT OF A PV SYSTEM</b>	<b>42</b>
4.1	Dependence of $R_s$ , $R_p$ , $I_S$ , $I_{ph}$ on Temperature . . . . .	42
4.2	Determining the MPP under Uniform Shading Condition . . . . .	43
4.2.1	The Iterative Expression of Current at MPP . . . . .	44
4.2.2	The Iterative Expression of Voltage at MPP . . . . .	48
4.3	Determining the GMPP of a PV String under Partial Shading Condition	48
4.3.1	Calculating for $I_{ph}$ of Panel at Measured Points . . . . .	51
4.3.2	Segmentation . . . . .	52
4.3.3	Determining the Expression of String Voltage . . . . .	53
4.3.3.1	Expression of panel voltage $V_P^i$ when $I_{Str} \leq I_{ph}^i$ . . . . .	53
4.3.3.2	Expression of Panel Voltage $V_P^i$ when $I_{Str} > I_{ph}^i$ . . . . .	54
4.3.3.3	The Expression of String Voltage in Segment $m$ . . . . .	54
4.3.4	The Expression of Voltage at Local MPP in Segment $m$ , $V_M^m$ . . . . .	55
4.3.5	Searching the Local Peak Voltage in Segment $m$ . . . . .	56
4.4	Determining the GMPP of Parallel Strings Under Uniform Shading Condition . . . . .	57
4.4.1	Voltage Scanning . . . . .	59
4.4.2	$V_G$ Approximation . . . . .	60
<b>V</b>	<b>EXPERIMENTS, CALCULATION AND SIMULATION RESULTS OF PROPOSED EXTRACTION METHOD</b>	<b>61</b>
5.1	Extracting for Referenced Solar Cell and Panel. . . . .	61
5.1.1	Extracting for Referenced Solar Cell Bases on Given Dataset. . . . .	61
5.1.2	Extracting for Referenced Solar Panel Bases on Given Dataset. . . . .	63
5.2	Extraction for Real Solar Panels Basing on Measured values. . . . .	65
5.2.1	Extracting for a Polycrystalline Panel . . . . .	65
5.2.2	Extracting for a Monocrystalline Panel Model . . . . .	67
5.3	Extracting for Solar Panels Basing on Product Datasheet. . . . .	69
5.3.1	Extracting for Polycrystalline Solar Panels . . . . .	69
5.3.2	Extracting for Monocrystalline Solar Panels . . . . .	71
5.3.3	Extracting for Thin Film Solar Panels . . . . .	72

<b>VI EXPERIMENTS, CALCULATION AND SIMULATION FOR DETERMINING THE GMPP</b>	<b>76</b>
6.1 Single Panel: Experiment, Simulation Compare to Calculated Results by Proposed Method . . . . .	76
6.2 Single String: Experiments, Simulations Compare to the Calculated Results by Proposed method . . . . .	78
6.2.1 <i>Case 1</i> : The Irradiance on All Panels Are Equivalent (Uniform Shading Condition) . . . . .	79
6.2.2 <i>Case 2</i> : The Irradiance on Panels Are Different (Partial Shading)	81
6.3 Confirming the Correctness, Robustness and Reliability of Proposed by Simulations . . . . .	83
6.4 Calculation and Simulation for Single String under Partial Shading . .	87
6.4.1 <i>Case 1</i> : The irradiance Distributes on a Wide Range . . . . .	87
6.4.2 <i>Case 2</i> : The Irradiance Distributes in a Narrower Range . . . . .	89
6.4.3 <i>Case 3</i> : One Panel Received Lower Irradiance Compare to Others	91
6.5 Calculation and Simulation for Parallel Strings under Partial Shading Conditions . . . . .	93
6.5.1 <i>Case 1</i> : Two Strings, Seven Panels per String . . . . .	93
6.5.2 <i>Case 2</i> : Three Strings, Five Panels per String . . . . .	95
<b>VII CONCLUSION &amp; FUTURE WORK</b>	<b>98</b>
<b>REFERENCES</b>	<b>100</b>
<b>APPENDICES</b>	
<b>A INTRODUCE THE EXTRACTION PROGRAM AND THE CALCULATED PARAMETERS</b>	<b>105</b>
A.1 Using the Extraction Program . . . . .	105
A.2 The Extracted Results by The Proposed Method . . . . .	106
A.3 The I-V Curves, P-V Curves, MPP by Simulation and Calculation . . .	115
<b>B INTRODUCE THE CALCULATION AND SIMULATION PROGRAM FOR THE PV SYSTEM</b>	<b>119</b>
B.1 The Program for Determination MPPs and Simulation PV System . .	119
B.1.1 The Program Interface . . . . .	119
B.1.2 Example for Using the Program . . . . .	122
B.2 Calculation and Simulation for Single String . . . . .	125
B.2.1 <i>Case 1</i> : Four Panels String . . . . .	126
B.2.2 <i>Case 2</i> : Eight Panels String . . . . .	127
B.2.3 <i>Case 3</i> : Ten Panels String . . . . .	129
B.3 Calculation and Simulation for Two Strings in Parallel . . . . .	131
B.3.1 <i>Case 1</i> : Three Panels per String . . . . .	131
B.3.2 <i>Case 2</i> : Ten Panels per String . . . . .	133
B.4 Calculation and Simulation for Three Strings in Parallel . . . . .	135
<b>Biography</b>	<b>140</b>



## List of Tables

### Table

5.1	The calculated cell parameters by the proposed method and by the other reference methods. The values in parenthesis are the difference when the values obtained by the proposed methods are compared with those of other reference methods. . . . .	62
5.2	The errors when the measured current in the third column from left is compared with those predicted by the proposed method and other reference methods. The measurements was performed at 20 different I-V pairs. . . . .	63
5.3	A panel parameters extracted by the proposed and other methods. The panel is composed of 36 cells ( $\mathcal{C} = 36$ ). The figures in parenthesis are the difference when the values obtained by the proposed methods are compared with those of other methods. . . . .	64
5.4	The errors when the measured current in the third column from left is compared with those predicted by the proposed method and other reference methods. The measurements was scanned at 21 different I-V pairs along the I-V curve. . . . .	64
5.5	Measured I-V pairs and the absolute difference between the measured and the calculated current. The experiment is performed on polycrystalline, model <i>STP6</i> – 120/36 by Schutten Solar. . . . .	67
5.6	The parameters of real solar panel are calculated by proposed method using three measured points. . . . .	68
5.7	Measured I-V pairs and the absolute difference between the measured and the calculated current. The experiment is performed on a monocrystalline, model <i>STM6</i> – 40/36 by Schutten Solar. . . . .	69
5.8	The input values and calculated parameters of the polycrystalline silicon solar cells, Series TS 240-255P-60, H&T Power GmbH manufacturer. . . . .	70
5.9	The input values and calculated parameters of monocrystalline silicon solar cells, Series TS 250-265D-60, H&T Power GmbH manufacturer. . . . .	71
5.10	The input values and calculated parameters of TeCd thin film solar cells, Series 4 <sup>TM</sup> (FS 4102-2 to FS 4112-2), First Solar manufacturer. . . . .	73
5.11	Code of solar panel models (right column). . . . .	74
5.12	The parameters of polycrystalline panels obtained by using only the information in their datasheet. . . . .	75
5.13	The parameters of monocrystalline panels obtained by using only the information in their datasheet. . . . .	75
5.14	The parameters of thin-film panels obtained by using only the information in their datasheet. . . . .	75
6.1	Measured $V$ and $I$ and their calculated $P$ . . . . .	76
6.2	Four I-V datasets, calculated MPPs, and effect of additive zero-mean Gaussian noise. . . . .	77
6.3	The measured values are used for calculation by proposed method in <i>Case 2</i> and the corresponding obtained values. . . . .	80

## Table

6.4	The measured peak powers and calculated peak powers from four samples in <i>Case 2</i> . . . . .	81
6.5	The measured peak voltages and the error in voltage between experiment and calculation of <i>Case 2</i> . . . . .	81
6.6	The measured values are used for calculation by proposed method in <i>Case 1</i> and the corresponding obtained values. . . . .	82
6.7	The measured peak powers and calculated peak powers from four samples in <i>Case 1</i> . . . . .	83
6.8	The measured peak voltages and the error in voltage between experiment and calculation of <i>Case 1</i> . . . . .	83
6.9	Five pairs measured values ( $V, I$ ) of a simulation are used in calculation and the corresponding calculated results of them. . . . .	85
6.10	The average errors of $V_M$ ( $\bar{e}_M, \bar{e}_{M+}, \bar{e}_{M-}$ ), their variances ( $\sigma_M^2, \sigma_{M+}^2, \sigma_{M-}^2$ ) and the average number of iterative loops ( $\bar{l}, \bar{l}_-$ and $\bar{l}_+$ ). Each calculated from 50 random pairs of $V$ and $I$ , $V+$ and $I+$ , and, $V-$ and $I-$ . . . . .	87
6.11	The measured values for Case 1 and the calculated $I_{ph}^i$ of all panels. . . . .	88
6.12	Six local MPPs found by the proposed method and by Simulink P-V scan. . . . .	88
6.13	The measured values for Case 2 and the calculated $I_{ph}^i$ of all panels. For Panel 1, Panel 2, and Panel 3, the estimated $T_d^i$ are shown instead of $T_P^i$ . . . . .	89
6.14	Four local MPPs found by the proposed method and by Simulink P-V scan. . . . .	90
6.15	The measured values for Case 3 and the calculated $I_{ph}^i$ of all panels. . . . .	91
6.16	Two local MPPs found by the proposed method and by Simulink P-V scan. . . . .	91
6.17	Voltage (left) and estimated power at local MPPs (right). . . . .	93
6.18	Operating condition of panels (left) and measured values for calculation (right). . . . .	94
6.19	The operating conditions of 3x5 PV system and panel voltages are used in proposed calculation. . . . .	95
6.20	The local peak voltage of strings by calculation, simulation and error between them (A). The estimated power of system at local peak voltages(B). . . . .	96
A.1	List of extracted models . . . . .	108
A.2	The extracted parameters of series model $ASxxx - 6P30$ at STC. . . . .	109
A.3	The extracted parameters of series model $ASxxx - 6P30$ at NOCT. . . . .	109
A.4	The extracted parameters of series model $TS - xxxPB - 60$ at STC. . . . .	109
A.5	The extracted parameters of series model $TS - xxxPB - 60$ at NOCT. . . . .	109
A.6	The extracted parameters of series model $TS - xxxPB - 72$ at STC. . . . .	110
A.7	The extracted parameters of series model $TS - xxxPB - 72$ at NOCT. . . . .	110
A.8	The extracted parameters of series $Goldline - xxx - P6 - 60$ at STC. . . . .	110
A.9	The extracted parameters of series $Goldline - xxx - P6 - 60$ at NOCT. . . . .	110
A.10	The extracted parameters of series model $ND - Rxxx - A5$ at STC. . . . .	111
A.11	The extracted parameters of series model $ND - Rxxx - A5$ at NOCT. . . . .	111
A.12	The extracted parameters of series $PlusSW$ at STC. . . . .	111

## Table

A.13	The extracted parameters of series <i>PlusSW</i> at NOCT. . . . .	112
A.14	The extracted parameters of series <i>TS – xxxD – 72</i> at STC. . . . .	112
A.15	The extracted parameters of series <i>TS – xxxD – 72</i> at NOCT. . . . .	112
A.16	The extracted parameters of series <i>TS – xxxD – 60</i> at STC. . . . .	112
A.17	The extracted parameters of series <i>TS – xxxD – 60</i> at NOCT. . . . .	113
A.18	The extracted parameters of series <i>TS – xxxD – 72</i> at STC. . . . .	113
A.19	The extracted parameters of series <i>TS – xxxD – 72</i> at NOCT. . . . .	113
A.20	The extracted parameters of series <i>FS – 4xxx – 2</i> at STC. . . . .	113
A.21	The extracted parameters of series <i>FS – 4xxx – 2</i> at NOCT. . . . .	114
A.22	The extracted parameters of series <i>FS – 3xxx – 2</i> at STC. . . . .	114
A.23	The extracted parameters of series <i>FS – 3xxx – 2</i> at NOCT. . . . .	114
B.1	The function of buttons in Main interface of program. . . . .	120
B.2	The data file are generated by program. . . . .	126
B.3	The operating conditions (A) and corresponding peaks by calculation and simulation (B). . . . .	127
B.4	Operating conditions of panels and the local peaks of string obtained by calculation and simulation. . . . .	128
B.5	The local peak powers and the corresponding voltage error. . . . .	128
B.6	Operating conditions, the voltage at MPPs by calculation and simulation. . . . .	130
B.7	The local peak powers and voltage errors at these peaks. . . . .	130
B.8	The operating conditions and measured panel’s voltage. . . . .	131
B.9	Voltage at local peaks (A) and estimated peak power (B). . . . .	132
B.10	Operating condition of panels (left) and measured values for calculation (right). . . . .	133
B.11	Voltage at local MPPs (left) and estimated powers at these voltages (right). . . . .	134
B.12	The operating conditions of 3x10 PV system. . . . .	136
B.13	The measured panel voltages are applied in calculation by proposed method for of 3x10 PV system. . . . .	136
B.14	The local peak powers by calculation ( $P_{Mcal}^{ij}$ ) and simulation ( $P_{Msim}^{ij}$ ) of strings. . . . .	137
B.15	The estimated power of system at determined local peaks. . . . .	137
B.16	The local peak voltage and voltage error at these points of two strings. . . . .	138

# List of Figures

Figure	
1.1 Solar radiation is converted to DC electricity by solar cells. It may be consumed by local consumers or sent to grid for distant consumers or stored to be used later. . . . .	1
1.2 Estimated Renewable Energy Share of Global Electricity Production, End-2013 ( <i>Source: REN21</i> ) . . . . .	2
1.3 In 2014, Growth Rate of Solar PV is the highest with an estimated 40 GW installed for a total global capacity of about 177 GW. ( <i>Source: REN21</i> ) . . . . .	2
1.4 The best research cell efficiencies from 1975 to 2015. ( <i>Source: NREL</i> ) .	3
1.5 The cell surface is not perpendicular to the sun light. That is one of reasons leads to increasing of losing energy. . . . .	4
1.6 Four photo sensors (N,S,E and W) are used to determine the direction of the sunlight (a), (b). Two articulations in a sun tracking system (c).	5
1.7 A sun tracking system base on real time clock, panel position and tilt sensor (or accelerator sensor). . . . .	6
1.8 For using produced electricity absolutely, a battery system is used to store redundant electricity. . . . .	7
1.9 Two different operating conditions (shaded (a) and unshaded(b). The I-V curves (b) and P-V curves (c) of solar cell when the conditions change. . . . .	7
1.10 The electricity is not delivered to load during offline time. The output voltage is equal zero in case short circuit current (a) and the output current is equal zero in case open circuit voltage (b). . . . .	8
1.11 The GMPP of a string is drifted under changing of irradiance. . . . .	9
2.1 Structure of a solar cell (a). Cross section of a solar cell (b). Single diode equivalent circuit of a solar cell (c). . . . .	12
2.2 The schematic is used to scan load and plot the I-V, P-V curves (a). The solar cell's I-V curve (b). The solar cell's P-V curve (c). . . . .	13
2.3 A string is composed of $N_s$ panels in series under partial shading (a) and the I-V, P-V curves (b). . . . .	15
2.4 The scanning for MPP with step $2V$ . . . . .	16
2.5 The searching strategy use voltage step-size $\Delta V = K_{OC}V_{OC}/2N_s$ [4] for the first scanning. . . . .	17
2.6 The I-V curves of seperated modules(a); The array I-V and P-V curves (b); The searching strategy of proposed method in [5] (c). . . . .	17
2.7 The voltage scanning range in [6] and expressions are used to determine the limited points. . . . .	18
2.8 In (A), the itersections and the GMPP locate at same part [7]. Points A, B, C, D, E belong to GPA of S1, S2, S3, S4, S5 respectively; In (B), the strategy searching based on the line OM which has slope $k = \frac{V_{OC}}{I_{SC}}$ . The intersection is determined and used as initial point of climbing algorithm. . . . .	19

## Figure

2.9	The I-V curve of PV system and I-V input curves of DC/DC converter (a). The P-V curve of PV system and the P-V input curves of the load (b).	19
2.10	The method in [9] bases on modified Fibonacci search method with fuzzy controller	20
2.11	The central control system for uniform shading condition (A); The combination central control system and wireless communication system is proposed by [13] (B). The structure of an array with a micro converter for every panel(C).	21
2.12	The proposed PV system for string GMPP tracking.	22
2.13	The proposed PV system for paralell string GMPP tracking.	23
2.14	Three well known estimations of $I_{ph}$ , $R_p$ and $R_s$ .	24
2.15	The flow-chart of the extraction method combines estimations and MMSE searching in [17].	25
2.16	Three points and one condition for establishing system equation in proposed method.	29
3.1	The equivalent circuit of a solar cell.	30
3.2	The structure of a solar panel.	31
3.3	Searching flowchart of proposed method.	35
3.4	Flowchart for searching $R_s$ .	37
3.5	An example of scanning for the most suitable value of $n$ . It is increased and decreased twice. Each direction changing the <i>step_size</i> is reduced ten times.	41
4.1	The solar farm under uniform condition.	44
4.2	Algorithm for searching the GMPP under uniform shading.	49
4.3	The bypass diode with a series resistor inside.	49
4.4	The solar farm under uniform condition.	50
4.5	The equivalent circuit of composed component solar panel - diode (a). The I-V curve of the composed component (b).	50
4.6	Algorithm for searching the GMPP under uniform shading.	52
4.7	$\mathcal{P}$ segments of string current.	52
4.8	The role of diode in two cases.	53
4.10	Algorithm for calculate panel voltage at a given current.	54
4.11	An MPP exist only when two relations are true: 1) at the current $I_{ph}^{m-1}$ , $V1 > V2$ and 2) at $I_{ph}^m$ , $V1 < V2$ . A modified bisection method is proposed to locate the local MPP in segment $m$ .	57
4.12	$\mathcal{S}$ parallel strings in PV system share a grid-connect inverter.	58
4.13	$\mathcal{P}$ segments in current and voltage of string $i$ .	58
4.14	Algorithm for estimating the GMPP of parallel strings.	60
5.1	I-V curves of a cell modeled by the proposed and three other reference methods.	62
5.2	The IV curves of a panel modeled by the proposed and three other methods.	65
5.3	Experiment for acquiring an I-V dataset from a solar panel.	66

Figure

5.4 Schematic for measuring the current and voltage of solar panel by scanning load (left) and status of switches for measurements (right). . . . . 66

5.5 The variable load is used in scanning. The range of resistance is from 0 to 13.8  $\Omega$ . This range ensures that the MPP is tracked. . . . . 66

5.6 I-V curve is produced based on the calculated parameters and several masured points. . . . . 67

5.7 The variable load is used in scanning. The load is scanned from 0 to 71.7  $\Omega$ . This range ensures that the MPPs of single panels and 4 panels-string are tracked. . . . . 68

5.8 I-V curve of the monocrystalline panel, modeled by the proposed method, and some masured points. . . . . 68

5.9 The I-V curves of calculated polycrystalline silicon solar panel (60 cells) basing on datasheet of Series TS 235-255P-60, H&T Power GmbH. . . . . 70

5.10 The relationship of parameteres and the efficiency of polycrystalline solar cell. . . . . 71

5.11 The relationship of parameteres and the efficiency of monocrystanlline silicon solar cell. . . . . 72

5.12 The I-V curves of calculated monocrytalline silicon solar panel (60 cells) basing on datasheet of Series TS 250-265D-60, H&T Power GmbH . . . . . 72

5.13 The relationship of parameteres and the efficiency of monocrystanlline silicon solar cell. . . . . 73

5.14 The I-V curves of calculated thin film CdTe solar panel (216 cells). Panel peak powers are 105W, 107.5W, 110W and 112.5W (Series 4<sup>TM</sup>, First Solar.) . . . . . 73

6.1 The P-V curves by load scanning and by simulation. The voltage at MPPs by measurement, simulation and calculation are closed together. . . . . 77

6.2 A string is composed of four mono panels *STM6 – 40/36* of Solar Schutten manufacturer. . . . . 78

6.3 The schematic is setup for the experiment. . . . . 79

6.4 The string P-V curve by scanning load and the local peaks which are obtained from calculation basing on measured sets of values. . . . . 80

6.5 The string P-V curve by scanning load and the local peaks which are obtained from calculation basing on measured sets of values. . . . . 82

6.6 Simulink model that is used to draw the I-V and the P-V curves. . . . . 84

6.7 The calculated peaks are always close to the Simulink peaks. . . . . 85

6.8 The calculated peaks and the P-V simulation curve. . . . . 88

6.9 The graphs of  $V^m$  and  $V_M^m$ . Their intersections locate the peaks of PV string. . . . . 89

6.10 The calculated peaks under changing of irradiance. . . . . 90

6.11 The calculated values are close to the intesection points of  $V^m$  and  $V_M^m$ . . . . . 90

6.12 The calculated peaks under changing of irradiance. . . . . 92

6.13 The calculated peaks under changing of irradiance. . . . . 92

6.14 I-V curves (left) and P-V curves (right) . . . . . 94

6.16 The intersections in segments of two strings. . . . . 95

6.18 I-V curves, P-V curves and intersections in segments of PV system. . . . . 97

A.1 First dialog permits user to provide data by two ways. . . . . 105

## Figure

A.2	The second interface permits user to choose panel from data base. Both test conditions STC and NOCT of panel are available. . . . .	106
A.3	The dialog permits the user to type their measured values. . . . .	106
A.4	An example for calculation with given data. . . . .	107
A.5	An example for calculating from manual data set. . . . .	107
A.6	The I-V curves (left) and the P -V curves (right) of series <i>ASxxx-6P30</i> at STC (upper) and NOCT (lower). . . . .	115
A.7	The I-V curves (left) and the P -V curves (right) of series <i>TS-xxxPB-60</i> at STC (upper) and NOCT (lower). . . . .	115
A.8	The I-V curves (left) and the P -V curves (right) of series <i>TS-xxxPB-72</i> at STC (upper) and NOCT (lower). . . . .	115
A.9	The I-V curves (left) and the P -V curves (right) of series <i>Goldline-xxx-P6-60</i> at STC (upper) and NOCT (lower). . . . .	116
A.10	The I-V curves (left) and the P -V curves (right) of series <i>ND-Rxxx-A5</i> at STC (upper) and NOCT (lower). . . . .	116
A.11	The I-V curves (left) and the P -V curves (right) of series <i>PlusSW</i> at STC (upper) and NOCT (lower). . . . .	116
A.12	The I-V curves (left) and the P -V curves (right) of series <i>TS-xxxD-72</i> at STC (upper) and NOCT (lower). . . . .	117
A.13	The I-V curves (left) and the P -V curves (right) of series <i>TS-xxxD-60</i> at STC (upper) and NOCT (lower). . . . .	117
A.14	The I-V curves (left) and the P -V curves (right) of series <i>TS-xxxD-72</i> at STC (upper) and NOCT (lower). . . . .	117
A.15	The I-V curves (left) and the P -V curves (right) of series <i>FS-4xxx-2</i> at STC (upper) and NOCT (lower). . . . .	118
A.16	The I-V curves (left) and the P -V curves (right) of series <i>FS-3xxx-2</i> at STC (upper) and NOCT (lower). . . . .	118
B.1	The interface of program permits user to choose the size of PV system. The maximum size is 10x10 (10 strings, each string contents 10 panels in series). The number of cells in each panel is unlimited. There are seven buttons in Main interface. The functions of these buttons are introduced in Table B.1 . . . . .	119
B.2	The interface for user to set up the operating conditions of all panels. Each panel requires three input data: $I_r, T_p, T_d$ . The button "SEND TO PV SYSTEM" updates the setting values to model in schematic for simulation. . . . .	120
B.3	The interface permits user to enter the measured values ( $T, V_{OC}, I_{SC}, V_M, I_M$ and $C$ ) in left column. Click the button "SEARCH & DISPLAY" to extract the parameters based on input data and display them to right column. Button "UPDATE PARAMETERS" send the parameters to model for simulation. . . . .	121
B.4	The interface for loading the measured values from database. Similar to the program which is introduced in Fig. A.2. However, this dialog has two other buttons for update the parameters to the models ("UPDATE Parameters STC" and "UPDATE Parameters NOCT"). . . . .	121

## Figure

B.5	The dependence of $R_{load}$ on time. The variable load is scanned from $0\Omega$ to $10850\Omega$ . The zoomed part shows that the load is scanned slowly at small values for tracking the MPP. The step size will be increase when the load value is large. . . . .	122
B.6	Main interface with default both number of string and number of panel per string are 1. . . . .	122
B.7	Setting the PV system structure. . . . .	123
B.8	Main interface with default both number of string and number of panel per string are 1. . . . .	123
B.9	Setting the parameters for solar cell follow model $TS - 235PB - 60$ of GmbH manufacturer. . . . .	124
B.10	Setting the operating conditions for all panels in 2x3 PV system. . . . .	125
B.11	I-V curves (A) and P-V curves (B) of a four panels string. . . . .	127
B.13	The I-V curve, MPP by simulation. The intersections between curves of $V^m(I)$ and $V_M^m(I)$ are the local MPP. . . . .	127
B.14	I-V curve (A), P-V curve (B) of eight panels-string by simulation and the calculated local peaks. . . . .	129
B.15	The I-V curve by simulation and calculation and MPP curve by calculation of 8 panel-string. The intersections between curves of $V^m(I)$ and $V_M^m(I)$ are closed to the local peaks by simulation. . . . .	129
B.16	I-V, P-V curves (A) and local peaks (B) by calculation and simulation. . . . .	130
B.18	Intersections in segments of ten panels-string. . . . .	131
B.19	I-V curves (left), P-V curves (right) and local MPP. . . . .	132
B.21	Intersections correspond to local MPPs in every segment of two strings. . . . .	132
B.23	I-V curves (left) and P-V curves (right) of strings and whole PV system. . . . .	134
B.25	The intersections in segments of two strings. . . . .	135
B.27	I-V curves (A), P-V curves (B) of strings and whole PV system . . . . .	138
B.29	Intersections in every segment of three strings. . . . .	139



## Abbreviations

<b>MPP</b>	<b>Maximum Power Point</b>
<b>MPPT</b>	<b>Maximum Power Point Tracking</b>
<b>MPPTS</b>	<b>Maximum Power Point Tracking System</b>
<b>GMPP</b>	<b>Global Maximum Power Point</b>
<b>PV</b>	<b>PhotoVoltaic</b>
<b>P-V</b>	<b>Power-Voltage</b>
<b>I-V</b>	<b>Current-Voltage</b>
<b>LHS</b>	<b>Left Hand Side</b>
<b>RHS</b>	<b>Right Hand Side</b>
<b>PWM</b>	<b>Pulse Width Modulation</b>
<b>ADC</b>	<b>Analog to Digital Converter</b>
<b>STC</b>	<b>Standard Test Conditions</b>
<b>NOCT</b>	<b>Nominal Operating Cell Temperature</b>
<b>OC</b>	<b>Open Circuit</b>
<b>SC</b>	<b>Short Circuit</b>

## Physical Constants

Boltzmann constant  $k = 1.3806488 \times 10^{-23} \text{ JK}^{-1}$

Elementary charge  $q = 1.60217657 \times 10^{-19} \text{ C}$

Speed of light  $c = 299792458 \text{ m s}^{-1}$

## Symbols

$I_r$	irradiance intensity	W/m <sup>2</sup>
$I$	current	A
$P$	power	W (Js <sup>-1</sup> )
$V$	voltage	V
$I_c$	current of cell	A
$V_c$	voltage of cell	V
$V_P^i$	voltage of panel $i^{th}$	V
$V_{Str}$	voltage of string	V
$V_{Str}^m$	voltage of string with current $I \in [I_{m-1}, I_m]$	V
$I_{SC}$	short circuit current	A
$V_{OC}$	open circuit voltage	V
$V_T$	thermal voltage	V
$n$	emission coefficient or ideality factor	
$R_s$	series resistance	Ω
$R_p$	parallel (shunt) resistance	Ω
$I_{ph}$	induced (photo generated) current	A
$I_S$	reverse saturation current	A
$I_M$	current at MPP	A
$V_M$	voltage at MPP	A
$TIPH$	temperature coefficient of induced current	
$TXIS$	temperature power coefficient of reverse saturation current	
$TRS$	temperature power coefficient of series resistance	
$TRP$	temperature power coefficient of parallel resistance	
$EG$	Energy band Gap	eV
$E$	Photon Energy	eV
$\omega$	angular frequency	rads <sup>-1</sup>
$\varepsilon$	very small value, cost function, photon energy	
$\lambda$	wave length of light	m

# Chapter I

## MOTIVATION

### 1.1 Solar PV - A Promising Electricity Source

Sunlight is an important factor for the survival of almost all creatures in the planet. Humans, animals and plants rely on the sun for warmth and food. The sun transfers its energy to nearly all energy form. From millions of years ago, plants and algae stored solar energy and they are compressed under many thick sediment layers. After a long time, it became fossil fuels such as oil and coal, which are used for transportation and electricity generation. The other example is biomass which converts solar energy into a fuel. Wind turbine produces electricity based on air flows that are created by solar heated air. Hydro-electricity has close relationship with the sun via the evaporation of water which cause rain. The rain provides water for dams of hydro power plant. Photovoltaics (PV), one kind of modern renewable energy source, is relatively a new technology in harvesting solar energy. PV devices (or solar cells) convert the incident solar radiation to electricity. Fig. 1.1 shows the chain from sun light to electric device. Because PV has advantages such as no sound and carbondioxide, no moving parts, easy to set up and maintain and low operating cost. The solar photovoltaic is used more and more in civil life, in industry and in space technology.

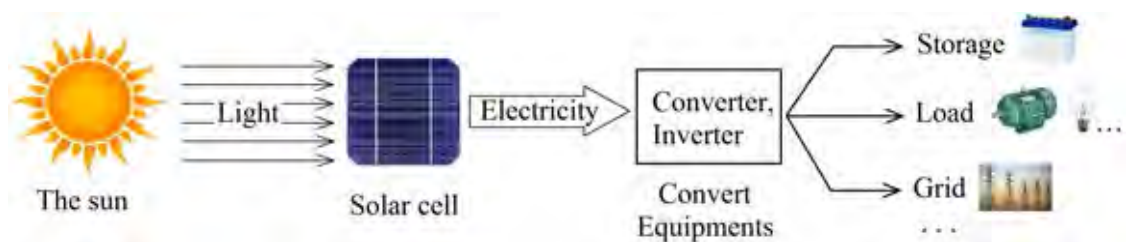


FIGURE 1.1: Solar radiation is converted to DC electricity by solar cells. It may be consumed by local consumers or sent to grid for distant consumers or stored to be used later.

The growth rate of solar PV is the highest in modern renewable sources with 30% in 2014 and 50% in stage 2008 through 2014 (Fig. 1.3(a)). The installed capacity of solar

PV has grown strongly since early years of this millennium. Beginning with 3.7GW in 2004, after 10 years, the capacity is 177GW at the end of 2014. Specially, 40 GW solar PV is installed within 2014 (Fig. 1.3(b)). According to *Renewables 2015 – Global Status Report of REN21* [39], solar PV contributed 0.9% of total global capacity in 2014 (Fig. 1.2), increasing 0.2 % compare to that in 2013. The solar PV attracts investors and researchers because it is not only green energy source but also its beneficial economic. The PV has been used more and more in many fields and applications. Because of environmental reason and people’s concern, nuclear and coal power plants are gradually replaced by solar farms or other renewable resources.

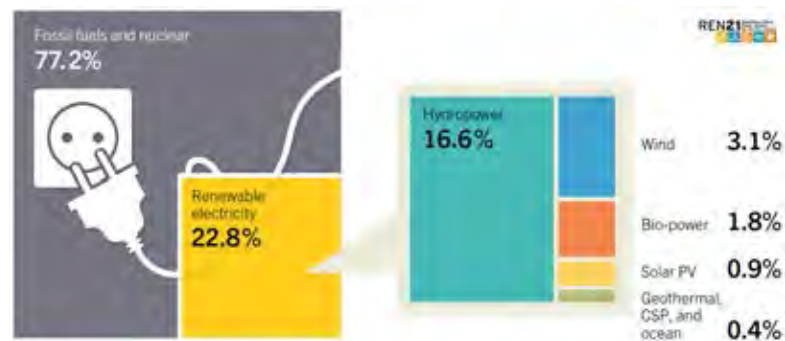


FIGURE 1.2: Estimated Renewable Energy Share of Global Electricity Production, End-2013 (Source: REN21)

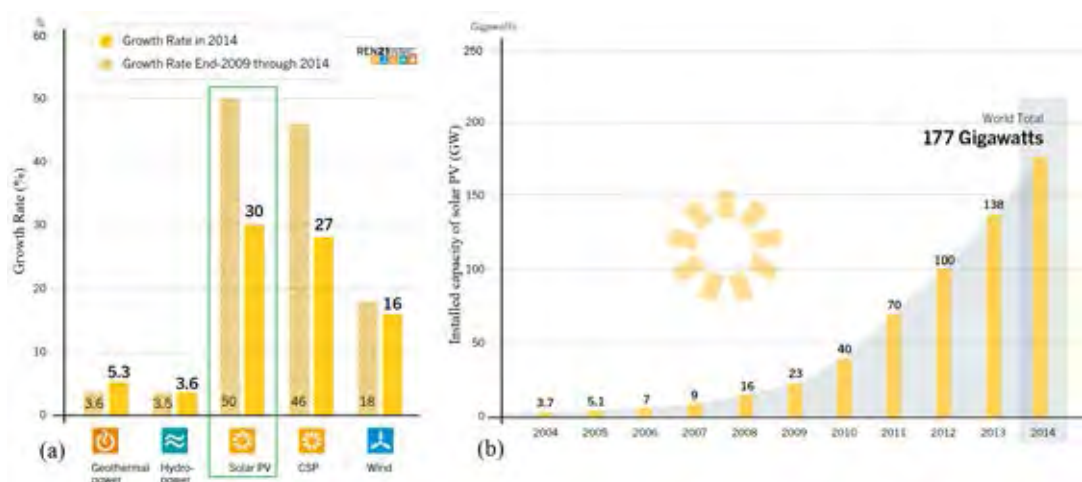


FIGURE 1.3: In 2014, Growth Rate of Solar PV is the highest with an estimated 40 GW installed for a total global capacity of about 177 GW. (Source: REN21)

According to the report of National Renewable Energy Laboratory of United State [40], the solar cell technologies are divided into five groups: single-junction, multi-junction, crystalline, thin-film and the other-emerging PV. In laboratory, the efficiency of these techniques have increased from a few recently decades. Particularly, the multi-junction

(concentrator) can yield 46% in efficiency. The crystalline and thin-film have the efficient records around 20% to 28%. Fig. 1.4 shows the highest efficiency of all solar cell technologies since 1976 to 2016. Although solar PV is a promising source,

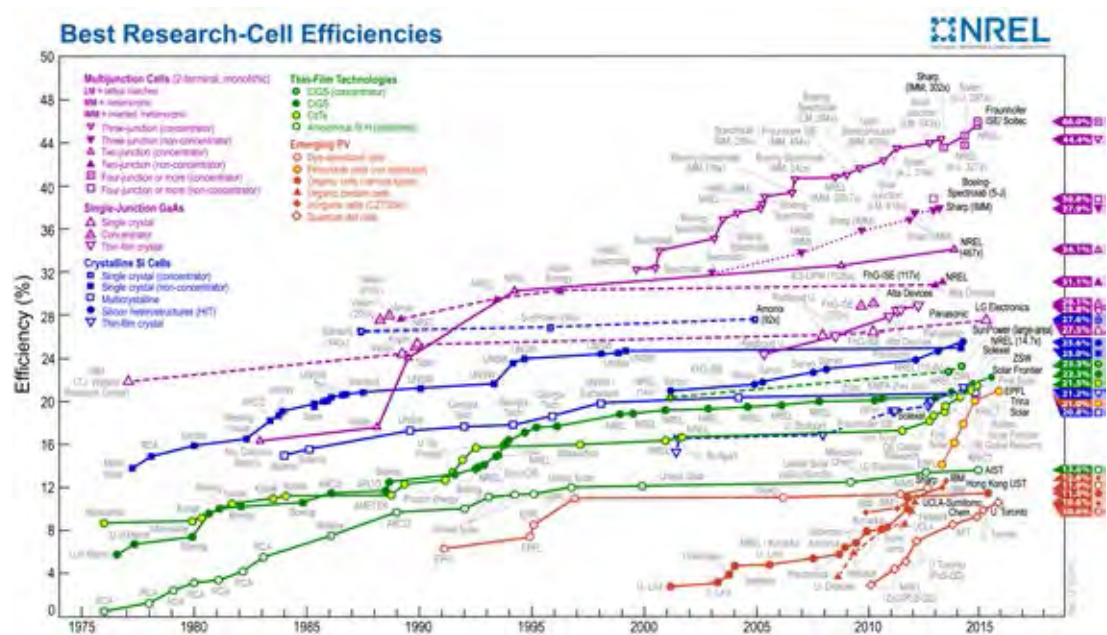


FIGURE 1.4: The best research cell efficiencies from 1975 to 2015. (Source: NREL)

the efficiency in conversion from light to electricity is still very low. Furthermore, photovoltaic is a special electricity resource. The solar cell just transfers its produced power at the highest level if it is connected to a suitable load (converter or inverter). There exists only one operating point, where the load can receive the maximum power from a PV system. This point is called *maximum power point* (MPP). So, harvesting energy by PV systems requires techniques, which ensure that the PV systems receive the highest light intensity and operate at MPP all time despite of the sun and environmental conditions. These techniques will be introduced and analyzed in the following parts.

## 1.2 Optimizing the Efficiency of PV System

The efficiency of an existing PV system can be optimized by two ways: maximize the input light power (*sun tracking*) and maximize the output power (*maximum power point tracking*).

### 1.2.1 Sun Tracking

Sun tracking is a process that moves the solar panel so that its surface is always perpendicular to the incident sun light. This ensures the solar cell receives the highest power from the sun. See Fig. 1.5, let  $\alpha$  be the angle between the sunshine and the normal line of surface,  $I_r$  represent the irradiance of the sun light, and  $S$  denotes the area of cell. The cell receives input power  $P_{light}$  which is calculated by the following

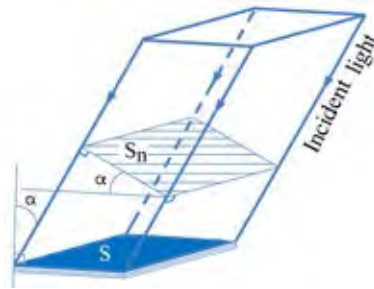


FIGURE 1.5: The cell surface is not perpendicular to the sun light. That is one of reasons leads to increasing of losing energy.

formula:

$$P_{light} = I_r S_n = I_r S \cos \alpha$$

where  $S_n$  is cross section of the incident light.

There are many methods for tracking the solar position. These methods can be separated into two groups: the first group is based on the photo sensors, and the other is based on the real time clock, location of PV system. In all sun tracking systems, the PV panel are put on a dynamic frame which can rotate around the horizon axis in order to keep the panel's surface perpendicular to the incident sunlight by the time of day; In some sun tracking systems, the panels can rotate around the vertical axis to track the sun according to the time of year.

#### 1.2.1.1 Sun Tracking Based on Photo Sensor

The photo sensors are fixed on the surface of solar panels. They are used to detect the angle between panel and incident sun light. Fig. 1.6(a) and 1.6(b) show two combinations of photo sensors. There are two pairs of light sensor (E-W and N-S). The solar panel is put on a frame which can rotate on a horizontal axis and some system can rotate around a vertical axis (see Fig. 1.6(c)). The difference of voltages

$\Delta V_{EW} = V_E - V_W$  and  $\Delta V_{NS} = V_N - V_S$  are used to control two motors in order to rotate the frame. Motor stops if its corresponding feedback signal yields zero. When both of motors stop, the incident light is perpendicular to the surface of panel. The light sensor may be photo-transistor, photo-diode, light-dependent resistor (LDR). This method works well with clear sky and strong sun light. Under shading condition

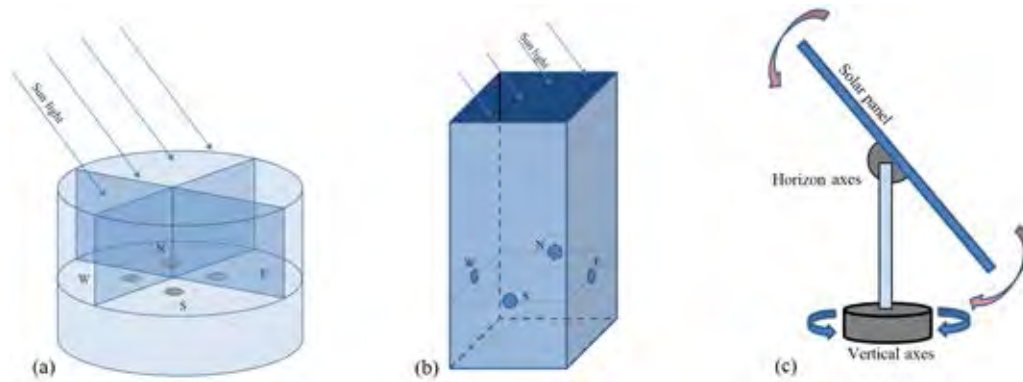


FIGURE 1.6: Four photo sensors (N,S,E and W) are used to determine the direction of the sunlight (a), (b). Two articulations in a sun tracking system (c).

by cloud, trees, dust ect., the sensors can not determine the direction of the sunlight exactly. Hence, the panel is fixed or rotated forward wrong position. This increases the angle  $\alpha$  (Note that the earth rotates around the sun and its own axis continuously). When the sunlight comes back with large  $\alpha$ , the tracking system spends long time to catch the perpendicular position. The energy is lost during catching time. To avoid the mismatch angle by shading, when the condition  $V_E = V_W$  occurs, motor drives the frame to rotates around the horizontal axis continuously with a suitable speed. At that time, the sun tracking system operating in sightless tracking mode.

### 1.2.1.2 Sun Tracking Basing on Real Time Clock, Panel Location and Tilt Angle Sensor

This method permits the panel tracking the solar without sun light. The real time clock is combined with the location information of PV system (longitude and latitude) to calculate the tilt angle of the incident light (see in Fig. 1.7). The solar panel will be controlled forward the sun based the comparison of the real tilt angles and the calculated angles.



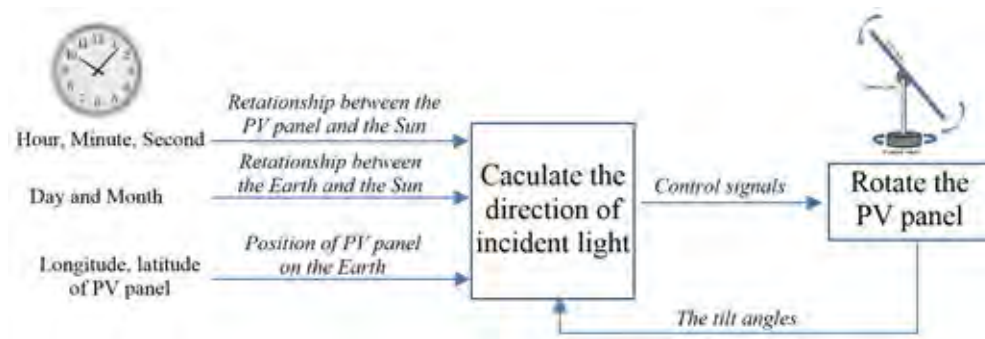


FIGURE 1.7: A sun tracking system base on real time clock, panel position and tilt sensor (or accelerator sensor).

Generally, optimization for the input power is implemented many years ago. The sun can be tracked by several techniques. These methods have done very well for not only for PV panel but also the solar parabolic dish, solar parabol trough, ect.

### 1.2.2 Maximum Power Point Tracking

It is well-known that the output power of a solar cell depends on its load. The PV system transfers most of its produced electricity when it operates at the MPP. To ensure the output power is always maximum under changing of the weather conditions such as light intensity and temperature, a *Maximum Power Point Tracking* (MPPT) module is inserted between PV modules and converter-inverter. Combination of PV panels MPPT module and converter-inverter is called *Maximum Power Point Tracking System*(MPPTS). Because the irradiance and temperature are time varying values; The MPP is shifted by these factors. If the load, which connected to PV system is fixed, the system will not operates at the MPP. In this case, only a part of its produced electricity is transfered to load, the rest is dissipated on itself in the form of heat. Furthermore, high temperature reduces the life time and efficiency. In small PV systems, the MPPT modules are usually integrated with converter, solar inverter. The combinations are called solar converter or solar inverter. To utilize the produced electricity maximally, the exceed energy will be stored in a battery as in Fig. 1.8.

*Why the energy will be lost if the PV system does not operate at the MPP ?*

The following example answers above question. Fig. 1.9(a) and 1.9(b) show two different operating conditions of a PV system. The I-V and P-V curves are changed by the irradiance and temperature. At first, assume that the load is adjusted to the most suitable value for the input condition ( $I_{r1}, T_1$ ) and fixed at this value. The PV

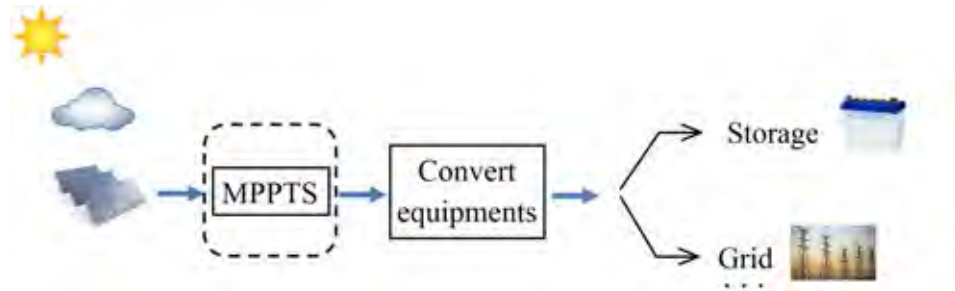


FIGURE 1.8: For using produced electricity absolutely, a battery system is used to store redundant electricity.

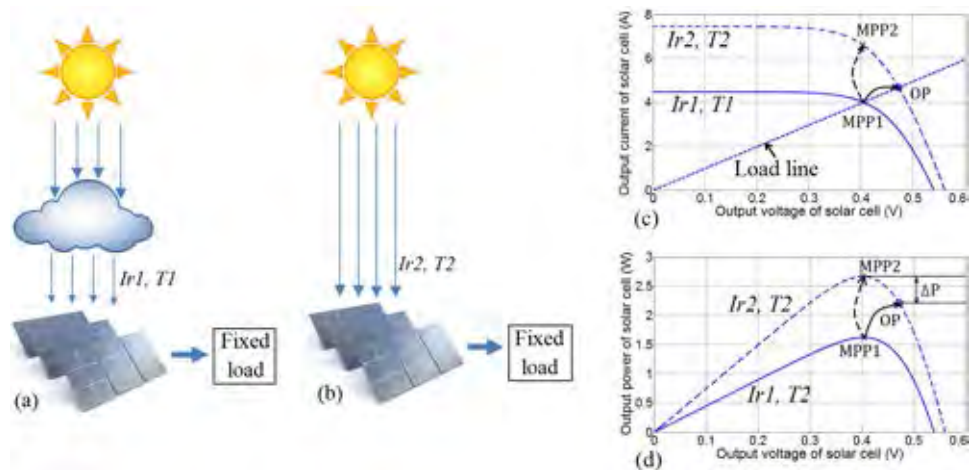


FIGURE 1.9: Two different operating conditions (shaded (a) and unshaded(b)). The I-V curves (b) and P-V curves (c) of solar cell when the conditions change.

system operates at  $MPP1(V_M = V_{M1}, I_M = I_{M1})$ . The outdoor conditions change to  $(I_r2, T2)$  with  $I_r2 > I_r1$ . The I-V, P-V curves become the dash lines (Fig. 1.9(c) and Fig. 1.9(d)). Because the load is constant then load line is fixed. The operating point changes from  $MPP1$  to  $OP$  on this load line and the output power is  $P_{OP}$ . Unfortunately,  $OP$  is not maximum power point on the new I-V curve. The new maximum power point is  $MPP2(V = V_{M2}, I = I_{M2})$  which is yielded with another load value. The desired power is  $P_{M2} = V_{M2}I_{M2}$ . The difference of power,  $P_{M2} - P_{OP}$  is lost in the form of heat and cause the panel to be hotter.

Although there are many MPPT methods which are proposed in recent time. Depend on the techniques, these methods face at least one of the following problems.

### 1.2.3 Problems of Existing MPPT Techniques

#### 1.2.3.1 Gaps of Offline Tracking Methods

For the offline tracking techniques [1] [2], the PV systems and their load are isolated for measurement. During measuring time, the produced energy is consumed on solar cell instead of transferred to the load. Fig. 1.10 shows two cases of offline tracking.

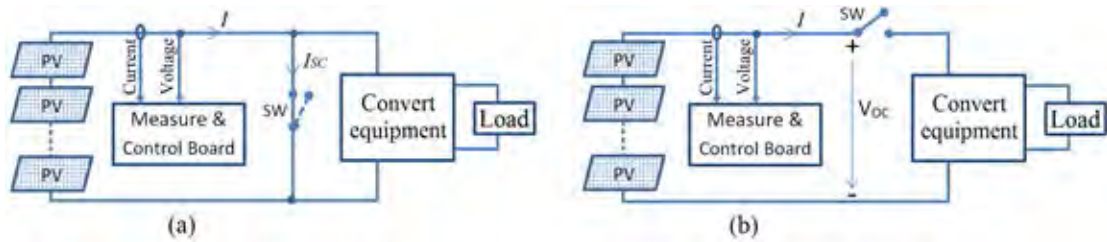


FIGURE 1.10: The electricity is not delivered to load during offline time. The output voltage is equal zero in case short circuit current (a) and the output current is equal zero in case open circuit voltage (b).

The short circuit current is measured by the schematic in Fig. 1.10(a). While the SW is switched on, the output current is short circuit current,  $I_{SC}$  but the terminal voltage of panel becomes zero. The output power is zero. In Fig. 1.10(b), if the SW is turned off, the output voltage is open circuit voltage,  $V_{OC}$  but the output current is zero. The string can not provide energy for the load. The intermittent output power of PV string reduces the output power as well the quality of the output. In general, “losing energy” and “fluctuant power” are two disadvantages of the offline tracking techniques.

#### 1.2.3.2 Gap in Online Tracking

Unlike the offline techniques, online tracking techniques do not require any isolation for measurement. The terminal voltages and currents are measured while the systems are in operation. To determine the maximum power point, these methods measure  $(V, I)$  at many different points on the I-V curve (voltage scanning). The power at all scanned points are calculated for comparison in later steps. During scanning, the PV systems do not operate at the MPP. This means some energy is lost until the PV systems reach the MPP. The scanning time is curtailed significantly if the number of scanned point is reduced. The hybrid tracking uses the offline values  $(V_{OC}, I_{SC})$  for determination scanned points. After the rough scan, a narrow range of  $V_M$  is obtained.

A high accurate online technique is deployed to drive PV system to the MPP quickly. Although there are many improvements in online and hybrid, “*the losing energy during tracking*” is still a disadvantage of these tracking techniques.

### 1.2.3.3 Mismatch the GMPP in Partial Shading Condition

Fig. 1.11 shows four P-V curves of a PV string composed of partial shading panels. Assume that the irradiance increases, the P-V curve changes from the lowest to the

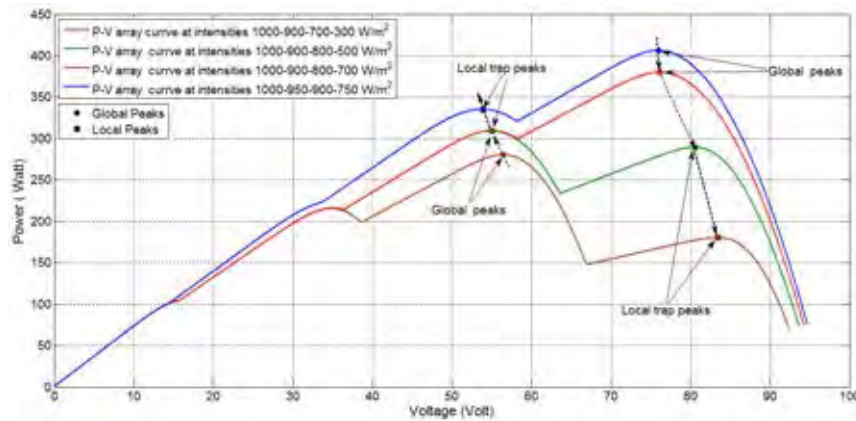


FIGURE 1.11: The GMPP of a string is drifted under changing of irradiance.

highest. It is well-known that partial shading cause. At beginning, the local Peak 2 (from right) is global maximum power point (GMPP). In the highest curve, the GMPP is peak 1. Some conventional methods can not jump to the new global peak and trapped by the local peak. This is another reason of energy loss.

## 1.3 The Target and Scope

“*Reducing the negative effects of MPPs tracking under partial shading conditions*” is the target of this dissertation. The backbone of this dissertation is “*Finding new algorithms which permit the PV systems to determine the GMPP exactly based on a few online measurements within short time*”. Five parameters (or single diode) model is chosen for calculation and simulation. The relation current-voltage of single diode model, condition at MPP are used flexibly to find all local MPPs and GMPP. All required values of proposed method are measured online simultaneously only one time. The GMPP is determined within short time in order to increase the efficiency of the PV system. Because the accuracy of proposed method depends on the parameters of solar cell tightly. Determining the parameters of solar cell model is key factor of calculation

method. Unfortunately, these parameters are not provided by solar cell manufacturers. Hence, “*Extraction parameters for solar cell using information in product datasheet or measured values at three special points*” is the second main task of this dissertation.

After the proposed algorithms for finding the GMPP is developed, their software will be written for calculation and simulation. In GUI, user can build a PV system, set the operating conditions and parameters of solar cells before running the simulation. In calculation, user provide measured values first. After execution, the obtained results including current, voltage and power at all local MPPs (if exist) and GMPP will be analyzed.

In addition, for extracting experiment, two solar modules are measured for extraction parameters at operating condition. One panel and a string of panels are used for determining experiments. The proposed method is evaluated by the comparison between the results by measurement, calculation and simulation of these experiments.

Numerical methods (Bisection, Newton-Raphson) are used in calculation regularly. In some cases, these method are modified to speed up the searching. The algorithms are analyzed carefully and improved many times in order to reduce the complexity.

## Chapter II

# LITERATURE REVIEW

PV systems should always operate at MPP in order to transfer its produced electricity to load as much as possible. Since 2000, many MPP tracking methods have been proposed and applied in practice. This chapter presents the overview of MPP tracking techniques. The emphases will be upon their advantages and their tracking methods are also introduced briefly. The brief introduction of proposed tracking method is also mentioned. In addition, extraction methods for determining the parameters of solar cell are presented in this chapter. Before going deep into the research, the background knowledge in solar cell is reminded in Section 2.1.

### 2.1 Solar Cell

#### 2.1.1 Structure

The structure of typical solar cell model is similar to that of the diode but the *p-n* junction area of solar cells is built specifically large for absorbing the sun light energy (Fig 2.1(a)). The anti-reflect layer on the top (surface) of solar cell prevents the reflective light, hence increase the efficiency. Fig 2.1(b) depicts the cross section of a solar cell. The incident lights which have longer wave length, penetrate deeper than shorter ones ( $\lambda_1 < \lambda_2 < \lambda_3$ ). When an electron at valence shell is hit by a photon  $E = hc/\lambda$ , if  $E > E_g$  ( $E_g$ , band gap energy) the electron will jump to the conduction band. Following that, two charged carriers, a hole and an electron, are created. Inside the solar cell, the electrons move from *p* to *n* area, and the holes move in the opposite direction. One potential,  $V$  appears between anode and cathode. If the anode and cathode are isolated, this potential is called open circuit voltage ( $V_{OC}$ ). If the anode connects to cathode by a load, the electrons move through the load from cathode to anode to make the current  $I$ . Electrons recombine with the holes at *p* area and complete the circuit. But when the anode and cathode is connected without any load, the current is called short circuit current ( $I_{SC}$ ). It may be approximated by the photo

generated current  $I_{ph}$  of solar cell. The value of  $I_{ph}$  is proportional to the incident light intensity, so the sun tracking maximize the possible output current. The equivalent circuit of solar cell is shown in Fig. 2.1(c). The parallel resistor,  $R_p$  is high (thousands of  $\Omega\text{cm}^2$ ) while the series resistor,  $R_s$  is relatively small (less than  $1 \Omega\text{cm}^2$ ).

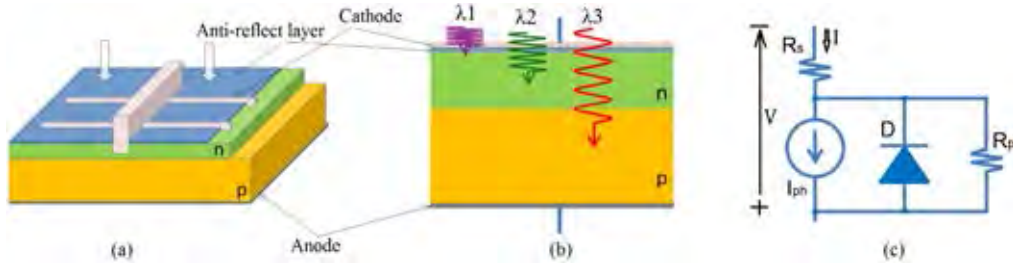


FIGURE 2.1: Structure of a solar cell (a). Cross section of a solar cell (b). Single diode equivalent circuit of a solar cell (c).

### 2.1.2 I-V Relation

The I-V equation of solar cell model in Fig. 2.1(c) is shown by (2.1) or (2.2) as follow:

$$I = I_{ph} - I_S \left( e^{\frac{V+I \cdot R_s}{nV_T}} - 1 \right) - \frac{V + I \cdot R_s}{R_p} \approx I_{ph} - I_S e^{\frac{V+I \cdot R_s}{nV_T}} \quad (2.1)$$

where:  $I_S$ : saturation current (dark current) of the diode

$n$ : diode emission coefficient (ideality factor)

$$V_T = \frac{kT}{q}, \quad \text{where: } k: \text{ Boltzmann constant } \cong 1.38 \times 10^{-23} \text{ J/K}$$

$q$ : elementary charge  $\cong 1.6 \times 10^{-19} \text{ C}$

$T$ :  $p$ - $n$  junction temperature, K

The I-V relation can be written by other form as follow:

$$V = nV_T \ln \left( \frac{I_{ph} + I_S - I \left( 1 + \frac{R_s}{R_p} \right) - \frac{V}{R_p}}{I_S} \right) - IR_s \quad (2.2)$$

$$\approx nV_T \ln \left( \frac{I_{ph} - I - \frac{V}{R_p}}{I_S} \right) - IR_s$$

In practice, five solar cell parameters  $n$ ,  $R_s$ ,  $R_p$ ,  $I_S$  and  $I_{ph}$  may be extracted by many methods [15]. This dissertation proposes an extraction method which uses  $I_{SC}$ ,  $V_{OC}$ , and current, voltage at maximum power point only. These values are provided in product datasheet, otherwise they can be measured easily. Fig. 2.2(a) depicts the

schematic for scanning load. At a fixed operating condition, the load  $R_L$  is scanned from zero to  $1.0\text{k}\Omega$  by a step  $0.01\Omega$ . Corresponding to each value of  $R_L$ , voltage and current ( $V, I$ ) is measured and used to plot a point on I-V curve in Fig. 2.2(b). The output power of solar cell,  $P$  is equal  $VI$ . The P-V curve of solar cell is drawn in Fig. 2.2(c). The unique point on the P-V curve (MPP) where the output power is maximum, is the MPP. The voltage, current and power at MPP are denoted as  $V_M$ ,  $I_M$  and  $P_M$  respectively.

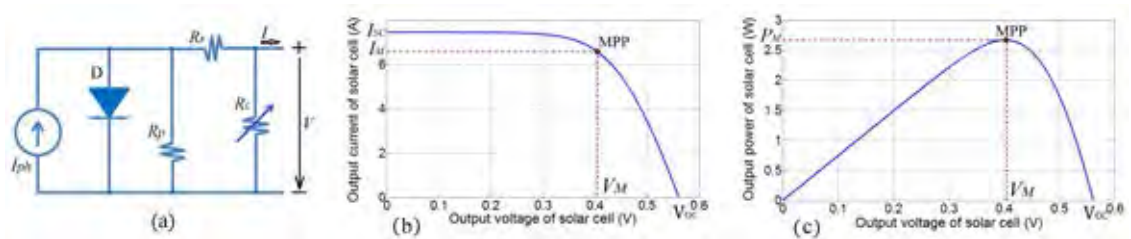


FIGURE 2.2: The schematic is used to scan load and plot the I-V, P-V curves (a). The solar cell's I-V curve (b). The solar cell's P-V curve (c).

## 2.2 Maximum Power Point Tracking

The MPP tracking techniques are categorized in three kinds: *Offline*, *Online* and *Hybrid*. In the Offline methods, the PV panels or strings will be isolated from the load during measuring time. In Online methods, the values are measured while the PV system delivering their produced energy to load. The Hybrid methods are combination of the two. At first, the Hybrid methods use an Offline method for limiting the range of searching. Then they employ an Online method to locate the MPP in a narrow voltage range [1].

### 2.2.1 Offline Tracking

Fractional Open Circuit Voltage (*FOCV*) and Fractional Short Circuit Current (*FSCC*) are two well known offline methods which were invented several years ago. Both of them are suitable for tracking the MPP for small PV systems but they do not suffer the effect of partial shading.

*FOCV* method bases on the relationship between voltages at maximum power point and at open circuit point to estimate the MPP. The accepted expression is  $V_M = K_{OC}V_{OC}$ , where  $K_{OC}$  is a constant from 0.7 to 0.8 [2]. At beginning, the PV system is isolated from its load for measuring  $V_{OC}$  and reconnect immediately. Next, the  $V_M$  is



estimated by  $K_{OC}V_{OC}$  and applied to calculate new duty cycle of inverter or converter (load). The suitable duty cycle help to keep the output voltage at  $V_M$ . During tracking time, the output power is updated continuously in order to find the most suitable value of duty cycle. The searching stop when output voltage yields the desired value. The currently duty cycle is kept until the next offline measurement. The isolation occurs regularly cause of the losing energy and intermittent output. Furthermore, the value of  $K_{OC}$  actually varies with irradiance slightly. That means the estimated MPP may not be close to the true value.

Different from *FOCV*, in *FSCC* method, the relationship between short circuit current and current at MPP ( $I_M = K_{SC}I_{SC}$ , where  $K_{SC}$  is a constant from 0.78 to 0.92 [1] ) is used to estimate the desired current ( $I_M$ ). After the short circuit current is obtained by offline measurement. Current  $I_M$  is calculated and used as referent value. The duty cycle of inverter or converter is adjusted continuously to drive the output current forward referent value. Similar to *FOCV*, this method has the same weak points those are less accurate and long tracking time.

### 2.2.2 Online Tracking

These methods measure voltages and/or currents without isolation of solar PV from system. In conventional methods, the voltage (or current) is scanned from zero to  $V_{OC}$  (or  $I_{SC}$ ) for searching the GMPP. Two well known methods are *Perturb & Observe* (*P&O*) and *Incremental Conductance* (*IC*).

In *P&O*, the voltage are measured simultaneous with current regularly. The calculated power  $P = VI$  is used to compare with the previous ones. Basing on the result of comparison, the duty cycle will be adjusted to increase the output power basing on the measured value. The observe power is slight changed every short period (ms). The PV system reaches the MPP if the condition of MPP, ( $\frac{\partial P}{\partial V} = 0$ ) is satisfied. The duty cycle which corresponds to MPP is maintained until the next measurement. This method can track the MPP well despite the fluctuation of the weather. However, *P&O* method can not determine GMPP if the PV system has many local MPPs because of the local peak trap.

Similar to the *P&O*, *IC* method requires the measured value of voltage and current at the same time. Two consecutive pairs ( $V^i, I^i$ ) and ( $V^{i+1}, I^{i+1}$ ) are used to calculate

the new value of duty cycle. At the MPP, it is well-known that  $\frac{\partial V}{\partial I} = -\frac{V}{I}$ . The duty cycle which corresponds to this point is maintained until the next measurement. The *IC* method can not apply for tracking string of panel.

The other online tracking method, *Current Sweep* bases on the solar cell characteristics (I-V curve). Load scanning conducts to a set of points which belong to the I-V curve of the solar PV system. The current and voltage at MPP are interpolated from these points. After that, the PV system is driven directly to MPP by the solar converter or inverter. The time spend for load scanning and the error in calculation are weak points of this method.

In practice, an array or a farm is composed of many panels and spread on a wide area. The partial shading occurs frequently. This is a reason of mismatching the GMPP and losing energy. To detect the GMPP exactly under fluctuant operating conditions, many improvements of tracking technique have been proposed and employed. Based on the structure of PV system, the corresponding method is put into single string group or parallel strings group.

### 2.2.2.1 Single String Tracking

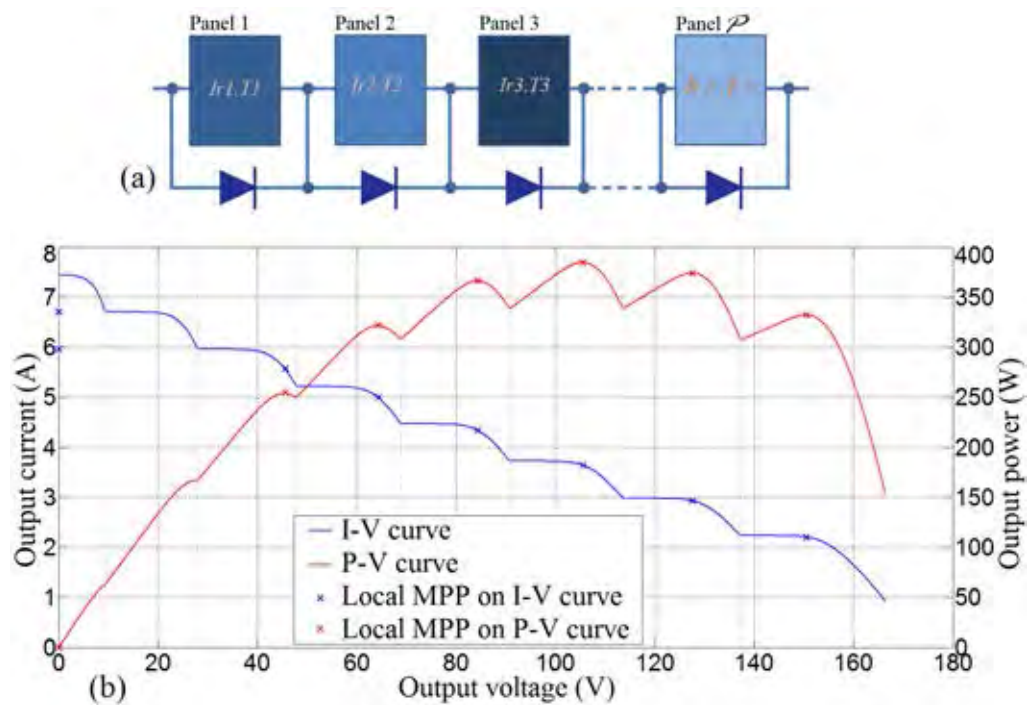


FIGURE 2.3: A string is composed of  $N_s$  panels in series under partial shading (a) and the I-V, P-V curves (b).

Under partial shading condition (Fig. 2.3(a)), a string may have several local MPPs as shown in Fig. 2.3(b). Finding out the GMPP exactly among these local MPPs is not a simple thing. The simplest idea is scanning the output voltage from zero to  $V_{OC}$  of string by a fixed small step. All local peaks are detected and the highest peak is the GMPP. The corresponding voltage of this point is the desired value for the PV system. Using this method, the scanning in [3] uses a step size of 0.5V. For illustration, Fig. 2.4 shows the measured points of a voltage scanning process with a step size of 2V. Although

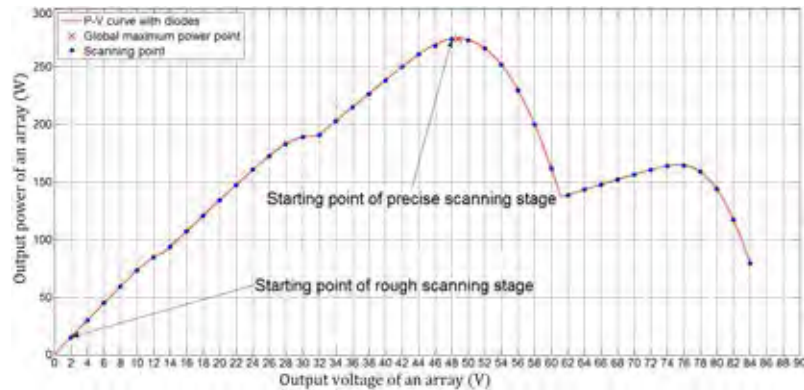


FIGURE 2.4: The scanning for MPP with step 2V

the value of  $V_{OC}$  is smaller than 90V, there is more than 40 required measurements for one scanning time. Furthermore, to detect the GMPP under fluctuant operating condition, the scanning task must be repeated regularly. That thing cause the losing energy.

In [4], the scanning process is separated into two step. The first step is rough scan with the step size  $\Delta V = K_{OC}V_{OC}/2N_s$ , where  $N_s$  is number of panel in the string. There is around  $2N_s$  scanned points in this step. The maximum value of these points is closed to the real MPP. It is the initial point of the second scanning step. An online method such as  $P\&O$  or  $IC$  is used in the second step to drive the PV system from initial point to the MPP in short time. Fig. 2.5 shows the strategy in searching the GMPP of this method.

An other improvement in scanning strategy is presented in [5]. Similar to the method in [4] but the large step size of voltage in rough scanning step is determined by  $\Delta V = 0.8V_{OC}^{array}/N_s$  where  $N_s$  is number of panels in a string. Following that, the number of measured points is curtailed significantly. Only  $N_s$  scanned points are required by the first step. However, the highest power point is not real MPP and it may not close to

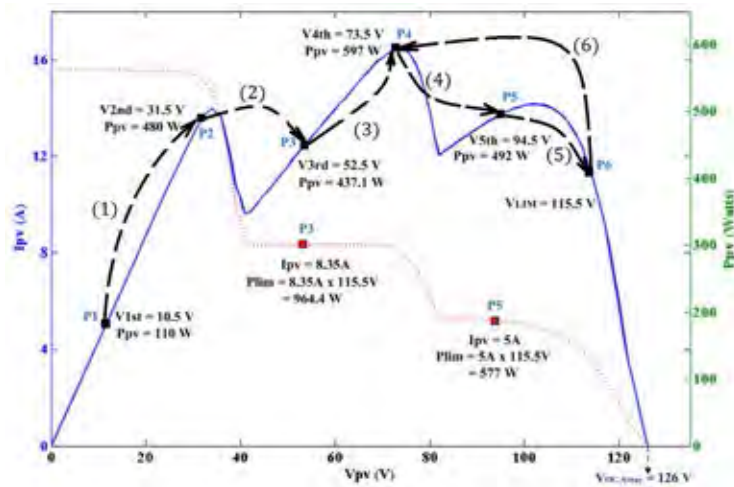


FIGURE 2.5: The searching strategy use voltage step-size  $\Delta V = K_{OC}V_{OC}/2N_s$  [4] for the first scanning.

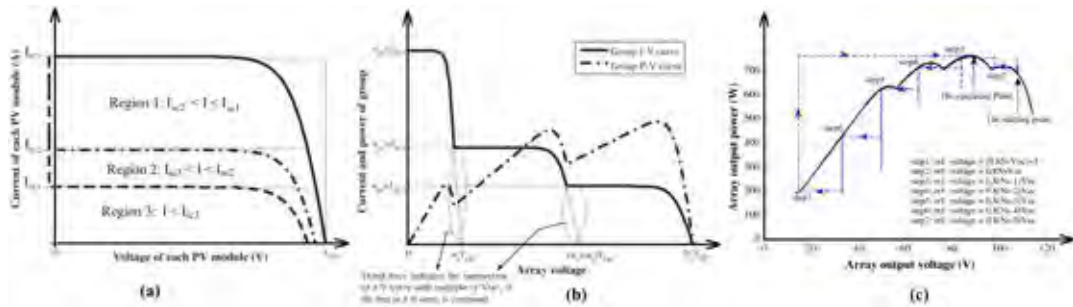


FIGURE 2.6: The I-V curves of separated modules(a); The array I-V and P-V curves (b); The searching strategy of proposed method in [5] (c).

the true MPP. An online method with the reasonable initial point helps to drive the PV system to the true MPP (see Fig. 2.6) in short time but longer than that in [4].

A method which allows the PV system to yield the GMPP quickly basing on a few measurements, is presented in [6]. The parameters of PV system and the input conditions are used to calculate the high and the low limitations of voltage. Fig. 2.7 shows the area for scanning and the relative expressions. The area which contains global maximum power point is divided into three smaller areas basing on the potentially optimal intervals (POIs). The output voltage is driven to middle point of each area for measuring the corresponding powers. These powers are analyzed to determine the new area for the GMPP. The area which contents GMPP is curtailed three times after each measurement. The tracking process continue until the error between two consecutive output powers is smaller than a certain value. This method can track the GMPP in short time. The short circuit current and the open circuit voltage at the highest and the lowest irradiance intensity are required for calculation. But determining these

values is difficult thing and they are not constants. Furthermore, this method may provide the wrong GMPP in case the string too long.

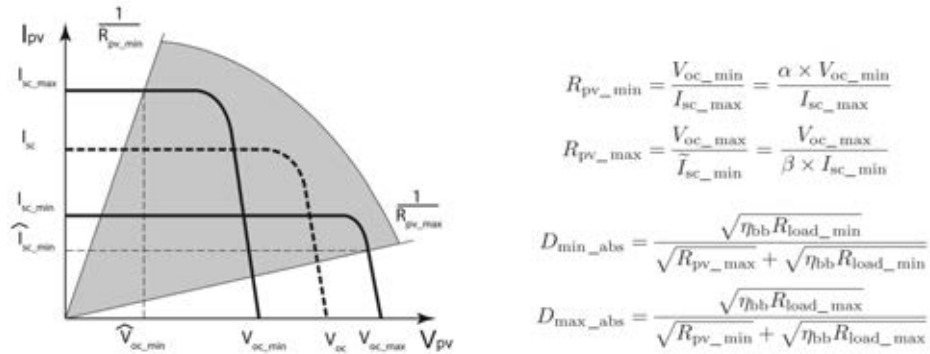


FIGURE 2.7: The voltage scanning range in [6] and expressions are used to determine the limited points.

One method which is presented in [7] bases on the experiment: In almost cases,  $X$  and GMPP belong to the same part of array I-V curve (or Global Peak Area, GPA)(see Fig. 2.8(a)), where  $X$  is the intersection of  $OM$  and I-V curve and  $M(V_{OC}, I_{SC})$  is ideal operating point. The tracking strategy of this method include three stages. In the first stage, the PV system is isolated for measuring  $V_{OC}$  and  $I_{SC}$ . The referential point  $M(V_M = V_{OC}; I_M = I_{SC})$  is determined and displayed in the same graph with the I-V curve. The segment  $OM$  which has slope  $\frac{I_{SC}}{V_{OC}}$  is used to determine the area of GMPP. In the second step, a simple algorithm is deployed to move the operating point to  $X$ .  $X$  is the initial point of the last stage. In the last stage,  $P\&O$  method is exploited to track the global MPP from initial point  $X$ . Fig. 2.8(b) shows an example of this tracking strategy. At beginning, the PV system is driven to the intersection point  $A$ . After that, a climbing method is deployed with initial point  $A$ . The global maximum power point  $B$  will be tracked. The change of irradiance causes the operating point move to  $C$  and the new intersection point  $D$  is determined. Again,  $P\&O$  with the initial point  $D$  leads to new GMPP. The disadvantages of this method can be listed as follow: 1)The isolation is required every tracking cycle; 2)Long time spend for searching intersection point  $X$  and after that for the global peak tracking; 3)In some cases, the intersection point and global peak are not belong to the same part of P-V curve. The local peak will be tracked instead of the global peak.

Based on the I-V array curve and the characteristic of DC/DC converter (load) curve, an interesting method is introduced in [8]. Fig 2.9(a) shows the output I-V curve of

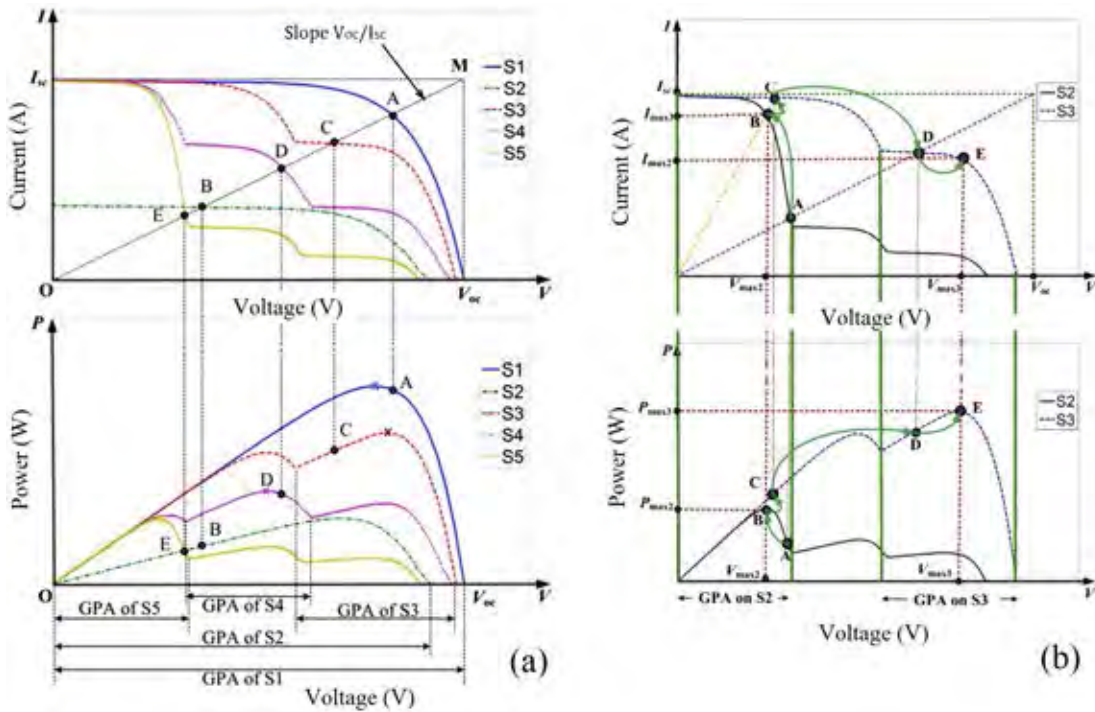


FIGURE 2.8: In (A), the intersections and the GMPP locate at same part [7]. Points A, B, C, D, E belong to GPA of S1, S2, S3, S4, S5 respectively; In (B), the strategy searching based on the line OM which has slope  $k = \frac{V_{oc}}{I_{sc}}$ . The intersection is determined and used as initial point of climbing algorithm.

a PV string and the input I-V curves of load (dash line). After the load connects to PV string, the operating points must be the intersections of two these curves. For

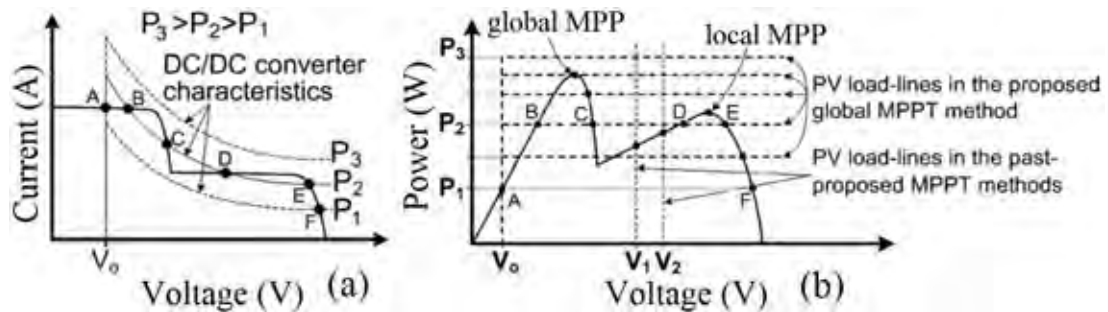


FIGURE 2.9: The I-V curve of PV system and I-V input curves of DC/DC converter (a). The P-V curve of PV system and the P-V input curves of the load (b).

example, at the smallest power  $P_1$ , there are two operating points (A and F). If the power of converter increases to  $P_2$ , there are four operating points (B, C, D and E). Power can not increase to  $P_3$ , because there is no intersections at this value. The power is dropped abruptly after the operating point crosses the MPP. In Fig. 2.9(b), PV load lines are horizon lines. Hence, easy to determine the GMPP based on the changing of operating point. This method helps PV system to avoid the local peak trap. However, the DC/DC converter which can keep the input power at constant

value is not a simple design. Furthermore, the output power of PV system is scanned for searching the GMPP regularly. Hence, the PV array can not yield the MPP in all time.

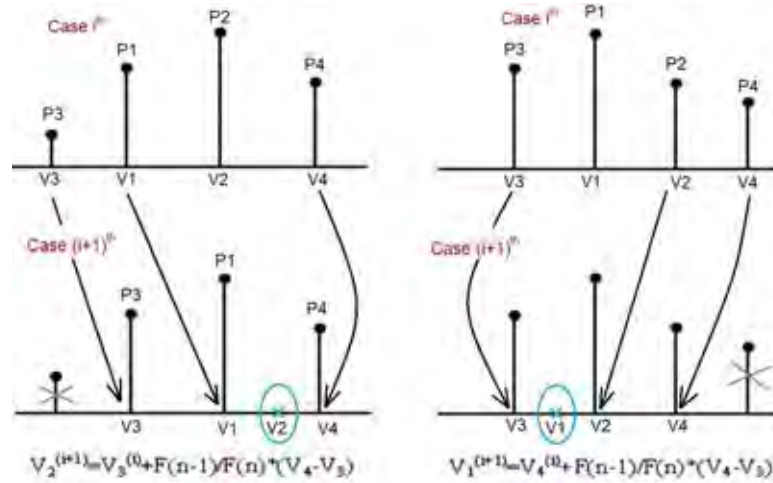


FIGURE 2.10: The method in [9] bases on modified Fibonacci search method with fuzzy controller

The modified Fibonacci search which based on Maximum Power Point Tracking scheme, is presented in [9]. The power at a few initial voltages are measured first. Two proposed expression use these values for determining the next voltage for tracking (see in Fig. 2.10). This method requires the power scanning but it help PV system reaches the MPP in short time. However, the wrong detection may occur if there are a low local peak which locates among two high local peaks.

There is an exciting method which bases on the inherent characteristic resistances and I-V relation of solar cell [10]. The MPP of identical PV system can be predicted exactly but  $I_{SC}$ ,  $V_{OC}$  are required for searching. This means the offline measurement must be implemented. In [11], Particle Swarm Optimization algorithm is adapted and employed for searching local and global power maxima of a string in the *Local* mode and the *Global* mode, respectively. However, long searching time makes this method less interesting. An interesting technique for tracking MPP is proposed in [12]. It avoids the disadvantage of conventional techniques, but it is suitable only for the uniform shading condition.

### 2.2.2.2 Multi-Strings Tracking

A tracking method for the large PV system which uses distributed micro converters, is introduced in [13]. Each panel connects to one distributed micro DC/DC converters.

The information of panels in a string is sent to the others by Zigbee wireless modules. A DC/AC inverter converts the output of all strings and synchronous with grid (Fig. 2.11(a) and Fig. 2.11(b)). The Global MPP of each string is tracked individually. Each

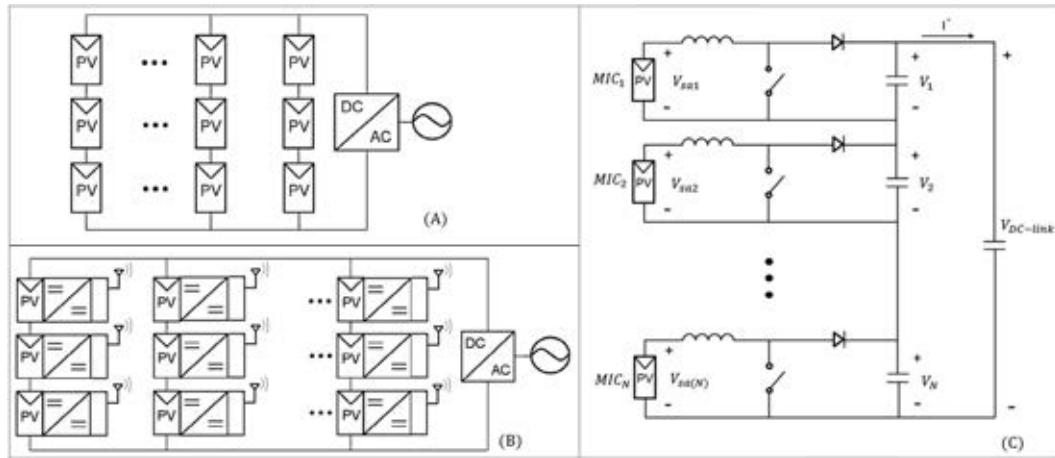


FIGURE 2.11: The central control system for uniform shading condition (A); The combination central control system and wireless communication system is proposed by [13] (B). The structure of an array with a micro converter for every panel(C).

of all panel runs itself tracking procedure consecutively. At beginning, only one panel in array is tracked. The information of  $n$  tracked panels is transferred to  $(n + 1)^{th}$  panel for tracking the maximum output power of group  $(n + 1)$  panels. Repeat until whole string yields the global peak power. This method has some the weak points. First, all strings are connected in parallel means that they have the same output voltage. Under partial shading, the voltage at GMPP of a string is different from each other. So, all of string can not reach the highest output power at the same voltage. The second weak point is long tracking time. The time is spent for searching global peak too long if the string is composed of many panels. Third, in solar farm, there are many parallel strings and they make effects together. Blocking diodes are used but its consumption is undesired and also make the negative effect to PV system.

A method uses the MPP condition and I-V relationship to formulate a Lambert function equation [14]. A numerical method is employed to search all local maxima from several initial points. Although the method does not require offline measurement, but it requires undesirable light intensity measurement on all panels in order to calculate the photo generated current. Moreover, it does not consider the effect of the bypass diodes, which may affect the location of the MPP, especially when many panels are bypassed.



### 2.3 Introducing The Proposed Tracking Method

GMPP tracking system is an essential part in a PV system. It ensures that the produced power is always transferred to load at the highest level. Three important requirements in GMPP tracking are: 1) Determine the MPP within short time, 2) Adapt to changing of weather, 3) Minimize the negative effects. To respond these requirements, the proposed method combines online measured values and characteristics of solar cell for calculation the GMPP of every string as well as of parallel strings. Using only one set of panel voltages, panel temperatures and string currents, all local MPPs and certainly the GMPP of strings and whole PV system will be determined exactly. After that, the PV system is driven to GMPP directly without power scanning. The measurement is repeated regularly in order to update the operating conditions continuously. The proposed PV string and parallel strings are shown in Fig. 2.12 and Fig. 2.13 respectively. The required data is collected by a GMPP tracking module or Center. This module uses the solar cell parameters and measured data to build the I-V curves of strings and system. Based on the obtained curves, the maximum output power of PV system can be evaluated. The PV system is controlled to reach this point directly. In the proposed method for determining the GMPP

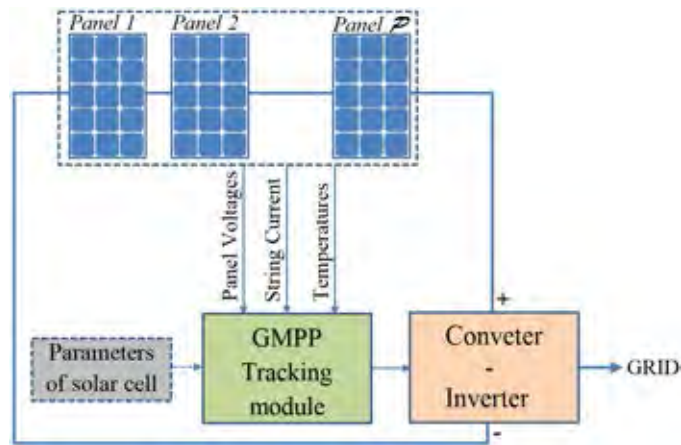


FIGURE 2.12: The proposed PV system for string GMPP tracking.

of a PV system, the precise I-V curve is required strictly. So, the parameters of solar model must be extracted as exact as possible. There are many methods for extracting the parameters of solar cell model. However, these methods have at least one of the following disadvantage: less accuracy, high complexity with a lot required measurements. To solve above problems, a new accurate extracting method which uses only information in product datasheet, is proposed in this dissertation. The

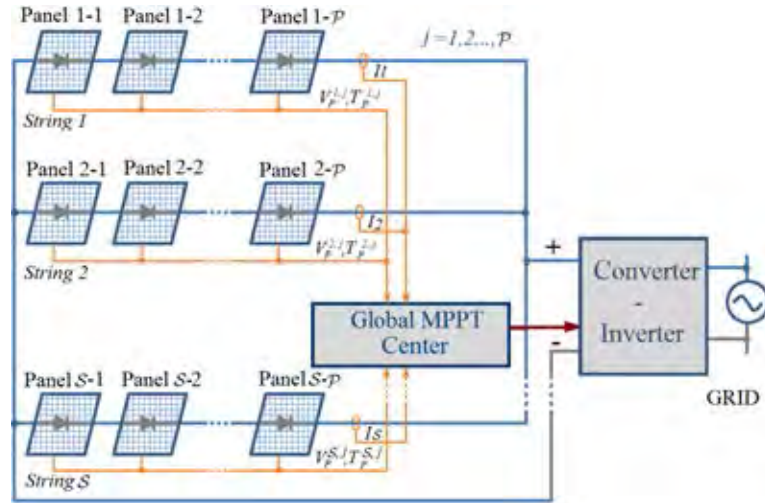


FIGURE 2.13: The proposed PV system for parallel string GMPP tracking.

following section introduces solar parameters extraction technologies and the brief ideal of proposed method. Chapter 4 will presents this method completely.

## 2.4 Extraction Parameters of Solar Cell

“How to determine the parameters of solar cell model ?” is an interesting question. In recent years, many research are carried out to answer this question. They contribute to the increasing of PV system efficiency.

A paper [15] present the overview of extraction techniques in 2013 and earlier. Up to now, many extraction methods are proposed. Most of methods used to determine the parameters of the single diode solar cell model because the interpretation of the equation describing the mathematical model is useful and simpler than double diode solar cell model. The following equation reminds the relationship between current and voltage of panel:

$$I = I_{ph} - I_S \left( e^{\frac{V + I \cdot R_s}{nV_T}} - 1 \right) - \frac{V + I \cdot R_s}{R_p}$$

Five parameters of a single diode solar cell model include:

- 1) Induced current (or photo generated current),  $I_{ph}$ ;
- 2) Saturation current (or dark current) of diode,  $I_S$ ;
- 3) Emission coefficient (or ideality factor),  $n$ ;

- 4) Series resistor,  $R_s$ ;
- 5) Parallel (or shunt) resistor,  $R_p$ .

There are two groups of extraction method. One group bases on approximations of one or two parameters to calculate for the others. The other group uses set of measured points and curve a fitting method to search the parameters.

The first group of methods bases on the slope of I-V curve at short circuit current point ( $SCC$  or  $SC$  in short name) and open circuit voltage point ( $OCV$  or  $OV$  in short name) (see Fig. 2.14). Notice that, the voltage and current at  $SC$  and  $OV$  are

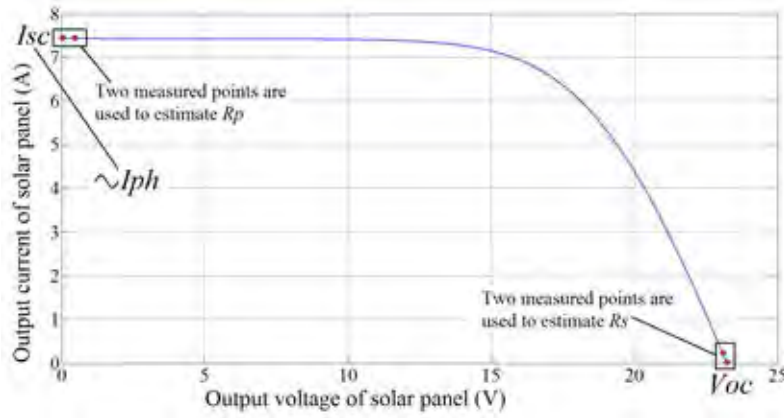


FIGURE 2.14: Three well known estimations of  $I_{ph}$ ,  $R_p$  and  $R_s$ .

easy to measure. Basing on measured values,  $\frac{dV}{dI}|_{I_{SC}}$  and  $\frac{dV}{dI}|_{V_{OC}}$  are determined first. Next, the parameters will be estimated by many methods. One of them is Five Points, which is introduced in [16]. According to this method, the voltage and current at two points which are close to  $OV$  are measured for calculation of  $R_s$  by:

$$R_s = -\frac{dV}{dI}\Big|_{V_{OC}} = -\frac{\Delta V}{\Delta I}\Big|_{V_{OC}} \quad (2.3)$$

The voltage and current at two points which are close to  $SC$  are measured for calculation of  $R_p$  by:

$$R_p = -\frac{dV}{dI}\Big|_{I_{SC}} = -\frac{\Delta V}{\Delta I}\Big|_{I_{SC}} \quad (2.4)$$

After that,  $R_s$ ,  $R_p$  are employed to I-V equation at three points  $SC$ ,  $OV$  and  $M$  to calculate the other parameters:  $I_S$ ,  $I_{ph}$  and  $n$ .

The other method [17] uses two similar estimations:  $R_p \approx -\frac{dV}{dI}\bigg|_{I_{SC}}$  and  $I_{ph} + I_S \approx I_{SC} + \frac{R_s I_{SC}}{R_p}$  to build a function  $\delta(n, R_s)$ . In next step,  $n$  and  $R_s$  are scanned to find the suitable set of parameters based on mean square error technique. Each set will be used to calculate the  $MSE$  of a set measured points. The minimum of  $MSE$  indicates the parameters of solar cell. Fig. 2.15 shows the flow-chart of this method.

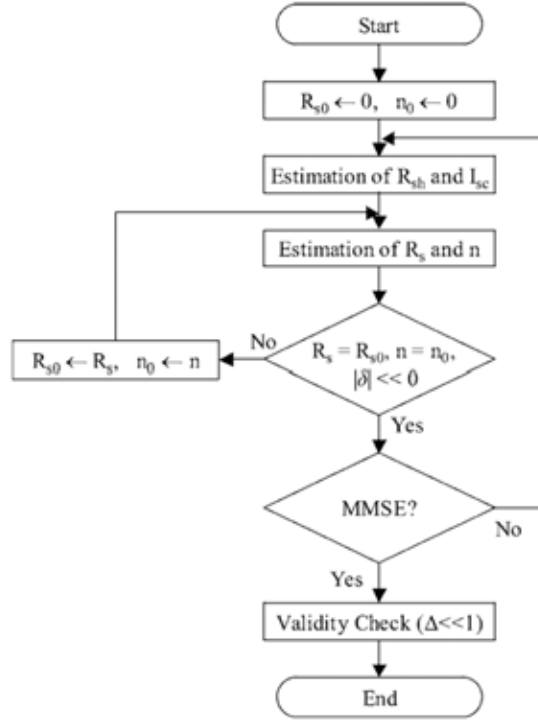


FIGURE 2.15: The flow-chart of the extraction method combines estimations and MMSE searching in [17].

Similar to the method in [16], five measured points must be determined before extracting by the method in [18]. They are combined with the approximation  $I_{ph} \approx I_{SC}$  to build the following equations:

$$-\frac{dI}{dV}\bigg|_{V=0} = a = \frac{nVT}{-I_S + \frac{I_{SC}R_s - nVT}{R_p}} - R_s \quad (2.5)$$

$$-\frac{dI}{dV}\bigg|_{I=0} = b = \frac{nVT}{-I_S - I_{SC} + \frac{V_{OC} - nVT}{R_p}} - R_s \quad (2.6)$$

Since (2.5) and (2.6), inferring the expressions of other parameters as follows:

$$R_s = -\frac{1}{2} \left( \left( (a-b)^2 + \frac{2q}{I_{SC}} (a-b) + \left( \frac{V_{OC}}{I_{SC}} \right)^2 \right)^{1/2} + a + b + \frac{V_{OC}}{I_{SC}} \right) \quad (2.7)$$

$$R_p = \frac{V_{OC}}{\frac{nV_T}{b+R_s} - \frac{nV_T}{a+R_s} + I_{SC}} \quad (2.8)$$

$$I_S = \frac{I_{SC}}{e^{\frac{V_{OC}}{nV_T}} - 1} - \frac{V_{OC}}{\left( e^{\frac{V_{OC}}{nV_T}} - 1 \right) R_p} \quad (2.9)$$

$$n = V_T \frac{(V_M - I_M R_s) \left( I_{SC} + I_S - I_M - \frac{V_M}{R_p} \right)}{I_M - \frac{V_M}{R_p}} \quad (2.10)$$

With above four equations, four unknowns ( $R_s, R_p, I_S, n$ ) can be found by numerical method easily.

The second group extract solar cell parameters based on the measured value of current and voltage at several operating points. Minimum mean square error (*MMSE*) is main tool of methods in this group. In [19], a function is proposed for calculation as follow:

$$F(I) = aI + b \ln(I_{ph} - I) + c \quad (2.11)$$

$$\text{where: } a = -R_s; \quad b = nV_T - V_a; \quad c = -nV_T \ln I_s$$

$V_a$  is an arbitrary value of voltage.

This method requires a set of measured points which distribute through the I-V curve. With a value of  $V_a$ , the value  $F(I)$  of all points ( $V, I$ ) is calculated.  $a, b$  and  $c$  will be found by using the nonlinear least square fit method. At the last step, the values of  $R_s, n$  and  $I_S$  will be calculated from  $a, b$  and  $c$ . The photo generated current is approximated by  $I_{SC}$  while the last parameter,  $R_p$ , is calculated from measured values at  $I_{SC}$  by the well known formula:  $R_p = -\frac{dV}{dI}|_{I=I_{SC}}$

A method which is presented in [20] uses the non-linear least squares optimization algorithm to determine the parameters. The modified Newton method with the Levenberg parameter is proposed for algorithm. The objective function for solar cell

model is defined by:

$$S(P) = \sum_{i=1}^N (I_i - I(V_i, P))^2 \quad (2.12)$$

where:  $I_i, V_i$  are measured values.

$P$  is set of five parameters.

The set  $P$ , which helps  $S(P)$  to yield the minimum value, is the extracted parameters of solar cell. The measured values in this paper are also used as the standard input data for many later researches.

Another method uses the linear fit for the negative bias area of I-V curve to determine two objects  $G_A = \frac{G_{sh}}{1+G_{sh}R_s}$  and  $I_A$  first [21]. Next, the following function  $f(I)$  is proposed for least square method:

$$f(I) = C_0 + C_1I + C_2 \ln \left( 1 - \frac{I}{I_A} \right) \quad (2.13)$$

After  $C_0, C_1, C_2$  are obtained by using set of measured points in linear fit method, the parameters are calculated by:

$$R_s = -C_1; \quad R_p = \frac{1 - R_s G_A}{G_A}; \quad n = C_2/V_T; \quad I_{ph} = \frac{I_A}{1 - R_s G_A}; \quad I_S = \frac{I_A e^{-\frac{C_0}{C_2}}}{1 - R_s G_A}$$

Similar to [21], the extraction method in [22] uses the least mean square error but with *Co-Content* function ( $CC(I, V)$ ) as follow:

$$CC(I, V) = C_{V1}V + C_{I1}(I - I_{SC}) + C_{I1V1}V(I - I_{SC}) + C_{V2}V^2 + C_{I2}(I - I_{SC})^2$$

Five coefficients,  $C_{V1}, C_{I1}, C_{V2}, C_{I2}, C_{I1V1}$  will be obtained when fitting the function to measured points. The solar cell parameters are calculated from them as follows:

$$R_p = \frac{1}{2C_{V2}}$$

$$R_s = \frac{\sqrt{1 + 16C_{V2}C_{I2}} - 1}{4C_{V2}}$$

$$n = \frac{C_{V1}(\sqrt{1 + 16C_{V2}C_{I2}} - 1) + 4C_{I1}C_{V2}}{4V_T C_{V2}}$$

$$I_{ph} = -\frac{(1 + \sqrt{1 + 16C_{V2}C_{I2}})(C_{V1} + I_{SC})}{2} - 2C_{I1}C_{V2}$$

The last parameter, saturation current  $I_S$  is calculated by applying above extracted parameters and one measured point:

$$I_S = \frac{I - (V - IR_s)/R_p + I_{ph}}{e^{\frac{V-IR_s}{nV_T}} - 1}$$

An extraction method that uses the pattern search is presented in [24]. This method can extract for both single and double diodes solar cell models. Extraction of solar cell parameters from a single I-V characteristic which uses teaching learning based optimization algorithm, is introduced in [32]. There are two phases (teacher and learner) in searching process. The values of parameters by this method are almost the same to that from [20]. In another method, a new equivalent circuit of dye-sensitized solar cells is proposed for calculation of the parameters [33]. The I-V curve is obtained by measurement first. The parameters which corresponding to the closet calculated points to the curve will be chosen. The mutative-scale parallel chaos optimization algorithm (*MPCOA*) with crossover and merging operation is presented in [34]. This method content two searching phases. The obtained parameter are accurate but the algorithm is complex and this method also requires many measured points .

At present, the extraction of parameters for solar cell is still interesting topic. "*How to determine five parameters of solar panel exactly using only given information in product datasheet ?*" is another problem which must be solved in this dissertation.

## 2.5 Proposed Extraction Method

The proposed method uses only three points which are always given in product datasheet to extract the parameters of single diode solar cell model. Fig. 2.16(a) shows three special points ( $SC_{(V=0, I=I_{SC})}$ ,  $OV_{(V=V_{OC}, I=0)}$ ,  $M_{(V=V_M, I=I_M)}$ ) which are applied in the I-V equation. Note that, the I-V and P-V curves are not determined yet and plotted by two dash lines in Fig. 2.16. However, three points  $SC, VC, M$  are always given in datasheet. Each point corresponds to an equation. In case the datasheet is not provided, measuring  $I_{SC}$ ,  $V_{OC}$ ,  $V_M$ ,  $I_M$  and temperature  $T$  at operating condition is

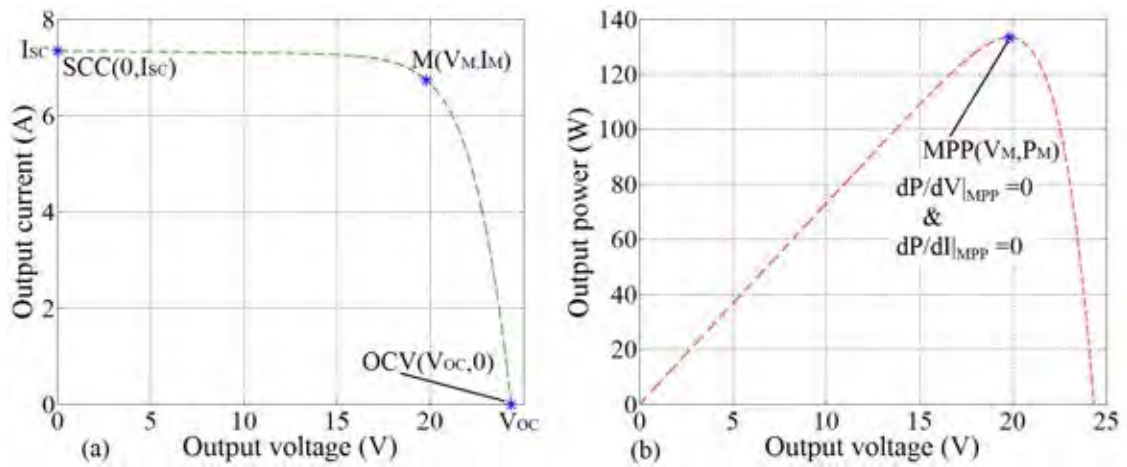


FIGURE 2.16: Three points and one condition for establishing system equation in proposed method.

not difficult work. So, three equations are obtained based on I-V relation. The fourth equation is inferred from the condition at MPP :  $dV/dI|_{MPP} = -V_M/I_M$  (see Fig. 2.16(b)). The last equation is based on a good estimation and the I-V relation at SC point. A cost function is built for evaluating the most suitable set parameters for solar model. During scanning  $n$ , the Newton-Raphson iterative method is deployed for searching  $R_s$  from each given value of  $n$ . After that, three parameters  $R_p, I_S, I_{ph}$  are evaluated using  $n$  and  $R_s$ . Cost function is calculated and compared to previous value for selecting new value of  $n$  and detect the most suitable set parameters. The proposed extraction is mentioned in Chapter 3.



## Chapter III

# NEW EXTRACTION METHOD FOR SINGLE DIODE SOLAR CELL MODEL

This chapter proposes a new method which permits to extract the parameters of solar cell model exactly basing only knowledge of three special points  $SC$ ,  $OC$  and  $M$  which are usually given in product datasheet.

### 3.1 Introduction

A solar cell is modeled by a circuit as Fig. 3.1 with five parameters  $n$ ,  $R_s$ ,  $R_p$ ,  $I_S$  and  $I_{ph}$ . These parameters depend on the  $p - n$  junction temperature  $T$  as well as the irradiance  $I_r$ .

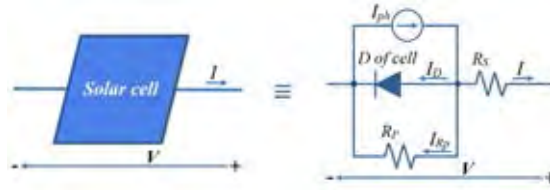


FIGURE 3.1: The equivalent circuit of a solar cell.

The main idea of this extraction method is “Applying the condition of MPP and a good estimation into  $I-V$  equations to determine the most suitable set parameters”. The measured voltage and current at  $OC(V_{OC}, 0)$ ,  $SC(0, I_{SC})$  and MPP ( $V_M, I_M$ ) replace for  $(V, I)$  in  $I-V$  equation in turn to conduct three equations. Fourth equation bases on MPP condition ( $dP/dV|_{MPP} = 0$ ). The last equation which bases on an estimation and special point  $SC$ , is used to verify the validity of every set parameters.

Because almost solar cells are produced and packaged as solar panel. Each panel is composed of many single cells in series. The calculations in this chapter will be carried out using measured values of a panel. Fig. 3.2 shows the structure of the panel with  $C$  cells. Assume that all cells are identical, the current of panel and cells are the same

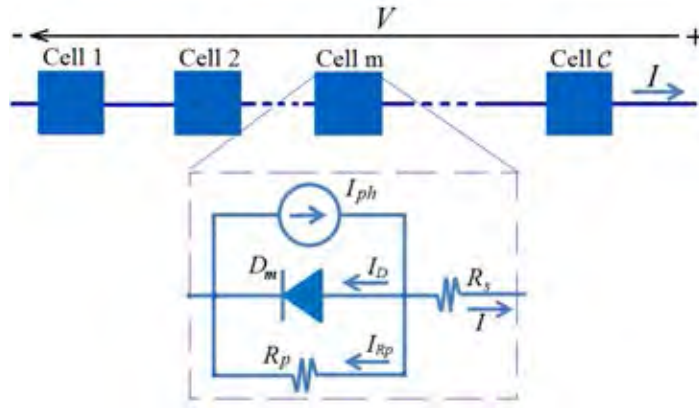


FIGURE 3.2: The structure of a solar panel.

but the voltage of panel is equal sum of all cell's voltage. The relations between panel and cell are described as follow:

$$\begin{cases} I = I_{c1} = I_{c2} = \dots = I_{cC} = I_c \\ V = \sum_{i=1}^{i=C} V_{ci} = CV_c \end{cases}$$

### 3.2 Equations for Proposed Method

The current-voltage equation of a panel is rewritten as:

$$I = I_{ph} - I_S \left( e^{\frac{V + CI R_s}{CnV_T}} - 1 \right) - \frac{V + CI R_s}{CR_p} \quad (3.1)$$

or:

$$V = CnV_T \ln \left( \frac{I_{ph} + I_S - I \left( 1 + \frac{R_s}{R_p} \right) - \frac{V}{CR_p}}{I_S} \right) - IC R_s \quad (3.2)$$

Applying three measured points (short circuit, open circuit and maximum power) into (3.1) to obtain the following equations:

**At OC point,  $V = V_{OC}$ ,  $I = 0$ :**

$$0 = I_{ph} - I_S \left( e^{\frac{V_{OC}}{CnV_T}} - 1 \right) - \frac{V_{OC}}{CR_p} \quad (3.3)$$

**At SC point,  $V = 0$ ,  $I = I_{SC}$ :**

$$I_{SC} = I_{ph} - I_S \left( e^{\frac{CI_{SC}R_s}{CnV_T}} - 1 \right) - \frac{CI_{SC}R_s}{CR_p} \quad (3.4)$$

**At MPP point,  $V = V_M, I = I_M$ :**

$$I_M = I_{ph} - I_S \left( e^{\frac{V_M + CI_M R_s}{CnV_T}} - 1 \right) - \frac{V_M + CI_M R_s}{CR_p} \quad (3.5)$$

**The condition equation at MPP:** At the MPP well known that the derivative of power with respect to voltage and current are equal zero:

$$\begin{cases} \frac{dP}{dV}|_M = 0 \\ \frac{dP}{dI}|_M = 0 \end{cases} \Leftrightarrow \begin{cases} \frac{dIV}{dV}|_M = I_M + V_M \frac{dI}{dV}|_M = 0 \\ \frac{dIV}{dI}|_M = V_M + I_M \frac{dV}{dI}|_M = 0 \end{cases} \Leftrightarrow \begin{cases} \frac{dI}{dV}|_M = -\frac{I_M}{V_M} \\ \frac{dV}{dI}|_M = -\frac{V_M}{I_M} \end{cases}$$

Derivative  $I$  with respect to  $V$ , (3.1) leads to:

$$\frac{dI}{dV} = -I_S \frac{1 + CR_s \frac{dI}{dV}}{CnV_T} e^{\frac{V + CR_s I}{nV_T}} - \frac{1 + CR_s \frac{dI}{dV}}{CR_p} \quad (3.6)$$

At MPP, replace  $\frac{dI}{dV}|_M$  in (3.6) by  $-\frac{I_M}{V_M}$  to obtain:

$$\begin{aligned} -\frac{I_M}{V_M} &= -I_S \frac{1 - CR_s \frac{I_M}{V_M}}{CnV_T} e^{\frac{V_M + CR_s I_M}{nV_T}} - \frac{1 - CR_s \frac{I_M}{V_M}}{CR_p} \\ \Leftrightarrow \frac{I_M}{V_M} &= I_S \frac{1 - CR_s \frac{I_M}{V_M}}{CnV_T} e^{\frac{V_M + CR_s I_M}{nV_T}} + \frac{1 - CR_s \frac{I_M}{V_M}}{CR_p} \\ \Leftrightarrow \frac{I_M}{V_M} - \frac{V_M - CR_s I_M}{CR_p V_M} &= I_S \frac{V_M - CR_s I_M}{CnV_T V_M} e^{\frac{V_M + CR_s I_M}{nV_T}} \\ \Leftrightarrow \frac{I_M CR_p - V_M + CR_s I_M}{R_p} &= I_S \frac{V_M - CR_s I_M}{nV_T} e^{\frac{V_M + CR_s I_M}{nV_T}} \\ \Leftrightarrow I_S &= \frac{nV_T (I_M C (R_p + R_s) - V_M)}{R_p (V_M - CR_s I_M) e^{\frac{V_M + CR_s I_M}{CnV_T}}} \end{aligned} \quad (3.7)$$

The equation (3.7), together with (3.3), (3.4) and (3.5) are used to calculate the parameters of solar cell model based on the given value of  $n$ .

**The verifying equation:** Subtracting (3.3) from (3.4) leads to equation:

$$\begin{aligned} I_{SC} &= I_S \left( e^{\frac{V_{OC}}{CnV_T}} - e^{\frac{CI_{SC} R_s}{CnV_T}} \right) + \frac{V_{OC} - CI_{SC} R_s}{CR_p} \\ \Leftrightarrow I_{SC} &= I_S e^{\frac{V_{OC}}{CnV_T}} \left( 1 - e^{-\frac{V_{OC} - CI_{SC} R_s}{CnV_T}} \right) + \frac{V_{OC} - CI_{SC} R_s}{CR_p} \end{aligned} \quad (3.8)$$

Rearrange (3.4) to obtain:

$$I_{SC}R_{ps} = R_p I_{pS} (1 - \psi) \quad (3.9)$$

$$\text{where } \psi = \frac{I_S}{I_{pS}} e^{\frac{I_{SC}R_s}{nV_T}}, \quad R_{pS} = R_p + R_s, \quad I_{pS} = I_{ph} + I_S$$

Naturally, the value of  $\psi \cong 0$  (see the value of  $\psi$  extracted from more than 100 panels at [38]). Thus (3.9) may be reduced to

$$\frac{R_p}{R_{ps}} I_{pS} \cong I_{SC} \quad (3.10)$$

Derivative  $V$  in (3.2) with respect to  $I$  to obtain the equation:

$$\begin{aligned} V &= \mathcal{C}nV_T \ln \left( \frac{I_{ph} + I_S - I \left( 1 + \frac{R_s}{R_p} \right) - \frac{V}{\mathcal{C}R_p}}{I_S} \right) - IC R_s \\ \Leftrightarrow \frac{dV}{dI} &= \mathcal{C}nV_T \left( \frac{I_S}{I_{ph} + I_S - I \left( 1 + \frac{R_s}{R_p} \right) - \frac{V}{\mathcal{C}R_p}} \right) \left( \frac{-1 - \frac{R_s}{R_p} - \frac{1}{\mathcal{C}R_p} \frac{dV}{dI}}{I_S} \right) - \mathcal{C}R_s \\ \Leftrightarrow \frac{dV}{dI} &= -\mathcal{C}nV_T \left( \frac{\mathcal{C}(R_p + R_s) + \frac{dV}{dI}}{\mathcal{C}R_p(I_{ph} + I_S) - IC(R_p + R_s) - V} \right) + \mathcal{C}R_s \\ \Rightarrow \frac{dV}{dI} &= \frac{-\mathcal{C}^2(nV_T(R_p + R_s) + R_p R_s(I_{ph} + I_S) - R_s(R_p + R_s)I) + \mathcal{C}R_s V}{(I_{ph} + I_S)\mathcal{C}R_p - IC(R_p + R_s) + \mathcal{C}nV_T - V} \quad (3.11) \end{aligned}$$

Right side of equation (3.11) is used to calculate the slope of I-V curve at any point  $(V, I)$ . At  $SC$ , equation (3.11) becomes:

$$\left. \frac{dV}{dI} \right|_{SCC} = \frac{-\mathcal{C}(nV_T(R_p + R_s) + R_p R_s(I_{ph} + I_S) - R_s(R_p + R_s)I_{SC})}{(I_{ph} + I_S)R_p - I_{SC}(R_p + R_s) + nV_T} \quad (3.12)$$

On the other hand, applying the estimation (3.10) into (3.11) to obtain:

$$\frac{dV}{dI} \approx \frac{-\mathcal{C}^2(nV_T(R_p + R_s) + R_s I_{SC}(R_p + R_s) - R_s(R_p + R_s)I) + \mathcal{C}R_s V}{\mathcal{C}I_{SC}(R_p + R_s) - \mathcal{C}I(R_p + R_s) + \mathcal{C}nV_T - V} \quad (3.13)$$

Using equation (3.13) to calculate slope of I-V curve at  $SC$ :

$$\begin{aligned} \left. \frac{dV}{dI} \right|_{SCC} &\approx \frac{-\mathcal{C}^2(nV_T(R_p + R_s) + R_s I_{SC}(R_p + R_s) - R_s(R_p + R_s)I_{SC})}{\mathcal{C}I_{SC}(R_p + R_s) - \mathcal{C}I_{SC}(R_p + R_s) + \mathcal{C}nV_T} \\ \Leftrightarrow \left. \frac{dV}{dI} \right|_{SCC} &\approx \mathcal{C}(R_p + R_s) \quad (3.14) \end{aligned}$$

Since (3.12) and (3.14), the verifying equation is written as follow:

$$\begin{aligned} \frac{-\mathcal{C}(nV_T(R_p + R_s) + R_p R_s (I_{ph} + I_S) - R_s (R_p + R_s) I_{SC})}{(I_{ph} + I_S) R_p - I_{SC} (R_p + R_s) + nV_T} &= \mathcal{C} (R_p + R_s) \\ \Leftrightarrow \frac{-(R_p + R_s)(nV_T - R_s I_{SC}) + R_p R_s (I_{ph} + I_S)}{(I_{ph} + I_S) R_p - I_{SC} (R_p + R_s) + nV_T} &= R_p + R_s \end{aligned} \quad (3.15)$$

Finally, the five parameters  $n, R_s, R_p, I_S, I_{ph}$  will be obtained by solving the system:

$$\left\{ \begin{array}{l} 0 = I_{ph} - I_S \left( e^{\frac{V_{OC}}{CnV_T}} - 1 \right) - \frac{V_{OC}}{CR_p} \quad (3.3) \\ I_{SC} = I_{ph} - I_S \left( e^{\frac{CI_{SC}R_s}{CnV_T}} - 1 \right) - \frac{CI_{SC}R_s}{CR_p} \quad (3.4) \\ I_M = I_{ph} - I_S \left( e^{\frac{V_M + CI_M R_s}{CnV_T}} - 1 \right) - \frac{V_M + CI_M R_s}{CR_p} \quad (3.5) \\ I_S = \frac{nV_T(I_M C(R_p + R_s) - V_M)}{R_p(V_M - CR_s I_M)e^{\frac{V_M + CI_M R_s}{CnV_T}} - V_M} \quad (3.7) \\ R_p + R_s = \frac{-(R_p + R_s)(nV_T - R_s I_{SC}) + R_p R_s (I_{ph} + I_S)}{(I_{ph} + I_S) R_p - I_{SC} (R_p + R_s) + nV_T} \quad (3.15) \end{array} \right. \quad (3.16)$$

These are nonlinear equations and not independent absolutely. Hence, solving them directly by algebra is very difficult task. This extraction uses numerical method and an searching strategy to find the approximate values of five solutions.

### 3.3 Searching Strategy

In single diode solar cell model, the value of ideality factor  $n$  is from 1 to 2. Scanning  $n$  is the best choice for searching the parameters. To avoid missing the lower than 1 value of  $n$ , the initial 0.8 is chosen. With each value of  $n$ , the corresponding  $R_s$  is searched first. Next, both  $n$  and  $R_s$  are used to calculate  $R_p, I_S$  and  $I_{ph}$ . In the third step, all parameters are used to calculate a cost function. Comparison of two consecutive cost functions shows which is the most suitable set parameters. There is three steps in one loop which corresponds to a value of  $n$  (Fig. 3.3). Each step in will be explained in the following parts.

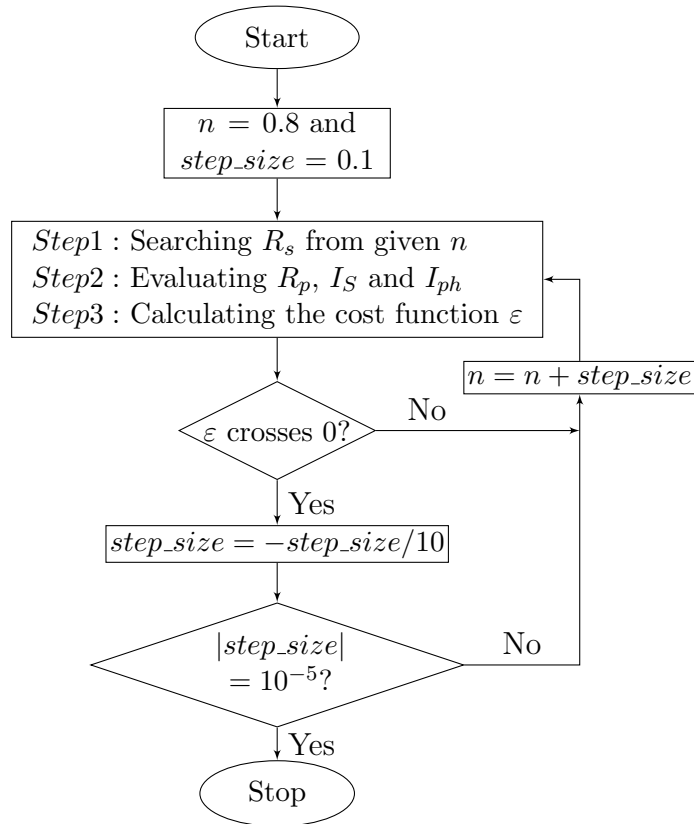


FIGURE 3.3: Searching flowchart of proposed method.

### 3.3.1 Searching the Series Resistor $R_s$ Bases on a Given Value of $n$

This step uses four equations in (3.16) for searching  $R_s$ . Subtracting (3.3) from (3.4) to obtain equation:

$$\begin{aligned}
 I_{SC} &= I_S \left( e^{\frac{V_{OC}}{CnV_T}} - e^{\frac{CI_{SC}R_s}{CnV_T}} \right) + \frac{V_{OC} - CI_{SC}R_s}{CR_p} \\
 \Rightarrow I_S &= \frac{CI_{SC}(R_p + R_s) - V_{OC}}{CR_p \left( e^{\frac{V_{OC}}{CnV_T}} - e^{\frac{CI_{SC}R_s}{CnV_T}} \right)} \quad (3.17)
 \end{aligned}$$

Combination of (3.7) and (3.17) leads to the following equation:

$$\begin{aligned}
 \frac{nV_T(I_M C(R_p + R_s) - V_M)}{R_p(V_M - CR_s I_M) e^{\frac{V_M + CR_s I_M}{CnV_T}}} &= \frac{CI_{SC}(R_p + R_s) - V_{OC}}{CR_p \left( e^{\frac{V_{OC}}{CnV_T}} - e^{\frac{CI_{SC}R_s}{CnV_T}} \right)} \\
 \Leftrightarrow \frac{nV_T(I_M C(R_p + R_s) - V_M)}{V_M - CR_s I_M} &= \frac{CI_{SC}(R_p + R_s) - V_{OC}}{C \left( e^{\frac{V_{OC} - V_M - CR_s I_M}{CnV_T}} - e^{\frac{CI_{SC}R_s - V_M - CR_s I_M}{CnV_T}} \right)} \quad (3.18)
 \end{aligned}$$

Let  $A = e^{\frac{V_{OC} - V_M - \mathcal{C}R_s I_M}{\mathcal{C}nV_T}}$  and  $B = e^{\frac{\mathcal{C}I_{SC}R_s - V_M - \mathcal{C}R_s I_M}{\mathcal{C}nV_T}}$ , equation (3.18) becomes:

$$\begin{aligned}
\frac{nV_T(I_M \mathcal{C}(R_p + R_s) - V_M)}{V_M - \mathcal{C}R_s I_M} &= \frac{\mathcal{C}I_{SC}(R_p + R_s) - V_{OC}}{\mathcal{C}(A - B)} \\
\Leftrightarrow \mathcal{C}nV_T(I_M \mathcal{C}(R_p + R_s) - V_M)(A - B) &= (V_M - \mathcal{C}R_s I_M)(\mathcal{C}I_{SC}(R_p + R_s) - V_{OC}) \\
\Leftrightarrow R_p(\mathcal{C}^2 nV_T I_M(A - B) - (V_M - \mathcal{C}R_s I_M)\mathcal{C}I_{SC}) &= \\
&= (V_M - \mathcal{C}R_s I_M)(\mathcal{C}I_{SC}R_s - V_{OC} + \mathcal{C}nV_T(A - B)) \\
\Leftrightarrow R_p &= \frac{(V_M - \mathcal{C}R_s I_M)(\mathcal{C}I_{SC}R_s - V_{OC} + \mathcal{C}nV_T(A - B))}{\mathcal{C}(\mathcal{C}nV_T I_M(A - B) - (V_M - \mathcal{C}R_s I_M)I_{SC})} \quad (3.19)
\end{aligned}$$

On the other hand, subtracting (3.3) from (3.5) to obtain equation:

$$\begin{aligned}
I_M &= I_S \left( e^{\frac{V_{OC}}{\mathcal{C}nV_T}} - e^{\frac{V_M + \mathcal{C}I_M R_s}{\mathcal{C}nV_T}} \right) + \frac{V_{OC} - V_M - \mathcal{C}I_M R_s}{\mathcal{C}R_p} \\
\Rightarrow I_S &= \frac{\mathcal{C}I_M(R_p + R_s) - V_{OC} + V_M}{\mathcal{C}R_p \left( e^{\frac{V_{OC}}{\mathcal{C}nV_T}} - e^{\frac{V_M + \mathcal{C}I_M R_s}{\mathcal{C}nV_T}} \right)} \quad (3.20)
\end{aligned}$$

Combination of (3.7) and (3.20) leads to the following equation:

$$\begin{aligned}
\frac{nV_T(I_M \mathcal{C}(R_p + R_s) - V_M)}{R_p(V_M - \mathcal{C}R_s I_M)e^{\frac{V_M + \mathcal{C}R_s I_M}{\mathcal{C}nV_T}}} &= \frac{\mathcal{C}I_M(R_p + R_s) - V_{OC} + V_M}{\mathcal{C}R_p \left( e^{\frac{V_{OC}}{\mathcal{C}nV_T}} - e^{\frac{V_M + \mathcal{C}I_M R_s}{\mathcal{C}nV_T}} \right)} \\
\Leftrightarrow \frac{nV_T(I_M \mathcal{C}(R_p + R_s) - V_M)}{R_p(V_M - \mathcal{C}R_s I_M)} &= \frac{\mathcal{C}I_M(R_p + R_s) - V_{OC} + V_M}{\mathcal{C}R_p \left( e^{\frac{V_{OC} - V_M - \mathcal{C}I_M R_s}{\mathcal{C}nV_T}} - 1 \right)} \\
\Leftrightarrow \frac{nV_T(I_M \mathcal{C}(R_p + R_s) - V_M)}{V_M - \mathcal{C}R_s I_M} &= \frac{\mathcal{C}I_M(R_p + R_s) - V_{OC} + V_M}{\mathcal{C}(A - 1)} \\
\Leftrightarrow \frac{\mathcal{C}nV_T I_M R_p + nV_T(\mathcal{C}I_M R_s - V_M)}{V_M - \mathcal{C}R_s I_M} &= \frac{\mathcal{C}I_M R_p + \mathcal{C}I_M R_s - V_{OC} + V_M}{\mathcal{C}(A - 1)} \\
\Leftrightarrow R_p \mathcal{C}(\mathcal{C}nV_T I_M(A - 1) - I_M(V_M - \mathcal{C}R_s I_M)) &= \\
&= (V_M - \mathcal{C}R_s I_M)(\mathcal{C}I_M R_s - V_{OC} + V_M + \mathcal{C}nV_T(A - 1)) \\
\Leftrightarrow R_p &= \frac{(V_M - \mathcal{C}R_s I_M)(\mathcal{C}I_M R_s - V_{OC} + V_M + \mathcal{C}nV_T(A - 1))}{\mathcal{C}(\mathcal{C}nV_T I_M(A - 1) - I_M(V_M - \mathcal{C}R_s I_M))} \quad (3.21)
\end{aligned}$$

Since (3.19) and (3.21), inferring the equation of  $R_s$ :

$$\begin{aligned}
& \frac{(V_M - \mathcal{C}R_s I_M)(\mathcal{C}I_{SC}R_s - V_{OC} + \mathcal{C}nV_T(A - B))}{\mathcal{C}(\mathcal{C}nV_T I_M(A - B) - (V_M - \mathcal{C}R_s I_M)I_{SC})} = \\
& = \frac{(V_M - \mathcal{C}R_s I_M)(\mathcal{C}I_M R_s - V_{OC} + V_M + \mathcal{C}nV_T(A - 1))}{\mathcal{C}(\mathcal{C}nV_T I_M(A - 1) - I_M(V_M - \mathcal{C}R_s I_M))} \\
& \Leftrightarrow \frac{\mathcal{C}I_{SC}R_s - V_{OC} + \mathcal{C}nV_T(A - B)}{\mathcal{C}nV_T I_M(A - B) - (V_M - \mathcal{C}R_s I_M)I_{SC}} = \frac{\mathcal{C}I_M R_s - V_{OC} + V_M + \mathcal{C}nV_T(A - 1)}{\mathcal{C}nV_T I_M(A - 1) - I_M(V_M - \mathcal{C}R_s I_M)}
\end{aligned} \tag{3.22}$$

After expanding and reducing, the equation (3.22) is rewritten as:

$$\begin{aligned}
& \mathcal{C}nV_T(I_{SC}V_M(A - 1) - I_M V_{OC}(B - 1) - 2I_M V_M(A - B)) + I_{SC}V_M^2 + \\
& \mathcal{C}I_{SC}I_M R_s(V_{OC} - V_M) - V_{OC}V_M(I_{SC} - I_M) - \mathcal{C}I_M^2 R_s V_{OC} = 0
\end{aligned} \tag{3.23}$$

Because  $A, B$  are exponential functions, (3.23) must be solve by the numerical method. The Newton-Raphson iterative is used in this case to find  $R_s$  from  $n, T$  and measured currents and voltages. Let the left side of (3.23) is  $F(R_s)$ . Derivative  $F'(R_s)$  with

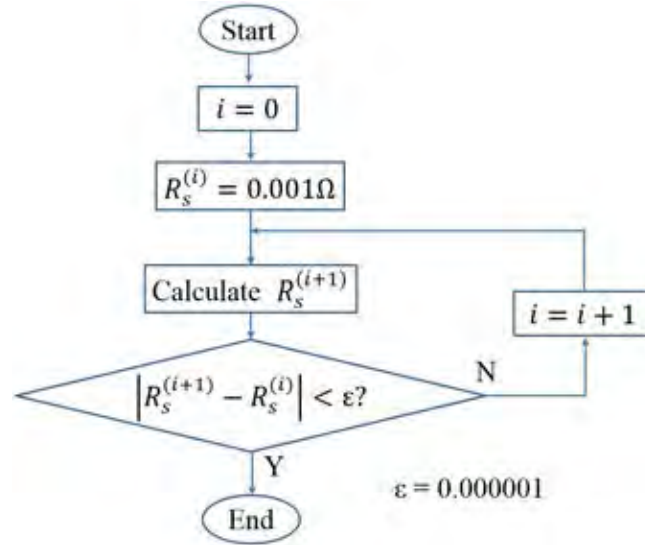


FIGURE 3.4: Flowchart for searching  $R_s$ .

respect to  $R_s$ :

$$\begin{aligned}
& F'(R_s) = \\
& = \mathcal{C}nV_T(I_{SC}V_M A' - I_M V_{OC} B' - 2I_M V_M(A' - B')) + \mathcal{C}I_{SC}I_M(V_{OC} - V_M) - \mathcal{C}I_M^2 V_{OC}
\end{aligned}$$



Easy to infer the derivative of  $A$  and  $B$  with respect to  $R_s$  as follows:

$$A' = \frac{dA}{dR_s} = -\frac{I_M}{CnV_T}A \quad (3.24)$$

$$B' = \frac{dB}{dR_s} = -\frac{I_M}{CnV_T}B \quad (3.25)$$

Using (3.24) and (3.25),  $F'(R_s)$  is rewritten as:

$$\begin{aligned} F'(R_s) &= CnV_T \left( -\frac{I_M}{CnV_T} \right) (I_{SC}V_M A - I_M V_{OC} B - 2I_M V_M (A - B)) - CI_M^2 V_{OC} \\ &\quad + CI_{SC} I_M (V_{OC} - V_M) \\ &= -I_M (I_{SC} V_M A - I_M V_{OC} B - 2I_M V_M (A - B)) + CI_{SC} I_M (V_{OC} - V_M) \\ &\quad - CI_M^2 V_{OC} \end{aligned} \quad (3.26)$$

According to Newton-Raphson method, the approximated solution of equation “ $F(R_s) = 0$ ” is calculated by the iterative formula:

$$R_s^{(i+1)} = R_s^{(i)} - \frac{F(R_s^{(i)})}{F'(R_s^{(i)})} \quad (3.27)$$

Because the real values of  $R_s$  is small then the initial value of  $R_s$ ,  $R_s^{(0)}$  is set at  $0.001\Omega$ . The new value of  $R_s$  is updated to formula (3.27) for calculating the next value. The calculation end if the absolute error between two consecutive  $R_s$  smaller than  $0.000001$  ( $|R_s^{(i+1)} - R_s^{(i)}| < 0.000001$ ). Fig. 3.4 shows the flow-chart of searching  $R_s$ .

### 3.3.2 Determine $R_p$ , $I_S$ and $I_{ph}$ Based on Given $n$ and Calculated $R_s$

#### 3.3.2.1 Parallel Resistor $R_p$

The value of parallel resistance  $R_p$  is calculated basing on both  $n$  and  $R_s$  by using (3.19) or (3.21) as follows:

$$R_p = \frac{(V_M - CR_s I_M)(CI_{SC} R_s - V_{OC} + CnV_T(A - B))}{C(CnV_T I_M(A - B) - (V_M - CR_s I_M)I_{SC})}$$

or:

$$R_p = \frac{(V_M - \mathcal{C}R_s I_M)(\mathcal{C}I_M R_s - V_{OC} + V_M + \mathcal{C}nV_T(A - 1))}{\mathcal{C}(\mathcal{C}nV_T I_M (A - 1) - I_M(V_M - \mathcal{C}R_s I_M))}$$

### 3.3.2.2 Saturation Current $I_S$

Combination of two subtractions ((3.4)-(3.3)) and ((3.5)-(3.3)) leads to the system:

$$\begin{aligned} & \begin{cases} I_{SC} = I_S \left( e^{\frac{V_{OC}}{\mathcal{C}nV_T}} - e^{\frac{\mathcal{C}I_{SC}R_s}{\mathcal{C}nV_T}} \right) - \frac{V_{OC} - \mathcal{C}I_{SC}R_s}{\mathcal{C}R_p} \\ I_M = I_S \left( e^{\frac{V_{OC}}{\mathcal{C}nV_T}} - e^{\frac{V_M + \mathcal{C}I_M R_s}{\mathcal{C}nV_T}} \right) - \frac{V_{OC} - V_M - \mathcal{C}I_M R_s}{\mathcal{C}R_p} \end{cases} \\ \Leftrightarrow & \begin{cases} \frac{V_{OC} - \mathcal{C}I_{SC}R_s}{\mathcal{C}R_p} = I_S \left( e^{\frac{V_{OC}}{\mathcal{C}nV_T}} - e^{\frac{\mathcal{C}I_{SC}R_s}{\mathcal{C}nV_T}} \right) - I_{SC} \\ \frac{V_{OC} - V_M - \mathcal{C}I_M R_s}{\mathcal{C}R_p} = I_S \left( e^{\frac{V_{OC}}{\mathcal{C}nV_T}} - e^{\frac{V_M + \mathcal{C}I_M R_s}{\mathcal{C}nV_T}} \right) - I_M \end{cases} \\ \Rightarrow & \frac{V_{OC} - \mathcal{C}I_{SC}R_s}{V_{OC} - V_M - \mathcal{C}I_M R_s} = \frac{I_S \left( e^{\frac{V_{OC}}{\mathcal{C}nV_T}} - e^{\frac{V_M + \mathcal{C}I_M R_s}{\mathcal{C}nV_T}} \right) - I_M}{I_S \left( e^{\frac{V_{OC}}{\mathcal{C}nV_T}} - e^{\frac{\mathcal{C}I_{SC}R_s}{\mathcal{C}nV_T}} \right) - I_{SC}} \\ \Leftrightarrow & (V_{OC} - \mathcal{C}I_{SC}R_s)(I_S(A - B) - I_{SC}D) = (V_{OC} - V_M - \mathcal{C}I_M R_s)(I_S(A - 1) - I_M D) \\ & \text{where: } D = e^{-\frac{V_M + \mathcal{C}I_M R_s}{\mathcal{C}nV_T}} \\ \Rightarrow I_S = & \frac{D(I_{SC}(V_{OC} - \mathcal{C}I_{SC}R_s) - I_M(V_{OC} - V_M - \mathcal{C}I_M R_s))}{(V_{OC} - \mathcal{C}I_{SC}R_s)(A - B) - (V_{OC} - V_M - \mathcal{C}I_M R_s)(A - 1)} \quad (3.28) \end{aligned}$$

The expression (3.28) is used to calculate value of  $I_S$  from  $R_s$ ,  $n$  and measured values.

### 3.3.2.3 Calculating for Photo-generated Current $I_{ph}$

System (3.3), (3.4) and (3.5) can be rewritten as follow:

$$\begin{cases} I_{ph} - \frac{V_{OC}}{\mathcal{C}R_p} = I_S \left( e^{\frac{V_{OC}}{\mathcal{C}nV_T}} - 1 \right) \\ I_{ph} - I_{SC} - \frac{\mathcal{C}I_{SC}R_s}{\mathcal{C}R_p} = I_S \left( e^{\frac{\mathcal{C}I_{SC}R_s}{\mathcal{C}nV_T}} - 1 \right) \\ I_{ph} - I_M - \frac{V_M + \mathcal{C}I_M R_s}{\mathcal{C}R_p} = I_S \left( e^{\frac{V_M + \mathcal{C}I_M R_s}{\mathcal{C}nV_T}} - 1 \right) \end{cases}$$

$$\begin{aligned}
&\Rightarrow \left\{ \begin{array}{l} \left( e^{\frac{CI_{SC}R_s}{CnV_T}} - 1 \right) \left( I_{ph} - \frac{V_{OC}}{CR_p} \right) = \left( e^{\frac{V_{OC}}{CnV_T}} - 1 \right) \left( I_{ph} - I_{SC} - \frac{CI_{SC}R_s}{CR_p} \right) \\ \left( e^{\frac{V_M + CI_M R_s}{CnV_T}} - 1 \right) \left( I_{ph} - \frac{V_{OC}}{CR_p} \right) = \left( e^{\frac{V_{OC}}{CnV_T}} - 1 \right) \left( I_{ph} - I_M - \frac{V_M + CI_M R_s}{CR_p} \right) \end{array} \right. \\
&\Leftrightarrow \left\{ \begin{array}{l} I_{ph} \left( e^{\frac{CI_{SC}R_s}{CnV_T}} - e^{\frac{V_{OC}}{CnV_T}} \right) = \frac{V_{OC}}{CR_p} \left( e^{\frac{CI_{SC}R_s}{CnV_T}} - 1 \right) - \left( I_{SC} + \frac{CI_{SC}R_s}{CR_p} \right) \left( e^{\frac{V_{OC}}{CnV_T}} - 1 \right) \\ I_{ph} \left( e^{\frac{V_M + CI_M R_s}{CnV_T}} - e^{\frac{V_{OC}}{CnV_T}} \right) = \frac{V_{OC}}{CR_p} \left( e^{\frac{V_M + CI_M R_s}{CnV_T}} - 1 \right) - \left( I_M + \frac{V_M + CI_M R_s}{CR_p} \right) \left( e^{\frac{V_{OC}}{CnV_T}} - 1 \right) \end{array} \right. \\
&\Leftrightarrow \left\{ \begin{array}{l} I_{ph} (B - A) = \frac{V_{OC}}{CR_p} (B - D) - \left( I_{SC} + \frac{CI_{SC}R_s}{CR_p} \right) (A - D) \\ I_{ph} (1 - A) = \frac{V_{OC}}{CR_p} (1 - D) - (A - D) \left( I_M + \frac{V_M + CI_M R_s}{CR_p} \right) \end{array} \right. \\
&\quad \text{where: } A = e^{\frac{V_{OC} - V_M - CR_s I_M}{CnV_T}}; B = e^{\frac{CI_{SC}R_s - V_M - CR_s I_M}{CnV_T}}; D = e^{-\frac{V_M + CI_M R_s}{CnV_T}} \\
&\Leftrightarrow \left\{ \begin{array}{l} I_{ph} (B - A) + I_{SC} (A - D) = \frac{1}{CR_p} (V_{OC} (B - D) - CI_{SC}R_s (A - D)) \\ I_{ph} (1 - A) + I_M (A - D) = \frac{1}{CR_p} (V_{OC} (1 - D) - (V_M + CI_M R_s) (A - D)) \end{array} \right. \\
&\Rightarrow \frac{I_{ph} (B - A) + I_{SC} (A - D)}{I_{ph} (1 - A) + I_M (A - D)} = \frac{V_{OC} (B - D) - CI_{SC}R_s (A - D)}{V_{OC} (1 - D) - (V_M + CI_M R_s) (A - D)} \\
&\Rightarrow [I_{ph} (B - A) + I_{SC} (A - D)][V_{OC} (1 - D) - (V_M + CI_M R_s) (A - D)] = \\
&\quad [I_{ph} (1 - A) + I_M (A - D)][V_{OC} (B - D) - CI_{SC}R_s (A - D)] \\
&\Leftrightarrow I_{ph} (B - A) [V_{OC} (1 - D) - (V_M + CI_M R_s) (A - D)] - \\
&\quad I_{ph} (1 - A) [V_{OC} (B - D) - CI_{SC}R_s (A - D)] = \\
&\quad I_M (A - D) [V_{OC} (B - D) - CI_{SC}R_s (A - D)] - \\
&\quad I_{SC} (A - D) [V_{OC} (1 - D) - (V_M + CI_M R_s) (A - D)] \\
&\Leftrightarrow I_{ph} = \frac{(B - D)I_M V_{SC} + (D - 1)I_{SC} V_{OC} + (A - D)I_{SC} V_M}{(B - 1)V_{OC} + (A - B)(V_M + CI_M R_s) - (A - 1)CI_{SC}R_s} \quad (3.29)
\end{aligned}$$

Generally, with a given  $n$ , using Newton-Raphson iterative method to search  $R_s$  first. Next applying  $n$  and  $R_s$  to calculate  $R_p$ ,  $I_S$  and  $I_{ph}$  by (3.21), (3.28) and (3.29) respectively. In the last step, the calculated set parameters  $(n, R_s, R_p, I_S, I_{ph})$  will be verified by applying them into equation (3.15).

### 3.3.3 Verifying by Cost Function $\varepsilon(n, R_s, R_p, I_S, I_{ph})$

This part present a techniques for verifying the calculated set parameters and an improvement to reduce the calculating time. Equation (3.15) can be rewritten as :

$$\frac{(R_p + R_s)(R_s I_{SC} - nV_T) + R_p R_s (I_{ph} + I_S)}{(I_{ph} + I_S) R_p - I_{SC}(R_p + R_s) + nV_T} - R_p - R_s = 0 \quad (3.30)$$

Let the left hand side of (3.30) is cost function  $\varepsilon(n, R_s, R_p, I_S, I_{ph})$ .

$$\varepsilon(n, R_s, R_p, I_S, I_{ph}) = \frac{(R_p + R_s)(R_s I_{SC} - nV_T) + R_p R_s (I_{ph} + I_S)}{(I_{ph} + I_S) R_p - I_{SC}(R_p + R_s) + nV_T} - R_p - R_s \quad (3.31)$$

Fig. 3.3 also shows the scanning strategy for finding the parameters that minimize

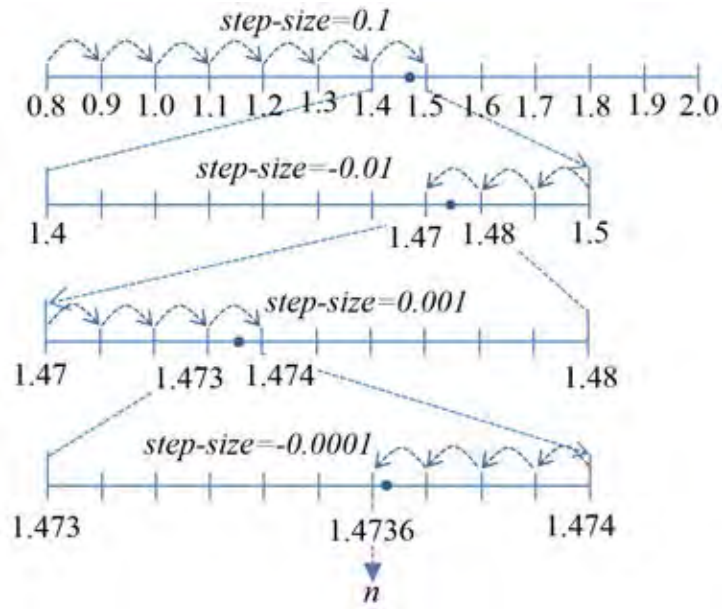


FIGURE 3.5: An example of scanning for the most suitable value of  $n$ . It is increased and decreased twice. Each direction changing the *step\_size* is reduced ten times.

the cost function. First  $n$  is fixed to 0.8 (lowest plausible value) and the *step\_size* is  $+0.1$ , complete the three steps said above. Check if  $\varepsilon$  crosses zero (or changes its sign) when compared to its previous value. If not, change the value of  $n$  with the same *step\_size*. But if  $\varepsilon$  crosses zero, which means the true  $n$  is between the current  $n$  and the previous one, change the direction of scanning and reduce the *step\_size* ten times before moving the next  $n$ . Continue the scanning until the *step\_size* is considerably insignificant ( $10^{-5}$ ).

Fig. 3.5 shows a scanning example. First,  $n$  is scanned up from 0.8 with the *step\_size* of  $+0.1$ . When  $n = 1.5$ ,  $\varepsilon$  changes its sign. Then, the value of  $n$  reduced from 1.5 with step size  $-0.01$  until  $n = 1.47$ ,  $\varepsilon$  changes its sign again. At this points the *step\_size*  $= +0.001$  so  $n$  increases again until  $n = 1.474$ . Then it is reduced with the step size of  $-0.0001$ . Finally when  $n = 1.4736$ , the scanning stops. The current set of parameters found in *Step 1* and *Step 2* is the answer.

## Chapter IV

# PROPOSED METHOD FOR CALCULATION THE GLOBAL MAXIMUM POWER POINT OF A PV SYSTEM

This chapter presents a new method which permits to calculate the voltage and current at GMPP of single or parallel strings exactly in short time basing on a few online measurements. The effect of temperature on solar cell parameters are considered in order to increase the accuracy and the robustness of method.

### 4.1 Dependence of $R_s$ , $R_p$ , $I_S$ , $I_{ph}$ on Temperature

The parameters of solar cell at testing condition  $T_{meas}$ ,  $I_{r_{meas}}$ , are always determined first. After that, these values are used to calculate the parameters at operating condition. The well-known testing condition is *Standard Test Condition* (STC),  $T_{meas} = 25^\circ\text{C}$  and  $I_{r_{meas}} = 1000\text{W/m}^2$  or 298K. Assuming that the solar cell parameters at STC ( $R_{s0}$ ,  $R_{p0}$ ,  $I_{S0}$  and  $I_{ph0}$ ) are determined already. At the operating temperature  $T$ , each of them must be recalculated by its corresponding expressions.

The series resistance at  $T$ :

$$R_s(T) = R_{s0} \times \left( \frac{T}{T_{meas}} \right)^{k_{R_s}} \quad (4.1)$$

where:  $k_{R_s}$  is temperature exponent for  $R_s$

The parallel resistance at  $T$ :

$$R_p(T) = R_{p0} \times \left( \frac{T}{T_{meas}} \right)^{k_{R_p}} \quad (4.2)$$

where:  $k_{R_p}$  is temperature exponent for  $R_p$

The saturation current of diode at  $T$ :

$$I_S(T) = I_{S0} \times \left( \frac{T}{T_{meas}} \right)^{k_{I_S}/n} \times e^{EG \times \left( \frac{T}{T_{meas}} - 1 \right) / (nV_T)} \quad (4.3)$$

where:  $k_{I_S}$  is temperature exponent for  $I_S$

$EG$  is the solar cell activation energy (Bandgap Energy)

$T$  and  $T_{meas}$  are presented in K. For silicon material, the typical value of  $k_{R_s}$ ,  $k_{R_p}$  are 0.2 and the value of  $k_{I_S}$  is 3. The band gap energy of silicon  $EG$  is 1.11eV. With the ambient temperature is 298K, the values of  $R_s$  and  $R_p$  are increase a little ( $\approx 1.6\%$ ) if the temperature increase amount  $25^\circ$  K. The saturation current of diode is change to much under changing of temperature [41]. For example, with  $n = 1.5$ , if temperature increase  $10^\circ$  K, it changes from  $T_{meas} = 298$ K to  $T = 308$ K. The saturation current will be increase  $\left( \frac{308}{298} \right)^{3/1.5} \times e^{1.11 \times \left( \frac{308}{298} - 1 \right) / (1.5 \times k \times 308 / q)} \approx 2.72$  times. Similarly, if the temperature change  $20^\circ$  K, the saturation current will be increase  $\left( \frac{318}{298} \right)^{3/1.5} \times e^{1.11 \times \left( \frac{318}{298} - 1 \right) / (1.5 \times k \times 318 / q)} \approx 6.97$  times. The photo generated current depends on temperature as the following formula:

$$I_{ph}(T) = I_{ph0} \times \left( 1 + k_{I_{ph}} \times (T - T_{meas}) \right) \quad (4.4)$$

where:  $k_{I_S}$  is temperature coefficient for  $I_{ph}$

In practice, the value of temperature coefficient is given in data sheet. Its value is from  $0.038\%^\circ\text{C}^{-1}$  to  $0.081\%^\circ\text{C}^{-1}$ . In calculation by the proposed method, the photo generated current is calculated basing on the measured values ( $V, I$ ) and other parameters. So, the equation (4.4) and  $k_{I_{ph}}$  are not used in any case.

## 4.2 Determining the MPP under Uniform Shading Condition

Under uniform condition, all cells of panels are received the same rate of irradiance. The current, voltage and temperature of all cells are equal. So, basing on measured values of one panel, the voltage and current of MPP of whole is calculated quickly. Fig. 4.1 shows a solar farm (parallel strings) under uniform condition. The measured voltage and current of a panel are  $V_P$ ,  $I_P$  and  $T$ . Reminding that the relationship of

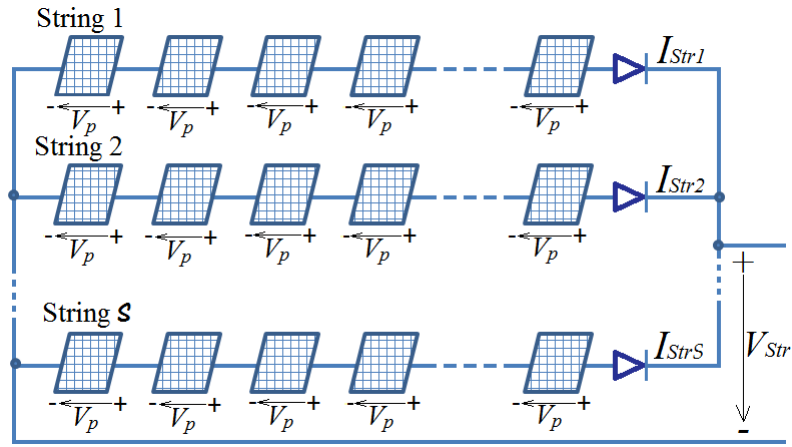


FIGURE 4.1: The solar farm under uniform condition.

them is depicted in following equation:

$$I_P = I_{ph} - I_S \left( e^{\frac{V_P + C I_P R_s}{C n V_T}} - 1 \right) - \frac{V_P + C I_P R_s}{C R_p} \quad (4.5)$$

or:

$$V_P = C n V_T \ln \left( \frac{C(I_{ph} + I_S)R_p - C I_P (R_p + R_s) - V_P}{C R_p I_S} \right) - C I_P R_s \quad (4.6)$$

where  $n$ ,  $R_s$ ,  $R_p$ ,  $I_S$ ,  $I_{ph}$  are five determined parameters of solar cell;  $C$  is number of cells in a panel; Temperature  $T$  is estimated by cell surface's temperature that is measured by IR thermometer easily. In uniform shading, the voltage and current at MPP of a panel are determined instead of GMPP of whole PV system.

Let  $M$  is maximum power point of panel.  $V_M$ ,  $I_M$  are voltage and current at  $M$  respectively. The current at  $M$  can be calculated basing on the voltage at this point,  $V_M$  and solar cell parameters. On the other hand,  $V_M$  can be calculated basing  $I_M$  also. These formulae are used in the iterative calculation for determining MPP of panel as well as GMPP of PV system.

#### 4.2.1 The Iterative Expression of Current at MPP

To build the expression of  $I_M$  as a function of  $V_M$ , the photo generated current at fixed  $I_r$  and  $T$  must be determined first. Since (4.5), the photo generated current  $I_{ph}$  is calculated basing on measured values by the following expression:

$$I_{ph} = I_P + I_S \left( e^{\frac{V_P + C I_P R_s}{C n V_T}} - 1 \right) + \frac{V_P + C I_P R_s}{C R_p} \quad (4.7)$$

On the other hand, derivative  $V_P$  in (4.6) with respect to  $I_P$ :

$$\begin{aligned} \frac{dV_P}{dI_P} &= \mathcal{C}nV_T \left( \frac{\mathcal{C}R_p I_S}{\mathcal{C}(I_{ph} + I_S)R_p - \mathcal{C}I_P(R_p + R_s) - V_P} \right) \frac{-\mathcal{C}(R_p + R_s) - \frac{dV_P}{dI_P}}{\mathcal{C}R_p I_S} - \mathcal{C}R_s \\ \Leftrightarrow \frac{dV_P}{dI_P} &= \mathcal{C}nV_T \left( \frac{-\mathcal{C}(R_p + R_s) - \frac{dV_P}{dI_P}}{\mathcal{C}(I_{ph} + I_S)R_p - \mathcal{C}I_P(R_p + R_s) - V_P} \right) - \mathcal{C}R_s \end{aligned}$$

At the MPP,  $\frac{dV_P}{dI_P}|_M = -\frac{V_M}{I_M}$ , so inferring that:

$$-\frac{V_M}{I_M} = \mathcal{C}nV_T \left( \frac{-\mathcal{C}(R_p + R_s) + \frac{V_M}{I_M}}{\mathcal{C}(I_{ph} + I_S)R_p - \mathcal{C}I_M(R_p + R_s) - V_M} \right) - \mathcal{C}R_s \quad (4.8)$$

Let  $R_{ps} = R_p + R_s$  and  $I_{phS} = I_{ph} + I_S$ . Equation (4.8) becomes:

$$\begin{aligned} -\frac{V_M}{I_M} &= \mathcal{C}nV_T \left( \frac{-\mathcal{C}R_{ps}I_M + V_M}{\mathcal{C}I_M I_{phS}R_p - \mathcal{C}I_M^2 R_{ps} - I_M V_M} \right) - \mathcal{C}R_s \\ \Leftrightarrow \frac{V_M}{I_M} &= \frac{\mathcal{C}^2 n V_T R_{ps} I_M - \mathcal{C}n V_T V_M}{\mathcal{C}I_M I_{phS}R_p - \mathcal{C}I_M^2 R_{ps} - I_M V_M} + \mathcal{C}R_s \\ \Leftrightarrow \frac{V_M}{I_M} &= \frac{\mathcal{C}^2 n V_T R_{ps} I_M - \mathcal{C}n V_T V_M + \mathcal{C}R_s(\mathcal{C}I_M I_{phS}R_p - \mathcal{C}I_M^2 R_{ps} - I_M V_M)}{\mathcal{C}I_M I_{phS}R_p - \mathcal{C}I_M^2 R_{ps} - I_M V_M} \\ \Leftrightarrow V_M &= \frac{\mathcal{C}^2 n V_T R_{ps} I_M - \mathcal{C}n V_T V_M + \mathcal{C}R_s(\mathcal{C}I_M I_{phS}R_p - \mathcal{C}I_M^2 R_{ps} - I_M V_M)}{\mathcal{C}I_{phS}R_p - \mathcal{C}I_M R_{ps} - V_M} \\ \Leftrightarrow V_M(\mathcal{C}I_{phS}R_p - \mathcal{C}I_M R_{ps} - V_M) &= \\ \mathcal{C}^2 n V_T R_{ps} I_M - \mathcal{C}n V_T V_M + \mathcal{C}R_s(\mathcal{C}I_M I_{phS}R_p - \mathcal{C}I_M^2 R_{ps} - I_M V_M) & \\ \Leftrightarrow \mathcal{C}V_M I_{phS}R_p - \mathcal{C}R_{ps} V_M I_M - V_M^2 &= \\ \mathcal{C}^2 n V_T R_{ps} I_M - \mathcal{C}n V_T V_M + \mathcal{C}^2 R_s R_p I_{phS} I_M - \mathcal{C}^2 R_s R_{ps} I_M^2 - \mathcal{C}R_s V_M I_M & \\ \Leftrightarrow \mathcal{C}^2 R_s R_{ps} I_M^2 - \mathcal{C}R_{ps} V_M I_M - \mathcal{C}^2 n V_T R_{ps} I_M - \mathcal{C}^2 R_s R_p I_{phS} I_M + \mathcal{C}R_s V_M I_M + & \\ \mathcal{C}V_M I_{phS}R_p + \mathcal{C}n V_T V_M - V_M^2 &= 0 \\ \Leftrightarrow R_s R_{ps} I_M^2 - \left( R_p \frac{V_M}{\mathcal{C}} + n V_T R_{ps} + R_s R_p I_{phS} \right) I_M + \frac{V_M}{\mathcal{C}} (I_{phS}R_p + n V_T) - \left( \frac{V_M}{\mathcal{C}} \right)^2 & \\ &= 0 \quad (4.9) \end{aligned}$$

Let  $a = R_s R_{ps}$ ,  $b = R_p \frac{V_M}{\mathcal{C}} + n V_T R_{ps} + R_s R_p I_{phS}$  and  $c = \frac{V_M}{\mathcal{C}} (I_{phS}R_p + n V_T) - \left( \frac{V_M}{\mathcal{C}} \right)^2$ .



Equation (4.9) is rewritten in shorter form as follow:

$$aI_M^2 - bI_M + c = 0 \quad (4.10)$$

This is a quadratic equation of  $I_M$ . The expression of  $\Delta = b^2 - 4ac$  is determined by:

$$\begin{aligned} \Delta &= \left( R_p \frac{V_M}{\mathcal{C}} + nV_T R_{ps} + R_s R_p I_{phS} \right)^2 - 4R_s R_{ps} \left( \frac{V_M}{\mathcal{C}} (I_{phS} R_p + nV_T) - \left( \frac{V_M}{\mathcal{C}} \right)^2 \right) \\ &= \left( R_p \frac{V_M}{\mathcal{C}} + nV_T R_{ps} + R_s R_p I_{phS} \right)^2 - 4R_s R_{ps} \frac{V_M}{\mathcal{C}} \left( I_{phS} R_p + nV_T - \frac{V_M}{\mathcal{C}} \right) \end{aligned}$$

The quadratic equation (4.10) has two solution are:

$$I_{PM1} = \frac{-b - \sqrt{\Delta}}{2a} \quad \text{and} \quad I_{PM2} = \frac{-b + \sqrt{\Delta}}{2a}$$

They are written in details:

$$I_{PM1} = \frac{R_p \frac{V_M}{\mathcal{C}} + nV_T R_{ps} + R_s R_p I_{phS}}{2R_s R_{ps}} - \frac{\sqrt{\left( R_p \frac{V_M}{\mathcal{C}} + nV_T R_{ps} + R_s R_p I_{phS} \right)^2 - 4R_s R_{ps} \frac{V_M}{\mathcal{C}} \left( I_{phS} R_p + nV_T - \frac{V_M}{\mathcal{C}} \right)}}{2R_s R_{ps}}$$

$$I_{PM2} = \frac{R_p \frac{V_M}{\mathcal{C}} + nV_T R_{ps} + R_s R_p I_{phS}}{2R_s R_{ps}} + \frac{\sqrt{\left( R_p \frac{V_M}{\mathcal{C}} + nV_T R_{ps} + R_s R_p I_{phS} \right)^2 - 4R_s R_{ps} \frac{V_M}{\mathcal{C}} \left( I_{phS} R_p + nV_T - \frac{V_M}{\mathcal{C}} \right)}}{2R_s R_{ps}}$$

However, only the solution  $I_{PM1}$  is valid. The other root,  $I_{PM2}$  is implausible because it is more than  $I_{ph}$ . This thing is proved as follow. The expression of  $\Delta$  can be rewritten as:

$$\begin{aligned} \Delta &= \left( R_p \frac{V_{PM}}{\mathcal{C}} + nV_T R_{ps} + R_s R_p I_{phS} \right)^2 - 4R_s R_{ps} I_{phS} R_p \frac{V_{PM}}{\mathcal{C}} + \\ &\quad 4R_s R_{ps} \frac{V_{PM}}{\mathcal{C}} \left( \frac{V_{PM}}{\mathcal{C}} - nV_T \right) \end{aligned} \quad (4.11)$$

Well known that the voltage of one cell,  $\frac{V_{PM}}{C}$  is always larger than  $nV_T$ . That leads to the inequality:

$$\frac{V_{PM}}{C} - nV_T > 0 \Leftrightarrow 4R_s R_{ps} \frac{V_{PM}}{C} \left( \frac{V_{PM}}{C} - nV_T \right) > 0 \quad (4.12)$$

On the other hand, because  $R_s \ll R_p$  so  $R_{ps} = R_p + R_s \approx R_p$  and inferring that:

$$4R_s R_{ps} I_{phS} R_p \frac{V_{PM}}{C} \approx 4R_s R_p I_{phS} R_p \frac{V_{PM}}{C} \quad (4.13)$$

Since (4.11), (4.12) and (4.13), to obtain the following inequality:

$$\begin{aligned} \Delta &> \left( R_p \frac{V_{PM}}{C} + nV_T R_{ps} + R_s R_p I_{phS} \right)^2 - 4R_s R_p I_{phS} R_p \frac{V_{PM}}{C} \\ \Rightarrow \Delta &> \left( R_p \frac{V_{PM}}{C} + nV_T R_{ps} + R_s R_p I_{phS} \right)^2 - 4R_s R_p I_{phS} R_p \frac{V_{PM}}{C} - 4nV_T R_{ps} R_s R_p I_{phS} \\ \Leftrightarrow \Delta &> \left( R_p \frac{V_{PM}}{C} + nV_T R_{ps} - R_s R_p I_{phS} \right)^2 \end{aligned} \quad (4.14)$$

Because the higher solution,  $I_{PM2}$  is determined by :

$$\begin{aligned} I_{PM2} &= \frac{R_p \frac{V_{PM}}{C} + nV_T R_{ps} + R_s R_p I_{phS}}{2R_s R_{ps}} + \frac{\sqrt{\Delta}}{2R_s R_{ps}} \\ \Rightarrow I_{PM2} &> \frac{R_p \frac{V_{PM}}{C} + nV_T R_{ps} + R_s R_p I_{phS}}{2R_s R_{ps}} + \frac{\sqrt{\left( R_p \frac{V_{PM}}{C} + nV_T R_{ps} - R_s R_p I_{phS} \right)^2}}{2R_s R_{ps}} \\ \Leftrightarrow I_{PM2} &> \frac{R_p \frac{V_{PM}}{C} + nV_T R_{ps} + R_s R_p I_{phS} + \left| R_p \frac{V_{PM}}{C} + nV_T R_{ps} - R_s R_p I_{phS} \right|}{2R_s R_{ps}} \end{aligned} \quad (4.15)$$

If  $R_p \frac{V_{PM}}{C} + nV_T R_{ps} \geq R_s R_p I_{phS}$ , the inequality (4.15) becomes:

$$\begin{aligned} I_{PM2} &> \frac{R_p \frac{V_{PM}}{C} + nV_T R_{ps} + R_s R_p I_{phS} + R_p \frac{V_{PM}}{C} + nV_T R_{ps} - R_s R_p I_{phS}}{2R_s R_{ps}} \\ \Leftrightarrow I_{PM2} &> \frac{2 \left( R_p \frac{V_{PM}}{C} + nV_T R_{ps} \right)}{2R_s R_{ps}} \geq \frac{2R_s R_p I_{phS}}{2R_s R_{ps}} \approx I_{phS} \approx I_{ph} \end{aligned} \quad (4.16)$$

If  $R_p \frac{V_{PM}}{C} + nV_T R_{ps} < R_s R_p I_{phS}$ , the inequality (4.15) becomes:

$$\begin{aligned} I_{PM2} &> \frac{R_p \frac{V_{PM}}{C} + nV_T R_{ps} + R_s R_p I_{phS} - R_p \frac{V_{PM}}{C} - nV_T R_{ps} + R_s R_p I_{phS}}{2R_s R_{ps}} \\ \Leftrightarrow I_{PM2} &> \frac{2R_s R_p I_{phS}}{2R_s R_{ps}} \approx I_{phS} \approx I_{ph} \end{aligned} \quad (4.17)$$

Basing on two inequalities (4.16) and (4.17), the second solution  $I_{PM2}$  is always more than  $I_{ph}$ , this is impossible so  $I_{PM2}$  is implausible.

Finally, the expression of current at  $M$  is written as:

$$\begin{aligned} I_M &= \frac{R_p \frac{V_M}{C} + nV_T R_{ps} + R_s R_p I_{phS}}{2R_s R_{ps}} - \\ &\frac{\sqrt{(R_p \frac{V_M}{C} + nV_T R_{ps} + R_s R_p I_{phS})^2 - 4R_s R_{ps} \frac{V_M}{C} (I_{phS} R_p + nV_T - \frac{V_M}{C})}}{2R_s R_{ps}} \end{aligned} \quad (4.18)$$

#### 4.2.2 The Iterative Expression of Voltage at MPP

The current  $I_M$  can be calculated by using  $V_M$  in (4.18) and the voltage  $V_M$  is also calculated by using itself approximate and  $I_M$  in the I-V equation (4.19) as follow:

$$V_M = \mathcal{C} n V_T \ln \left( \frac{\mathcal{C}(I_{ph} + I_S) R_p - \mathcal{C} I_M (R_p + R_s) - V_M}{\mathcal{C} R_p I_S} \right) - \mathcal{C} I_M R_s \quad (4.19)$$

Fig. 4.2 shows the flow chart of searching for the voltage and current at MPP. The requirement for calculation is only one set of measured value ( $T, V_P, I_P$ ).

After  $I_{ph}$  is determined from measured values, the iterative begin with  $i = 0$ ,  $V_M^{(0)}$  is set equal  $\mathcal{C} \times 0.5V$ . This value is applied into (4.18) to calculate the current  $I_M^{(i+1)}$ . Next, both  $I_M^{(i+1)}$  and  $V_M^{(i)}$  are used to calculate  $V_M^{(i+1)}$  by using (4.19). If the absolute error of two consecutive calculated voltage,  $|V_M^{(i+1)} - V_M^{(i)}|$  is smaller than a certain value  $\varepsilon$ , the iterative calculation end. Otherwise, the new value will be updated for next iteration. In this study, the value of  $\varepsilon$  is set at 0.01V.

### 4.3 Determining the GMPP of a PV String under Partial Shading Condition

A string is composed from many panels in series. In this paper,  $\mathcal{P}$  indicates the number of panel in a string. Under partial shading, the panels receive different light intensities

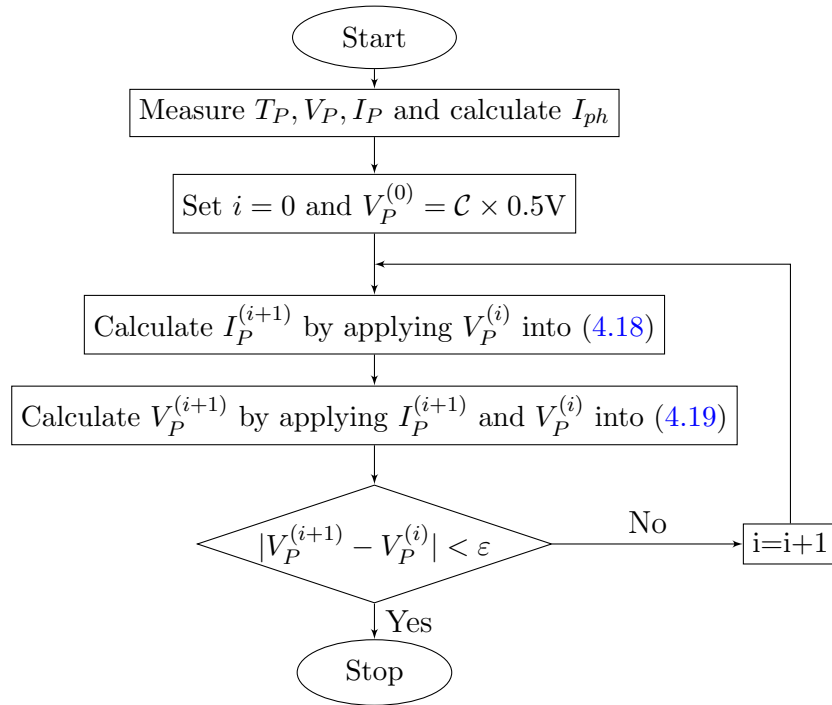


FIGURE 4.2: Algorithm for searching the GMPP under uniform shading.

and following that, many local MPPs are created (see Fig. 2.4 in Chapter 2). The proposed method determines all local MPPs and selects the GMPP among these peaks. Fig. 4.3 shows the proposed structure of a PV string which is used to implement the deterministic method for determining the MPPs. Let  $V_P^i$  is measured voltage of panel  $i$ , for  $i = 1 \dots \mathcal{P}$ . Symbol  $I$  is reused with new meaning that is string current and also is panel current.

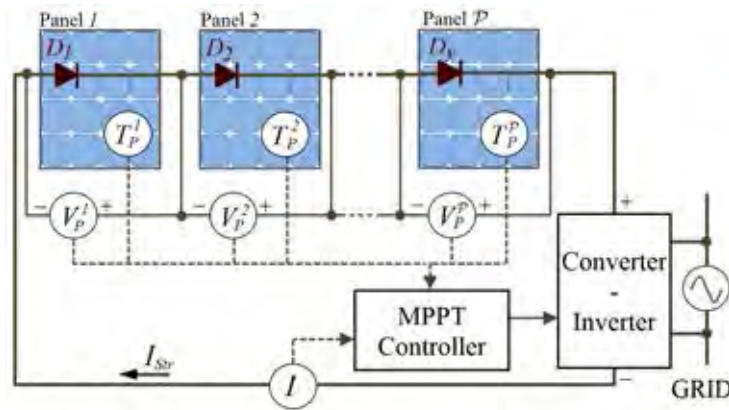


FIGURE 4.3: The bypass diode with a series resistor inside.

In Fig. 4.3, each panel connects in parallel with a bypassed diode. The Schottky diodes with low forward bias voltage are used to reduce the losing energy. The bypass diode has a low series resistor  $R_b$  inside (see in Fig. 4.4). The relationship between

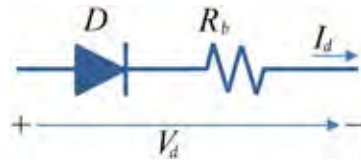


FIGURE 4.4: The solar farm under uniform condition.

voltage  $V_d$  and current  $I_d$  of diode is presented in the equation:

$$I_d = I_{Sd} \left( e^{\frac{V_d - I_d R_b}{n_d V_{Td}}} - 1 \right) \quad (4.20)$$

where:  $I_{Sd}$  is saturation current of bypass diode.

$n_d$  is ideality factor of bypass diode.

$V_{Td} = \frac{kT_d}{q}$  is **threshold** voltage of bypass diode.

$T_d$  is temperature of bypass diode.

The equivalent circuit of solar panel parallel with a diode is shown in Fig. 4.5(a) and the I-V curve of composed component is shown in 4.5(b). If the panel is not

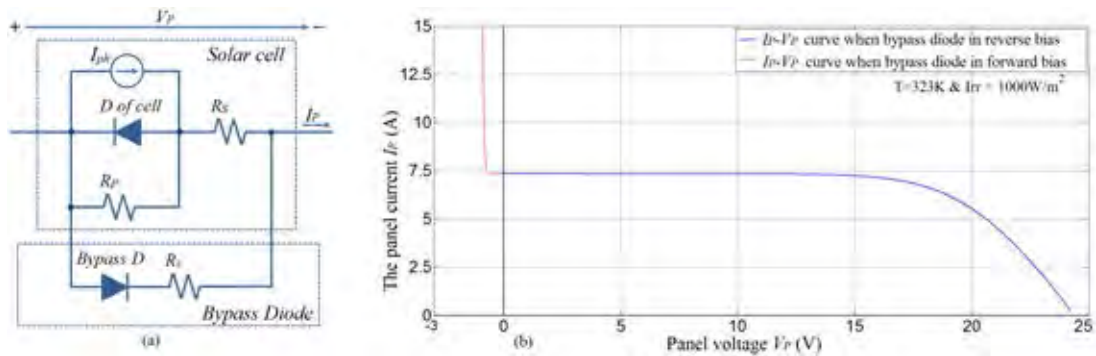


FIGURE 4.5: The equivalent circuit of composed component solar panel - diode (a).  
The I-V curve of the composed component (b).

bypassed, the current of diode is considered zero, the curve of solar panel and composed component is the same (the blue line). If the panel is bypassed, the current of diode is higher than zero while the current of solar cell yield maximum value  $I_{ph}$ . The output current in this time is equal sum of  $I_D$  and  $I_{ph}$  (the red dash line). The photo generated current is calculated from the measured voltage, current and temperature of panel. The temperature of diode, if required, will be approximated by the proposed iterative method. For increasing the accuracy of results, the temperature and current of bypassed diode can be determined at same time basing on iterative formulae.

### 4.3.1 Calculating for $I_{ph}$ of Panel at Measured Points

In string GMPP tracking, after measurement, the followings values are obtained:

The voltage of all panels:  $V_P^i$ , for  $i = 1, \dots, \mathcal{P}$ .

The string current  $I_{Str}$ . This is also the current of every panel.

The surface temperature of all panels:  $T_P^i$ , for  $i = 1, \dots, \mathcal{P}$ .

The temperature of bypass diode  $i$ :  $T_d^i$ , for  $i = 1, \dots, \mathcal{P}$ .

The photo generated current of panels are calculated first. Corresponding to the measured panel voltage, it will be calculated by one of two ways.

**If the measured panel voltage is positive ( $V_P^i > 0$ ):** Using (4.5) to infer the expression of  $I_{ph}$  of panel  $i$ ,  $I_{ph}^i$  as follow:

$$I_{ph}^i = I_{Str} + I_S \left( e^{\frac{V_P^i + \mathcal{C}I_{Str}R_s^i}{cnV_{Td}^i}} - 1 \right) + \frac{V_P^i + \mathcal{C}I_{Str}R_s^i}{\mathcal{C}R_p^i} \quad (4.21)$$

**If the measured panel voltage is negative ( $V_P^i < 0$ ):** The current  $I_{ph}^i$  can not determined directly by (4.5). The diode current is calculated first. The solar cell induced current is equal  $I_{Str} - I_D$ .  $I_D$  is calculated from (4.20). The parameters of diode  $n_d$  and  $R_b$  are given by manufacturer but measuring the temperature of diode,  $T_d$  is difficult. Fortunately,  $T_d$  and power consumption on diode has a relationship as follow:

$$T_d = T_A + \theta_{JA}P_d = T_A + \theta_{JA}V_dI_d \quad (4.22)$$

where:  $T_A$  is the ambient temperature of diode.

$\theta_{JA}$  is thermal resistance junction-to-ambient constant.

With  $T_A$  and  $\theta_{JA}$  are given in product datasheet, a iterative calculation base on two equation (4.20) and (4.22) leads the values of current and temperature of diode. Fig. 4.6 shows the flow chart for the searching  $I_d$  and  $T_d$ . The value of  $\varepsilon$  is 0.001A.

Generally, by directly calculation or indirectly via diode if panel is bypassed, the photo generated current of solar panel  $i$ ,  $I_{ph}^i$  for  $i = 1, 2, \dots, \mathcal{P}$ , is always determined.

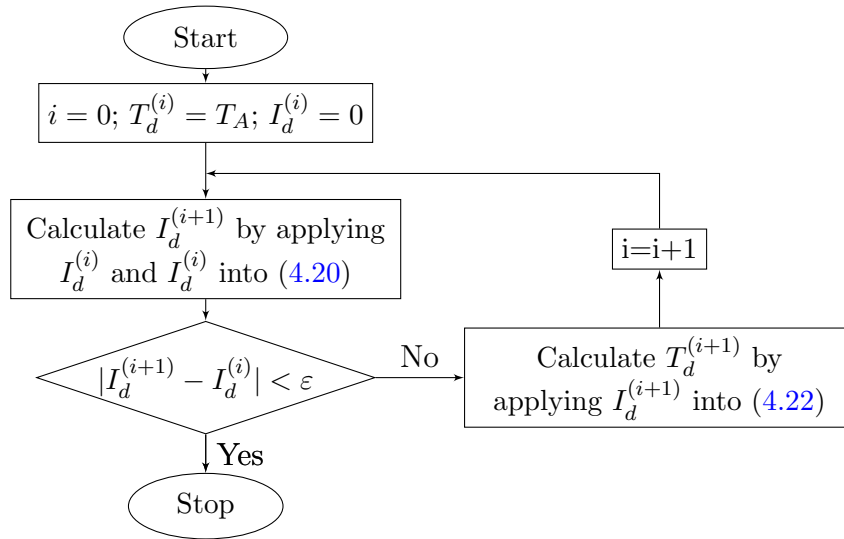


FIGURE 4.6: Algorithm for searching the GMPP under uniform shading.

### 4.3.2 Segmentation

After all panel photo generated currents  $I_{ph}^i$ ,  $i = 1, 2, \dots, \mathcal{P}$  are obtained. Without any effect to the results, assume that  $I_{ph}^1 < I_{ph}^2 < \dots < I_{ph}^{\mathcal{P}}$ . Let  $V_S^i$  is string voltage which corresponds with current  $I_{ph}^i$ . Note that the higher current, the lower voltage. So,  $V_S^1 > V_S^2 > \dots > V_S^{\mathcal{P}} = 0$ . Putting these values on two axes ( $I$  and  $V$ ) to determine  $\mathcal{P}$  segments of current and voltage as Fig. 4.7. If the load is scanned from zero to

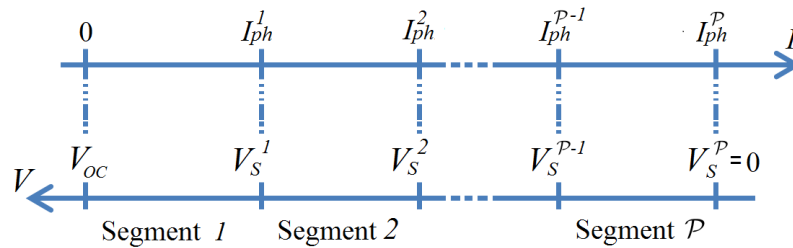


FIGURE 4.7:  $\mathcal{P}$  segments of string current.

infinite, the string current,  $I_{Str}$  changes from  $I_{ph}^{\mathcal{P}}$  to zero. The number of local peak in every segment is never more than 1. The proposed method will search the local peak of every segment basing on the I-V curve and condition of MPP. The expression of string voltage depends on the segment which the scanning string current belong to. With  $\mathcal{P}$  panel-string, the number of local peaks can be from 1 to  $\mathcal{P}$ .

### 4.3.3 Determining the Expression of String Voltage

In searching process, this expression is used to calculate string voltage from a given string current. The string voltage is equal sum of panel voltages:

$$V_{Str} = V_P^1 + V_P^2 + \dots + V_P^P = \sum_{i=1}^P V_P^i \quad (4.23)$$

The panel voltage is calculated basing on solar panel if its induced current is more than  $I_{Str}$  and basing on bypass diode if its induced current is smaller than  $I_{Str}$ .

#### 4.3.3.1 Expression of panel voltage $V_P^i$ when $I_{Str} \leq I_{ph}^i$

In this case, the current of bypass diode is zero and the diode can be ignored (see Fig. 4.9a). The panel voltage  $V_P^i$  of panel  $i$  can be obtain by using the following iterative

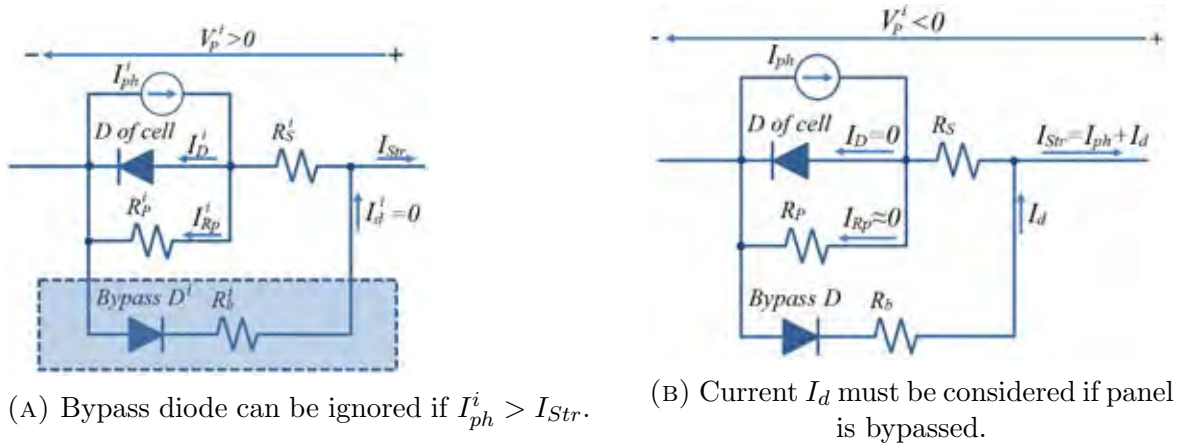


FIGURE 4.8: The role of diode in two cases.

formula:

$$V_P^i = C n V_T^i \ln \left( \frac{C(I_{ph}^i + I_S^i)R_p^i - C I_{Str} (R_p^i + R_s^i) - V_P^i}{C R_p^i I_S^i} \right) - C I_{Str} R_s^i \quad (4.24)$$

The flow chart for searching panel voltage is shown in Fig. 4.10. The initial value of panel voltage  $V_P^{i(0)}$  is chosen equal  $C \times 0.5V$ . This value is applied in right hand side of (4.24) to calculate the new value of  $V_P^i$ :  $V_P^{i(1)}$ . Similarly,  $V_P^{i(1)}$  is used to calculate  $V_P^{i(2)}$  in next calculation and so on. The iteration stops when the absolute error of two consecutive voltages,  $|V_P^{i(j+1)} - V_P^{i(j)}|$  is smaller than a certain value  $\epsilon$ . In this iterative,  $\epsilon$  is set equal 0.001V. The voltage is converged just after a few iterative times.



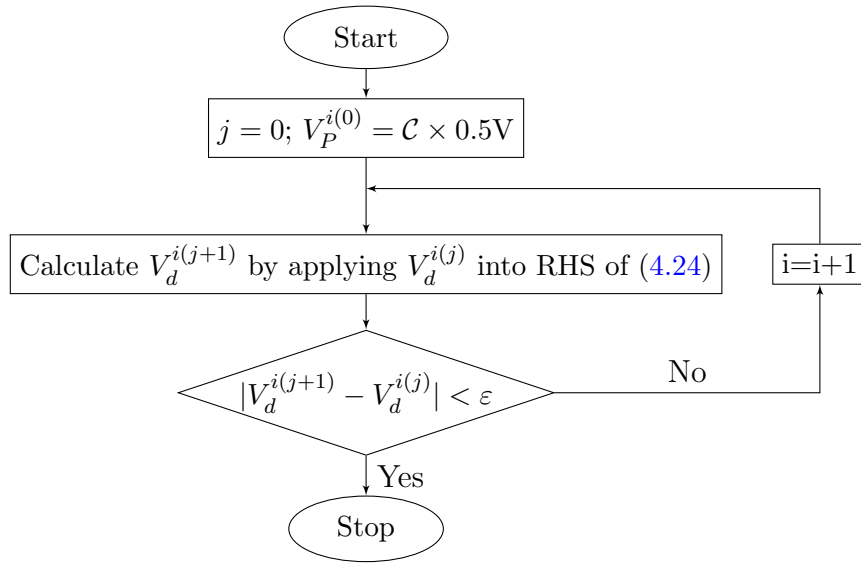


FIGURE 4.10: Algorithm for calculate panel voltage at a given current.

#### 4.3.3.2 Expression of Panel Voltage $V_P^i$ when $I_{Str} > I_{ph}^i$

The current in elements of composed component is depicted in Fig.4.9b. With a given string current and calculated photo generated current, the bypass diode current is determined by:  $I_d^i = I_{Str} - I_{ph}^i$ . The voltage of panel (or opposite of bypassed diode voltage) is calculated by:

$$V_P^i = -V_D^i = - \left( n_d V_{Td}^i \ln \left( \frac{I_d^i + I_{Sd}}{I_{Sd}} \right) + I_d^i R_b^i \right) \quad (4.25)$$

#### 4.3.3.3 The Expression of String Voltage in Segment $m$

Note that in Segment  $m$ , the current satisfies  $(I_{ph}^{(m-1)} < I_{Str} < I_{ph}^m)$ . Panels 1 to  $(m-1)$  are bypassed while panels  $m$  to  $\mathcal{P}$  deliver power to the load. String voltage is equal sum of panels voltages.

$$\begin{aligned}
 V_{Str}^m &= \sum_{i=1}^{m-1} V_P^i + \sum_{i=m}^{\mathcal{P}} V_P^i = - \sum_{i=1}^{m-1} V_D^i + \sum_{i=m}^{\mathcal{P}} V_P^i \\
 \Rightarrow V_{Str}^m &= - \sum_{i=1}^{m-1} \left( n_d V_{Td}^i \ln \left( \frac{I_d^i + I_{Sd}}{I_{Sd}} \right) + I_d^i R_b^i \right) + \\
 &\quad \sum_{i=m}^{\mathcal{P}} \left( C n V_T^i \ln \left( \frac{C(I_{ph}^i + I_S^i) R_p^i - C I_{Str} (R_p^i + R_s^i) - V_P^i}{C R_p^i I_S^i} \right) - C I_{Str} R_s^i \right) \quad (4.26)
 \end{aligned}$$

The voltage  $V_P^i$  are determined already by iterative formula (4.24). So, with a given value of string current and using the measured values, the value of string voltage will be calculated base on (4.26).

#### 4.3.4 The Expression of Voltage at Local MPP in Segment $m$ , $V_M^m$

The relationship between voltage  $V_{Str}^m$  and current  $I_{Str}$  in Segment  $m$  of string can be written as follow:

$$V_{Str}^m = \sum_{i=1}^{m-1} \left( n_d V_{Td}^i \ln \left( \frac{I_{Str} - I_{ph}^i + I_{Sd}}{I_{Sd}} \right) + (I_{Str} - I_{ph}^i) R_b^i \right) + \sum_{i=m}^{\mathcal{P}} \left( C n V_T^i \ln \left( \frac{C(I_{ph}^i + I_S^i) R_p^i - C I_{Str} (R_p^i + R_s^i) - V_P^i}{C R_p^i I_S^i} \right) - C I_{Str} R_s^i \right) \quad (4.27)$$

At a maximum power point in Segment  $m$  (if exist):

$$\begin{aligned} \frac{\partial P_{Str}^m}{\partial I_{Str}^m} \Big|_M = 0 &\Leftrightarrow \frac{\partial (V_{Str}^m I_{Str}^m)}{\partial I_{Str}^m} \Big|_M = 0 \Leftrightarrow V_{Str}^m \Big|_M + I_{Str}^m \Big|_M \frac{\partial V_{Str}^m}{\partial I_{Str}^m} \Big|_M = 0 \\ &\Leftrightarrow V_M^m = -I_{Str}^m \Big|_M \frac{\partial V_{Str}^m}{\partial I_{Str}^m} \Big|_M \Rightarrow V_M^m = - \left( I_{Str} \frac{\partial V_{Str}^m}{\partial I_{Str}} \right) \Big|_M \end{aligned} \quad (4.28)$$

On the other hand, derivative (4.27) with respect to  $I_{Str}$  leads to:

$$\begin{aligned} \frac{\partial V_{Str}^m}{\partial I_{Str}} = \sum_{i=1}^{m-1} \left( n_d V_{Td}^i \left( \frac{I_{Sd}}{I_{Str} - I_{ph}^i + I_{Sd}} \right) \left( \frac{-1}{I_{Sd}} \right) - R_b^i \right) + \sum_{i=m}^{\mathcal{P}} \left( C n V_T^i \left( \frac{-C (R_p^i + R_s^i) - \frac{\partial V_P^i}{\partial I_{Str}}}{C (I_{ph}^i + I_S^i) R_p^i - C I_{Str} (R_p^i + R_s^i) - V_P^i} \right) - C R_s^i \right) \end{aligned} \quad (4.29)$$

According to previous part, the panel voltages  $V_P^i$  can be calculated from current  $I_{Str}$  easily. Hence, the derivative  $\frac{\partial V_P^i}{\partial I_{Str}}$  is determined as a real number by the following expression:

$$\frac{\partial V_P^i}{\partial I_{Str}} = \frac{C(2R_s^i (R_p^i + R_s^i) I_{Str} - n V_T^i (R_p^i + R_s^i) - R_p^i R_s^i (I_{ph}^i + I_S^i)) + R_s^i V_P^i}{(I_{ph}^i + I_S^i) R_p^i - I_{Str} (R_p^i + R_s^i) + n V_T^i - \frac{V_P^i}{C}}$$

Let  $I_M^m$  is current of string at local MPP in Segment  $m$ . Combination of (4.28) and (4.29) leads to the formula of voltage at MPP in segment  $m$ :

$$V_M^m = - \left( I_{Str} \frac{\partial V_{Str}^m}{\partial I_{Str}} \right) \Big|_M = \sum_{i=1}^{m-1} \left( \frac{n_d V_{Td}^i I_M^m}{I_{Str} - I_{ph}^i + I_{Sd}} + R_b^i I_M^m \right) + \sum_{i=m}^{\mathcal{P}} \left( \frac{I_M^m \mathcal{C} n V_T^i \left( \mathcal{C} (R_p^i + R_s^i) + \frac{\partial V_P^i}{\partial I_{Str}} \right)}{\mathcal{C} (I_{ph}^i + I_S^i) R_p^i - \mathcal{C} I_M^m (R_p^i + R_s^i) - V_P^i} + I_M^m \mathcal{C} R_s^i \right) \quad (4.30)$$

#### 4.3.5 Searching the Local Peak Voltage in Segment $m$

The voltage and current at local MPP in segment  $m$  ( $V_M^m$  and  $I_M^m$ ) satisfy both equations (4.26) and (4.30):

$$\left\{ \begin{array}{l} V_M^m = \sum_{i=1}^{m-1} \left( n_d V_{Td}^i \ln \left( \frac{I_M^m - I_{ph}^i + I_{Sd}}{I_{Sd}} \right) + (I_M^m - I_{ph}^i) R_b^i \right) + \\ \quad \sum_{i=m}^{\mathcal{P}} \left( \mathcal{C} n V_T^i \ln \left( \frac{\mathcal{C} (I_{ph}^i + I_S^i) R_p^i - \mathcal{C} I_M^m (R_p^i + R_s^i) - V_P^i}{\mathcal{C} R_p^i I_S^i} \right) - \mathcal{C} I_M^m R_s^i \right) \\ V_M^m = \sum_{i=1}^{m-1} \left( \frac{n_d V_{Td}^i I_M^m}{I_{Str} - I_{ph}^i + I_{Sd}} + R_b^i I_M^m \right) + \\ \quad \sum_{i=m}^{\mathcal{P}} \left( \frac{I_M^m \mathcal{C} n V_T^i \left( \mathcal{C} (R_p^i + R_s^i) + \frac{\partial V_P^i}{\partial I_{Str}} \right)}{\mathcal{C} (I_{ph}^i + I_S^i) R_p^i - \mathcal{C} I_{MPP}^m (R_p^i + R_s^i) - V_P^i} + I_M^m \mathcal{C} R_s^i \right) \end{array} \right. \quad (4.31)$$

For convenience, replace  $I_M^m$  by  $I$  in (4.31). Let  $V_1, V_2$  are two functions of  $I$  as follows:

$$V_1(I) = \sum_{i=1}^{m-1} \left( n_d V_{Td}^i \ln \left( \frac{I - I_{ph}^i + I_{Sd}}{I_{Sd}} \right) + (I - I_{ph}^i) R_b^i \right) + \sum_{i=m}^{\mathcal{P}} \left( \mathcal{C} n V_T^i \ln \left( \frac{\mathcal{C} (I_{ph}^i + I_S^i) R_p^i - \mathcal{C} I (R_p^i + R_s^i) - V_P^i}{\mathcal{C} R_p^i I_S^i} \right) - \mathcal{C} I R_s^i \right) \quad (4.32)$$

$$V_2(I) = \sum_{i=1}^{m-1} \left( \frac{n_d V_{Td}^i I}{I_{Str} - I_{ph}^i + I_{Sd}} + R_b^i I \right) + \sum_{i=m}^{\mathcal{P}} \left( \frac{I \mathcal{C} n V_T^i \left( \mathcal{C} (R_p^i + R_s^i) + \frac{\partial V_P^i}{\partial I_{Str}} \right)}{\mathcal{C} (I_{ph}^i + I_S^i) R_p^i - \mathcal{C} I (R_p^i + R_s^i) - V_P^i} + I \mathcal{C} R_s^i \right) \quad (4.33)$$

In segment  $m$  ( $I_{ph}^{m-1} < I < I_{ph}^m$ ),  $V_1(I)$  is decreasing function while  $V_2(I)$  is increasing function. So, the local MPP is intersection between their curves. Again, finding the intersection by solving the two equations directly is impossible. A modified bisection method will be employed to locate the MPP. Fig. 4.11 describes the mechanism of searching the MPP which is combined of bisection and linear estimation method.

Starting with the bisection method,  $V_1$  and  $V_2$  are evaluated at Guess Bisection current

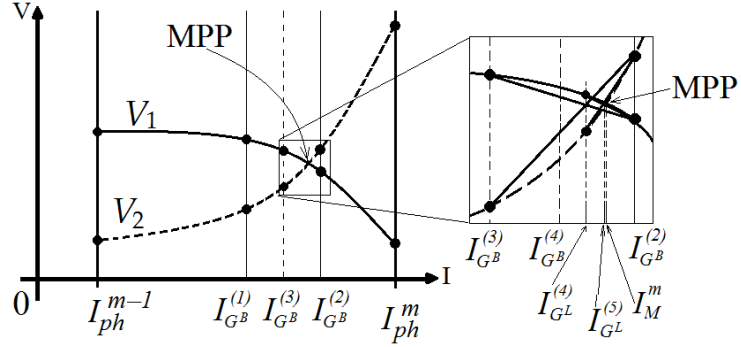


FIGURE 4.11: An MPP exist only when two relations are true: 1) at the current  $I_{ph}^{m-1}$ ,  $V_1 > V_2$  and 2) at  $I_{ph}^m$ ,  $V_1 < V_2$ . A modified bisection method is proposed to locate the local MPP in segment  $m$ .

1,  $I_{GB}^{(1)}$  that is the mid point between  $I_{ph}^{m-1}$  and  $I_{ph}^m$ . The next two guesses also follow the rule of the bisection method. But for the fourth guess, the search portion is small enough (12.5% that of the first guess). The chance that both  $V_1$  and  $V_2$  curves may be estimated to be straight lines, is high. Instead of  $I_{GB}^{(4)}$  following Bisection method, the intersection of the linearised  $V_1$  and  $V_2$  lines,  $I_{GL}^{(4)}$  is a better guess. As seen in Fig 4.11, the fifth guess is very close to the actual intersection. The search stops when at the guessed point  $|V_1 - V_2| < 0.01V$ . The modified bisection method always finishes the search faster than the conventional one. If a segment is short ( $I_{ph}^m \approx I_{ph}^{m+1}$ ), it may not content any local MPP. After a limited calculating times, if the current  $I_M^m$  still does not converge. Conclude that there is no peak in this segment.

After local peaks in all segment are found, the maximum of them corresponds to the GMPP of PV string. The tracking system drive string to this point directly without power scanning.

#### 4.4 Determining the GMPP of Parallel Strings Under Uniform Shading Condition

If a PV system has many string which are connected in parallel, the proposed determining method for single string which is presented above, can be employed to estimate the GMPP of whole system. The GMPP of each string is searching individually first. Basing on the estimation of system power at local peak voltages, an approximated of voltage at GMPP of whole system will be predicted in high accuracy.

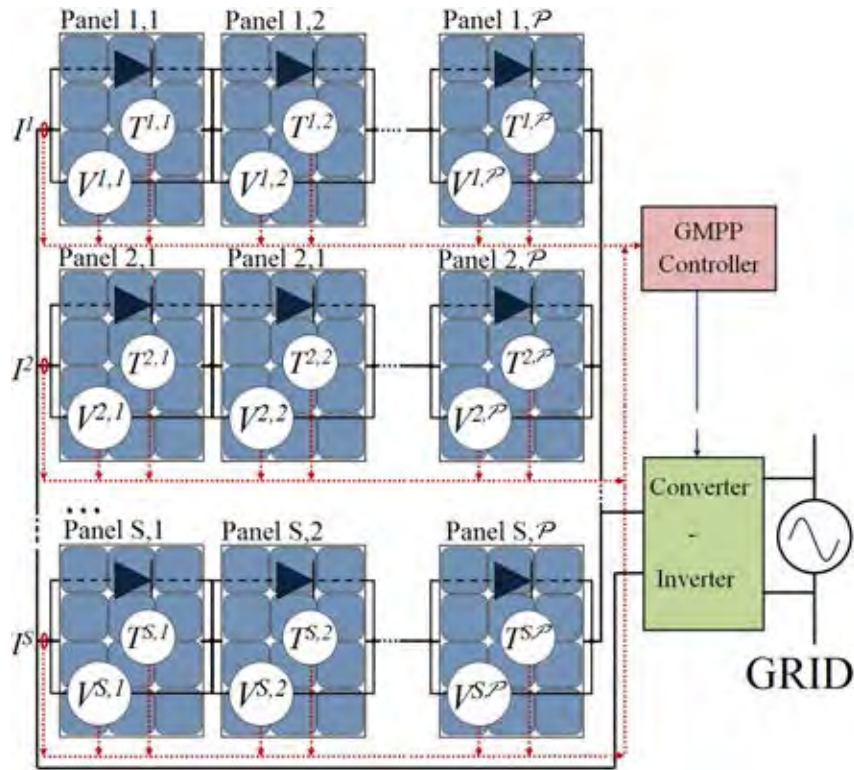


FIGURE 4.12:  $\mathcal{S}$  parallel strings in PV system share a grid-connect inverter.

Fig. 4.12 shows the structure of parallel strings for the proposed method. A PV system may be configured such that some of its strings are connected in parallel. In other words, all strings are forced to operate at the same voltage. Let  $V_P^{i,j}$  denote the voltage of Panel  $j$  in String  $i$ , so the string voltage  $V_S = \sum_{j=1}^{\mathcal{P}} V_P^{i,j}$  for  $i = 1, \dots, \mathcal{S}$ . The goal of this method is to find  $V_G$  that is a value of string voltage (also is system voltage), which maximizes the total power of all strings. Let  $I_{ph}^{i,j}$  denotes the photo-generated

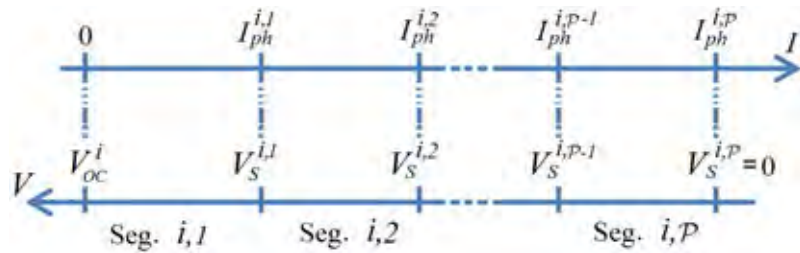


FIGURE 4.13:  $\mathcal{P}$  segments in current and voltage of string  $i$ .

current of Panel  $j$  in String  $i$ , and  $V_S^{i,j}$  is the string voltage that corresponds to the string current  $I_{ph}^{i,j}$ . Fig. 4.13 shows  $I_{ph}^{i,j}$ ,  $j = 1, \dots, \mathcal{P}$  and their corresponding  $V_S^{i,j}$  of only String  $i$ . If the string voltage is known to be  $V_S$ , the number of bypassed panel,  $m_i - 1$ , of String  $i$  is determined by the fact that  $V_S^{i,m_i} \leq V_S < V_S^{i,m_i-1}$ . Similar to (4.26), the voltage expression for String  $i$ , Segment  $m_i$  is the summation of the

bypassed and non-bypassed panels, and can be written as

$$\begin{aligned}
V_S = & - \sum_{j=1}^{m_i-1} \left( n_d V_{Td}^{i,j} \ln \left( \frac{I^i - I_{ph}^{i,j} + I_{Sd}^{i,j}}{I_{Sd}^{i,j}} \right) + (I^i - I_{ph}^{i,j}) R_b \right) \\
& + \sum_{j=m_i}^{\mathcal{P}} \left( \mathcal{C} n V_T^{i,j} \ln \left( \frac{\mathcal{C} I_{pS}^{i,j} R_p^{i,j} - \mathcal{C} I^i R_{ps}^{i,j} - V_P^{i,j}}{\mathcal{C} R_p^{i,j} I_S^{i,j}} \right) - \mathcal{C} I^i R_s^{i,j} \right) \quad (4.34)
\end{aligned}$$

where  $V_{Td}^{i,j}$ ,  $V_T^{i,j}$ ,  $V_P^{i,j}$ ,  $I_{ph}^{i,j}$ ,  $I_{pS}^{i,j}$ ,  $I_S^{i,j}$ ,  $I_{Sd}^{i,j}$ ,  $R_p^{i,j}$ ,  $R_{ps}^{i,j}$ , and  $R_s^{i,j}$  represent similar notation to those in (4.26); the superscript  $i$  and  $j$  indicate that of Panel  $j$  in String  $i$ . In (4.34) there is only one variable, which is the current of string  $i$ ,  $I^i$ . Solving this equation can be archived by the Newton-Raphson method with its initial  $(I_{ph}^{i,m_i-1} + I_{ph}^{i,m_i})/2$ . After all string currents  $I^i$  for  $i, \dots, \mathcal{S}$  which correspond to  $V_S$  are evaluated, the system power  $P_{\mathcal{S}}$  may simply calculated from:

$$P_{\mathcal{S}} = V_S \sum_{i=1}^{\mathcal{S}} I^i \quad (4.35)$$

#### 4.4.1 Voltage Scanning

The peak powers of string can be found simply by scanning. For example,  $V_S$  may be given to be 0 and then increased to the maximum of open circuit voltage of all strings with a fixed step size. For each  $V_S$ , evaluate  $I^i$ , for  $i = 1, \dots, \mathcal{S}$ , then calculate  $P_{\mathcal{S}}$  using (4.35). After the scan finishes, the voltage that yields maximum  $P_{\mathcal{S}}$ , can be used as desired value of the physical maximum power searching. In practice, the range of string voltage can be several hundred volts. Scanning with a small step size may take a long time. But a large step size may leads to the wrong global peak. Fortunately, this problem is similar to that of the P&O, so there exists a few techniques [4], [5], which can be adapted and then employed in order to speed up the GMPP searching.

To speed up the searching further, good initial points can be estimated from the prior knowledge of all the local power peaks. Let  $V_M^{i,j}$  denote the string voltage at Peak  $j$  of String  $i$ . Each and all  $V_M^{i,j}$  may be chosen as an initial points, but sometimes scanning with  $V_M^{i,j}$  as the initial point may already pass over the voltage  $V_M^{i+1,j}$ , so scanning with  $V_M^{i+1,j}$  as the initial point is unnecessary.

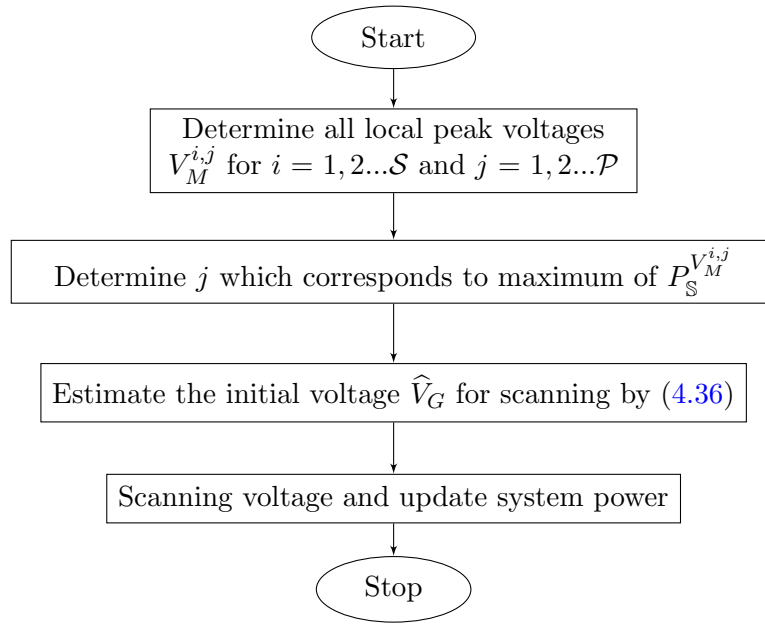


FIGURE 4.14: Algorithm for estimating the GMPP of parallel strings.

#### 4.4.2 $V_G$ Approximation

An algorithm as depicted in Fig. 4.14 is proposed to cut down the scanning time even more. First, using the technique proposed in previous parts to find all the voltages that correspond to all local string power peak, denoted by  $V_{Max}^{i,j}$ , for  $i = 1, \dots, \mathcal{S}$  and for  $j = 1, \dots, \mathcal{P}$ . If there exists a local peak in segment  $j$  of String  $i$ , then  $V_{Max}^{i,j} = V_M^{i,j}$  and  $I_{Max}^{i,j} = I_M^{i,j}$  otherwise  $V_{Max}^{i,j} = V_S^{i,j}$  and  $I_{Max}^{i,j} = I_{ph}^{i,j}$ . Calculate  $P_S$  at each of all  $V_{Max}^{i,j}$  using (4.35). Assume that  $P_S$  is maximum when  $i = I$  and  $j = J$ , an estimate of  $V_G$ , denoted by  $\hat{V}_G$ , is the average of  $V_{Max}^{i,J}$  for  $i = 1, \dots, \mathcal{S}$ , weighted by its corresponding power, and can be express as

$$\hat{V}_G = \frac{\sum_{i=1}^{\mathcal{S}} V_{Max}^{i,J} P_{Max}^{i,J}}{\sum_{i=1}^{\mathcal{S}} P_{Max}^{i,J}} \quad (4.36)$$

The scanning with  $\hat{V}_G$  as its initial is supposed to end in a few steps if  $\hat{V}_G$  is really near  $V_G$ .

## Chapter V

# EXPERIMENTS, CALCULATION AND SIMULATION RESULTS OF PROPOSED EXTRACTION METHOD

To confirm and evaluate the extraction method, three parts will be presented in this chapter. In the first part, the new proposed method is employed to determine the parameters of solar cell and panel based on experiment dataset in [20]. The results are used to compare to those by other methods. Two real panels are extracted based on measured values at its operating condition in the second part. The model *STP6 – 120/36* and *STM6 – 40/36* (Schutten manufacturer) are chosen for experiment. The last part shows more than hundred extracted set parameters of solar panels (three type polycrystalline, monocrystalline and thin film solar cell) basing on the information in product datasheet.

### 5.1 Extracting for Referenced Solar Cell and Panel.

#### 5.1.1 Extracting for Referenced Solar Cell Bases on Given Dataset.

A dataset  $(I, V)$ , which is shown in the second and third columns of Table 5.2, is measured from a 57mm-diameter commercial solar cell [20]. The dataset does not contain OC, SC, nor MPP. They can be, however, obtained by interpolated from the dataset. Their values are as follows:  $V_{OC} = 0.5727V$ ,  $I_{SC} = 0.7605A$ ,  $V_M = 0.45V$  and  $I_M = 0.69A$ . Note the dataset is acquired when  $T = 33^\circ C$ . Table 5.1 shows the extracted parameters which are calculated by the proposed method and by the other reference techniques, namely LMSA [29], CPSO [27], SA [23], PS [24], BMO [26], ABSO [28], GA [25] and Newton [20]. Although the proposed method employs only three I-V pairs, the extracted parameters are in the same range with those calculated by other techniques. Particularly, when compared with those obtained by LMSA, the discrepancy in  $n$ ,  $R_s$ , and  $I_{ph}$  is  $-0.93\%$ ,  $-0.56\%$ , and  $-0.03\%$  respectively.



TABLE 5.1: The calculated cell parameters by the proposed method and by the other reference methods. The values in parenthesis are the difference when the values obtained by the proposed methods are compared with those of other reference methods.

	Proposed	LMSA	CPSO	SA	PS	BMO	ABSO	GA	Newton
$n$	1.4935 n/a	1.4798 -0.93%	1.5033 0.65%	1.5172 1.56%	1.6000 6.66%	1.4817 -0.79%	1.4758 -1.20%	1.5751 5.18%	1.4837 -0.66%
$R_s$ (m $\Omega$ )	36.60 n/a	36.43 -0.56%	35.40 -3.49%	34.50 -6.19%	31.30 -17.04%	36.36 -0.75%	36.60 -0.09%	29.90 -22.52%	36.40 -0.64%
$R_p$ ( $\Omega$ )	62.574 n/a	53.326 -17.3%	59.012 -6.0%	43.103 -45.2%	64.103 2.4%	53.872 -16.2%	52.290 -19.7%	42.373 -47.7%	53.763 -16.4%
$I_S$ ( $\mu$ A)	0.3635 n/a	0.3185 -14.1%	0.4000 9.1%	0.4798 24.2%	0.9980 63.6%	0.3248 -11.9%	0.3062 -18.7%	0.8087 55.0%	0.3223 -12.8%
$I_{ph}$ (A)	0.7610 n/a	0.7608 -0.03%	0.7607 -0.04%	0.762 +0.13%	0.7617 +0.09%	0.76077 -0.03%	0.7608 -0.03%	0.7619 +0.12%	0.7608 -0.03%

Sets of calculated parameters are applied to the solar cell model in *MATLAB – Simulink* for simulation. The simulated I-V curves and the measured points are plotted on Fig. 5.1. The curve created from parameters extracted with the proposed method are closed to all measured points, particularly around the MPP (zoomed part).

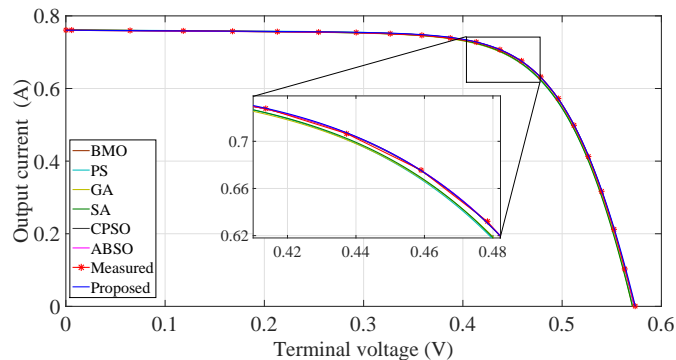


FIGURE 5.1: I-V curves of a cell modeled by the proposed and three other reference methods.

Table 5.2 shows the discrepancy in current between experiment and calculation on 20 points. Given  $V$ , the cell modeled by the proposed method estimate the current with MAE at 0.148%. For this dataset, the results from the proposed method agree very much with the values by experiment, as reflected by the MAE of all 20 points and that of the four points around the MPP. This means the proposed extracted method generates sets of parameters which are very reliable to compute the I-V pairs that are close to the MPP. This high accuracy depends on quality of the estimated  $I_M$

and  $V_M$ . For example, if the I-V pair at #13 (2.0% difference in  $V$  and -2.1% in  $I$  when compared to the interpolated point), which yields the highest product among the measured points is used as the MPP, the MAE would increase to 4.56%.

TABLE 5.2: The errors when the measured current in the third column from left is compared with those predicted by the proposed method and other reference methods. The measurements was performed at 20 different I-V pairs.

Measured values			Absolute of current error (%)								
#	$V(V)$	$I(A)$	Proposed	LMSA	CPSO	SA	PS	BMO	ABS0	GA	Newton
1	0.0057	0.7605	0.012	0.046	0.046	0.128	0.097	0.060	0.045	0.122	0.042
2	0.0646	0.7600	0.066	0.125	0.112	0.064	0.041	0.163	0.128	0.059	0.121
3	0.1185	0.7590	0.053	0.128	0.103	0.076	0.060	0.165	0.133	0.070	0.123
4	0.1678	0.7580	0.033	0.009	0.046	0.227	0.214	0.017	0.002	0.219	0.016
5	0.2132	0.7570	0.008	0.117	0.071	0.111	0.097	0.148	0.126	0.100	0.109
6	0.2545	0.7555	0.061	0.059	0.006	0.175	0.152	0.070	0.070	0.156	0.049
7	0.2924	0.7540	0.080	0.049	0.006	0.183	0.137	0.057	0.060	0.149	0.035
8	0.3269	0.7505	0.247	0.114	0.165	0.333	0.242	0.160	0.103	0.276	0.139
9	0.3585	0.7465	0.236	0.111	0.149	0.301	0.135	0.154	0.102	0.210	0.158
10	0.3873	0.7385	0.317	0.217	0.233	0.360	0.085	0.294	0.212	0.231	0.313
11	0.4137	0.7280	0.004	0.085	0.098	0.007	0.418	0.114	0.084	0.163	0.106
12	0.4373	0.7065	0.096	0.070	0.025	0.078	0.482	0.089	0.076	0.075	0.434
13	0.4590	0.6755	0.049	0.027	0.094	0.083	0.773	0.048	0.015	0.162	0.641
14	0.4784	0.6320	0.250	0.189	0.255	0.280	1.041	0.283	0.175	0.182	0.976
15	0.4960	0.5730	0.276	0.179	0.206	0.258	1.003	0.284	0.168	0.145	1.787
16	0.5119	0.4990	0.038	0.128	0.190	0.110	0.496	0.194	0.033	0.961	3.376
17	0.5265	0.4130	0.005	0.159	0.384	0.269	0.027	0.288	0.589	1.734	5.538
18	0.5398	0.3165	0.218	0.314	0.808	0.603	0.850	0.720	0.058	2.846	9.498
19	0.5521	0.2120	0.330	0.053	1.048	0.580	1.844	0.250	0.074	3.828	17.361
20	0.5633	0.1035	0.580	1.262	1.073	0.483	3.469	7.182	1.494	4.307	41.975
MAE (%)			<u>0.148</u>	0.172	0.256	0.236	0.583	0.537	0.187	0.800	4.140
MAE of 4 points (%)			0.100	<u>0.093</u>	0.118	0.112	0.678	0.134	0.088	0.145	0.539

### 5.1.2 Extracting for Referenced Solar Panel Bases on Given Dataset.

This repeats the previous set up. The only difference is the source of the dataset. Measurement is performed on a panel composed of 36 polycrystalline silicon cells connected in series [20], i.e.,  $\mathcal{C} = 36$ . The inputs to the proposed method are as follows:  $V_{OC} = 16.78V$ ,  $I_{SC} = 1.0315A$ ,  $V_M = 12.64V$ ,  $I_M = 0.913A$ , and  $T = 45^\circ C$ . For convenience in comparison,  $n$ ,  $R_s$ , and  $R_p$  are multiplied by  $\mathcal{C}$ .

Similar to Table 5.1, parameters extracted by the proposed approach are shown and compared with those obtained by six other methods in Table 5.3. Apply these calculated sets into the solar cell model in *Simulink* to obtain the I-V curves. Fig. 5.2 shows the I-V curves of four models (of the same panel) together with the measured points.

TABLE 5.3: A panel parameters extracted by the proposed and other methods. The panel is composed of 36 cells ( $\mathcal{C} = 36$ ). The figures in parenthesis are the difference when the values obtained by the proposed methods are compared with those of other methods.

	Proposed	PS	Newton	ref [21]	SA	MPCOA	GA
$C_n$	47.1816 (n/a)	48.289 (+2.29%)	48.45 (+2.62%)	48.1862 (+2.08%)	48.8211 (+3.36%)	48.5065 (+2.73%)	48.5862 (+2.98%)
$\mathcal{C}R_s(\Omega)$	1.2744 (n/a)	1.2053 (-5.73%)	1.2057 (-5.70%)	1.203 (-5.94%)	1.1989 (-6.30%)	1.20295 (-5.94%)	1.1968 (-6.09%)
$\mathcal{C}R_p(\Omega)$	715.824 (n/a)	714.29 (-0.26%)	555.56 (-28.9%)	555.556 (-28.8%)	833.333 (+14.1%)	849.693 (+15.8%)	555.556 (-22.4%)
$I_S(\mu A)$	2.3326 (n/a)	3.1756 (+26.6%)	3.2875 (+29.0%)	3.076 (+24.2%)	3.6642 (+36.3%)	3.3737 (+30.9%)	3.436 (+47.3%)
$I_{ph}(A)$	1.0333 (n/a)	1.0313 (-0.19%)	1.0318 (-0.15%)	1.0339 (+0.06%)	1.0331 (-0.02%)	1.03188 (-0.14%)	1.0441 (+1.05%)

TABLE 5.4: The errors when the measured current in the third column from left is compared with those predicted by the proposed method and other reference methods. The measurements was scanned at 21 different I-V pairs along the I-V curve.

#	Measured values		Absolute of current error (%)						
	V(V)	I(A)	Proposed	PS	Newton	ref [10]	SA	MPCOA	GA
1	0.1248	1.0315	0.016	0.207	0.213	0.008	0.006	0.119	0.988
2	1.8093	1.0300	0.097	0.294	0.367	0.160	0.062	0.168	0.845
3	3.3511	1.0260	0.071	0.123	0.258	0.048	0.137	0.037	0.966
4	4.7622	1.0220	0.254	0.055	0.138	0.076	0.341	0.247	1.099
5	6.0538	1.0180	0.425	0.222	0.023	0.194	0.531	0.443	1.224
6	7.2364	1.0155	0.404	0.196	0.099	0.122	0.521	0.440	1.155
7	8.3189	1.0140	0.187	0.041	0.383	0.153	0.292	0.223	0.876
8	9.3097	1.0100	0.010	0.250	0.636	0.395	0.082	0.029	0.626
9	10.2163	1.0035	0.309	0.600	1.028	0.769	0.281	0.307	0.237
10	11.0449	0.9880	0.334	0.668	1.139	0.855	0.374	0.368	0.135
11	11.8018	0.9630	0.312	0.675	1.189	0.869	0.418	0.371	0.102
12	12.4929	0.9255	0.205	0.587	1.144	0.780	0.378	0.288	0.174
13	13.1231	0.8725	0.057	0.269	0.867	0.451	0.115	0.008	0.495
14	13.6983	0.8075	0.012	0.286	0.919	0.446	0.188	0.035	0.505
15	14.2221	0.7265	0.151	0.016	0.648	0.113	0.061	0.194	0.868
16	14.6995	0.6345	0.189	0.198	0.487	0.107	0.192	0.309	1.154
17	15.1346	0.5345	0.056	0.115	0.575	0.076	0.067	0.226	1.240
18	15.5311	0.4275	0.140	0.270	0.405	0.295	0.187	0.311	1.666
19	15.8929	0.3185	0.031	0.122	0.735	0.004	0.232	0.057	1.738
20	16.2229	0.2085	0.144	0.775	1.222	0.496	0.906	0.302	2.030
21	16.5241	0.1010	0.297	5.153	5.002	4.438	5.287	0.990	0.520
MAE (%)			<u>0.176</u>	0.530	0.832	0.517	0.508	0.261	0.888
MAE of 4 points (%)			<u>0.147</u>	0.454	1.030	0.636	0.275	0.175	0.319

With similarity to the cell model, the I-V curve of panel, modeled with the proposed methods, is closed to the measured points, especially the points near the MPP (see the enlarged part). To evaluate the accuracy of the proposed method and the other

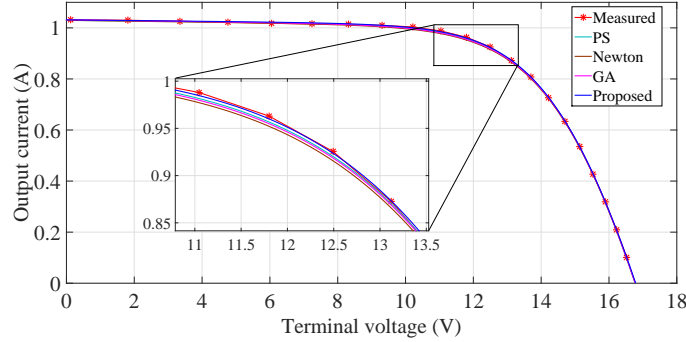


FIGURE 5.2: The IV curves of a panel modeled by the proposed and three other methods.

referenced techniques, the current errors on 21 measured points are analyzed and shown in Table 5.4. MAE of the model using calculated parameters by proposed method is 0.176%. This values is smaller than that of the models calculated by all reference methods.

## 5.2 Extraction for Real Solar Panels Basing on Measured values.

A simple load scanning experiment is set up to measure I-V datasets from two panels. Fig. 5.3 depicts the measurements while a monocrystalline panel supplies a variable load. Only an ampere-meter, a voltage-meter, a thermometer, a variable load, together with the panel of interest are required for the experiment. With measured  $T$ ,  $V_{OC}$ ,  $I_{SC}$ , and the I-V pair that yields highest product, the proposed algorithm can extract panel parameters. Then their mathematical models can be formulated. The models may calculate  $I$  when  $V$  is given. The results from calculation and from experiment will be compared in order to verify the correctness of the proposed methods.

### 5.2.1 Extracting for a Polycrystalline Panel

A real solar panel, model *SPT6 – 120/36* of Solar Schutten, is chosen to evaluate the proposed method in practice. This panel content 36 cell in series. Size of each cell is 156mm×156mm. The schematic in Fig. 5.4 is used for measurement. List of measured I-V pairs are shown in Table 5.5 (left). The measurement values which use in calculation are  $V_{OC} = 19.21V$ ,  $I_{SC} = 7.48A$ ,  $V_M = 14.93V$ ,  $I_M = 6.83A$  and

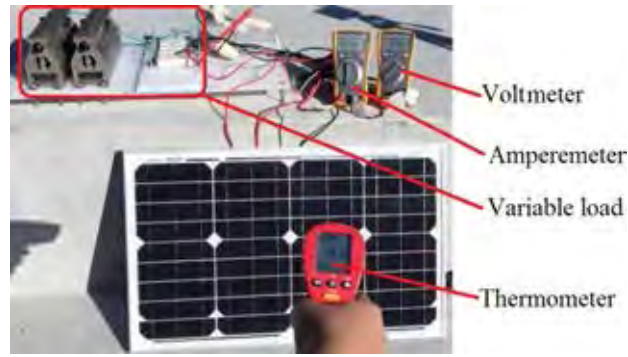


FIGURE 5.3: Experiment for acquiring an I-V dataset from a solar panel.

temperature  $T = 55^\circ\text{C}$ . The variable load is constructed as in Fig. 5.5. According

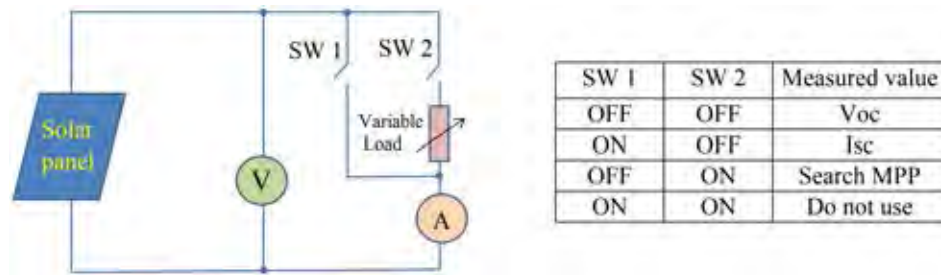


FIGURE 5.4: Schematic for measuring the current and voltage of solar panel by scanning load (left) and status of switches for measurements (right).



FIGURE 5.5: The variable load is used in scanning. The range of resistance is from 0 to  $13.8\ \Omega$ . This range ensures that the MPP is tracked.

to its datasheet, at STC,  $I_{SC}$  and  $V_{OC}$  can yield maximum 8A and 24V, respectively. Switch  $SW_s$  is controlled to closed or open in order to scan the full range of load.

Table 5.6 presents the parameters which were extracted by the proposed method. The determined set of parameters is applied to the solar cell model of *MATLAB – Simulink*. The simulated I-V curve and measured points are plotted in Fig. 5.6 for evaluating the accuracy of the calculated parameters. The curves are close to all measured points, which means the determined parameters are accurate and highly reliable. In detail, the maximum power point of the simulation is  $M_M^{sim}$  with  $V_M^{sim} = 14.9305\text{V}$  and  $I_M^{sim} = 6.8331\text{A}$ . The error between the measured and simulated panel voltage is  $0.0005\text{V} \approx 0.0034\%$ . Table 5.5 shows the current error at the same voltages between values by

TABLE 5.5: Measured I-V pairs and the absolute difference between the measured and the calculated current. The experiment is performed on polycrystalline, model *STP6 – 120/36* by Schutten Solar.

	Measured		Calculated	
	V (V)	I (A)	I(A)	Error  (%)
1	17.65	3.83	3.8360	0.157
2	17.41	4.29	4.2800	0.233
3	17.25	4.56	4.5541	0.042
4	17.10	4.79	4.7940	0.063
5	16.90	5.07	5.0930	0.454
6	16.76	5.27	5.2870	0.323
7	16.34	5.75	5.7940	0.765
8	16.08	6.00	6.0550	0.917
9	15.71	6.36	6.3691	0.143
10	15.39	6.58	6.5881	0.123
11	14.93	6.83	6.8334	0.050
12	14.58	6.97	6.9748	0.069
13	14.17	7.10	7.1014	0.020
14	13.59	7.23	7.2265	0.048
15	13.16	7.29	7.2898	0.003
16	12.74	7.34	7.3345	0.075
17	12.36	7.37	7.3643	0.077
18	11.81	7.38	7.3947	0.199
19	11.17	7.41	7.4174	0.100
20	10.32	7.44	7.4352	0.065
21	9.740	7.42	7.4426	0.305
22	9.060	7.45	7.4487	0.017
			MAE (%)	0.193

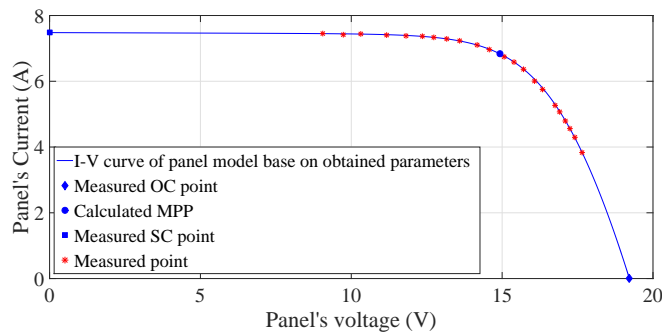


FIGURE 5.6: I-V curve is produced based on the calculated parameters and several measured points.

experiment and by calculation based on extracted parameters. The average error is 0.193%, this value, again confirms the correctness of proposed method.

### 5.2.2 Extracting for a Monocrystalline Panel Model

Solar panel model *STM6 – 40/36* manufactured also by Solar Schutten is chosen for extracting the parameters by the proposed method. The scanning load is described in Fig. 5.3. The panel is composed of 36 monocrystalline cells in series. Each cell has

TABLE 5.6: The parameters of real solar panel are calculated by proposed method using three measured points.

$n$	$R_s \Omega$	$R_p \Omega$	$I_S \mu A$	$I_{ph} A$
1.2072	0.0049	9.745	1.2	7.4828

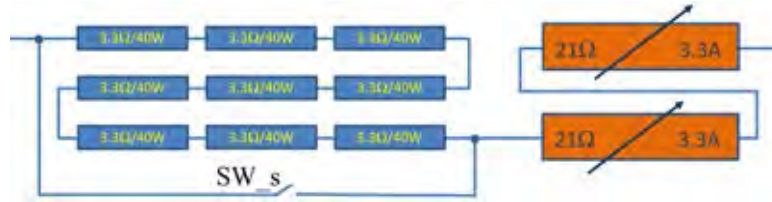


FIGURE 5.7: The variable load is used in scanning. The load is scanned from 0 to 71.7  $\Omega$ . This range ensures that the MPPs of single panels and 4 panels-string are tracked.

the size of 38mm $\times$ 128mm. Again, the schematic in Fig. 5.4 is used for measurement. However, the variable load is reconstructed as in Fig. 5.7. It includes 9 resistors 3.3 $\Omega$ -40W, two variable resistors 21 $\Omega$  (3.3A) which are connected in series. So the load can be scanned from 0 $\Omega$  to 71.7  $\Omega$ . Switch  $SW_s$  permits to scan load to 0 $\Omega$  when it is closed. At STC, the short circuit current of this panel is 2.36A lower but the open voltage is 21.6V higher compare with those of the polycrystalline panel in previous experiment. The load can track the MPPs of string 4 mono panels  $STM6 - 40/36$ . It can operate at the maximum current 2.5A and maximum voltage 100V. The maximum power is 700W, but this values is never yielded with four these panels.

Basing on the measurements, the input data for extraction are determined as:  $V_{OC} = 21.02V$ ,  $I_{SC} = 1.663A$ ,  $V_M = 16.98V$ ,  $I_M = 1.50A$ , and temperature, read from an IR thermometer, 51 $^{\circ}C$ . List of other measured I-V pairs are shown in Table 5.7 (left). After calculation, the extracted parameters are:  $n = 1.4986$ ,  $R_s = 4.87m\Omega$ ,

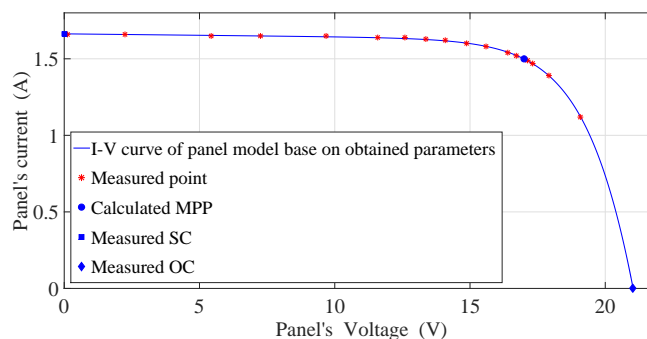


FIGURE 5.8: I-V curve of the monocrystalline panel, modeled by the proposed method, and some masured points.

TABLE 5.7: Measured I-V pairs and the absolute difference between the measured and the calculated current. The experiment is performed on a monocrystalline, model *STM6 – 40/36* by Schutten Solar.

	Measured		Calculated	
	$V$ (A)	$I$ (V)	$I$ (A)	$ Error $ (%)
1	0.118	1.663	1.6627	0.012
2	2.237	1.661	1.6590	0.120
3	5.434	1.653	1.6531	0.006
4	7.260	1.650	1.6497	0.018
5	9.680	1.645	1.6445	0.030
6	11.59	1.640	1.6383	0.104
7	12.60	1.636	1.6330	0.183
8	13.37	1.629	1.6267	0.141
9	14.09	1.619	1.6171	0.117
10	14.88	1.597	1.6030	0.376
11	15.59	1.581	1.5820	0.063
12	16.40	1.542	1.5432	0.078
13	16.71	1.524	1.5225	0.098
14	16.98	1.500	1.5006	0.040
15	17.13	1.485	1.4867	0.114
16	17.32	1.465	1.4674	0.164
17	17.91	1.388	1.3897	0.122
18	19.08	1.118	1.1208	0.250
			MAE (%)	0.113

$R_p = 15.41\Omega$ ,  $I_S = 1.4142\mu\text{A}$ , and  $I_{ph} = 1.6635\text{A}$ . They are applied into solar cell models in *MATLAB – Simulink* to obtain the I-V curve. The curves of solar model by this method as well as the others and the measured pairs are presented in Fig. 5.8. Its shows that all measured points are very near the curve.

Table 5.7 (right) shows the calculated current when  $V$  is given and absolute of error at 18 different measured point. At the MPP, discrepancy between the measured and calculated is only 0.040%. The maximum of the absolute error is 0.376% and MAE = 0.113%. Very low discrepancy between the measured and calculated values displayed in Table 5.5 and Table 5.7 suggests that the mathematical model built form calculated parameters is very close to the real panel.

### 5.3 Extracting for Solar Panels Basing on Product Datasheet.

#### 5.3.1 Extracting for Polycrystalline Solar Panels

The datasheet of series panels TS xxxP-60 which are produced by H&T Power GmbH manufacturer, are used for extraction. Table 5.8 shows the input values of four panels (left) and the corresponding extracted parameters by proposed method (right). The



power of the panels are 240W ( $\eta = 12.96\%$ ), 245W ( $\eta = 13.17\%$ ), 250W ( $\eta = 13.45\%$ ) and 255W ( $\eta = 13.73\%$ ). In next step, these parameter sets are applied in the solar cell models for load scanning simulation by *MATLAB – Simulink*. The obtained I-V

TABLE 5.8: The input values and calculated parameters of the polycrystalline silicon solar cells, Series TS 240-255P-60, H&T Power GmbH manufacturer.

Peak power of panel (W)		240	245	250	255
Input data of panel	$V_{oc}(V)$	37.23	37.34	37.42	37.53
	$I_{sc}(A)$	8.66	8.82	8.98	9.13
	$V_M(V)$	29.98	30.11	30.31	30.51
	$I_M(A)$	8.01	8.14	8.25	8.36
	$x$	60	60	60	60
Calculated parameters of each cell	$n$	1.4383	1.4809	1.5569	1.6036
	$R_s(\Omega)$	0.00293	0.00257	0.00181	0.00129
	$R_p(\Omega)$	15.3822	12.3558	8.0948	5.9324
	$I_s(A)$	4.36E-07	6.85E-07	1.50E-06	2.28E-06
	$I_{ph}(A)$	8.6616	8.8218	8.9820	9.1321

curves of four models are drawn in Fig. 5.12. The zoomed areas (a) and (c) of this figure show that, the curves of panel models are very close to *SC* and *OC* points by datasheet. In the zoomed area (b), the calculated MPP points (mark by  $\times$ ) and the given maximum power points (mark by  $\circ$ ) are closed together too. The voltage errors at these points are smaller than  $0.015V (\approx 0.05\%)$  for all panels. According to values

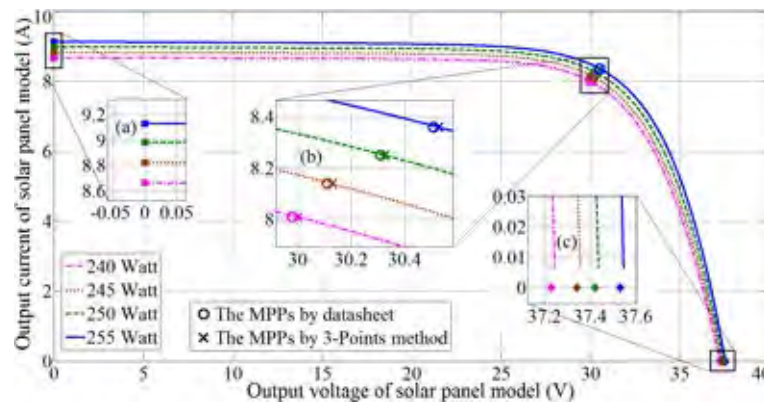


FIGURE 5.9: The I-V curves of calculated polycrystalline silicon solar panel (60 cells) basing on datasheet of Series TS 235-255P-60, H&T Power GmbH.

in TABLE 5.8, Fig. 5.10 performs the shift of parameters in order to increase the efficient of solar panel. Different from the slightly increase of  $n$  and  $I_{ph}$ , the saturation current  $I_s$  rises strongly while both resistances  $R_s$  and  $R_p$  decrease rapidly.

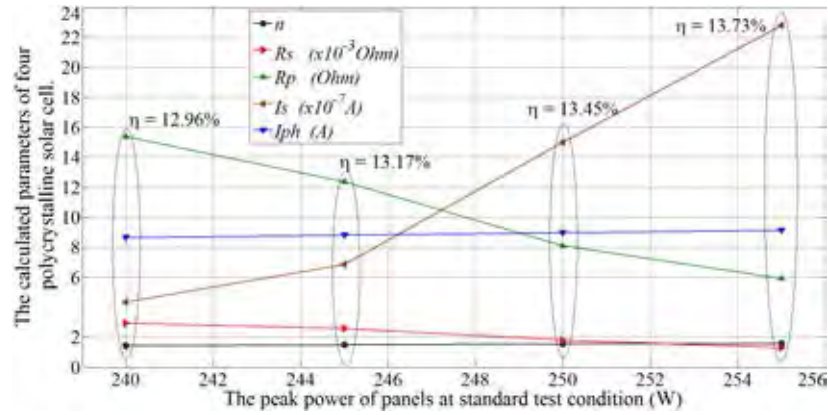


FIGURE 5.10: The relationship of parameters and the efficiency of polycrystalline solar cell.

### 5.3.2 Extracting for Monocrystalline Solar Panels

The datasheet of Series TS xxxD-60 (H&T Power GmbH) are chosen for extraction. The power and efficient of four panels are 250W ( $\eta = 15.4\%$ ), 255W ( $\eta = 15.71\%$ ), 260W ( $\eta = 16.02\%$ ) and 265W ( $\eta = 16.33\%$ ). The input values and calculated parameters of these panels are shown in TABLE 5.9. Basing on the results in Table

TABLE 5.9: The input values and calculated parameters of monocrystalline silicon solar cells, Series TS 250-265D-60, H&T Power GmbH manufacturer.

Peak power of panel (W)		250	255	260	265
Input data of panel	$V_{oc}(V)$	37.59	37.73	37.91	38.1
	$I_{sc}(A)$	8.79	8.93	9.06	9.19
	$V_M(V)$	30.59	30.69	30.79	30.9
	$I_M(A)$	8.17	8.31	8.44	8.58
	$x$	60	60	60	60
Calculated parameters of each cell	$n$	1.3931	1.3749	1.3584	1.3217
	$R_s(\Omega)$	0.00251	0.00265	0.00286	0.00317
	$R_p(\Omega)$	21.1324	23.9801	27.5759	36.0159
	$I_s(A)$	2.17E-07	1.64E-07	1.23E-07	6.88E-08
	$I_{ph}(A)$	8.7910	8.9310	9.0609	9.1908

6, the techniques which are applied to optimize the efficiency of monocrystalline solar cell, make the effects to parameters as: Decrease  $n$  and  $I_s$ , increase  $R_s$ ,  $I_{ph}$  and  $R_p$  (see Fig.5.11). Those changes are contrary to the changes in polycrystalline solar cell.

Using the calculated values in simulation, the I-V curves are drawn in Fig. 5.12. Similar to poly solar panels, the obtained curves from these panels are closed to three given points  $OC$ ,  $SC$  and  $M$  from corresponding datasheet. At maximum power point, the error between measured and calculated voltages are smaller than 0.016V ( $\approx 0.052\%$ )

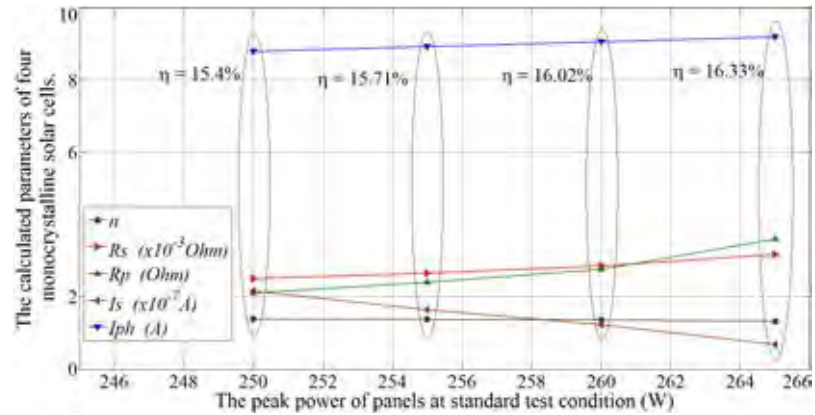


FIGURE 5.11: The relationship of parameters and the efficiency of monocrystalline silicon solar cell.

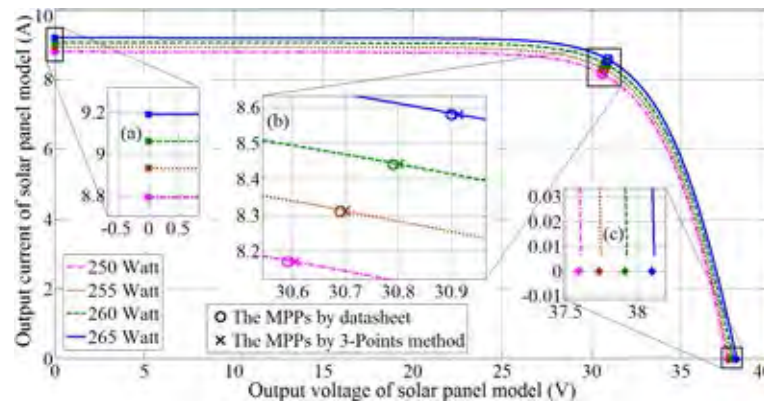


FIGURE 5.12: The I-V curves of calculated monocrystalline silicon solar panel (60 cells) basing on datasheet of Series TS 250-265D-60, H&T Power GmbH

### 5.3.3 Extracting for Thin Film Solar Panels

Datasheet of Series 4<sup>TM</sup> which produced by First Solar Company, US are used for calculation. These are TeCd thin film solar panels, each of them consist of 216 single thin film cells in series. The peak power at standard test condition of four chosen panels are 105W ( $\eta = 14.24\%$ ), 107.5W ( $\eta = 14.93\%$ ), 110W ( $\eta = 15.28\%$ ) and 12.5W ( $\eta = 15.63\%$ ). The input data and the calculated results are shown in TABLE 5.10.

Different from the panels are made by poly and mono crystal technologies, the thin film has the emission coefficient is closed to 1 and sometimes it is lower than 1. So, calculating for the thin film model by the proposed method, the initial value of  $n$  is reduced to 0.8. Fig. 5.13 shows the change of parameters in order to optimize the panels efficiency. Values in Table 5.8, Table 5.9 and Table 5.10 shows that: The efficiency of polycrystalline silicon solar cell can be optimized by increasing  $I_S$ ,  $I_{ph}$ ,  $n$  and decreasing  $R_s$  and  $R_p$ . In contrary, the efficiency of monocrystalline silicon and TeCd thin film solar cells can be optimized be reducing  $I_S$ ,  $I_{ph}$ ,  $n$  and increasing  $R_s$

TABLE 5.10: The input values and calculated parameters of TeCd thin film solar cells, Series 4<sup>TM</sup> (FS 4102-2 to FS 4112-2), First Solar manufacturer.

Peak power of panel (W)		105	107.5	110	112.5
Input data of panel	$V_{oc}(V)$	86	86.6	87.2	87.7
	$I_{sc}(A)$	1.74	1.75	1.75	1.75
	$V_M(V)$	67.8	68.6	69.4	70.2
	$I_M(A)$	1.55	1.57	1.59	1.6
	$x$	216	216	216	216
Calculated parameters of each cell	$n$	1.1965	1.1629	1.085	1.0441
	$R_s(\Omega)$	0.00666	0.00668	0.00801	0.00802
	$R_p(\Omega)$	8.3789	10.319	17.5298	23.6001
	$I_s(A)$	3.99E-06	2.53E-06	8.81E-07	4.60E-07
	$I_{ph}(A)$	1.7414	1.7511	1.7508	1.7506

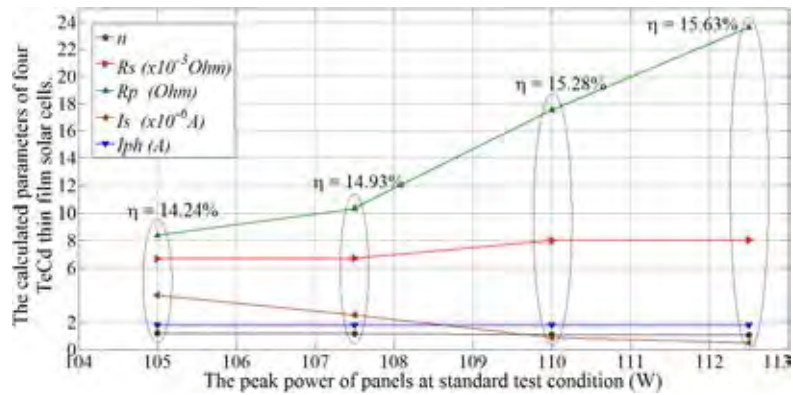


FIGURE 5.13: The relationship of parameters and the efficiency of monocrystalline silicon solar cell.

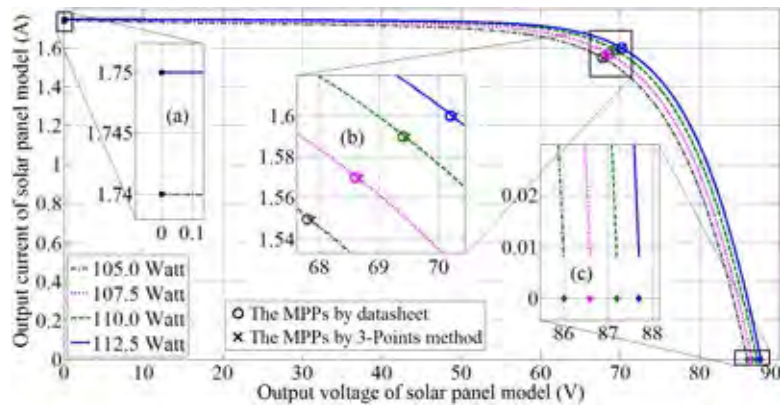


FIGURE 5.14: The I-V curves of calculated thin film CdTe solar panel (216 cells). Panel peak powers are 105W, 107.5W, 110W and 112.5W (Series 4<sup>TM</sup>, First Solar.)

and  $R_p$ . The calculated parameters are also applied in solar cell models for simulation. The simulative curve are closed to the given points from product datasheet (Fig. 5.14). At the maximum power point, the errors of voltages are still very small. All of them are lower than 0.07V ( $\approx 0.1\%$ )

Information from several datasheet is only the input for the extraction. This is to

check that extracted parameters are all within valid ranges. Table 5.11 shows the name, manufacturer and type of solar panels which collected from product datasheets. Table 5.12, Table 5.13 and Table 5.14 show the extracted parameters at STC of 20 solar panels using their datasheets. These datasheets are provided by some manufacturers as follows : H&T Power GmbH, Solarworld, Scheuten, Sharp, Kyocera and First Solar. The chosen panels vary in size and the number of cells. The extracted parameters from all datasheets are in their valid ranges.

TABLE 5.11: Code of solar panel models (right column).

Manufacturer	Model	Type	Model's Code
H&T GmbH	TS-300BP-72	Poly	P01
H&T GmbH	TS-300P-72	Poly	P02
Nemy	JB-255P-60	Poly	P03
Nemy	JB-300P-72	Poly	P04
SCHEUTEN	Goldline-210P6-54	Poly	P05
SCHEUTEN	i40-240P6-60	Poly	P06
Sharp	ND-R240-A5	Poly	P07
Kyocera	KD100-36	Poly	P08
Solarworld	SW-50-RMA	Poly	P09
Solarworld	Protect-SW-255	Poly	P10
Solarworld	Plus-SW-270	Mono	M01
H&T GmbH	TS-245D-60	Mono	M02
H&T GmbH	TS-260D-60	Mono	M03
H&T GmbH	TS-200D-72	Mono	M04
H&T GmbH	TS-305D-72	Mono	M05
Fisrt Solar	FS-4105-2	TF	T01
Fisrt Solar	FS-4107-2	TF	T02
Fisrt Solar	FS-375	TF	T03
Fisrt Solar	FS-377	TF	T04
Fisrt Solar	FS-380	TF	T05

Within polycrystalline panels:  $1.1254 \leq n \leq 1.6199$ ;  $1.10\text{m}\Omega \leq R_s \leq 5.24\text{m}\Omega$ ;  $5.857\Omega \leq R_p \leq 129.431\Omega$ ;  $0.0044 \mu\text{A} \leq I_S \leq 3.3440 \mu\text{A}$ .

Within monocrystalline panels:  $1.2809 \leq n \leq 1.5118$ ;  $1.80\text{m}\Omega \leq R_s \leq 5.55\text{m}\Omega$ ;  $14.772\Omega \leq R_p \leq 57.508\Omega$ ;  $0.0223 \mu\text{A} \leq I_S \leq 0.4900 \mu\text{A}$ .

Within polycrystalline panels:  $1.1606 \leq n \leq 1.2425$ ;  $2.32\text{m}\Omega \leq R_s \leq 6.77\text{m}\Omega$ ;  $4.354\Omega \leq R_p \leq 10.445\Omega$ ;  $2.4920 \mu\text{A} \leq I_S \leq 8.5610 \mu\text{A}$ .

The parameters of more than 100 solar panel models are extracted and presented at Appendix A and at [38].

TABLE 5.12: The parameters of polycrystalline panels obtained by using only the information in their datasheet.

Model's Code	Given values in datasheet					Extracted parameters by proposed method				
	$C$	$V_m$ (V)	$I_m$ (A)	$V_{OC}$ (V)	$I_{SC}$ (A)	$n$	$R_s$ (m $\Omega$ )	$R_p$ ( $\Omega$ )	$I_S$ ( $\mu$ A)	$I_{ph}$ (A)
P01	72	36.81	8.15	45.04	8.88	1.5760	1.10	6.408	1.7020	8.8815
P02	72	36.30	8.26	44.82	8.88	1.3596	2.94	24.615	0.1600	8.8811
P03	60	30.50	8.39	37.80	8.95	1.2163	4.14	71.112	0.0156	8.9505
P04	72	36.50	8.12	45.30	8.79	1.4793	2.77	14.058	0.5610	8.7917
P05	54	27.30	7.70	33.30	8.17	1.1254	3.68	129.431	0.0044	8.1702
P06	60	29.90	8.03	37.00	8.58	1.2268	3.90	55.823	0.0270	8.5806
P07	60	30.40	7.90	37.20	8.57	1.5108	1.44	9.129	0.9756	8.5714
P08	36	17.70	7.91	22.10	8.68	1.6199	2.17	5.857	3.3440	8.6832
P09	36	18.20	2.75	22.10	2.95	1.3412	5.24	65.649	0.0534	2.9502
P10	60	30.90	8.32	38.00	8.88	1.2554	3.46	57.404	0.0261	8.8805
Minimum value						1.1254	1.1	5.857	0.0044	2.9502
Maximum value						1.6199	5.24	129.431	3.3440	8.8815

TABLE 5.13: The parameters of monocrystalline panels obtained by using only the information in their datasheet.

Model's Code	Given values in datasheet					Extracted parameters by proposed method				
	$C$	$V_m$ (V)	$I_m$ (A)	$V_{OC}$ (V)	$I_{SC}$ (A)	$n$	$R_s$ (m $\Omega$ )	$R_p$ ( $\Omega$ )	$I_S$ ( $\mu$ A)	$I_{ph}$ (A)
M01	60	30.90	8.81	39.20	9.44	1.2809	5.55	57.508	0.0223	9.4409
M02	60	30.49	8.04	37.51	8.64	1.3674	2.76	24.774	0.1597	8.6410
M03	60	30.79	8.44	37.91	9.06	1.3601	2.85	27.451	0.1258	9.0609
M04	72	37.39	5.35	45.50	5.79	1.5118	1.80	14.772	0.4900	5.7907
M05	72	36.72	8.31	45.28	8.92	1.3488	3.01	28.714	0.1116	8.9209
Minimum value						1.2809	1.80	14.772	0.0223	5.7907
Maximum value						1.5118	5.55	57.508	0.4900	8.9209

TABLE 5.14: The parameters of thin-film panels obtained by using only the information in their datasheet.

Model's Code	Given values in datasheet					Extracted parameters by proposed method				
	$C$	$V_m$ (V)	$I_m$ (A)	$V_{OC}$ (V)	$I_{SC}$ (A)	$n$	$R_s$ (m $\Omega$ )	$R_p$ ( $\Omega$ )	$I_S$ ( $\mu$ A)	$I_{ph}$ (A)
T01	216	67.80	1.55	86.00	1.74	1.1951	6.77	8.487	3.9340	1.7414
T02	216	68.60	1.57	86.60	1.75	1.1616	6.77	10.445	2.4920	1.7511
T03	154	46.90	1.60	60.10	1.82	1.2425	6.83	5.876	8.5610	1.8221
T04	154	48.30	1.61	60.70	1.84	1.2387	2.51	4.354	7.2740	1.8411
T05	154	48.50	1.65	60.80	1.88	1.2248	2.32	4.477	6.3400	1.8810
Minimum value						1.1606	2.32	4.354	2.4920	1.7414
Maximum value						1.2425	6.77	10.445	8.5610	1.8810

## Chapter VI

# EXPERIMENTS, CALCULATION AND SIMULATION FOR DETERMINING THE GMPP

The correctness, robustness and reliability of proposed deterministic method will be confirmed by experiments and simulations. Three structures of PV system which are analyzed in this chapter include single panel, single string and multiple strings in parallel (parallel strings).

### 6.1 Single Panel: Experiment, Simulation Compare to Calculated Results by Proposed Method

A SCHUTTEN SOLAR *STM6-40/36* PV panel is employed in this experiment. It is composed of 36 cells connected in series ( $C = 36$ ). The cell dimension is  $38\text{mm} \times 128\text{mm}$ . Current and voltage of the panel are measured by two FLUKE-115 DMM meters; Its temperature is measured by a UNI-T *UT301A* IR thermometer; Its load is a power variable resistor or rheostat (see Fig. 6.2). The load is scanned within one minute, so that irradiance and ambient temperature may be assumed to be constant. Twenty I-V pairs are read from a movie recorded. The measured temperature is  $51^\circ\text{C}$ .

TABLE 6.1: Measured  $V$  and  $I$  and their calculated  $P$

#	$V$ (A)	$I$ (V)	$P$ (W)	#	$V$ (A)	$I$ (V)	$P$ (W)
1.	0.118	1.663	0.20	11.	15.59	1.581	24.65
2.	2.237	1.661	3.72	12.	16.40	1.542	25.29
3.	5.434	1.653	8.98	13.	16.71	1.524	25.47
4.	7.260	1.650	11.98	14.	16.98	1.500	25.47
5.	9.680	1.645	15.92	15.	17.13	1.485	25.54
6.	11.59	1.640	19.01	16.	17.32	1.465	25.37
7.	12.60	1.636	20.61	17.	17.91	1.388	24.86
8.	13.37	1.629	21.78	18.	19.08	1.118	21.39
9.	14.09	1.619	22.81	19.	19.93	0.773	15.39
10.	14.88	1.597	23.76	20	20.50	0.427	8.73

With a few measured values, the parameter extraction method in [37] yields  $n = 1.4986$ ,  $R_s = 4.87\text{m}\Omega$ ,  $R_p = 15.41\Omega$ ,  $I_S = 1.4142\mu\text{A}$ , and  $I_{ph} = 1.6635\text{A}$ . These parameters

are applied into the PV panel model of MATLAB Simulink in order to plot the I-V curve. The proposed method also use them in order to determine the MPP.

The proposed method requires only one dataset (voltage, current and temperature), but to test its reliability four (out of 20) datasets are chosen randomly and shown in TABLE 6.2 (left). With each dataset, the proposed method predicts  $V_M$  and power at MPP,  $P_M$ , whose values are shown in TABLE 6.2 (middle). The  $V_M$ , found by the experiment, is 16.98V. MATLAB simulation finds that  $V_M = 16.988V$ . The discrepancy between the experiment and  $V_M$  obtained from the proposed method are 0.25%, 0.26%, 0.26% and 0.27% for Dataset 1 (high voltage but low current) through to Dataset 4 (low voltage but high current) respectively. The agreement among results confirms accuracy and reliability of the method.

TABLE 6.2: Four I-V datasets, calculated MPPs, and effect of additive zero-mean Gaussian noise.

	Measured		Calculated MPPs		Effect of Noise	
	$V$ (V)	$I$ (A)	$V_M$ (V)	$P_M$ (W)	$\bar{\epsilon}$ (V)	$\sigma^2$ (V <sup>2</sup> )
Dataset 1	17.13	1.485	17.0232	25.964	-0.0012	0.0008
Dataset 2	16.40	1.542	17.0234	25.967	0.0012	0.0006
Dataset 3	14.09	1.619	17.0249	26.002	-0.0016	0.0006
Dataset 4	11.59	1.640	17.0253	26.011	0.0019	0.0005

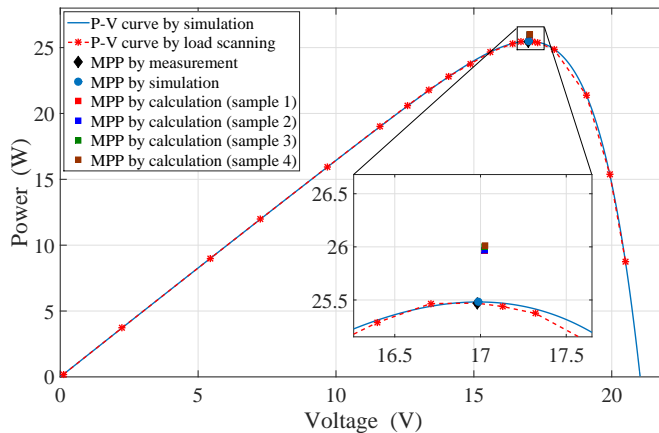


FIGURE 6.1: The P-V curves by load scanning and by simulation. The voltage at MPPs by measurement, simulation and calculation are closed together.

To simulate measurement error, each dataset in TABLE 6.2 is used as the baseline.

Voltage and current noises are added to the baseline. They are zero-mean and Gaussian-distributed

Their standard deviation is 2% of their baselines. All datasets with additive noises are then used to calculate their own  $\tilde{V}_M$ . After 100 Monte Carlo simulations,  $\bar{\epsilon}$ , which is equal to  $\mathbf{E}(\tilde{V}_M - V_M)$ , and their variance  $\sigma^2$ , are calculated and shown in TABLE 6.2



(right). Both of them are so small. This confirms that the proposed method is robust to small measurement noise.

Fig. 6.1 displays 20 measured datasets, their corresponding I-V curves (red dash line), MATLAB simulation I-V curve (blue solid line). Moreover, four MPPs obtained through the proposed method are also plotted there. It is clearly seen that the MATLAB simulation curve matches perfectly with the experiment data. All calculated MPPs are very close to the actual point.

## 6.2 Single String: Experiments, Simulations Compare to the Calculated Results by Proposed method

Panels *STM6 – 40/36* of Solar Schutten manufacturer are chosen to build a string for experiment. A string is composed of 4 above single panel in series. The irradiance level on each panel is controlled by adjusting its tilt angle. The required equipment for measurement are: 4 Voltage-meter, 1 Ampere-meter, 1 IR Thermometer (Fig. 6.2). A camera is used to record the panel voltages, string current at the same time during load scanning. The platform for experiment are configured as in Fig. 6.3.



FIGURE 6.2: A string is composed of four mono panels *STM6 – 40/36* of Solar Schutten manufacturer.

A variable resistor is used as a load. Scanning the load to draw the I-V and p-V curves of PV string. The voltage at the real MPP are compared with the estimated by proposed method. In calculation, the parameters of panel can be obtained from the information which are shown in commercial product datasheet [37]. For model *STM6 – 40/36*, the given data at STC are:  $V_{OC} = 21.6\text{V}$ ,  $I_{SC} = 2.36$ ,  $V_M = 18\text{V}$ ,  $I_M = 2.23\text{A}$  and  $C = 36$ . The extracted parameters from given data are:  $n = 1.0833$ ,  $R_s = 8.5857\text{m}\Omega$ ,  $R_p = 476.80\Omega$ ,  $I_S = 1.0134\text{nA}$  and  $I_{ph} = 2.36\text{A}$ . The parameters

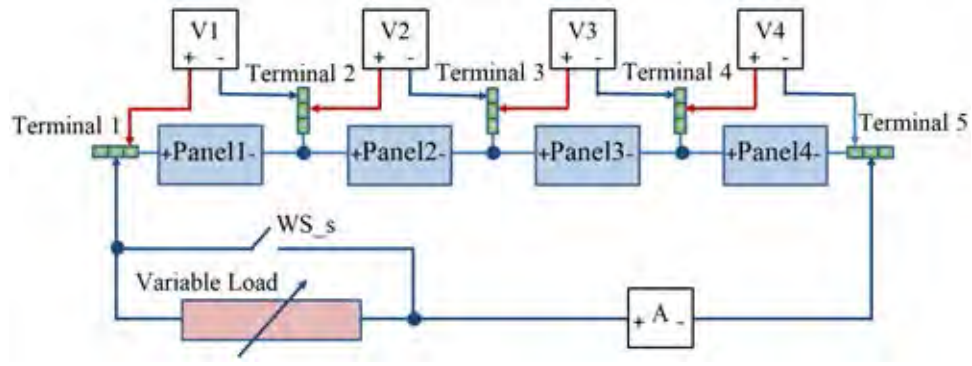


FIGURE 6.3: The schematic is setup for the experiment.

of bypass diode are used for calculation as follows:  $n_d = 1.00$ ,  $R_b = 10\text{m}\Omega$  and  $I_{sd} = 10^{-12}\text{A}$ . The measurements are conducted for two cases: the  $I_r$  are equivalent (as under uniform shading) and different (as under partial shading). The operating conditions of panels ( $T_p^i$ ,  $I_r^i$  for  $i = 1, 2, 3, 4$ ) are considered as constants during load scanning. The scanning are carried out in short time to reduce the effects by fluctuation of irradiance and temperature. Only one set of panel voltages and string current are sufficient for calculating all local maximum power points.

The panel voltages and string current are measured by five multimeters concurrently. The indicated values on multimeter are recorded by camera and read for drawing I-V, P-V curve later. A few sets of measured values are employed into proposed method to determine the local maximum power points.

### 6.2.1 Case 1: The Irradiance on All Panels Are Equivalent (Uniform Shading Condition)

The operating temperature of panels are:  $T_p^1 = 49^\circ\text{C}$ ,  $T_p^2 = 50^\circ\text{C}$ ,  $T_p^3 = 51^\circ\text{C}$  and  $T_p^4 = 52^\circ\text{C}$ . The load scanning provides the measured P-V curve which shown by dash line in Fig. 6.4. There are four samples of measured values which are employed into proposed method to determine the GMPP of string. Each sample includes four panel voltages and a string current measured at the same time (the top part). The calculated value of photo-generated current of every panel, the current and voltage of all local peaks (if exist) are shown in the middle and bottom of TABLE 6.3. Sample 1 and Sample 2 are corresponding to two bypassed panels and one bypassed panel, respectively. Sample 3 and Sample 4 are measured without bypassed panel.

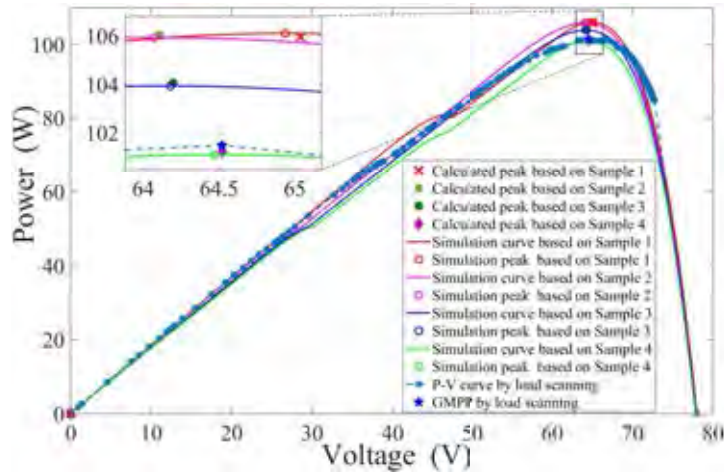


FIGURE 6.4: The string P-V curve by scanning load and the local peaks which are obtained from calculation basing on measured sets of values.

TABLE 6.3: The measured values are used for calculation by proposed method in *Case 2* and the corresponding obtained values.

		Sample1	Sample2	Sample3	Sample4
Measured values	$V_P^1(V)$	-0.709	-0.616	10.34	15.74
	$V_P^2(V)$	-0.656	9.98	12.16	16.18
	$V_P^3(V)$	12.39	14.85	15.57	16.78
	$V_P^4(V)$	17.72	17.93	18.02	18.14
Calculated photo generated current	$I(A)$	1.849	1.755	1.705	1.546
	$I_{ph}^1(A)$	1.685	1.748	1.706	1.626
	$I_{ph}^2(A)$	1.822	1.756	1.709	1.674
	$I_{ph}^3(A)$	1.849	1.794	1.778	1.752
Calculated local peak's current	$I_{Peak}^4(A)$	1.855	1.802	1.794	1.803
	$I_{Peak}^1(A)$	1.637	1.654	1.621	1.569
	$I_{Peak}^2(A)$	n/a	n/a	n/a	n/a
	$I_{Peak}^3(A)$	n/a	n/a	n/a	n/a
Calculated local peak's voltage	$I_{Peak}^4(A)$	n/a	n/a	n/a	n/a
	$V_{Peak}^1(V)$	64.95	64.11	64.2	64.52
	$V_{Peak}^2(V)$	n/a	n/a	n/a	n/a
	$V_{Peak}^3(V)$	n/a	n/a	n/a	n/a
	$V_{Peak}^4(V)$	n/a	n/a	n/a	n/a

The values of input data and calculated results are perform in TABLE 6.3. In *Case 1*, the approximation of  $I_r^1, I_r^2, I_r^3, I_r^4$  leads to the calculated photo-generated current of four panels are close together. Therefore, the string has only one peak with all samples. The calculated values in this table, again confirm the correctness and the reliability of the proposed method. TABLE 6.4 shows that there are only one peak is determined in each of all sample. TABLE 6.5 shows the error in voltage between

measured voltage at GMPP and the voltages by calculation of for samples in *Case 1*. The maximum error in voltage of four samples is -0.66%.

TABLE 6.4: The measured peak powers and calculated peak powers from four samples in *Case 1*.

	Measured	Error of measured and calculated peak voltage (%)			
	$P(W)$	Sample 1	Sample 2	Sample 3	Sample 4
Peak 1	101.49 (1 <sup>st</sup> )	106.32 (1 <sup>st</sup> )	106.06 (1 <sup>st</sup> )	104.06 (1 <sup>st</sup> )	101.21 (1 <sup>st</sup> )
Peak 2	n/a	n/a	n/a	n/a	n/a
Peak 3	n/a	n/a	n/a	n/a	n/a
Peak 4	n/a	n/a	n/a	n/a	n/a
GMPP	Peak 1	Peak 1	Peak 1	Peak 1	Peak 1

TABLE 6.5: The measured peak voltages and the error in voltage between experiment and calculation of *Case 1*.

Peak	Measured	Error of voltage (%)			
	$V(V)$	Sample 1	Sample 2	Sample 3	Sample 4
1	64.520	-0.66%	0.64%	0.50%	0.004%
2	n/a	n/a	n/a	n/a	n/a
3	n/a	n/a	n/a	n/a	n/a
4	n/a	n/a	n/a	n/a	n/a

Fig. 6.4 shows the P-V curve by scanning load and the local MPPs by calculation from 4 samples of *Case 1*. The power and voltage in four sample are different because the effect of outdoor factor. The operating condition are not constants during scanning time. Nevertheless, the peak voltages are still determined in high accuracy. The operating conditions which correspond to for samples are applied in simulation. The obtained PV curves are plotted in Fig. 6.4 also. In the zoomed area, the peaks by calculation and by simulation are close together.

### 6.2.2 *Case 2: The Irradiance on Panels Are Different (Partial Shading)*

The operating temperature of panels are:  $T_P^1 = 49^\circ\text{C}$ ,  $T_P^2 = 52^\circ\text{C}$ ,  $T_P^3 = 53^\circ\text{C}$  and  $T_P^4 = 54^\circ\text{C}$ . The load scanning performs the P-V curve which shown by dash line in Fig 6.5. TABLE 6.6 shows four samples which are used in calculation for the local maximum power points of *Case 2*. There is one bypassed panel in Sample 1 and Sample 2 and none bypassed panel in Sample 3 and Sample 4. The irradiance and temperature are slightly fluctuated under effects of outdoor environment such as cloud and wind.

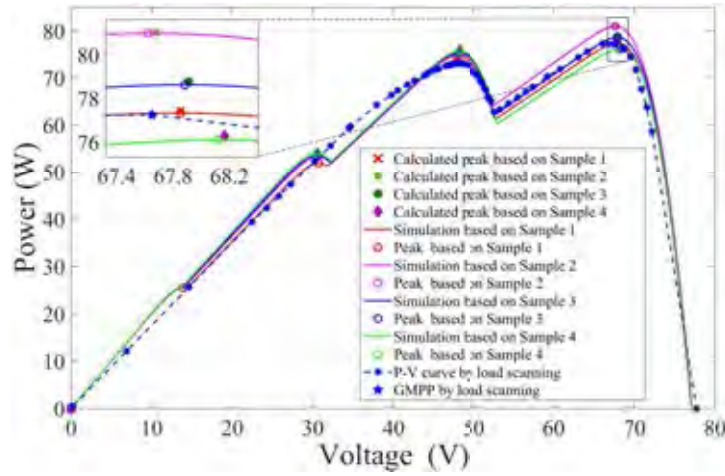


FIGURE 6.5: The string P-V curve by scanning load and the local peaks which are obtained from calculation basing on measured sets of values.

TABLE 6.6: The measured values are used for calculation by proposed method in *Case 2*. and the corresponding obtained values.

		Sample1	Sample2	Sample3	Sample4
Measured values	$V_P^1(V)$	-0.710	-0.658	9.700	14.91
	$V_P^2(V)$	16.84	17.25	17.47	17.68
	$V_P^3(V)$	17.31	17.69	17.86	18.03
	$V_P^4(V)$	17.72	17.93	18.02	18.14
Calculated photo generated current	$I(A)$	1.345	1.246	1.180	1.106
	$I_{ph}^1(A)$	1.162	1.219	1.181	1.139
	$I_{ph}^2(A)$	1.601	1.607	1.614	1.620
	$I_{ph}^3(A)$	1.767	1.825	1.844	1.864
Calculated local peak's current	$I_{Peak}^4(A)$	2.001	2.018	2.002	2.003
	$I_{Peak}^1(A)$	1.141	1.197	1.160	1.125
	$I_{Peak}^2(A)$	1.552	1.561	1.567	1.575
	$I_{Peak}^3(A)$	n/a	1.7393	1.7531	1.811
Calculated local peak's voltage	$I_{Peak}^4(A)$	n/a	n/a	n/a	n/a
	$V_{Peak}^1(V)$	67.86	67.68	67.91	67.96
	$V_{Peak}^2(V)$	47.99	48.19	48.17	48.27
	$V_{Peak}^3(V)$	n/a	30.66	30.57	30.35
	$V_{Peak}^4(V)$	n/a	n/a	n/a	n/a

That thing together with the error in measurement lead to the difference of calculated values between samples. However, in all samples, the calculated values by proposed method are change not much.

TABLE 6.7 shows the calculated values of power at local peaks. The GMPPs by proposed method are resembled that by measured in experiment (Peak 1). In Sample

TABLE 6.7: The measured peak powers and calculated peak powers from four samples in *Case 2*.

	Measured	The calculated power $P_{Peak}^j$ (W)			
	$P$ (W)	Sample 1	Sample 2	Sample 3	Sample 4
Peak 1	76.92 (1 <sup>st</sup> )	77.44 (1 <sup>st</sup> )	81.03 (1 <sup>st</sup> )	78.77 (1 <sup>st</sup> )	76.43 (1 <sup>st</sup> )
Peak 2	73.21 (2 <sup>nd</sup> )	74.47 (2 <sup>nd</sup> )	75.19 (2 <sup>nd</sup> )	75.47 (2 <sup>nd</sup> )	76.01 (2 <sup>nd</sup> )
Peak 3	n/a	n/a	53.32 (3 <sup>rd</sup> )	53.60 (3 <sup>rd</sup> )	54.95 (3 <sup>rd</sup> )
Peak 4	n/a	n/a	n/a	n/a	n/a

TABLE 6.8: The measured peak voltages and the error in voltage between experiment and calculation of *Case 1*.

	Measured	Error of measured and calculated peak voltage (%)			
	$V$ (V)	Sample 1	Sample 2	Sample 3	Sample 4
Peak 1	67.650	-0.30%	-0.05%	-0.38%	-0.46%
Peak 2	48.451	0.96%	0.55%	0.57%	0.37%
Peak 3	n/a	n/a	n/a	n/a	n/a
Peak 4	n/a	n/a	n/a	n/a	n/a

4, there are three local peaks are determined because of irradiance change. However, that thing does not affect the voltage of GMPP. The local peaks by calculation are also plotted in Fig. 6.5). Four P-V curves which obtained by set four samples condition for simulation, are also presented in this figure for comparison. So, the order of local MPPs and certainly, the GMPP will be chosen exactly from calculation. To evaluate the reliability and correctness of proposed method, TABLE 6.8 presents the errors in voltage between calculated and the measured values. The voltage at all MPP are determined in high accurate. The highest error for the GMPP is -0.46% and that of second peak is 0.96%.

### 6.3 Confirming the Correctness, Robustness and Reliability of Proposed by Simulations

The proposed method is deployed to calculate MPPs in different conditions and settings. Its findings are compared with peaks obtained by Simulink P-V scanning. At the standard test conditions ( $T_0 = 25^\circ\text{C}$  and  $I_{r0} = 1,000\text{W}/\text{m}^2$ ), the parameters are set as follows:  $I_{ph0} = 7.34\text{A}$ ,  $I_{S0} = 10^{-6}\text{A}$ ,  $R_{s0} = 5\text{m}\Omega$  and  $R_{p0} = 10\Omega$ . The values of temperature coefficients for  $I_{ph}$ ,  $I_S$ ,  $R_s$  and  $R_p$  or  $k_{I_{ph}}$ ,  $k_{I_S}$ ,  $k_{R_s}$ , and  $k_{R_p}$  are 0.0007, 3,

0.2 and 0.2 respectively. Though [35] and [36] showed that the value of  $n$  is changed slightly according to  $T$  and  $Ir$  respectively, it hardly affect the results of the following experiments. Hence,  $n$  is assumed to be constant and its value is always 1.5. Note that the values of  $Ir$  and  $k_{Iph}$  are needed only for Simulink simulation, but are not required in the proposed calculation. Assume that all the bypass diodes are identical. Their parameters are set as follows:  $n_d = 1.25$ ,  $R_b = 12\text{m}\Omega$ ,  $I_{Sd0} = 30\mu\text{A}$ , the temperature coefficient for  $I_{Sd} = 0.3$ , and  $\theta_{JA} = 5\text{K W}^{-1}$ . The ambient temperature is  $35^\circ\text{C}$ . The value of  $T_d^i$  will be iteratively estimated from its measured voltage and calculated current.

Under uniform irradiance conditions, the outputs of all cells are indistinguishable. Therefore, finding the GMPP of a cell is equivalent to finding that of the whole system. The simplified schematic in Fig. 6.6 is employed to plot the I-V and the P-V curves of a cell using *MATLAB – Simulink* software. In the following experiments, similar schematics are employed to find those of a panel and a string. Using the proposed

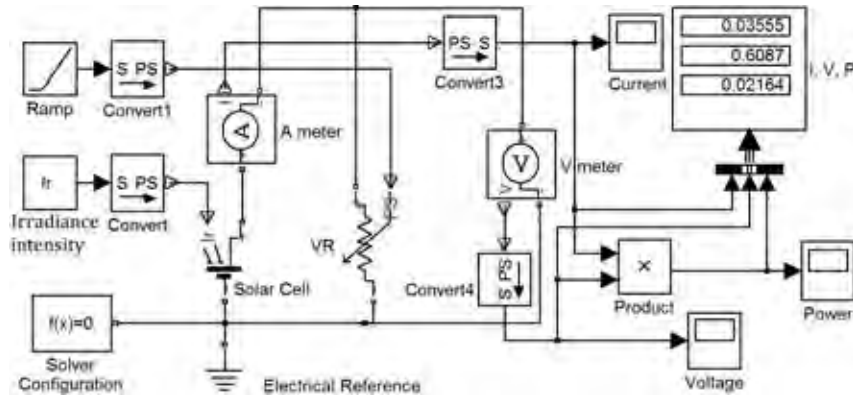


FIGURE 6.6: Simulink model that is used to draw the I-V and the P-V curves.

method, only a set of measurements, composed of  $V$ ,  $I$ , and  $T$ , is sufficient to find  $V_M$  and  $I_M$ . However to show reliability of the method, five pairs of  $V$  and  $I$  are chosen randomly (from the I-V curve) to simulate different operating points. The measured temperature is assumed to be  $50^\circ\text{C}$  in all operating points. And the unknown  $Ir$  is fixed at  $1,000\text{W/m}^2$ . Obtained results are shown in Table 6.9. Though operating at different points, the proposed method find almost the same  $V_M$  from all the measurements. The discrepancy between the calculated voltage and the peak of the P-V curve is smaller than 0.15%.

TABLE 6.9: Five pairs measured values ( $V, I$ ) of a simulation are used in calculation and the corresponding calculated results of them.

	Measured		Calculated				$V_M$ error (%)
	$I$ (A)	$V$ (V)	$I_{ph}$ (A)	$I_M$ (A)	$V_M$ (V)	$P_M$ (W)	
1	7.16	0.36	7.50	6.66	0.4015	2.67	0.12
2	5.85	0.44	7.50	6.66	0.4015	2.68	0.12
3	3.92	0.49	7.52	6.68	0.4014	2.68	0.14
4	2.92	0.51	7.53	6.69	0.4014	2.68	0.15
5	2.10	0.53	7.51	6.67	0.4014	2.68	0.13

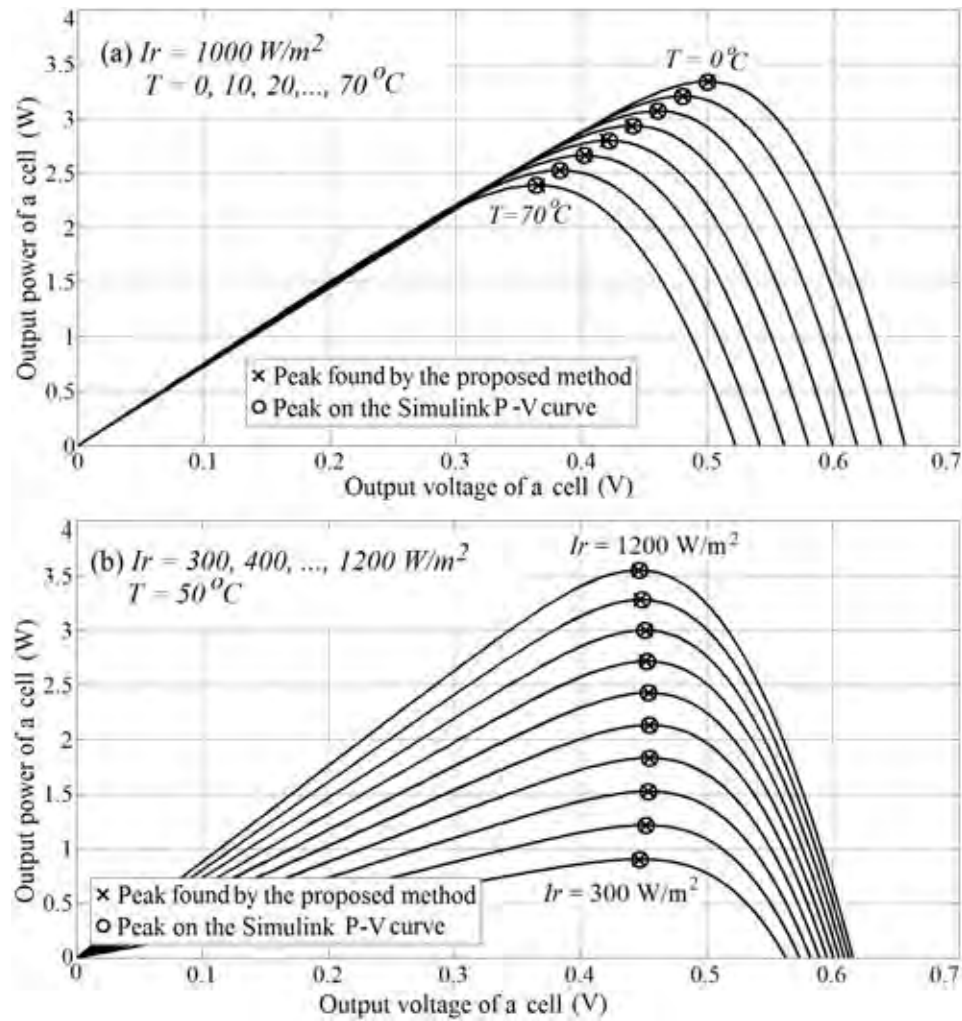


FIGURE 6.7: The calculated peaks are always close to the Simulink peaks.

The proposed calculation method gives reliable results, even if the temperature and the irradiance are changed in steps abruptly. In Fig. 6.7(a), the panel temperature rises from  $0^\circ\text{C}$  to  $70^\circ\text{C}$  by a step size of  $10^\circ\text{C}$ , while the irradiance is kept at  $1,000\text{W/m}^2$ . In Fig. 6.7(b) the irradiance falls from  $1,200\text{W/m}^2$  down to  $300\text{W/m}^2$  by a step size of  $-100\text{W/m}^2$ , while the temperature is kept at  $50^\circ\text{C}$ . Both figures show that the calculated results were always close to the Simulink peaks.



To verify robustness of the method, with each input conditions ( $Ir$  and  $T$ ), 50 pairs of operating points,  $V$  and  $I$ , are picked randomly from an I-V curve. Furthermore, random errors are added and subtracted to the chosen  $V$  and  $I$ . The errors are uniformly distributed between 0% and 2% relatively to the  $V$  and  $I$  themselves. Fifty pairs of  $V+$  and  $I+$ , and another fifty pairs of  $V-$  and  $I-$  are created from pairs of  $V$  and  $I$  plus and minus the random errors respectively. This is to test robustness of the method to the measurement errors. Moreover, during calculation all the voltages and currents were rounded to the nearest thousandth (three digits after the decimal points) in order to test if the method is robust to the round-off error as well.

Compared to the Simulink peaks, the average errors  $\bar{e}_M$ ,  $\bar{e}_{M+}$ , and  $\bar{e}_{M-}$  (in %) and the variance of calculated MPP  $\sigma_M^2$ ,  $\sigma_{M+}^2$ ,  $\sigma_{M-}^2$  (in %<sup>2</sup>) are shown in Table 6.10. The subscripts  $M$ ,  $M+$  and  $M-$  denote that the MPP were calculated with the  $V$  and  $I$  pair, the  $V+$  and  $I+$  pair, and the  $V-$  and  $I-$  pair respectively. Note that  $V_M^{(0)}$  was reset to 0.5V before every calculation.

Calculated with the  $V$  and  $I$  pair,  $\bar{e}_M$  has the smallest amplitude in most cases. Its biggest value is lower than 0.31% and its variance  $\sigma_M^2 < 0.006\%^2$  in all cases ( $Ir$  and  $T$ ). When the random negative errors are added,  $\bar{e}_{M-}$  has the amplitude less than 0.97%, and the variances  $\sigma_{M-}^2$  is less than 0.011%<sup>2</sup>. Calculated with the  $V+$  and  $I+$  pair,  $\bar{e}_{M+}$  has the amplitude less than 1.7%, and its variances  $\sigma_{M+}^2$  is less than 0.004%<sup>2</sup> in all cases.

The voltages converge to its final values just after a few iterative loops ( $\bar{l}$ ,  $\bar{l}_-$  and  $\bar{l}_+$  are less than 4 in all cases). Low errors in all calculations show that the method can withstand the measurement and the round-off errors. Moreover, very low variances confirm determinism of the method.

As seen in Fig. 6.7,  $V_M$  does not vary much with the incident photon flux, but  $V_M$  reduces when temperature increases, so  $V_M^{(0)}$  shall be adapted according to the measured temperature. For example, in the last experiment, at  $T = 0^\circ\text{C}$ ,  $V_M^{(0)} = 0.5\text{V}$  permits the voltage to converge just after one loop. But at  $25^\circ\text{C}$  and  $50^\circ\text{C}$ , using the same initial value,  $V_M$  converges after 2 to 3 loops. In other words, a better initial guess can reduce computation time. With the eight  $V_M$  found on the curves in Fig. 6.7(a), a good guess of  $V_M^{(0)}$  for any temperature can be obtained easily.

TABLE 6.10: The average errors of  $V_M$  ( $\bar{e}_M, \bar{e}_{M+}, \bar{e}_{M-}$ ), their variances ( $\sigma_M^2, \sigma_{M+}^2, \sigma_{M-}^2$ ) and the average number of iterative loops ( $\bar{l}, \bar{l}_-$  and  $\bar{l}_+$ ). Each calculated from 50 random pairs of  $V$  and  $I$ ,  $V+$  and  $I+$ , and,  $V-$  and  $I-$ .

$Ir(\text{W/m}^2)$	$T = 0^\circ\text{C}$			$T = 25^\circ\text{C}$			$T = 50^\circ\text{C}$		
	600	800	1000	600	800	1000	600	800	1000
$V_M$ (V)	0.505	0.504	0.501	0.455	0.454	0.452	0.405	0.405	0.403
$\bar{e}_M$ (%)	0.238	0.026	-0.147	-0.023	-0.084	-0.228	-0.128	-0.099	-0.305
$\bar{e}_{M-}$ (%)	-0.063	0.401	0.963	-0.451	0.073	0.554	-0.566	-0.075	0.320
$\bar{e}_{M+}$ (%)	-0.353	-1.626	-2.574	-0.243	-1.146	-2.080	-0.075	-0.798	-1.702
$\sigma_M^2$ (% <sup>2</sup> )	0.005	0.004	0.002	0.005	0.002	0.002	0.006	0.003	0.002
$\sigma_{M-}^2$ (% <sup>2</sup> )	0.011	0.007	0.004	0.009	0.006	0.004	0.008	0.005	0.003
$\sigma_{M+}^2$ (% <sup>2</sup> )	0.003	0.002	0.002	0.004	0.002	0.002	0.003	0.002	0.002
$\bar{l}$ (loops)	1.0	1.0	1.0	2.0	2.0	2.0	3.0	3.0	3.0
$\bar{l}_-$ (loops)	1.0	1.0	1.0	2.0	2.0	2.0	2.5	3.0	3.0
$\bar{l}_+$ (loops)	1.0	1.0	2.0	2.0	2.0	2.0	3.0	3.0	3.0

## 6.4 Calculation and Simulation for Single String under Partial Shading

The following calculations and simulations are carried out on a string, which consists of eight identical panels in series. Each panel is composed of 40 cells, also connected in series. On each panel, all the 40 cells is assumed to receive the same irradiance. But the irradiance and the temperature on different panels may vary. Results from three cases might disprove the reliability and accuracy of the proposed algorithm.

### 6.4.1 Case 1: The irradiance Distributes on a Wide Range

The irradiance on panels changes from  $300\text{W/m}^2$  up to  $1,000\text{W/m}^2$  with a uniform step of  $100\text{W/m}^2$ . Also the panel temperature varies from  $53^\circ\text{C}$  up to  $60^\circ\text{C}$  with a step of  $1^\circ\text{C}$ . The string current  $I$  is selected randomly, and in this case is  $1.75\text{A}$ . Given all the panel temperatures and the string current, all the corresponding panel voltages could be obtained from the Simulink I-V curves. The panel voltages are found to be all positive. So, no panel is bypassed during the measurement. Table 6.11 shows the measured values of  $T^i$ ,  $V_P^i$ , and  $I$  for  $i = 1, \dots, 8$ . The calculated  $I_{ph}^i$  of all panels are more than  $I$ . This reconfirms that no panel is bypassed during the measurement. The proposed method finds out six local MPPs. The number and the values of MPPs, found by Simulink (shown on Table 6.12), prove the accuracy of the method. The discrepancy between the power at the calculated MPPs and those of Simulink is less than  $1\text{W}$  (0.3%), and those of  $V_M^i$  are less than  $0.08\text{V}$  (0.06%).

TABLE 6.11: The measured values for Case 1 and the calculated  $I_{ph}^i$  of all panels.

Panel	Measured			Calculated
	$T_P^i$ (°C)	$V_P^i$ (V)	$I$ (A)	$I_{ph}^i$ (A)
1	53	17.26		2.25
2	54	18.75		3.00
3	55	19.46		3.75
4	56	19.92		4.50
5	57	20.25	1.75	5.25
6	58	20.51		6.00
7	59	20.71		6.75
8	60	20.87		7.50

TABLE 6.12: Six local MPPs found by the proposed method and by Simulink P-V scan.

Peak	Proposed Method			Simulink	
	$V_M$ (V)	$I_M$ (A)	$P_M$ (W)	$V_M$ (V)	$P_M$ (W)
1	149.74	2.22	332.81	149.76	332.30
2	127.64	2.95	376.65	127.56	376.71
3	106.03	3.67	389.32	105.97	389.82
4	85.16	4.38	372.63	85.13	373.42
5	65.18	5.05	328.85	65.14	329.75
6	46.17	5.65	260.82	46.15	261.66

Fig. 6.8 reconfirms that the calculated peaks are very close to those found by Simulink. At GMPP, their voltage difference is 0.06V ( $\approx 0.06\%$ ). Because the GMPP belongs to Seg. 3, when the MPPTcontroller moves the operating point to this point, two panels will be bypassed.

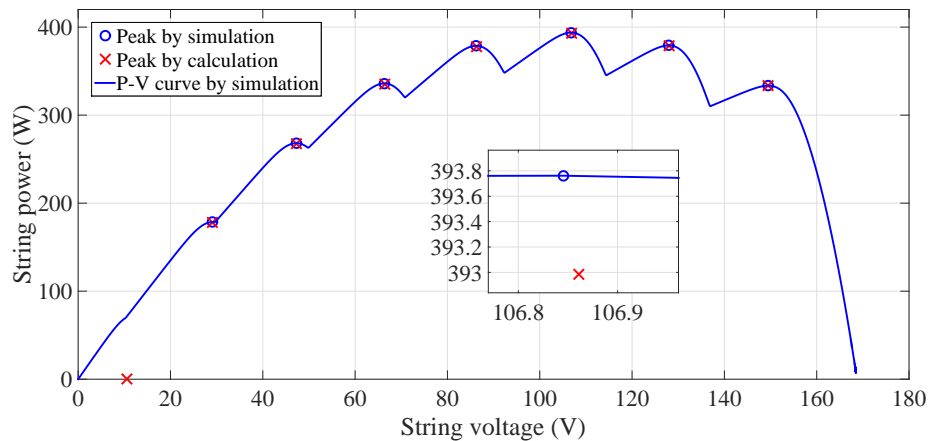


FIGURE 6.8: The calculated peaks and the P-V simulation curve.

Only for the illustration purpose, Fig. 6.9 shows the curves of  $V^m$  and  $V_M^m$  for  $m = 1, \dots, 8$ . They cross each other six times. Seg. 7 and Seg. 8 which correspond to the two highest segments do not contain any peaks due to no crosses. The MPPT

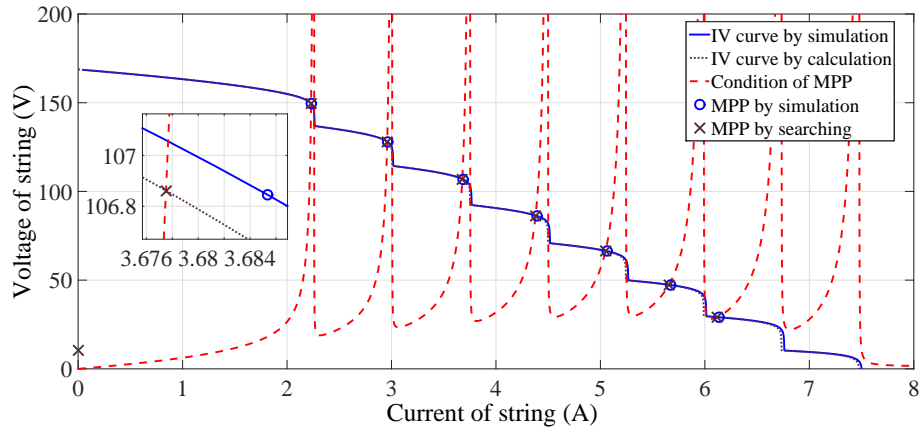


FIGURE 6.9: The graphs of  $V^m$  and  $V_M^m$ . Their intersections locate the peaks of PV string.

controller does not need these curves. For a segment, only 5-8 calculations of  $V^m$  and  $V_M^m$  are needed to locate their common value. Notice that the higher  $V_M^m$ , the smaller difference between  $I_M^m$  and  $I_{ph}^m$ . For example, for Seg. 6,  $V_M^6$  is at 46.2V and  $I_{ph}^6 - I_M^6 = 0.35A$ ; while for Seg. 1,  $V_M^1$  is at 149V and  $I_{ph}^1 - I_M^1 = 0.03A$ .

#### 6.4.2 Case 2: The Irradiance Distributes in a Narrower Range

The surface temperature of all the panels are the same as in *Case 1*. But the irradiance variation is reduced by half. With a step size of  $50W/m^2$ , the first panel receives the intensity of  $650W/m^2$  and the last gets  $1,000W/m^2$ .

TABLE 6.13: The measured values for Case 2 and the calculated  $I_{ph}^i$  of all panels. For Panel 1, Panel 2, and Panel 3, the estimated  $T_d^i$  are shown instead of  $T_P^i$ .

Panel	Measured/Estimated			Calculated
	$T_P^i/T_d^i(^{\circ}C)$	$V_P^i(V)$	$I(A)$	$I_{ph}^i(A)$
1	37	-0.32		4.87
2	36	-0.30		5.26
3	35	-0.26		5.64
4	56	13.99	5.85	6.02
5	57	16.15		6.40
6	58	17.00		6.79
7	59	17.52		7.18
8	60	17.88		7.56

Table 6.13 shows that, operating at 5.85A, the measured voltages (from the Simulink I-V curves) of Panel 1, Panel 2, and Panel 3 are negative, hence they are bypassed. Their temperatures, displayed in the table are those of the diodes instead of those of the panel surfaces. Recall that temperatures and currents are iteratively calculated

TABLE 6.14: Four local MPPs found by the proposed method and by Simulink P-V scan.

Peak	Proposed Method			Simulink	
	$V_M$ (V)	$I_M$ (A)	$P_M$ (W)	$V_M$ (V)	$P_M$ (W)
1	140.44	4.77	669.54	140.34	670.70
2	120.38	5.11	614.83	120.36	616.15
3	100.90	5.43	547.94	100.86	549.33
4	82.05	5.73	469.94	82.01	471.30

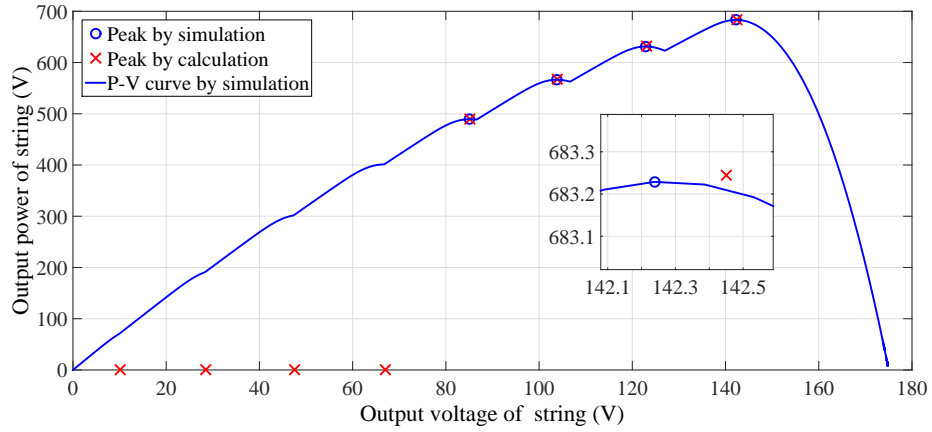


FIGURE 6.10: The calculated peaks under changing of irradiance.

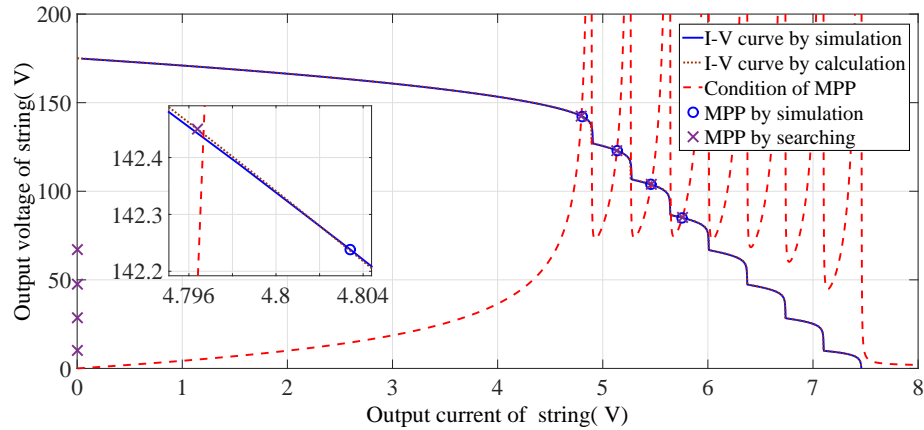


FIGURE 6.11: The calculated values are close to the intesection points of  $V^m$  and  $V_M^m$ .

using (4.20) and (4.22). The fact that the calculated  $I_{ph}^i < I$  for  $i = 1, 2, 3$  and  $I_{ph}^i > I$  for  $i = 4, \dots, 8$ , assures us that only Panel 1, Panel 2, and Panel 3 are bypassed.

Only four local MPPs are found by calculation. Only Seg. 1, Seg. 2, Seg. 3, and Seg. 4 yield the MPPs. The peaks found by Simulink, depicted in Fig. 6.10 reconfirm the accuracy of the proposed method. Even with the approximation of  $T_d^i$ , all the calculated peaks are very close to those of the Simulink. The discrepancy of the voltage is smaller than 0.1V and that of power is smaller than 1.5W. At GMPP the

voltage difference is  $0.10V \approx 0.13\%$ . Because the GMPP belongs to Seg. 1, when the MPPT controller moves the operating point to this point, no panel will be bypassed.

Fig. 6.11 shows the intersection points of the  $V^m$  and the  $V_M^m$  curves. The two curves crossed each other four times. Again these points belong to the four lowest current segments.

### 6.4.3 Case 3: One Panel Received Lower Irradiance Compare to Others

In this case, Panel 1 is shaded, and  $Ir^1 = 500W/m^2$ . Panel 2 to Panel 8 receive higher photon flux levels as follows:  $Ir^2 = 940W/m^2$ ,  $Ir^3 = 950W/m^2$ ,  $Ir^4 = 960W/m^2$ ,  $Ir^5 = Ir^6 = 980W/m^2$  and  $Ir^7 = Ir^8 = 1,000W/m^2$ . The panel surface temperatures are the same as in the other cases. At the measured point, the string current  $I$  is 2.77A and the panel voltages are all positive as shown in Table 6.15. The calculated  $I_{ph}^i$  for all panels are more than the measured string current  $I$ .

TABLE 6.15: The measured values for Case 3 and the calculated  $I_{ph}^i$  of all panels.

Panel	Measured			Calculated
	$T_P^i(^{\circ}C)$	$V_P^i(V)$	$I(A)$	$I_{ph}^i(A)$
1	53	18.89		3.71
2	54	20.55		7.07
3	55	20.90	—	7.12
4	56	20.85	2.77	7.20
5	57	20.67	—	7.36
6	58	20.67	—	7.36
7	59	20.33		7.54
8	60	20.33		7.54

TABLE 6.16: Two local MPPs found by the proposed method and by Simulink P-V scan.

Peak	Proposed Method			Simulink	
	$V_M(V)$	$I_M(A)$	$P_M(W)$	$V_M(V)$	$P_M(W)$
1	154.12	3.66	564.71	153.92	566.40
2	116.60	6.55	763.23	116.51	762.14

The temperature might affect the panel voltage, but with the same  $Ir$ , the temperature difference is usually very low. That leads to  $I_{ph}^5 \cong I_{ph}^6$  and  $I_{ph}^7 \cong I_{ph}^8$ . Only six segments exist in this case. Table 6.16 displays that the proposed method finds only two MPPs.

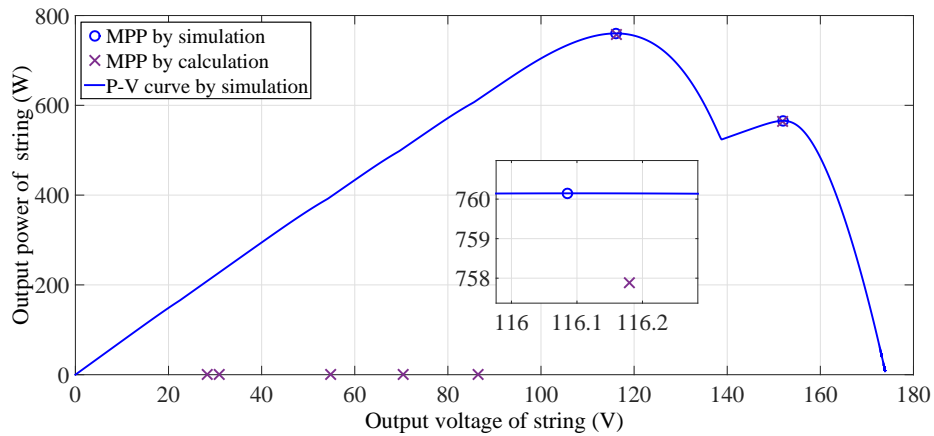


FIGURE 6.12: The calculated peaks under changing of irradiance.

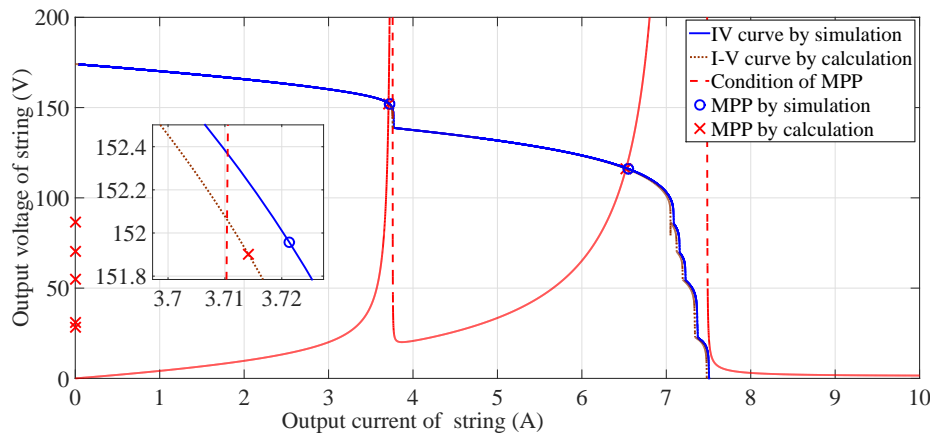


FIGURE 6.13: The calculated peaks under changing of irradiance.

Fig. 6.12 shows that the Simulink simulation finds the same the number and values of MPPs. Fig. 6.13 supports that the intersections of  $V^m$  and  $V_M^m$  are the MPPs. The error of global peak voltage is smaller than  $0.1V \approx 0.1\%$ . In this case, the string may operate at GMPP when the lowest power panel is bypassed because  $I_M > I_{ph}^1$ . Notice that the width of the first two low segments are much wider than the others.

In Fig. 6.13, there are only two intersections between curves of  $V^m$  and  $V_M^m$  and their currents are in Seg. 1 and Seg. 2. The results from all three cases lead to four notices: 1) The more irradiance variation, the more local peaks. 2) The first segment always contains an MPP. 3) If the current of the operating point is low enough such that no panel is by passed, there is no need to estimate the parameters of the bypassed diodes. And 4) The wide segments are more likely to contain MPPs than the smaller ones. One should find the MPP in descending order of the width. If a wider segment does not contain an MPP, there is no need to look for ones in narrower segments. The last notice reduces the search time further.

## 6.5 Calculation and Simulation for Parallel Strings under Partial Shading Conditions

### 6.5.1 Case 1: Two Strings, Seven Panels per String

The operation conditions of every panels are set as Table 6.17(A).

The string currents  $I_{Str}^1 = 4.3282A$ ,  $I_{Str}^2 = 3.7292A$  and following panel voltages ( $V_P^{i,j}(V)$ ,  $i, j$  correspond to string number and panel number in the PV system, shown in Table 6.18(A) are used for calculation.

TABLE 6.17: Voltage (left) and estimated power at local MPPs (right).

(A) The operating conditions of 2x7 PV system.				(B) The local peak voltage and voltage error at these points of two strings.			
		String 1	String 2			String 1	String 2
Panel 1	$I_r(W/m^2)$	500	350	Peak 1	$V_{Mcal}(V)$	188.7194	180.0850
	$T_P(^{\circ}C)$	52	50		$V_{Msim}(V)$	188.2890	179.6495
	$T_d(^{\circ}C)$	55	51		$ Err.V (\%)$	0.229	0.242
Panel 2	$I_r(W/m^2)$	600	400	Peak 2	$V_{Mcal}(V)$	n/a	n/a
	$T_P(^{\circ}C)$	54	51		$V_{Msim}(V)$	n/a	n/a
	$T_d(^{\circ}C)$	54	50		$ Err.V (\%)$	n/a	n/a
Panel 3	$I_r(W/m^2)$	700	450	Peak 3	$V_{Mcal}(V)$	131.2276	n/a
	$T_P(^{\circ}C)$	57	52		$V_{Msim}(V)$	131.0073	n/a
	$T_d(^{\circ}C)$	53	48		$ Err.V (\%)$	0.168	n/a
Panel 4	$I_r(W/m^2)$	800	500	Peak 4	$V_{Mcal}(V)$	n/a	n/a
	$T_P(^{\circ}C)$	58	53		$V_{Msim}(V)$	n/a	n/a
	$T_d(^{\circ}C)$	54	47		$ Err.V (\%)$	n/a	n/a
Panel 5	$I_r(W/m^2)$	900	550	Peak 5	$V_{Mcal}(V)$	n/a	n/a
	$T_P(^{\circ}C)$	60	54		$V_{Msim}(V)$	n/a	n/a
	$T_d(^{\circ}C)$	53	45		$ Err.V (\%)$	n/a	n/a
Panel 6	$I_r(W/m^2)$	1000	600	Peak 6	$V_{Mcal}(V)$	48.2040	n/a
	$T_P(^{\circ}C)$	62	55		$V_{Msim}(V)$	48.1253	n/a
	$T_d(^{\circ}C)$	52	42		$ Err.V (\%)$	0.164	n/a
Panel 7	$I_r(W/m^2)$	1000	600	Peak 7	$V_{Mcal}(V)$	n/a	n/a
	$T_P(^{\circ}C)$	62	55		$V_{Msim}(V)$	n/a	n/a
	$T_d(^{\circ}C)$	52	42		$ Err.V (\%)$	n/a	n/a

Table 6.17(B) shows the peak voltages of two string by calculation and simulation.

The estimated system power at five determined local peaks are shown in Table 6.18(B).

According to calculated results, the power at GMPP by estimation is  $V_S = 1804.3W$ .

Predicting that the real GMPP is belonged Segment 1 of both strings. Using (4.36) to



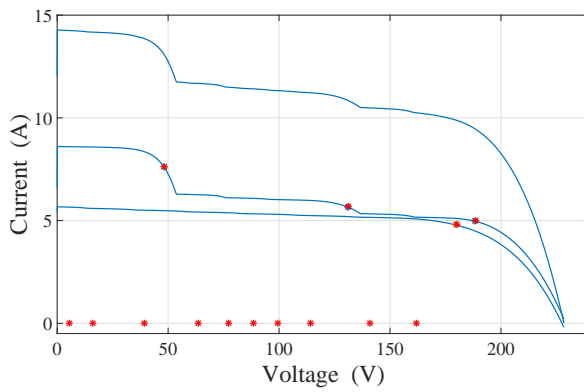
TABLE 6.18: Operating condition of panels (left) and measured values for calculation (right).

(A) The measured panel voltages are applied in calculation by proposed method for of 2x7 PV system.

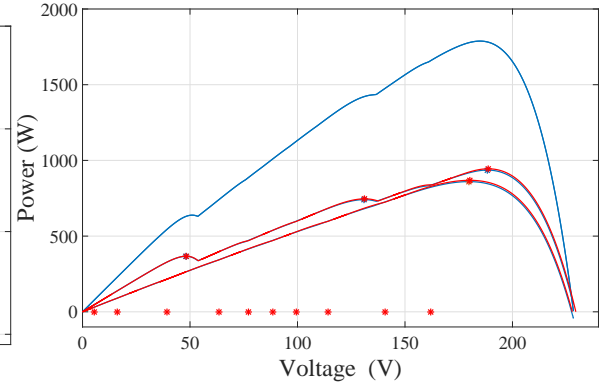
$V_P^{ij}$ (V)	String 1	String 2
Panel 1	26.7435	28.3859
Panel 2	27.2936	28.6828
Panel 3	28.5357	28.7103
Panel 4	28.6774	28.7300
Panel 5	28.8126	28.87163
Panel 6	30.6654	29.0063
Panel 7	30.6654	29.0067

(B) The estimated power of system at determined local peaks.

$P_S$ (W) at $V_P^{ij}$	$i=1$	$i=2$
$j=1$	1804.3	1797.4
$j=2$	n/a	n/a
$j=3$	1434.9	n/a
$j=4$	n/a	n/a
$j=5$	n/a	n/a
$j=6$	633.5	n/a
$j=7$	n/a	n/a



(A) I-V curves of PV system 2x7.



(B) P-V curves of PV system 2x7 and the local peaks of strings.

FIGURE 6.14: I-V curves (left) and P-V curves (right) .

calculate voltage at GMPP as:

$$\hat{V}_G = \frac{188.7194 \times 947.145 + 180.0850 \times 870.819}{947.145 + 870.819} = 184.5835(V)$$

The voltage error between simulation and estimation is  $\Delta V_G = 184.8955 - 184.5835 \approx 0.321(V \approx 0.169\%)$  Fig. 6.14(A) performs the I-V curves of two strings and whole system. The local MPPs by calculation and simulation are also plotted in this figure for comparison. The P-V curves are presented in Fig. 6.14(B). All pair of peaks by simulation and calculation are close. The intersections of String 1 and String 2 are shown in Fig 6.16(A) and Fig. 6.16(B), respectively.

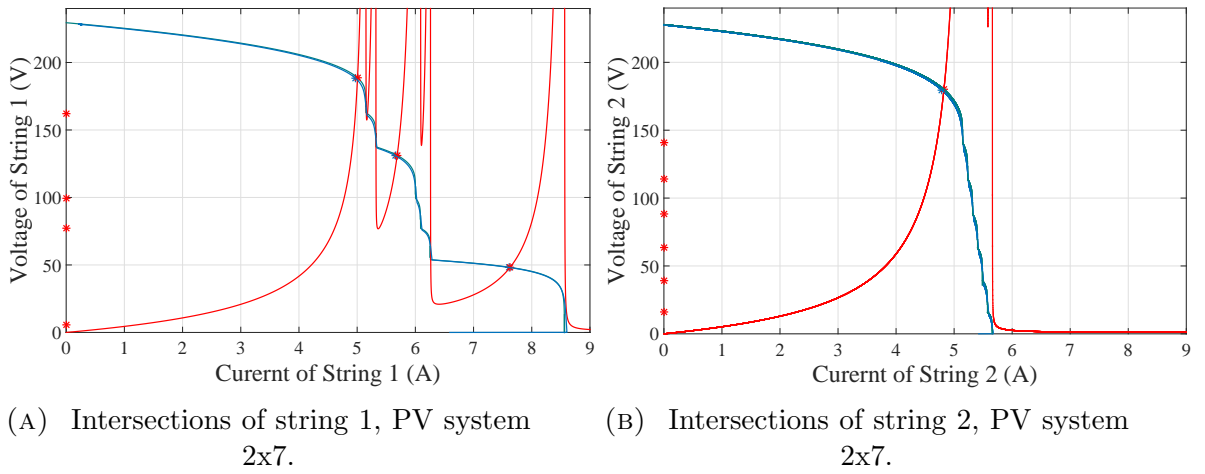


FIGURE 6.16: The intersections in segments of two strings.

### 6.5.2 Case 2: Three Strings, Five Panels per String

The operation conditions of every panels are set as in Table 6.19(A) for simulation. Basing on load scanning in simulation, the string currents  $I_{Str}^1 = 2.7253A$ ,  $I_{Str}^2 =$

TABLE 6.19: The operating conditions of 3x5 PV system and panel voltages are used in proposed calculation.

(A) The operating condition of all panels in PV system.

Panel		String 1	String 2	String 3
1	$I_r(W/m^2)$	600	200	800
	$T_P(^{\circ}C)$	45	40	53
	$T_d(^{\circ}C)$	50	48	49
2	$I_r(W/m^2)$	700	400	850
	$T_P(^{\circ}C)$	47	46	54
	$T_d(^{\circ}C)$	48	45	49
3	$I_r(W/m^2)$	800	600	900
	$T_P(^{\circ}C)$	51	47	59
	$T_d(^{\circ}C)$	46	46	46
4	$I_r(W/m^2)$	900	800	950
	$T_P(^{\circ}C)$	56	53	60
	$T_d(^{\circ}C)$	45	45	45
5	$I_r(W/m^2)$	1000	1000	1000
	$T_P(^{\circ}C)$	61	60	62
	$T_d(^{\circ}C)$	42	43	41

(B) The measured panel voltages are applied in proposed calculation.

$V_P^{i,j}(V)$	String 1	String 2	String 2
Panel 1	31.1454	28.7602	31.6918
Panel 2	31.7254	31.2814	31.8394
Panel 3	31.8734	32.5997	31.4837
Panel 4	31.7912	32.8224	31.5924
Panel 5	31.6377	32.7095	31.5659

0.9567A,  $I_{Str}^3 = 2.6463A$  and panel voltages ( $V_P^{i,j}(V)$ ,  $i, j$  correspond to string number and panel number in the PV system (Table 6.19(B)) are used for calculation. Table

6.20(A) shows the peak voltages of two string by calculation and simulation and the error between them.

TABLE 6.20: The local peak voltage of strings by calculation, simulation and error between them (A). The estimated power of system at local peak voltages(B).

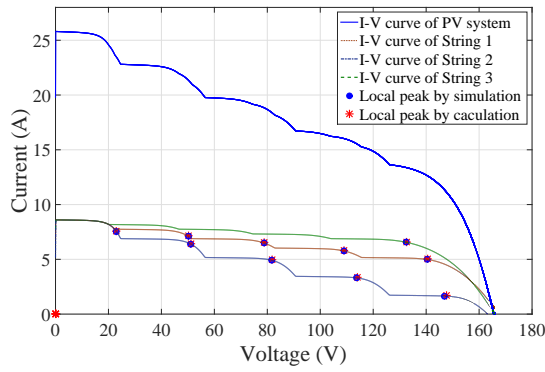
(A) The local peak voltage and voltage error at these points of two strings.					(B) The estimated power of system at determined local peaks voltage $V_P^{i,j}$ .			
		String 1	String 2	String 3	$P_s(W)$	$i=1$	$i=2$	$i=3$
Peak 1	$V_{Mcal}^{i,1}(V)$	140.603	147.736	132.560	$j=1$	1793.9	1669.6	1786.2
	$V_{Msim}^{i,1}(V)$	140.363	146.945	132.412	$j=2$	1751	1782.3	n/a
	$ Err.V (\%)$	0.171	0.538	0.142	$j=3$	1491.5	1511.5	n/a
Peak 2	$V_{Mcal}^{i,2}(V)$	109.041	113.985	n/a	$j=4$	1075.7	1082.1	n/a
	$V_{Msim}^{i,2}(V)$	108.916	113.674	n/a	$j=5$	n/a	538.8	n/a
	$ Err.V (\%)$	0.116	0.274	n/a				
Peak 3	$V_{Mcal}^{i,3}(V)$	78.857	81.765	n/a				
	$V_{Msim}^{i,3}(V)$	78.751	81.647	n/a				
	$ Err.V (\%)$	0.133	0.145	n/a				
Peak 4	$V_{Mcal}^{i,4}(V)$	50.316	51.141	n/a				
	$V_{Msim}^{i,4}(V)$	50.256	51.098	n/a				
	$ Err.V (\%)$	0.120	0.084	n/a				
Peak 5	$V_{Mcal}^{i,5}(V)$	n/a	22.991	n/a				
	$V_{Msim}^{i,5}(V)$	n/a	22.999	n/a				
	$ Err.V (\%)$	n/a	0.033	n/a				

The estimated system power at all determined local peaks are shown in Table 6.20(B). Basing on the Table 6.20(B), predicting that the GMPP is dropped in peaks 1 of all strings. Using formula (4.36) to determine the voltage at GMPP as follow:

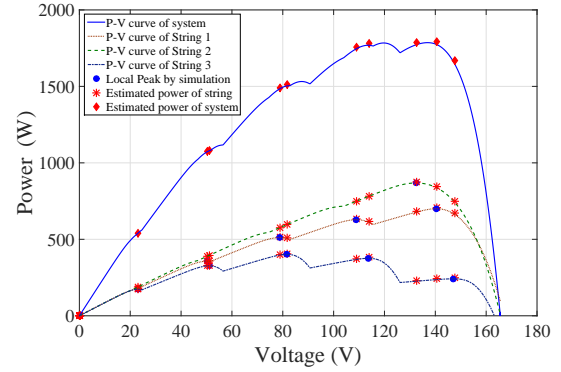
$$\widehat{V}_G = \frac{140.6026 \times 708.342 + 147.7364 \times 249.807 + 132.5998 \times 874.442}{708.342 + 249.807 + 874.442} = 137.7564(V)$$

The voltage at GMPP by simulation is  $V_{Gsim} = 136.9409V$ , so the voltage error is  $\Delta V_G \approx 0.8155V \approx 0.596\%$ . The I-V curves and P-V curves of three strings and whole PV system are plotted in Fig. 6.18A and Fig. 6.18B. All calculated peaks are close to corresponding simulated peaks. All estimated peaks by proposed method are match to the P-V curve by simulation. Fig. 6.18C,D,E show the peaks in segments which are determined basing on two function  $V_1$  and  $V_2$  in searching method.

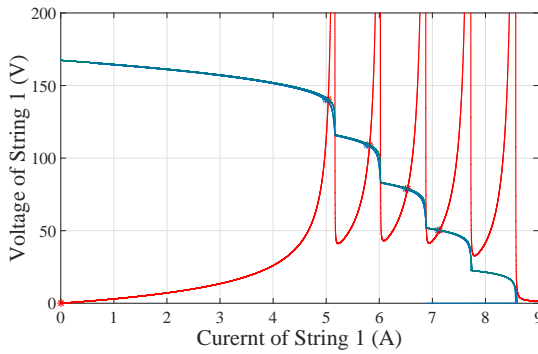
Others calculations and simulations results for single string, two parallel strings, three parallel strings are presented in Appendix B.



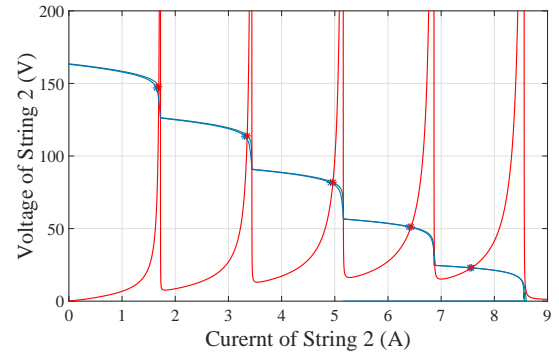
(A) I-V curves of PV system 3x5.



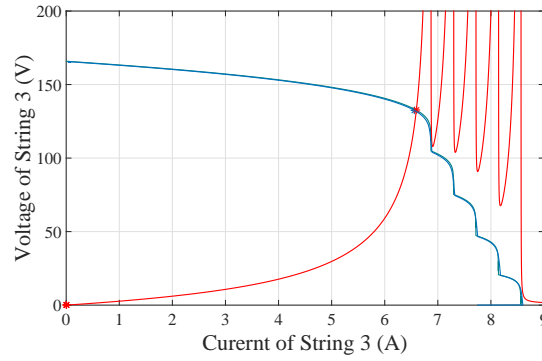
(B) P-V curves of PV system 3x5.



(C) Intersections of segments in String 1



(D) Intersections of segments in String 2



(E) Intersections of segments in String 3

FIGURE 6.18: I-V curves, P-V curves and intersections in segments of PV system.

## Chapter VII

### CONCLUSION & FUTURE WORK

This dissertation proposes a few techniques that maximize the efficiency of PV systems. That is “*Estimation of the GMPP of PV systems based on online measurement*”. The proposed methods requires only one set of measured string currents, voltage and temperature of panels in order to determine all local peaks of panels string and parallel strings. Because solar cell parameters are required for estimation, so “*Fast and precise extraction method for solar cell parameters using only three measured points*” is asked as an important condition. The parameters can be obtained with high accuracy quickly. The new method uses only  $I_{SC}$ ,  $V_{OC}$ ,  $I_M$ ,  $V_M$  and temperature during measurement to determine the parameters of single diode model ( $n$ ,  $R_s$ ,  $R_p$ ,  $I_s$ ,  $I_{ph}$ ). The condition of MPP is exploited extensively in all mentioned techniques. This book, includes original ideas, background theories, methodology (Chapter 3 and Chapter 4), experiment, calculation and simulation results (Chapter 5 and Chapter 6). Furthermore, two programs are built and introduced in Appendix A and Appendix B. Their results are also presented in these parts. Users can use two programs to extract the solar cell parameters and to determine the MPPs of a PV system.

The solar cell parameters play an important role in determination for MPPs. The accuracy of extracted results depends on the parameters tightly. So, the proposed extraction method is one of main factors which affects to values of calculated voltage at local MPPs. This method yields very accurate results. Two sets of measured voltages and currents of reference cell and panel are used in the proposed extraction method. The obtained parameters are used to estimate the error. When compared with other referenced methods, the proposed method shows smaller mean of absolute error. To verify the correctness of the methods, two types of solar panels are used in the experiments. After measurement, the required data are employed for extraction. The calculated parameters are applied in solar cell models in order to generate the I-V curves. The simulated curve match the curve by measured values perfectly. More than

one hundred solar panels are extracted by the proposed method using information in datasheet. All extractions yield parameters that are in valid ranges (possible values).

This dissertation introduces a few methods for finding the GMPP of a PV systems that may composed of a panels single string or of parallel strings under partial shading conditions. Because the voltage at GMPP is determined beforehand, the PV system is driven directly to this point without any power scanning. To track the operating conditions, the GMPP is recalculated periodically. Only the voltage obtained from calculation, is enough to track the GMPP. So a simple control technique can be employed. In addition, the proposed method for extracting the parameters of solar cell can be used to analyze the characteristics of solar cells at any operating conditions.

The experiments for GMPP estimation show that the peaks by the proposed methods are very near the peaks obtained by load scanning. The number of peaks obtained by calculation and by measurement are the same. The voltage discrepancies at all local MPPs are less than 1%. To confirm the reliability and correctness of the method, many calculation simulations with additional noise are implemented on the PV systems. The results at all peaks are acceptable, as the maximum error is less than 0.8%. The GMPP is estimated well, despite various operating conditions. Some notes, which help to evaluate the status of PV systems quickly, are also recommended in Chapter 6.

In the future, there are two interesting topics which are based on this dissertation: The first topic is “Development of MPPT controllers based on the proposed method”. This topic may evaluate the proposed method practically. For a large PV system, panel monitoring system, string controllers and/or farm controller may be needed. The second topic is “Relations of solar cell parameters with environmental conditions”. The parameters of one solar panel are extracted under many different operating conditions. Based on the calculated results and the measured values, the relationships between the parameters and the temperature, irradiance level, wave length, etc. may be formulated and verified for the last formulae.

## REFERENCES

- [1] T. Eswam, P.L. Chapman. **Comparison of Photovoltaic Array Maximum Power Point Tracking Techniques**, IEEE Transactions on Energy Conversion, vol. 22, no. 2, pp. 439-449, June 2007.
- [2] Jawad Ahmad. **A Fractional Open Circuit Voltage Based Maximum Power Point Tracker for Photovoltaic Arrays**, 2nd International Conference on Software Technology and Engineering(ICSTE), 2010.
- [3] Yan Cui, Wen Yao, Jinzhao Luo. **A Research and Improvement on a Maximum Power Point Tracking Method for PV System under Partially Shaded Conditions**, Procedia Engineering, Volume 29, pp. 2583-2589, 2012.
- [4] Ali Murtaza, Marcello Chiaberge, Filippo Spertino, Diego Boero, Mirko De Giuseppe. **A maximum power point tracking technique based on bypass diode mechanism for PV arrays under partial shading**, Energy and Buildings, Volume 73, pp. 13-25, 2014.
- [5] A. Kouchaki, H. Iman-Eini, B. Asaei. **A New Maximum Power Point Tracking Strategy for PV Strings under Uniform and Non-Uniform Insolation Conditions**, Solar Energy, Vol. 91, pp. 221-232, 2013.
- [6] Tat Luat Nguyen and Kay-Soon Low. **A Global Maximum Power Point Tracking Scheme Employing DIRECT Search Algorithm for Photovoltaic Systems**, IEEE Transaction on Industrial Electronics, Volume 57, No 10, pp. 3456-3467, 2010.
- [7] Jun Qi, Youbing Zhang, Yi Chen. **Modeling and maximum power point tracking (MPPT) method for PV array under partial shade conditions**, Renewable Energy, Volume 66, pp. 337-345, 2014.
- [8] Eftichios Koutroulis and Frede Blaabjerg. **A New Technique for Tracking the Global Maximum Power Point of PV Arrays Operating Under Partial-Shading Conditions**, IEEE Journal of Photovoltaic, Vol. 2, April, 2012.

- [9] R. Ramaprabha, M. Balaji, B.L. Mathur. **Maximum power point tracking of partially shaded solar PV system using modified Fibonacci search method with fuzzy controller** , Electrical Power and Energy Systems, Vol. 43, pp. 754-765, 2012.
- [10] J. S. Christy Mano Raj and A. E. Jeyakumar. **A Novel Maximum Power Point Tracking Technique for Photovoltaic Module Based on Power Plane Analysis of I–V Characteristics**, IEEE Transactions on Industrial Electronics, Vol. 61, No. 9, pp. 4734- 4745, Sep. 2014.
- [11] K. Ishaque and Z. Salam. **A Deterministic Particle Swarm Optimization Maximum Power Point Tracker for Photovoltaic System Under Partial Shading Condition**, IEEE Transactions on Industrial Electronics, Vol. 60, No. 8, pp. 3195- 3206, Aug. 2013.
- [12] D. R. Espinoza-Trejo and D. U. Campos-Delgado. **Voltage-Oriented Input–Output Linearization Controller as Maximum Power Point Tracking Technique for Photovoltaic Systems**, IEEE Transactions on Industrial Electronics, Vol. 62, No. 6, pp. 3499- 3507, June 2015.
- [13] Sol Moon, Seong-Jin Kim, Jeong-Won Seo, Joung-Hu Park, Changkun Park, Chan-Su Chung. **Maximum power point tracking without current sensor for photovoltaic module integrated converter using Zigbee wireless network**, Electrical Power and Energy Systems 56, pp. 286-297, 2014.
- [14] Y. Mahmoud and E. F. El-Saadany. **Fast Power-Peaks Estimator for Partially Shaded PV Systems**, IEEE Transactions on Energy Conversion, Vol. PP, Issue 99, 2015.
- [15] D.T. Cotfas, P.A. Cotfas, S. Kaplanis. **Methods to determine the dc parameters of solar cells: A critical review**. Renewable and Sustainable Energy Reviews, Vol. 28, pp. 588-596, 2013.
- [16] D. Chan, J. Phillips , J. Phang. **A comparative study of extraction methods for solar cell model parameters**. Solid-State Electronics, Vol. 29, pp. 329-337, 1986.



- [17] K. Ishibashi, Y. Kimura, and M. Niwano. **An extensively valid and stable method for derivation of all parameters of a solar cell from a single current-voltage characteristic.** Journal of Applied Physics, Vol. 103, 2008.
- [18] M. Tivanov, A. Patryn, N. Drozdov, A. Fedotov, A. Mazanik. **Determination of solar cell parameters from its current-voltage and spectral characteristics.** Solar Energy Materials & Solar Cells, Vol. 87, pp. 457-465, 2005.
- [19] M. Chegaar, G. Azzouzi, P. Mialhe. **Simple parameter extraction method for illuminated solar cells.** Solid-State Electronics, Vol. 50, pp. 1234-1237, 2006.
- [20] T. Easwarakhanthan, J. Bottin, I. Bouhouch, C. Boutrit. **Nonlinear minimization algorithm for determining the solar cell parameters with microcomputers.** International Journal of Solar Energy, Vol4, pp. 1-12, 1986.
- [21] K. Bouzidi, M. Chegaar and N. Nehaoua. **New method to extract the parameters of solar cells from their illuminated I-V curve.** 4th International Conference on Computer Integrated Manufacturing, Setif, Algeria, Nov. 2007.
- [22] A.O. Conde, F.J.G. Sanchez, J. Muci. **New method to extract the model parameters of solar cells from the explicit analytic solutions of their illuminated I-V characteristics.** Solar Energy Materials & Solar Cells, Vol. 90, pp. 352-361, 2006.
- [23] K.M. El-Naggar, M.R. AlRashidi, M.F. AlHajri and A.K. Al-Othman. **Simulated annealing algorithm for photovoltaic parameters identification.** Solar Energy, Vol. 86, pp. 266-274, 2012.
- [24] M.F. Al-Hajri, K.M. El-Naggar, M.R. Al-Rashidi and A.K. Al-Othman. **Optimal extraction of solar cell parameters using pattern search.** Renewable Energy, Vol. 44, pp. 238-245, 2012.
- [25] H. Wei, J. Cong, X. Lingyun and S. Deyun. **A new estimation approach for determining the I-V characteristics of solar cells.** Solar Energy, Vol. 85, pp. 1543-1550, 2011.

- [26] A. Askarzadeh and A. Rezazadeh. **Extraction of maximum power point in solar cells using bird mating optimizer-based parameters identification approach.** Solar Energy, Vol. 90, pp. 123-133, 2013.
- [27] H. Wei, J. Cong, X. Lingyun and S. Deyun. **Extracting Solar Cell Model Parameters Based on Chaos Particle Swarm Alogorithm.** International Conference on Electric Information and Control Engineering (ICEICE), pp. 398-402, 2011.
- [28] H. Wei, J. Cong, X. Lingyun, S. Deyun. **Artificial bee swarm optimization algorithm for parameters identification of solar cell models.** Applied Energy, Vol. 102, pp. 943-949, 2013.
- [29] F. Dkhichi, B. Oukarfi, A. Fakkar and N. Belbounaguia. **Parameter identification of solar cell model using Levenberg-Marquardt algorithm combined with simulated annealing.** Solar Energy, Vol. 110, pp. 781-788, 2014.
- [30] O. Hachana, K. E. Hemsas, G. M. Tina and C. Ventura. **Comparison of different metaheuristic algorithms for parameter identification of photovoltaic cell/module.** Journal of Renewable and Sustainable Energy, Vol. 5, 2014.
- [31] A. Askarzadeh, A. Rezazadeh, **Parameter identification for solar cell models using harmony search based algorithms.** Solar Energy, Vol. 86, pp. 3241-3249, 2012.
- [32] S.J. Patel, A.K. Panchal, V. Kheraj. **Extraction of solar cell parameters from a single current-voltage characteristic using teaching learning based optimization algorithm.** Applied Energy, Vol. 119, pp. 384-393, 2014.
- [33] S. Sarker, H.W. Seo, L. Ki-Seong , J. Young-Ku , J. Hyunchul, K. D. Min. **Exact analytical analysis of current density–voltage curves of dye-sensitized solar cells.** Solar Energy, Vol. 115, pp. 390–395, 2015.
- [34] Y. Xiaofang, X. Yongzhong, H. Yuqing, **Parameter extraction of solar cell models using mutative-scale parallel chaos optimization algorithm.** Solar Energy, Vol. 108, pp. 238-251, 2014

- [35] F. Khan, S.N. Singh and M. Husain. **Effect of illumination intensity on cell parameters of a silicon solar cell**, Solar Energy Materials & Solar Cells, Vol. 94, pp. 1473-1476, 2010.
- [36] B.P. Modi and J.M. Dhimmarr. **The temperature dependent ideality factor effect on I-V characteristics of Schottky diode**, 1st International Conference on Emerging Technology Trends in Electronics, Communication and Networking (ET2ECN-2012), Dec, 2012.
- [37] Nhan Thanh Tong and Wanchalerm Pora. **Parameter extraction for a solar cell model with three measured points only**, International Conference on Electronics, Information, and Communication (ICEIC 2016), Jan, 2016.
- [38] [http://www.esid.ee.eng.chula.ac.th/index\\_research.htm](http://www.esid.ee.eng.chula.ac.th/index_research.htm)
- [39] <http://www.ren21.net/status-of-renewables/global-status-report/>
- [40] <http://www.nrel.gov/>
- [41] <http://pveducation.org/>

## Appendix A

# INTRODUCE THE EXTRACTION PROGRAM AND THE CALCULATED PARAMETERS

### A.1 Using the Extraction Program

The extraction software permits user to load required values from data base or declare them directly. Fig. A.1 is the interface when this software start. After click to button

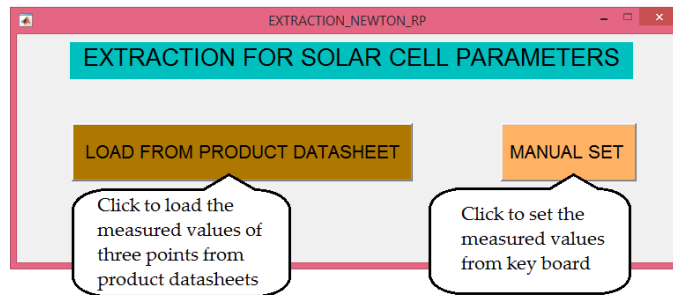


FIGURE A.1: First dialog permits user to provide data by two ways.

”LOAD FROM PRODUCT DATASHEET”, the Fig. A.2 is appeared for loading.

For example, Fig. A.4 shows the extracted parameters of a chosen panel from data base. The execute program for checking is available at website of ESID Lab [38]. The extracted parameters from commercial product data sheet are presented in Tables from A.4 to A.23. After that, the parameters are applied in to panel model in *MATLAB – Simulink* for simulation. The  $I - V$  curve and  $P - V$  curve are drawn in the corresponding figures.

The measured values can be provided for program from keyboard by click the button ”MANUAL SET”. A dialog permits users to type values of  $T$ ,  $V_{OC}$ ,  $I_{SC}$ ,  $V_M$ ,  $I_M$  and number of cell in panel  $x$  (Fig. A.3).

Next, click to button ”SEARCH & DISPLAY”, the program will calculate value of five parameters and show them on the left part. An example is shown in Fig A.5 . The value of 36 cells panel which are used as a referent module for many study, are applied for calculation.

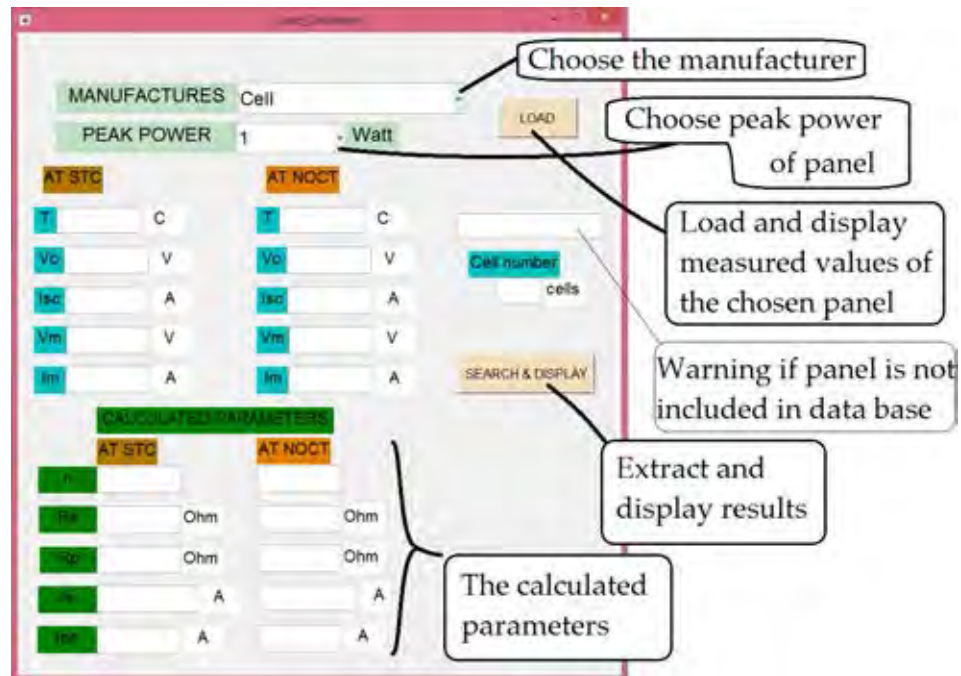


FIGURE A.2: The second interface permits user to choose panel from data base. Both test conditions STC and NOCT of panel are available.

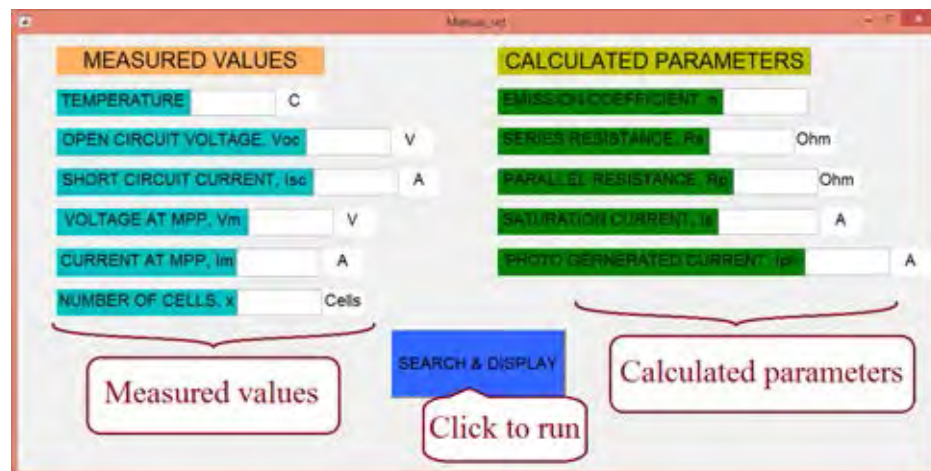


FIGURE A.3: The dialog permits the user to type their measured values.

## A.2 The Extracted Results by The Proposed Method

Eleven series of three type (Polycrystalline, Monocrystalline and Thin-film) are chosen for extracting. The information in datasheet and obtained parameters of each series model are shown in one table. The solar cell parameters at both condition STC and NOCT are extracted. These values are applied in corresponding parameter of solar cell model for creating the I-V and P-V curves. The curves with its MPP are plotted in the same figure for comparison with the given MPP in datasheet. All models are created by calculated parameters gives the MPPs which are closed to the measured

MANUFACTURES GmbH

PEAK POWER 240 Watt

LOAD

Valid values

Cell number 60 cells

SEARCH & DISPLAY

AT STC		AT NOCT	
T	25 C	T	47 C
Vo	37.23 V	Vo	33.7 V
Isc	8.66 A	Isc	7.01 A
Vm	29.98 V	Vm	26.8 V
Im	8.01 A	Im	6.38 A

CALCULATED PARAMETERS		
AT STC	AT NOCT	
n	1.4373	1.3855
Rs	0.0029456 Ohm	0.0030088 Ohm
Rp	15.8944 Ohm	6.8008 Ohm
Is	4.3105e-07 A	2.8587e-06 A
Iph	8.6616 A	7.0131 A

FIGURE A.4: An example for calculation with given data.

MEASURED VALUES

TEMPERATURE 45 C

OPEN CIRCUIT VOLTAGE, Voc 16.78 V

SHORT CIRCUIT CURRENT, Isc 1.0315 A

VOLTAGE AT MPP, Vm 12.64 V

CURRENT AT MPP, Im 0.913 A

NUMBER OF CELLS, x 36 Cells

SEARCH & DISPLAY

CALCULATED PARAMETERS

EMISSION COEFFICIENT, n 1.3107

SERIES RESISTANCE, Rs 0.035402 Ohm

PARALLEL RESISTANCE, Rp 19.884 Ohm

SATURATION CURRENT, Is 2.335e-06 A

PHOTO GERNERATED CURRENT, Iph 1.0333 A

FIGURE A.5: An example for calculating from manual data set.

MPP. Table A.1 lists name of models and its corresponding parameters tables, figures.

TABLE A.1: List of extracted models

#	Model	Manufacturer	Parameters Table		Figure
			At STC	At NOCT	
1	AS235-6P30	Worldwide Energy	Table <a href="#">A.2</a>	Table <a href="#">A.3</a>	Figure <a href="#">A.6</a>
2	AS240-6P30	Worldwide Energy	Table <a href="#">A.2</a>	Table <a href="#">A.3</a>	Figure <a href="#">A.6</a>
3	AS245-6P30	Worldwide Energy	Table <a href="#">A.2</a>	Table <a href="#">A.3</a>	Figure <a href="#">A.6</a>
4	AS250-6P30	Worldwide Energy	Table <a href="#">A.2</a>	Table <a href="#">A.3</a>	Figure <a href="#">A.6</a>
5	TS-235PB-60	H&T Power GmbH	Table <a href="#">A.4</a>	Table <a href="#">A.5</a>	Figure <a href="#">A.7</a>
6	TS-240PB-60	H&T Power GmbH	Table <a href="#">A.4</a>	Table <a href="#">A.5</a>	Figure <a href="#">A.7</a>
7	TS-245PB-60	H&T Power GmbH	Table <a href="#">A.4</a>	Table <a href="#">A.5</a>	Figure <a href="#">A.7</a>
8	TS-250PB-60	H&T Power GmbH	Table <a href="#">A.4</a>	Table <a href="#">A.5</a>	Figure <a href="#">A.7</a>
9	TS-280PB-72	H&T Power GmbH	Table <a href="#">A.6</a>	Table <a href="#">A.7</a>	Figure <a href="#">A.8</a>
10	TS-285PB-72	H&T Power GmbH	Table <a href="#">A.6</a>	Table <a href="#">A.7</a>	Figure <a href="#">A.8</a>
11	TS-290PB-72	H&T Power GmbH	Table <a href="#">A.6</a>	Table <a href="#">A.7</a>	Figure <a href="#">A.8</a>
12	TS-295PB-72	H&T Power GmbH	Table <a href="#">A.6</a>	Table <a href="#">A.7</a>	Figure <a href="#">A.8</a>
13	TS-300PB-72	H&T Power GmbH	Table <a href="#">A.6</a>	Table <a href="#">A.7</a>	Figure <a href="#">A.8</a>
14	GL-235-P6-60	Scheuten	Table <a href="#">A.8</a>	Table <a href="#">A.9</a>	Figure <a href="#">A.9</a>
15	GL-240-P6-60	Scheuten	Table <a href="#">A.8</a>	Table <a href="#">A.9</a>	Figure <a href="#">A.9</a>
16	GL-245-P6-60	Scheuten	Table <a href="#">A.8</a>	Table <a href="#">A.9</a>	Figure <a href="#">A.9</a>
17	GL-250-P6-60	Scheuten	Table <a href="#">A.8</a>	Table <a href="#">A.9</a>	Figure <a href="#">A.9</a>
18	ND-R230A5	Sharp	Table <a href="#">A.10</a>	Table <a href="#">A.11</a>	Figure <a href="#">A.10</a>
19	ND-R235A5	Sharp	Table <a href="#">A.10</a>	Table <a href="#">A.11</a>	Figure <a href="#">A.10</a>
20	ND-R240A5	Sharp	Table <a href="#">A.10</a>	Table <a href="#">A.11</a>	Figure <a href="#">A.10</a>
21	ND-R245A5	Sharp	Table <a href="#">A.10</a>	Table <a href="#">A.11</a>	Figure <a href="#">A.10</a>
22	ND-R250A5	Sharp	Table <a href="#">A.10</a>	Table <a href="#">A.11</a>	Figure <a href="#">A.10</a>
23	Plus SW 260	SUNmodule	Table <a href="#">A.12</a>	Table <a href="#">A.13</a>	Figure <a href="#">A.11</a>
24	Plus SW 265	SUNmodule	Table <a href="#">A.12</a>	Table <a href="#">A.13</a>	Figure <a href="#">A.11</a>
25	Plus SW 270	SUNmodule	Table <a href="#">A.12</a>	Table <a href="#">A.13</a>	Figure <a href="#">A.11</a>
26	Plus SW 275	SUNmodule	Table <a href="#">A.12</a>	Table <a href="#">A.13</a>	Figure <a href="#">A.11</a>
27	Plus SW 280	SUNmodule	Table <a href="#">A.12</a>	Table <a href="#">A.13</a>	Figure <a href="#">A.11</a>
28	TS-185D-72	H&T Power GmbH	Table <a href="#">A.14</a>	Table <a href="#">A.15</a>	Figure <a href="#">A.12</a>
29	TS-190D-72	H&T Power GmbH	Table <a href="#">A.14</a>	Table <a href="#">A.15</a>	Figure <a href="#">A.12</a>
30	TS-195D-72	H&T Power GmbH	Table <a href="#">A.14</a>	Table <a href="#">A.15</a>	Figure <a href="#">A.12</a>
31	TS-200D-72	H&T Power GmbH	Table <a href="#">A.14</a>	Table <a href="#">A.15</a>	Figure <a href="#">A.12</a>
32	TS-205D-72	H&T Power GmbH	Table <a href="#">A.14</a>	Table <a href="#">A.15</a>	Figure <a href="#">A.12</a>
33	TS-245D-60	H&T Power GmbH	Table <a href="#">A.16</a>	Table <a href="#">A.17</a>	Figure <a href="#">A.13</a>
34	TS-250D-60	H&T Power GmbH	Table <a href="#">A.16</a>	Table <a href="#">A.17</a>	Figure <a href="#">A.13</a>
35	TS-255D-60	H&T Power GmbH	Table <a href="#">A.16</a>	Table <a href="#">A.17</a>	Figure <a href="#">A.13</a>
36	TS-260D-60	H&T Power GmbH	Table <a href="#">A.16</a>	Table <a href="#">A.17</a>	Figure <a href="#">A.13</a>
37	TS-265D-60	H&T Power GmbH	Table <a href="#">A.16</a>	Table <a href="#">A.17</a>	Figure <a href="#">A.13</a>
38	TS-295D-72	H&T Power GmbH	Table <a href="#">A.18</a>	Table <a href="#">A.19</a>	Figure <a href="#">A.14</a>
39	TS-300D-72	H&T Power GmbH	Table <a href="#">A.18</a>	Table <a href="#">A.19</a>	Figure <a href="#">A.14</a>
40	TS-305D-72	H&T Power GmbH	Table <a href="#">A.18</a>	Table <a href="#">A.19</a>	Figure <a href="#">A.14</a>
41	TS-310D-72	H&T Power GmbH	Table <a href="#">A.18</a>	Table <a href="#">A.19</a>	Figure <a href="#">A.14</a>
42	TS-315D-72	H&T Power GmbH	Table <a href="#">A.18</a>	Table <a href="#">A.19</a>	Figure <a href="#">A.14</a>
43	FS-4102-2	First Solar	Table <a href="#">A.20</a>	Table <a href="#">A.21</a>	Figure <a href="#">A.15</a>
44	FS-4105-2	First Solar	Table <a href="#">A.20</a>	Table <a href="#">A.21</a>	Figure <a href="#">A.15</a>
45	FS-4107-2	First Solar	Table <a href="#">A.20</a>	Table <a href="#">A.21</a>	Figure <a href="#">A.15</a>
46	FS-4110-2	First Solar	Table <a href="#">A.20</a>	Table <a href="#">A.21</a>	Figure <a href="#">A.15</a>
47	FS-4112-2	First Solar	Table <a href="#">A.20</a>	Table <a href="#">A.21</a>	Figure <a href="#">A.15</a>
48	FS-375	First Solar	Table <a href="#">A.22</a>	Table <a href="#">A.23</a>	Figure <a href="#">A.16</a>
49	FS-377	First Solar	Table <a href="#">A.22</a>	Table <a href="#">A.23</a>	Figure <a href="#">A.16</a>
50	FS-380	First Solar	Table <a href="#">A.22</a>	Table <a href="#">A.23</a>	Figure <a href="#">A.16</a>
51	FS-382	First Solar	Table <a href="#">A.22</a>	Table <a href="#">A.23</a>	Figure <a href="#">A.16</a>
52	FS-385	First Solar	Table <a href="#">A.22</a>	Table <a href="#">A.23</a>	Figure <a href="#">A.16</a>

TABLE A.2: The extracted parameters of series model  $ASxxx - 6P30$  at STC.

	Measured values at STC					Calculated parameters				
	$P$ (W)	$Vm$ (V)	$Im$ (A)	$Voc$ (V)	$Isc$ (A)	$n$	$Rs$ ( $\Omega$ )	$Rp$ ( $\Omega$ )	$Is$ (A)	$Iph$ (A)
AS235-6P30	235	29.70	7.92	37.50	8.48	1.2252	0.00557	62.4198	1.9988E-08	8.4808
AS240-6P30	240	29.90	8.03	37.70	8.57	1.1725	0.00579	94.8700	7.4076E-09	8.5705
AS245-6P30	245	30.10	8.14	37.90	8.66	1.1193	0.00602	149.2193	2.4729E-09	8.6603
AS250-6P30	250	30.31	8.25	38.00	8.75	1.0715	0.00598	233.1454	8.8245E-10	8.7502

TABLE A.3: The extracted parameters of series model  $ASxxx - 6P30$  at NOCT.

	Measured values at NOCT					Calculated parameters				
	$P$ (W)	$Vm$ (V)	$Im$ (A)	$Voc$ (V)	$Isc$ (A)	$n$	$Rs$ ( $\Omega$ )	$Rp$ ( $\Omega$ )	$Is$ (A)	$Iph$ (A)
AS235-6P30	172	27	6.38	34.5	6.87	1.1168	0.00683	43.5185	4.7474E-08	6.8711
AS240-6P30	175	27.2	6.44	34.7	6.94	1.1398	0.00655	38.8354	6.2961E-08	6.9412
AS245-6P30	179	27.4	6.54	34.9	7.01	1.0636	0.00701	70.8337	1.5067E-08	7.0107
AS250-6P30	183	27.6	6.64	35	7.09	1.0137	0.00700	109.2310	5.3756E-09	7.0905

TABLE A.4: The extracted parameters of series model  $TS - xxxPB - 60$  at STC.

	Measured values at STC					Calculated parameters				
	$P$ (W)	$Vm$ (V)	$Im$ (A)	$Voc$ (V)	$Isc$ (A)	$n$	$Rs$ ( $\Omega$ )	$Rp$ ( $\Omega$ )	$Is$ (A)	$Iph$ (A)
TS-235PB-60	235	29.90	7.86	37.16	8.61	1.6177	0.00195	6.1578	2.8531E-06	8.6127
TS-240PB-60	240	29.98	8.01	37.23	8.66	1.4373	0.00295	15.8944	4.3105E-07	8.6616
TS-245PB-60	245	30.11	8.14	37.34	8.82	1.4798	0.00258	12.6124	6.7725E-07	8.8218
TS-250PB-60	250	30.31	8.25	37.42	8.98	1.5560	0.00182	8.0673	1.4827E-06	8.9820
TS-255PB-60	255	30.51	8.36	37.53	9.13	1.6029	0.00130	5.9371	2.2697E-06	9.1320

TABLE A.5: The extracted parameters of series model  $TS - xxxPB - 60$  at NOCT.

	Measured values at NOCT					Calculated parameters				
	$P$ (W)	$Vm$ (V)	$Im$ (A)	$Voc$ (V)	$Isc$ (A)	$n$	$Rs$ ( $\Omega$ )	$Rp$ ( $\Omega$ )	$Is$ (A)	$Iph$ (A)
TS-235PB-60	168	26.60	6.32	33.60	6.97	1.4142	0.00351	5.9220	3.9909E-06	6.9737
TS-240PB-60	171	26.80	6.38	33.70	7.01	1.3855	0.00301	6.8008	2.8587E-06	7.0131
TS-245PB-60	175	26.90	6.49	33.80	7.14	1.4039	0.00280	6.1823	3.3784E-06	7.1432
TS-250PB-60	178	27.00	6.60	33.90	7.27	1.4214	0.00260	5.6517	3.9396E-06	7.2733
TS-255PB-60	182	27.10	6.71	34.00	7.39	1.4247	0.00251	5.5666	3.9685E-06	7.3933



TABLE A.6: The extracted parameters of series model  $TS - xxxPB - 72$  at STC.

	Measured values at STC					Calculated parameters				
	$P$ (W)	$V_m$ (V)	$I_m$ (A)	$V_{oc}$ (V)	$I_{sc}$ (A)	$n$	$R_s$ ( $\Omega$ )	$R_p$ ( $\Omega$ )	$I_s$ (A)	$I_{ph}$ (A)
TS-280PB-72	280	35.81	7.82	44.59	8.53	1.5615	0.00244	8.3826	1.6590E-06	8.5325
TS-285PB-72	285	36.10	7.91	44.68	8.74	1.7058	0.00112	3.6110	6.0338E-06	8.7427
TS-290PB-72	290	36.18	8.02	44.81	8.85	1.7009	0.0012	3.8471	5.6358E-06	8.8528
TS-295PB-72	295	36.42	8.10	44.90	8.86	1.6155	0.00140	5.7548	2.5934E-06	8.8621
TS-300PB-72	300	36.81	8.15	45.04	8.88	1.5760	0.00110	6.4082	1.7017E-06	8.8815

TABLE A.7: The extracted parameters of series model  $TS - xxxPB - 72$  at NOCT.

	Measured values at NOCT					Calculated parameters				
	$P$ (W)	$V_m$ (V)	$I_m$ (A)	$V_{oc}$ (V)	$I_{sc}$ (A)	$n$	$R_s$ ( $\Omega$ )	$R_p$ ( $\Omega$ )	$I_s$ (A)	$I_{ph}$ (A)
TS-280PB-72	201	32.10	6.25	40.40	6.91	1.4449	0.00266	5.0669	5.2075E-06	6.9136
TS-285PB-72	206	32.20	6.39	40.50	7.08	1.4683	0.00241	4.4564	6.4412E-06	7.0838
TS-290PB-72	209	32.30	6.47	40.60	7.15	1.4488	0.00251	4.9499	5.2211E-06	7.1536
TS-295PB-72	211	32.40	6.51	40.70	7.17	1.4204	0.00269	5.8056	3.8197E-06	7.1733
TS-300PB-72	213	32.60	6.54	40.80	7.19	1.4092	0.00249	6.0823	3.2972E-06	7.1929

TABLE A.8: The extracted parameters of series  $Goldline - xxx - P6 - 60$  at STC.

	Measured values at STC					Calculated parameters				
	$P$ (W)	$V_m$ (V)	$I_m$ (A)	$V_{oc}$ (V)	$I_{sc}$ (A)	$n$	$R_s$ $\Omega$	$R_p$ $\Omega$	$I_s$ (A)	$I_{ph}$ (A)
Goldline										
235-P6-60	235	30.40	7.74	37.10	8.21	1.1209	0.00376	137.3618	3.8440E-09	8.2102
240-P6-60	240	30.50	7.87	37.20	8.33	1.0804	0.00396	198.6431	1.6419E-09	8.3302
245-P6-60	245	30.70	7.98	37.40	8.45	1.0983	0.00376	177.5322	2.1301E-09	8.4502
250-P6-60	250	30.90	8.10	37.50	8.57	1.0937	0.00349	188.8500	1.8552E-09	8.5702

TABLE A.9: The extracted parameters of series  $Goldline - xxx - P6 - 60$  at NOCT.

	Measured values at NOCT					Calculated parameters				
	$P$ (W)	$V_m$ (V)	$I_m$ (A)	$V_{oc}$ (V)	$I_{sc}$ (A)	$n$	$R_s$ $\Omega$	$R_p$ $\Omega$	$I_s$ (A)	$I_{ph}$ (A)
Goldline										
235-P6-60	172	27.90	6.15	34.70	6.65	1.2581	0.00372	19.5390	3.2561E-07	6.6513
240-P6-60	175	28.00	6.25	34.80	6.75	1.2457	0.00374	21.3031	2.6628E-07	6.7512
245-P6-60	178	28.10	6.34	35.00	6.85	1.2541	0.00388	21.0808	3.8839E-03	6.8513
250-P6-60	182	28.30	6.44	35.10	6.95	1.2499	0.00354	21.6262	2.5081E-07	6.9511

TABLE A.10: The extracted parameters of series model  $ND - Rxxx - A5$  at STC.

	Measured values					Calculated parameters				
	<b>P</b> (W)	<b>V<sub>m</sub></b> (V)	<b>I<sub>m</sub></b> (A)	<b>V<sub>oc</sub></b> (V)	<b>I<sub>sc</sub></b> (A)	<b>n</b>	<b>R<sub>s</sub></b> $\Omega$	<b>R<sub>p</sub></b> $\Omega$	<b>I<sub>s</sub></b> (A)	<b>I<sub>ph</sub></b> (A)
ND-R230A5	230	30.30	7.61	36.40	8.41	1.4652	0.00004	2.0089	8.0633E-07	8.4102
ND-R235A5	235	30.30	7.76	36.80	8.49	1.5600	0.00046	4.2219	1.8720E-06	8.4909
ND-R240A5	240	30.40	7.90	37.20	8.57	1.5108	0.00144	9.1287	9.7561E-07	8.5714
ND-R245A5	245	30.70	7.99	37.30	8.62	1.4462	0.00132	12.5187	4.6049E-07	8.6209
ND-R250A5	250	30.90	8.10	37.60	8.68	1.3462	0.00211	27.1733	1.1607E-07	8.6807

TABLE A.11: The extracted parameters of series model  $ND - Rxxx - A5$  at NOCT.

	Measured values					Calculated parameters				
	<b>P</b> (W)	<b>V<sub>m</sub></b> (V)	<b>I<sub>m</sub></b> (A)	<b>V<sub>oc</sub></b> (V)	<b>I<sub>sc</sub></b> (A)	<b>n</b>	<b>R<sub>s</sub></b> $\Omega$	<b>R<sub>p</sub></b> $\Omega$	<b>I<sub>s</sub></b> (A)	<b>I<sub>ph</sub></b> (A)
ND-R230A5	166	27.10	6.11	35.60	6.79	1.5023	0.00694	6.6934	4.1318E-06	6.7970
ND-R235A5	169	27.10	6.25	36.00	6.85	1.3089	0.00941	16.4659	4.2210E-07	6.8539
ND-R240A5	173	27.20	6.36	36.40	6.92	1.2055	0.01029	29.4436	9.3112E-08	6.9224
ND-R245A5	177	27.50	6.42	36.40	6.96	1.1739	0.01009	37.8965	5.1911E-08	6.9619
ND-R250A5	180	27.70	6.51	36.70	7.00	1.0506	0.01115	94.4190	4.8945E-09	7.0008

TABLE A.12: The extracted parameters of series  $PlusSW$  at STC.

	Measured values at STC					Calculated parameters				
	<b>P</b> (W)	<b>V<sub>m</sub></b> (V)	<b>I<sub>m</sub></b> (A)	<b>V<sub>oc</sub></b> (V)	<b>I<sub>sc</sub></b> (A)	<b>n</b>	<b>R<sub>s</sub></b> ( $\Omega$ )	<b>R<sub>p</sub></b> ( $\Omega$ )	<b>I<sub>s</sub></b> (A)	<b>I<sub>ph</sub></b> (A)
Plus SW 260	260	30.70	8.56	38.90	9.18	1.2918	0.00546	51.7038	2.9816E-08	9.1810
Plus SW 265	265	30.80	8.69	39.00	9.31	1.2772	0.00545	57.3245	2.2989E-08	9.3109
Plus SW 270	270	30.90	8.81	39.20	9.44	1.2809	0.00555	57.5075	2.2305E-08	9.4409
Plus SW 275	275	31.00	8.94	39.40	9.58	1.2830	0.00564	58.1687	2.1134E-08	9.5809
Plus SW 280	280	31.20	9.07	39.50	9.71	1.2793	0.00536	61.0653	1.9222E-08	9.7109

TABLE A.13: The extracted parameters of series *PlusSW* at NOCT.

	Measured values at NOCT					Calculated parameters				
	<b><i>P</i></b> (W)	<b><i>V<sub>m</sub></i></b> (V)	<b><i>I<sub>m</sub></i></b> (A)	<b><i>V<sub>oc</sub></i></b> (V)	<b><i>I<sub>sc</sub></i></b> (A)	<b><i>n</i></b>	<b><i>R<sub>s</sub></i></b> ( $\Omega$ )	<b><i>R<sub>p</sub></i></b> ( $\Omega$ )	<b><i>I<sub>s</sub></i></b> (A)	<b><i>I<sub>ph</sub></i></b> (A)
Plus SW 260	192	27.80	6.92	35.20	7.42	1.0843	0.00607	58.1819	2.3723E-08	7.4208
Plus SW 265	196	27.90	7.02	35.30	7.53	1.0955	0.00588	54.3179	2.7828E-08	7.5308
Plus SW 270	199	28.00	7.12	35.50	7.63	1.0803	0.00615	62.8048	1.9196E-08	7.6307
Plus SW 275	203	28.10	7.22	35.70	7.75	1.1087	0.00608	52.4969	2.9038E-08	7.7509
Plus SW 280	282	38.50	7.33	36.10	7.85	1.0845	0.00589	64.3544	1.8051E-08	7.8507

TABLE A.14: The extracted parameters of series *TS – xxxD – 72* at STC.

	Measured values at STC					Calculated parameters				
	<b><i>P</i></b> (W)	<b><i>V<sub>m</sub></i></b> (V)	<b><i>I<sub>m</sub></i></b> (A)	<b><i>V<sub>oc</sub></i></b> (V)	<b><i>I<sub>sc</sub></i></b> (A)	<b><i>n</i></b>	<b><i>R<sub>s</sub></i></b> ( $\Omega$ )	<b><i>R<sub>p</sub></i></b> ( $\Omega$ )	<b><i>I<sub>s</sub></i></b> (A)	<b><i>I<sub>ph</sub></i></b> (A)
TS-185D-72	185	36.42	5.08	45.05	5.41	1.1796	0.00686	144.1631	5.7844E-09	5.4103
TS-190D-72	190	36.50	5.21	45.20	5.53	1.1119	0.00754	251.8551	1.5633E-09	5.5302
TS-195D-72	195	36.94	5.28	45.28	5.58	1.0497	0.00700	454.8663	4.1148E-10	5.5801
TS-200D-72	200	37.39	5.35	45.50	5.79	1.5118	0.00180	14.7716	4.8997E-07	5.7907
TS-205D-72	205	37.83	5.42	45.68	5.90	1.5558	0.00055	7.4064	7.3781E-07	5.9004

TABLE A.15: The extracted parameters of series *TS – xxxD – 72* at NOCT.

	Measured values at NOCT					Calculated parameters				
	<b><i>P</i></b> (W)	<b><i>V<sub>m</sub></i></b> (V)	<b><i>I<sub>m</sub></i></b> (A)	<b><i>V<sub>oc</sub></i></b> (V)	<b><i>I<sub>sc</sub></i></b> (A)	<b><i>n</i></b>	<b><i>R<sub>s</sub></i></b> ( $\Omega$ )	<b><i>R<sub>p</sub></i></b> ( $\Omega$ )	<b><i>I<sub>s</sub></i></b> (A)	<b><i>I<sub>ph</sub></i></b> (A)
TS-185D-72	134	33.60	4.00	41.40	4.37	1.3843	0.00268	11.4922	1.1288E-06	4.3710
TS-190D-72	138	33.70	4.09	41.50	4.47	1.3912	0.00250	10.8820	1.1998E-06	4.4710
TS-195D-72	140	33.80	4.15	41.60	4.51	1.3354	0.00313	15.8110	6.2194E-07	4.5109
TS-200D-72	145	33.90	4.27	41.80	4.68	1.4277	0.00227	9.0227	1.6589E-06	4.6812
TS-205D-72	148	34.00	4.36	42.00	4.76	1.3964	0.00291	11.7146	1.1289E-06	4.7612

TABLE A.16: The extracted parameters of series *TS – xxxD – 60* at STC.

	Measured values at STC					Calculated parameters				
	<b><i>P</i></b> (W)	<b><i>V<sub>m</sub></i></b> (V)	<b><i>I<sub>m</sub></i></b> (A)	<b><i>V<sub>oc</sub></i></b> (V)	<b><i>I<sub>sc</sub></i></b> (A)	<b><i>n</i></b>	<b><i>R<sub>s</sub></i></b> ( $\Omega$ )	<b><i>R<sub>p</sub></i></b> ( $\Omega$ )	<b><i>I<sub>s</sub></i></b> (A)	<b><i>I<sub>ph</sub></i></b> (A)
TS-245D-60	245	30.49	8.04	37.51	8.64	1.3674	0.00276	24.7741	1.5968E-07	8.6410
TS-250D-60	250	30.59	8.17	37.59	8.79	1.3937	0.00250	20.9994	2.1890E-07	8.7910
TS-255D-60	255	30.69	8.31	37.73	8.93	1.3769	0.00263	23.8569	1.6822E-07	8.9310
TS-260D-60	260	30.79	8.44	37.91	9.06	1.3601	0.00285	27.4508	1.2578E-07	9.0609
TS-265D-60	265	30.90	8.58	38.10	9.19	1.3213	0.00317	36.4474	6.8367E-08	9.1908

TABLE A.17: The extracted parameters of series  $TS - xxxD - 60$  at NOCT.

	Measured values at NOCT					Calculated parameters				
	$P$ (W)	$V_m$ (V)	$I_m$ (A)	$V_{oc}$ (V)	$I_{sc}$ (A)	$n$	$R_s$ ( $\Omega$ )	$R_p$ ( $\Omega$ )	$I_s$ (A)	$I_{ph}$ (A)
TS-245D-60	176	27.60	6.38	34.30	6.98	1.3776	0.00232	7.5644	2.0125E-06	6.9821
TS-250D-60	180	27.70	6.49	34.40	7.10	1.3817	0.00223	7.3981	2.0488E-06	7.1021
TS-255D-60	183	27.80	6.60	34.50	7.22	1.3857	0.00214	7.2334	2.0828E-06	7.2221
TS-260D-60	187	27.90	6.70	34.60	7.32	1.3767	0.00215	7.6732	1.8330E-06	7.3221
TS-265D-60	191	28.10	6.80	34.80	7.43	1.3868	0.00201	7.3837	1.9041E-06	7.4320

TABLE A.18: The extracted parameters of series  $TS - xxxD - 72$  at STC.

	Measured values at STC					Calculated parameters				
	$P$ (W)	$V_m$ (V)	$I_m$ (A)	$V_{oc}$ (V)	$I_{sc}$ (A)	$n$	$R_s$ ( $\Omega$ )	$R_p$ ( $\Omega$ )	$I_s$ (A)	$I_{ph}$ (A)
TS-295D-72	295	36.48	8.09	45.01	8.71	1.3931	0.00280	21.2803	2.2363E-07	8.7111
TS-300D-72	300	36.60	8.20	45.11	8.81	1.3618	0.00290	25.8927	1.4557E-07	8.8110
TS-305D-72	305	36.72	8.31	45.28	8.92	1.3488	0.00301	28.7138	1.1588E-07	8.9209
TS-310D-72	310	36.84	8.41	45.49	9.01	1.3151	0.00332	36.9564	6.7455E-08	9.0108
TS-315D-72	315	36.91	8.53	45.62	9.12	1.2765	0.00360	48.5113	3.6717E-08	9.1207

TABLE A.19: The extracted parameters of series  $TS - xxxD - 72$  at NOCT.

	Measured values at NOCT					Calculated parameters				
	$P$ (W)	$V_m$ (V)	$I_m$ (A)	$V_{oc}$ (V)	$I_{sc}$ (A)	$n$	$R_s$ ( $\Omega$ )	$R_p$ ( $\Omega$ )	$I_s$ (A)	$I_{ph}$ (A)
TS-295D-72	214	33.30	6.43	41.40	7.03	1.3780	0.00241	7.9212	1.8658E-06	7.0321
TS-300D-72	218	33.50	6.51	41.50	7.11	1.3733	0.00215	7.9300	1.7273E-06	7.1119
TS-305D-72	221	33.60	6.59	41.70	7.20	1.3823	0.00227	7.9196	1.7958E-06	7.2021
TS-310D-72	225	33.80	6.66	41.90	7.28	1.3951	0.00211	7.4883	1.9410E-06	7.2821
TS-315D-72	229	33.90	6.75	42.00	7.36	1.3714	0.00224	8.6620	1.4586E-06	7.3619

TABLE A.20: The extracted parameters of series  $FS - 4xxx - 2$  at STC.

	Measured values at STC					Calculated parameters				
	$P$ (W)	$V_m$ (V)	$I_m$ (A)	$V_{oc}$ (V)	$I_{sc}$ (A)	$n$	$R_s$ ( $\Omega$ )	$R_p$ ( $\Omega$ )	$I_s$ (A)	$I_{ph}$ (A)
FS-4102-2	102.5	67.00	1.53	85.30	1.74	1.2518	0.00574	5.9110	7.7399E-06	1.7417
FS-4105-2	105	67.80	1.55	86.00	1.74	1.1951	0.00677	8.4873	3.9337E-06	1.7414
FS-4107-2	107.5	68.60	1.57	86.60	1.75	1.1616	0.00677	10.4447	2.4919E-06	1.7511
FS-4110-2	110	69.40	1.59	87.20	1.75	1.0838	0.00807	17.6661	8.6696E-07	1.7508
FS-4112-2	112.5	70.20	1.60	87.70	1.75	1.0439	0.00803	23.5738	4.5823E-07	1.7506

TABLE A.21: The extracted parameters of series  $FS - 4xxx - 2$  at NOCT.

	Measured values at NOCT					Calculated parameters				
	$P$ (W)	$V_m$ (V)	$I_m$ (A)	$V_{oc}$ (V)	$I_{sc}$ (A)	$n$	$R_s$ ( $\Omega$ )	$R_p$ ( $\Omega$ )	$I_s$ (A)	$I_{ph}$ (A)
FS-4102-2	76	62.10	1.23	80.40	1.40	1.1135	0.01137	7.7772	6.8215E-06	1.4021
FS-4105-2	78	62.60	1.25	81.00	1.40	1.0314	0.01448	12.9803	2.3734E-06	1.4016
FS-4107-2	80	63.10	1.27	81.60	1.41	0.9807	0.01634	18.4719	1.0922E-06	1.4112
FS-4110-2	82	64.10	1.28	82.10	1.41	0.9414	0.01534	24.7911	5.5710E-07	1.4109
FS-4112-2	84	65.00	1.29	82.60	1.41	0.8950	0.01510	36.1865	2.3692E-07	1.4106

TABLE A.22: The extracted parameters of series  $FS - 3xxx - 2$  at STC.

	Measured values at STC					Calculated parameters				
	$P$ (W)	$V_m$ (V)	$I_m$ (A)	$V_{oc}$ (V)	$I_{sc}$ (A)	$n$	$R_s$ ( $\Omega$ )	$R_p$ ( $\Omega$ )	$I_s$ (A)	$I_{ph}$ (A)
FS-375	75	46.90	1.60	60.10	1.82	1.2425	0.00683	5.8756	8.5610E-06	1.8221
FS-377	77.5	48.30	1.61	60.70	1.84	1.2387	0.00251	4.3544	7.2738E-06	1.8411
FS-380	80	48.50	1.65	60.80	1.88	1.2248	0.00232	4.4774	6.3399E-06	1.8810
FS-382	82.5	48.30	1.71	60.80	1.94	1.2240	0.00327	5.0689	6.5356E-06	1.9413
FS-385	85	48.50	1.76	61.00	1.98	1.1937	0.00394	6.3204	4.6892E-06	1.9812

TABLE A.23: The extracted parameters of series  $FS - 3xxx - 2$  at NOCT.

	Measured values at NOCT					Calculated parameters				
	$P$ (W)	$V_m$ (V)	$I_m$ (A)	$V_{oc}$ (V)	$I_{sc}$ (A)	$n$	$R_s$ ( $\Omega$ )	$R_p$ ( $\Omega$ )	$I_s$ (A)	$I_{ph}$ (A)
FS-375	56	44.00	1.28	55.90	1.49	1.1384	0.00318	3.7202	1.2326E-05	1.4913
FS-377	58	45.30	1.29	56.50	1.51	1.0657	0.00072	2.8930	4.8414E-06	1.5104
FS-380	60	45.50	1.32	56.50	1.54	1.0377	0.00053	2.8805	3.5227E-06	1.5403
FS-382	62	45.30	1.37	56.50	1.59	1.0644	0.00092	3.1682	5.0816E-06	1.5905
FS-385	64	45.50	1.41	56.70	1.62	1.0580	0.00121	3.7580	4.6493E-06	1.6205

### A.3 The I-V Curves, P-V Curves, MPP by Simulation and Calculation

Applying the obtained parameters into the models to plot the curve and MPPsin following figures.

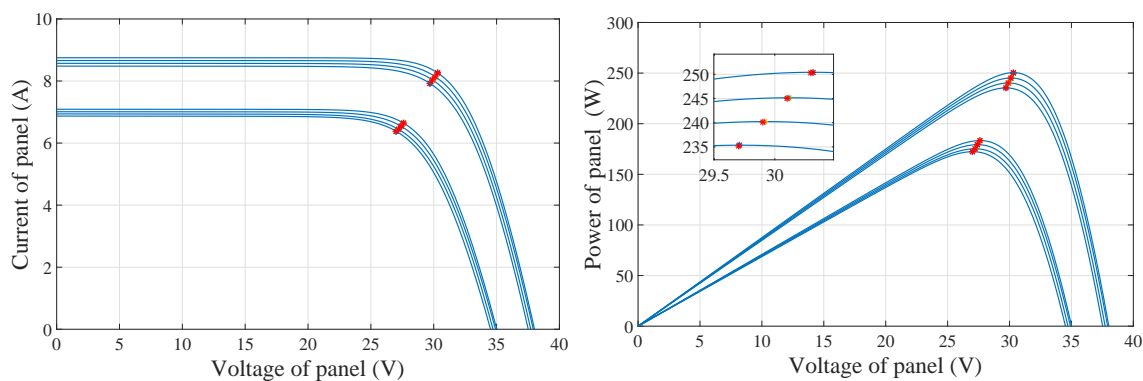


FIGURE A.6: The I-V curves (left) and the P -V curves (right) of series *ASxxx – 6P30* at STC (upper) and NOCT (lower).

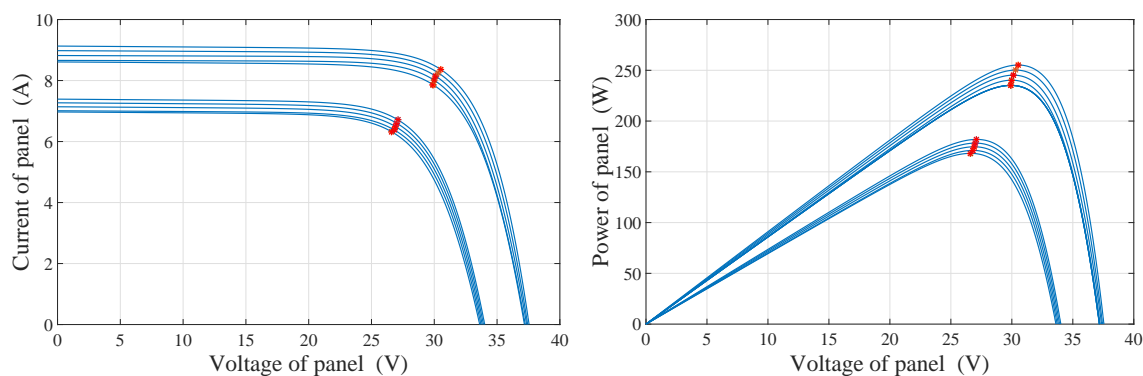


FIGURE A.7: The I-V curves (left) and the P -V curves (right) of series *TS – xxxPB – 60* at STC (upper) and NOCT (lower).

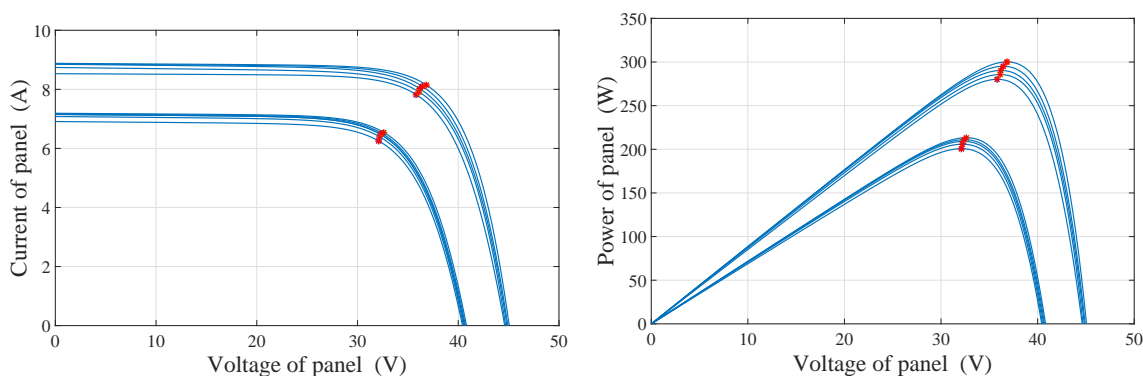


FIGURE A.8: The I-V curves (left) and the P -V curves (right) of series *TS – xxxPB – 72* at STC (upper) and NOCT (lower).

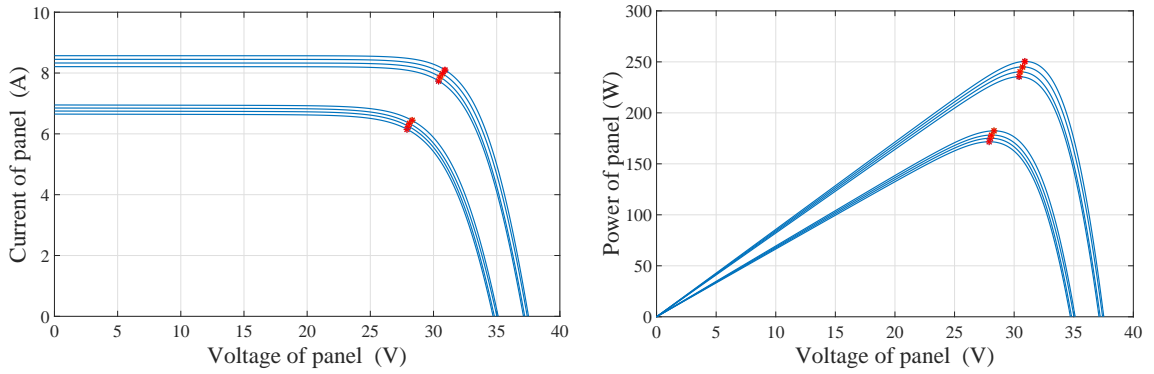


FIGURE A.9: The I-V curves (left) and the P -V curves (right) of series *Goldline – xxx – P6 – 60* at STC (upper) and NOCT (lower).

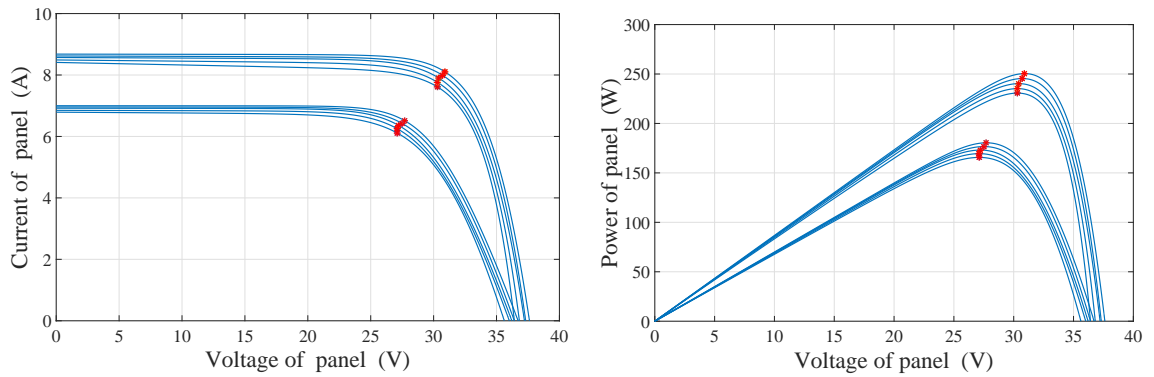


FIGURE A.10: The I-V curves (left) and the P -V curves (right) of series *ND – Rxxx – A5* at STC (upper) and NOCT (lower).

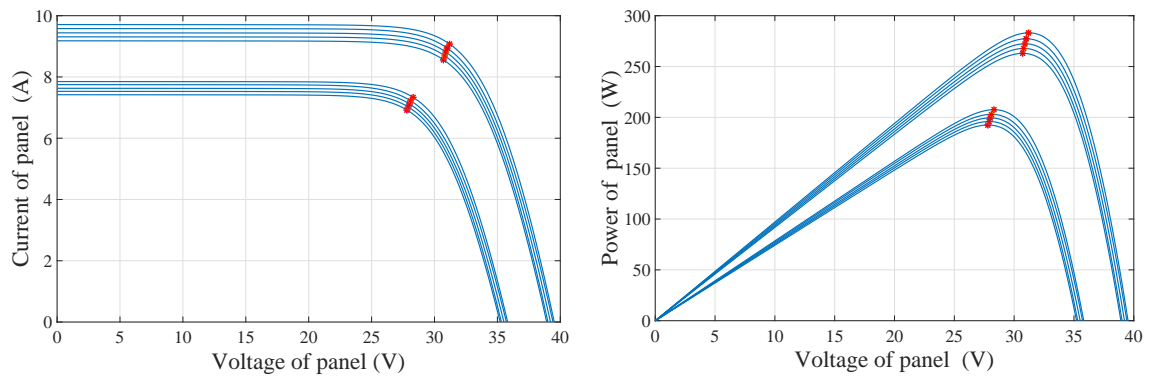


FIGURE A.11: The I-V curves (left) and the P -V curves (right) of series *PlusSW* at STC (upper) and NOCT (lower).

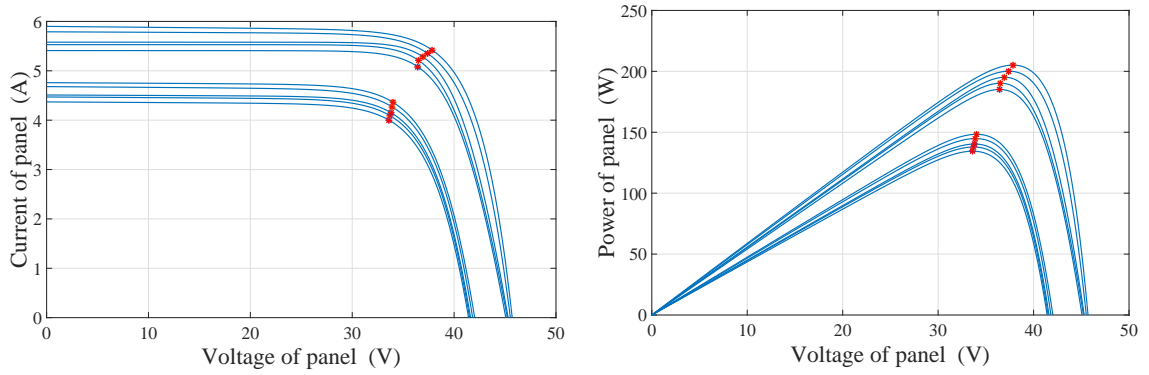


FIGURE A.12: The I-V curves (left) and the P -V curves (right) of series  $TS - xxxD - 72$  at STC (upper) and NOCT (lower).

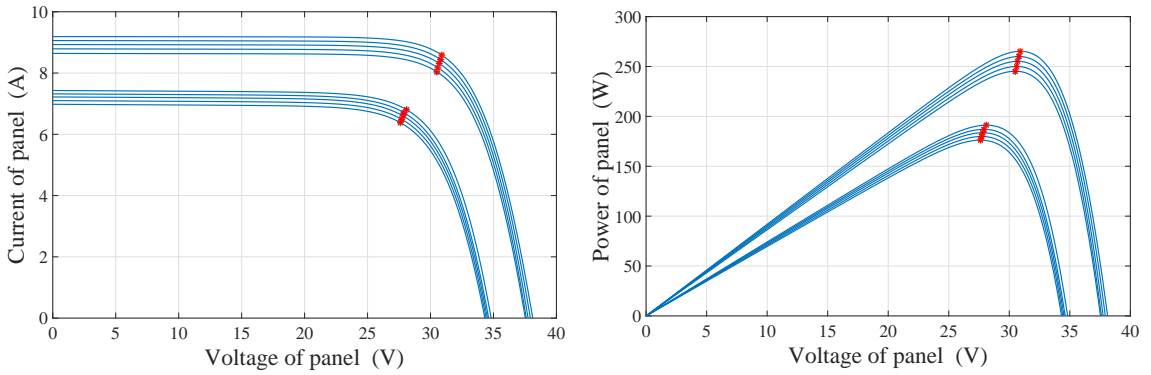


FIGURE A.13: The I-V curves (left) and the P -V curves (right) of series  $TS - xxxD - 60$  at STC (upper) and NOCT (lower).

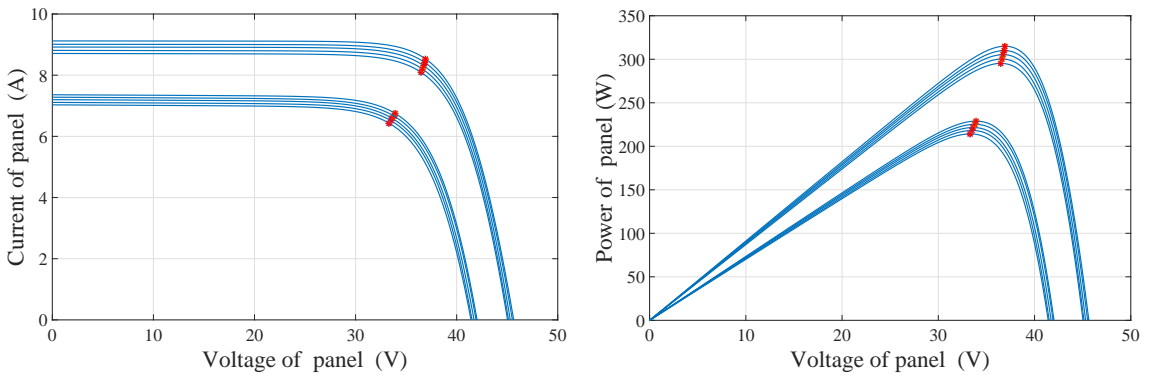


FIGURE A.14: The I-V curves (left) and the P -V curves (right) of series  $TS - xxxD - 72$  at STC (upper) and NOCT (lower).



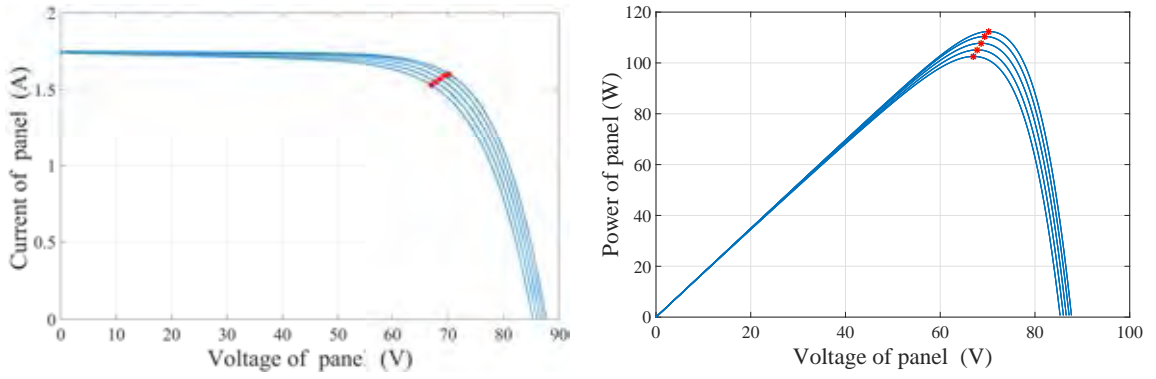


FIGURE A.15: The I-V curves (left) and the P -V curves (right) of series  $FS - 4xxx - 2$  at STC (upper) and NOCT (lower).)

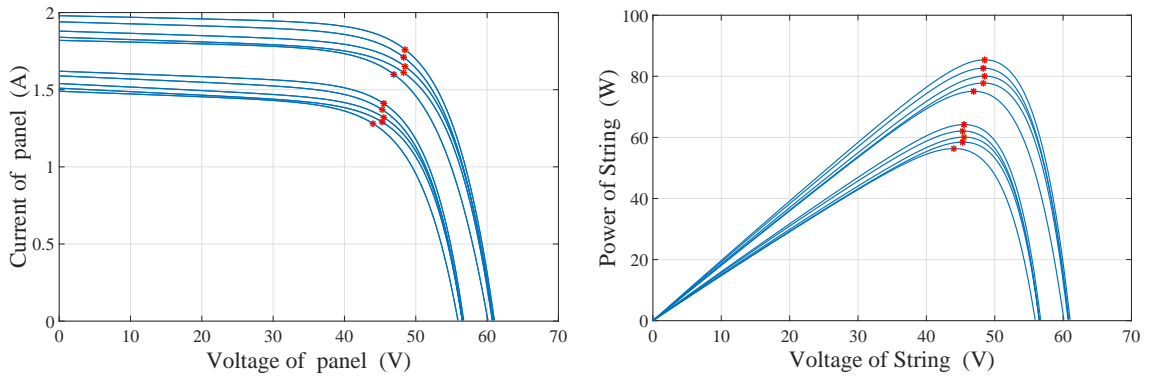


FIGURE A.16: The I-V curves (left) and the P -V curves (right) of series  $FS - 3xxx - 2$  at STC (upper) and NOCT (lower).)

## Appendix B

# INTRODUCE THE CALCULATION AND SIMULATION PROGRAM FOR THE PV SYSTEM

### B.1 The Program for Determination MPPs and Simulation PV System

#### B.1.1 The Program Interface

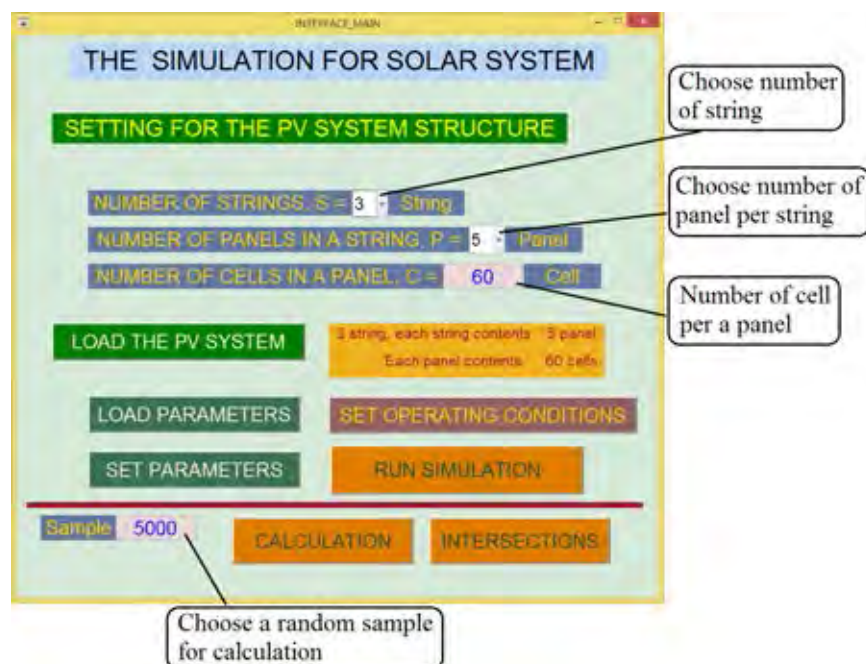


FIGURE B.1: The interface of program permits user to choose the size of PV system. The maximum size is 10x10 (10 strings, each string contents 10 panels in series). The number of cells in each panel is unlimited. There are seven buttons in Main interface. The functions of these buttons are introduced in Table B.1

The function of buttons in the main interface are described in Table B.1

TABLE B.1: The function of buttons in Main interface of program.

Button	Function
1 LOAD THE PV SYSTEM	Open the corresponding simulation file.
2 LOAD PARAMETERS	Open dialog for loading parameters from given data sheet.
3 SET PARAMETERS	Open dialog for calculating parameters from manual set.
4 SET OPERATING CON...	Open dialog for setting the $I_r, T_P, T_d$ of all panels.
5 RUN SIMULATION	Start the simulation. Drawing the curve and simulated peaks.
6 CALCULATION	Starting for calculation. Drawing the local calculated peaks.
7 INTERSECTIONS	Calculate and draw the curve for explaining obtained peaks.



FIGURE B.2: The interface for user to set up the operating conditions of all panels. Each panel requires three input data:  $I_r, T_P, T_d$ . The button “SEND TO PV SYSTEM” updates the setting values to model in schematic for simulation.

To scan for large values of the load, the value of load in simulation depends on time by the follow function:

$$R_{load}(t) = 50t + u(t - 0.5)500t + u(t - 1)5000t + u(t - 1.5)10000t \quad (\text{B.1})$$

where:

$$u(t) = \begin{cases} 0, & \text{if } t < 0 \\ 1, & \text{if } t \geq 0 \end{cases} \quad (\text{B.2})$$

The time for scanning is 2 seconds. That mean the load will be scanned from  $0\Omega$

FIGURE B.3: The interface permits user to enter the measured values ( $T$ ,  $V_{OC}$ ,  $I_{SC}$ ,  $V_M$ ,  $I_M$  and  $C$ ) in left column. Click the button “SEARCH & DISPLAY” to extract the parameters based on input data and display them to right column. Button “UPDATE PARAMETERS” send the parameters to model for simulation.

FIGURE B.4: The interface for loading the measured values from database. Similar to the program which is introduced in Fig. A.2. However, this dialog has two other buttons for update the parameters to the models (“UPDATE Parameters STC” and “UPDATE Parameters NOCT”).

to  $10850 \Omega$ . With the maximum of load, the power consumption is very low even if the output voltage is high. For example, the output voltage is 500V, the current is  $500/10850=0.0461\text{A}$  and power is 23.04 W.

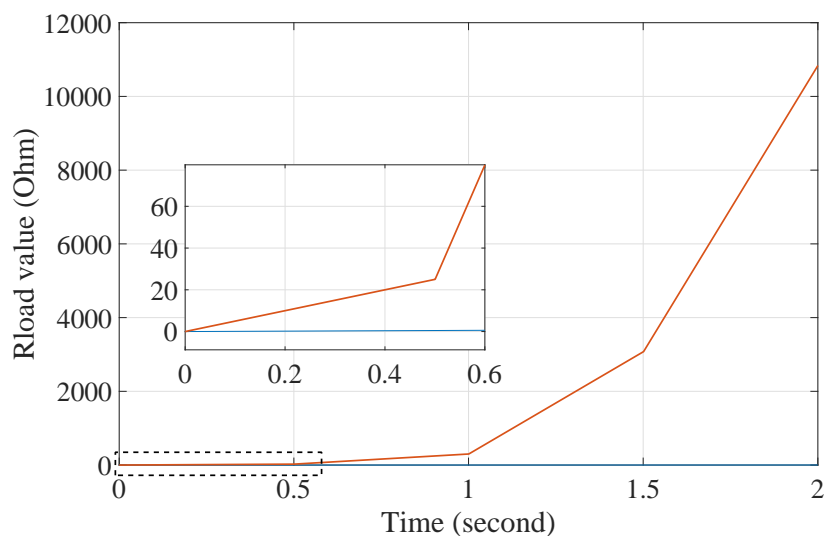


FIGURE B.5: The dependence of  $R_{load}$  on time. The variable load is scanned from  $0\Omega$  to  $10850\Omega$ . The zoomed part shows that the load is scanned slowly at small values for tracking the MPP. The step size will be increase when the load value is large.

### B.1.2 Example for Using the Program

*Step 1:* After user run the file “INTERFACE\_MAIN.exe”, it appears the dialog as Fig. B.6.

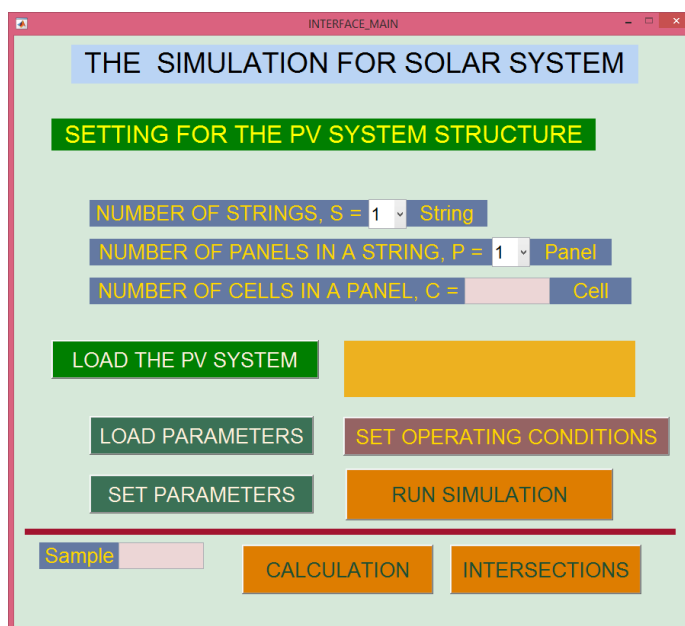
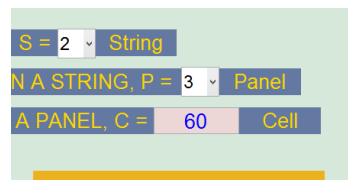


FIGURE B.6: Main interface with default both number of string and number of panel per string are 1.

*Step 2:* Choose the number of string in PV system, the number of panel per string and type number of cells per panel as the Fig. B.7.



Set the number of strings, and number of panels per string.



Set the number of cells per panel.

FIGURE B.7: Setting the PV system structure.

*Step 3:* Click to button “LOAD THE PV SYSTEM” to open the model PV system which is set at Step 2. After the loading is finished, there is a message to describe the current schematic which ready for simulation as in the Fig. B.8.

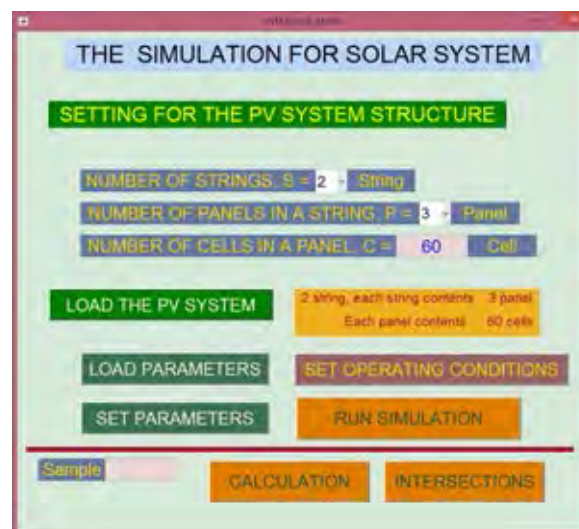


FIGURE B.8: Main interface with default both number of string and number of panel per string are 1.

*Step 4:* Click “LOAD PARAMETERS” or “SET PARAMETERS” to open dialogs for calculation the parameters of solar cell. In this case, click button “LOAD PARAMETERS”. The dialog will appear as the Fig. B.9. In the new dialog, choose MANUFACTURER “GmbH” and PEAK POWER “235”. Next click to button “LOAD” to load the data from data sheet of this product to program for calculation. These values are also



FIGURE B.9: Setting the parameters for solar cell follow model  $TS - 235PB - 60$  of GmbH manufacturer.

displayed on blanks of the dialog. Click to “SEARCH & DISPLAY” button to calculate and display the solar cell parameters which are extracted by proposed method. Click to “UPDATE Parameters STC” or “UPDATE Parameters NOCT” (depend on which condition is chosen).

*Step 5:* Back to “MAIN INTERFACE” dialog and click button “SET OPERATING CONDITIONS” to open the dialog which permit user enter the values of  $I_r, T_p, T_d$  for all panels in PV system. Set the conditions as in Fig. B.10. Click button “SEND TO PV SYSTEM” to update the operating conditions for all panels of system.

*Step 6:* Back to “MAIN INTERFACE”, click button “RUN SIMULATION” to simulate the PV system. The I-V curves, P-V curve and local MPP are plot and show in Figure 99 and 100 (default). The simulated peaks are also plotted in figure 11 and 12 for string 1 and string 2, respectively. The figures are shown in part B.3.1.

Step 7: User type the number of “Sample”, which will be used for calculation. The “Sample” value has a relationship with  $t$  by the formula:

$$t = \frac{\text{Sample}}{10000} \quad (\text{B.3})$$

Replace (B.3) into (B.1) to calculate value of  $R_{load}$  is used to measure and calculation. Set “Sample” is equal 5000 and click button “CALCULATION” to calculate the local



FIGURE B.10: Setting the operating conditions for all panels in 2x3 PV system.

peaks of strings. All local peaks which obtained by calculation are plotted on figure 99 and 100.

*Step 8:* Click “INTERSECTIONS” to build and draw the I-V curve, P-V curve, condition function curve ( $V_M(I)$ ) for illustration. All of figures are present in part B.3.1.

During executing time, the program generates the data files (.dat file) and auto save them at the same folder. The generated files are: *data\_str1.dat*, *data\_str2.dat*, *data\_system.dat*, *Datasheet.parameters.dat*, *Iphmatrix.dat*, *Irr.dat*, *IString\_System.dat*, *IVplocal\_matrix.dat*, *n\_C.dat*, *n\_P.dat*, *n\_S.dat*, *P\_est\_sys.dat*, *Parameters\_cal\_matrix.dat*, *Parameters\_calcu.dat*, *PString\_System.dat*, *Simlocal.dat*, *Td.dat*, *Tp.dat*, *VIPcal1.dat*, *VIPcal2.dat*, *VString\_System.dat*. These files can be loaded and shown from “Command window” for analyses. Table B.2 shows the content of data files.

## B.2 Calculation and Simulation for Single String

The parameters extracted from model *TS – 235PB – 60* at STC are applied in solar cell model for simulation:  $n = 1.6177$ ,  $R_{s0} = 1.954\text{m}\Omega$ ,  $R_{p0} = 6.1578$ ,  $I_{S0} = 2.8531\mu\text{A}$ ,  $I_{ph0} = 8.6127\text{A}$ .



TABLE B.2: The data file are generated by program.

	Name of file	Content
1	data_str1	String current and panel voltages of String 1 from scanning load.
2	data_str2	String current and panel voltages of String 2 from scanning load.
3	data_system	Voltage, Current and Power of PV system from scanning load.
4	Datasheet_parameters	The values of data are load from product datasheet.
5	Iphmatrix	Matrix of calculated photo-generated current $I_{ph}$ .
6	Irr	Matrix of irradiance
7	IString_System	Matrices of estimated string current at each of all string local peaks.
8	IVplocal_matrix	Matrix of calculated local peak currents and voltages.
9	n_P	Number of panels in each string.
10	n_S	Number of strings in PV system.
11	n_C	Number of cells per panel.
12	P_est_sys	Matrix of estimated power of PV system at all local peak voltages.
13	Parameters_cal_matrix	Matrix $V_T, R_S, R_p, I_S$ of panels at setting temperature.
14	Parameters_calcu	The parameters are extracted and used for simulation.
15	PString_System	Matrices of estimated string power at each of all string local peaks.
16	Simlocal	String currents, voltages and powers at all local peak by simulation.
17	Td	Matrix of bypass diode temperature.
18	Tp	Matrix of panels temperature.
19	VIPcal1	Matrices of voltage, current and power of String 1 for calculation.
20	VIPcal2	Matrices of voltage, current and power of String 2 for calculation.
21	VString_System	Matrices of estimated string voltage at each of all string local peaks.

### B.2.1 Case 1: Four Panels String

The operating condition are set for simulation as Table B.3(A). Together with the temperature, the random values of string current and panel voltages are chosen for calculation as follows:  $I_{Str} = 4.6096\text{A}$ ,  $V_P^1 = 26.0275\text{V}$ ,  $V_P^2 = 28.5033\text{V}$ ,  $V_P^3 = 30.2469\text{V}$ ,  $V_P^4 = 30.4389\text{V}$ . The calculated and simulative local peaks are shows in Table B.3(B). The power at local peaks are  $P_{Mcal}^1 = 552.99\text{W}$ (GMPP),  $P_{Mcal}^2 = 468.39\text{W}$  and  $P_{Mcal}^3 = 364.94\text{W}$ . The different voltage between calculation and simulation at local peaks:  $\Delta V1 = 0.1899\text{V} \approx 0.17\%$ ,  $\Delta V2 = 0.1211\text{V} \approx 0.15\%$  and  $\Delta V3 = 0.0718\text{V} \approx 0.14\%$ .

Fig. B.11 shows the I-V curves (A) and P-V curves (B). The peaks which obtained from simulation and calculation are plotted on this figure too. Fig. B.13 shows the intersections in segments, which indicate the local MPPs.

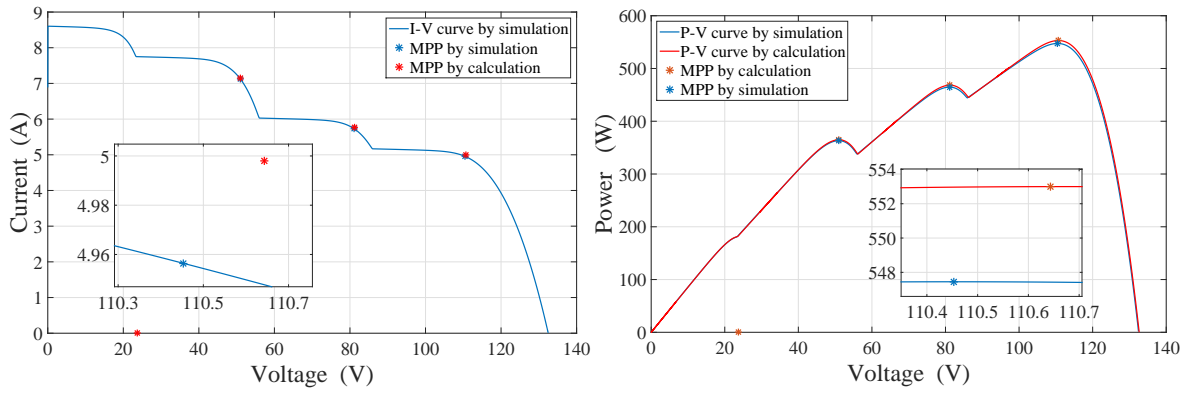
TABLE B.3: The operating conditions (A) and corresponding peaks by calculation and simulation (B).

(A) The operating condition are set for simulation.

Panel	$I_r$ (W/m <sup>2</sup> )	$T_P^i$ (°C)	$T_d^i$ (°C)
1	600	50	48
2	700	52	46
3	900	56	43
4	1000	60	40

(B) The voltage and current at peaks are obtained by calculation and simulation.

Peak	Calculation		Simulation	
	$V_{Mcal}^i$ (V)	$I_{Mcal}^i$ (A)	$V_{Msim}^i$ (V)	$I_{Msim}^i$ (A)
1	110.6432	4.9980	110.4533	4.9564
2	81.1966	5.7686	81.0755	5.7317
3	51.0308	7.1514	50.959	7.1271
4	23.6989	n/a	n/a	n/a



(A) The I-V curve, local MPPs by simulation and calculation.

(B) The P-V curve, local MPPs by simulation and calculation.

FIGURE B.11: I-V curves (A) and P-V curves (B) of a four panels string.

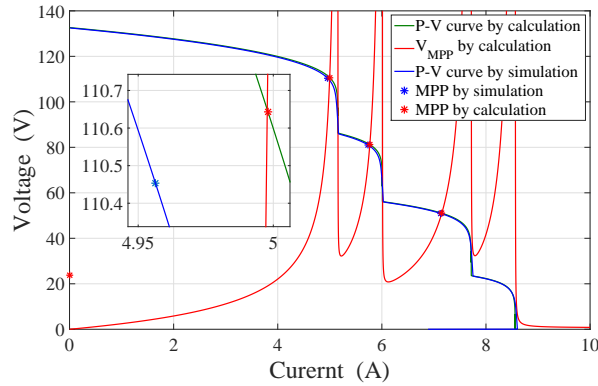


FIGURE B.13: The I-V curve, MPP by simulation. The intersections between curves of  $V^m(I)$  and  $V_M^m(I)$  are the local MPP.

## B.2.2 Case 2: Eight Panels String

This simulation uses eight panels, each of them is composed of 60 cells. The cell parameters are set follow  $TS - 235PB - 60$  model. The operating conditions are set for simulation as Table B.4(A). Together with the temperature, the random values of

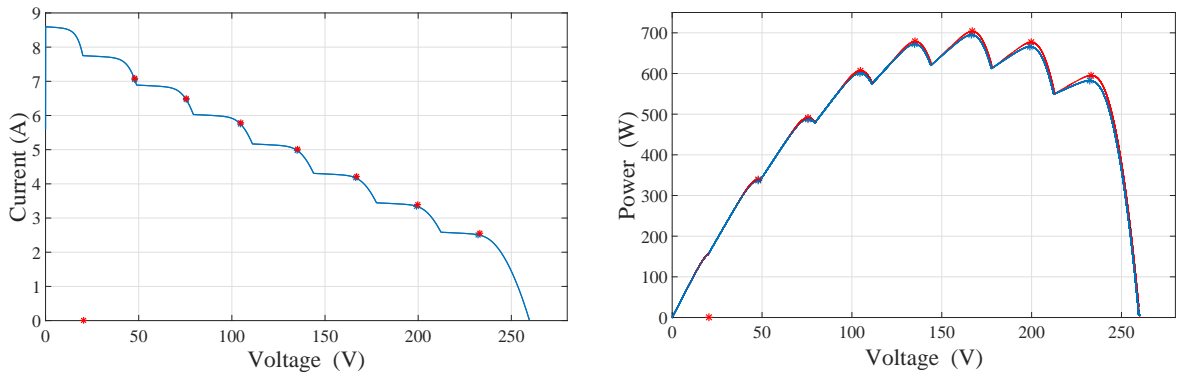
TABLE B.4: Operating conditions of panels and the local peaks of string obtained by calculation and simulation.

(A) The operating condition are set for simulation.				(B) The voltage and current at peaks are obtained by calculation and simulation.				
Panel	$I_r$ (W/m <sup>2</sup> )	$T_P^i$ (°C)	$T_d^i$ (°C)	Calculation		Simulation		
				$V_{Mcal}^i$ (V)	$I_{Mcal}^i$ (A)	$V_{Msim}^i$ (V)	$I_{Msim}^i$ (A)	
1	300	48	52	1	233.0934	2.5536	232.2386	2.5081
2	400	49	51	2	199.6845	3.3888	199.1417	3.3447
3	500	51	47	3	166.9264	4.2146	166.5195	4.1729
4	600	53	46	4	135.2186	5.0202	134.9415	4.9812
5	700	55	45	5	104.7291	5.7904	104.5574	5.7544
6	800	57	44	6	75.6061	6.4963	75.4869	6.4657
7	900	59	43	7	47.8587	7.0845	47.8264	7.0540
8	1000	60	42	8	20.4149	n/a	n/a	n/a

string current and panel voltages are chosen for calculation as follows:  $I_{Str} = 5.1117A$ ,  $V_P^1 = -0.8254V$ ,  $V_P^2 = -0.8027V$ ,  $V_P^3 = -0.7643V$ ,  $V_P^4 = 15.6244V$ ,  $V_P^5 = 26.7779V$ ,  $V_P^6 = 28.4413V$ ,  $V_P^7 = 29.3175V$ ,  $V_P^8 = 29.9977V$ . The calculated and simulative local peaks are shows in Table B.4(B). The calculated peak powers and the error voltages are shown in Table B.5 Fig. B.14(A) shows the I-V curve by simulation and the local MPPs by calculation and simulation. Fig. B.14(B) shows the PV curves by simulation and calculation. In both curve, the peaks at each segment are close together. The intersections which lead to the calculated peaks are shown in Fig. B.15. There are seven local peaks, that is also number of peaks by simulation.

TABLE B.5: The local peak powers and the corresponding voltage error.

Peak	$P_{Mcal}^i$ (W)	Voltage error  (%)
1	595.23	0.273
2	676.69	0.202
<b>3</b>	<b>703.53</b>	0.204
4	678.82	0.205
5	606.42	0.164
6	491.16	0.158
7	339.05	0.068
8	n/a	n/a



(A) The I-V curve and calculated local MPPs of 8 panel-string.

(B) The P-V curve and calculated local MPPs of 8 panel-string.

FIGURE B.14: I-V curve (A), P-V curve (B) of eight panels-string by simulation and the calculated local peaks.

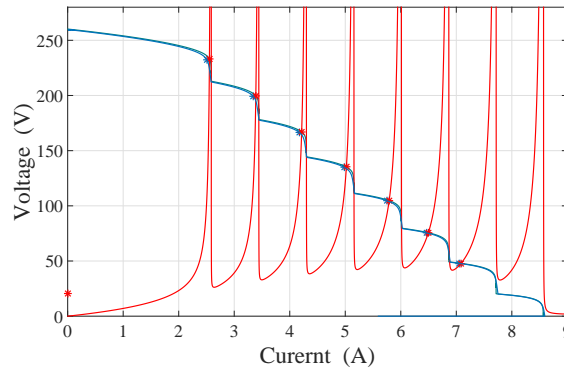


FIGURE B.15: The I-V curve by simulation and calculation and MPP curve by calculation of 8 panel-string. The intersections between curves of  $V^m(I)$  and  $V_M^m(I)$  are closed to the local peaks by simulation.

### B.2.3 Case 3: Ten Panels String

This simulation uses ten panels, each of them is composed of 60 cells. The cell parameters are set follow  $TS - 235PB - 60$  model. The operating conditions are set for simulation as Table B.6a. Together with the temperature, the random values of string current and panel voltages are chosen for calculation as follows:  $I_{Str} = 6.2275A$ ,  $V_P^1 = -0.8003V$ ,  $V_P^2 = -0.7840V$ ,  $V_P^3 = -0.7628V$ ,  $V_P^4 = -0.7264V$ ,  $V_P^5 = 22.2605V$ ,  $V_P^6 = 25.3988V$ ,  $V_P^7 = 26.7620V$ ,  $V_P^8 = 27.6019V$ ,  $V_P^9 = 28.1936V$ ,  $V_P^{10} = 28.5133V$ . The calculated and simulative local peaks are shows in Table B.6b. The calculated peak powers and the error voltages are shown in Table B.7. I-V curves and P-V curves by calculation and simulation are plotted in Fig. B.17a and Fig. B.17b. The local peaks are also presented for comparison.

TABLE B.6: Operating conditions, the voltage at MPPs by calculation and simulation.

(A) The operating condition are set for simulation.

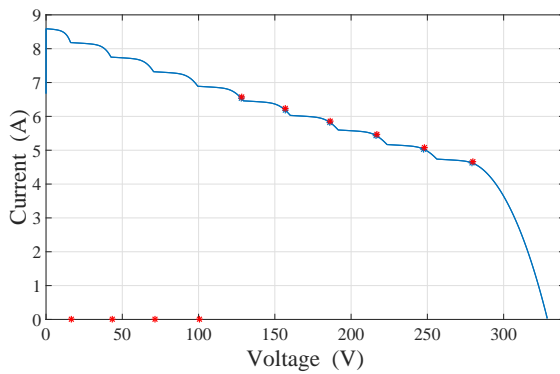
Panel	$I_r$ (W/m <sup>2</sup> )	$T_p^i$ (°C)	$T_d^i$ (°C)
1	550	50	52
2	600	51	51
3	650	53	50
4	700	54	50
5	750	55	48
6	800	57	47
7	850	58	46
8	900	59	45
9	950	60	45
10	1000	62	43

(B) The voltage and current at peaks are obtained by calculation and simulation.

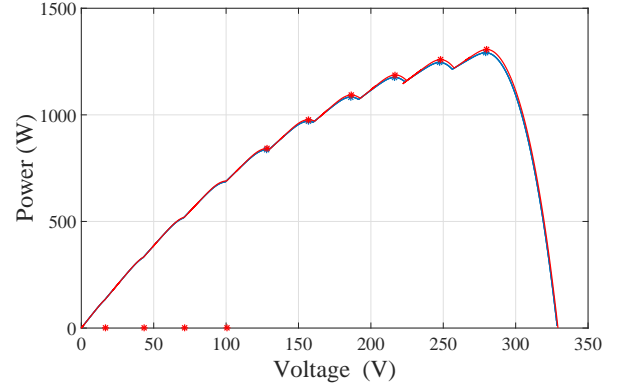
Peak	Calculation		Simulation	
	$V_{Mcal}^i$ (V)	$I_{Mcal}^i$ (A)	$V_{Msim}^i$ (V)	$I_{Msim}^i$ (A)
1	279.9015	4.6689	279.2148	4.6254
2	248.0233	5.0767	247.5682	5.0319
3	216.8011	5.4752	216.4514	5.4316
4	186.4407	5.8620	186.1561	5.8201
5	156.8791	6.2300	156.7249	6.1873
6	128.1765	6.5692	128.0522	6.5299
7	100.5990	n/a	n/a	n/a
8	71.4792	n/a	n/a	n/a
9	43.3931	n/a	n/a	n/a
10	16.6696	n/a	n/a	n/a

TABLE B.7: The local peak powers and voltage errors at these peaks.

Peak	$P_{Mcal}^i$ (W)	Voltage error  (%)
1	<b>1306.83</b>	0.246
2	1259.14	0.184
3	1187.03	0.162
4	1092.92	0.153
5	977.36	0.098
6	842.02	0.097
7,8,9,10	n/a	n/a



(A) The I-V curve and calculated local MPPs of 10 panel-string.



(B) The I-V curve and calculated local MPPs of 10 panel-string.

FIGURE B.16: I-V, P-V curves (A) and local peaks (B) by calculation and simulation.

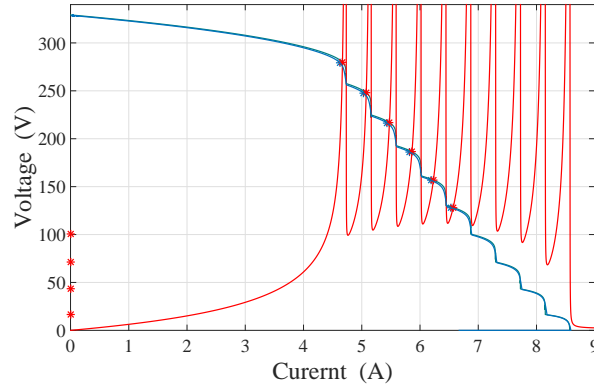


FIGURE B.18: Intersections in segments of ten panels-string.

### B.3 Calculation and Simulation for Two Strings in Parallel

#### B.3.1 Case 1: Three Panels per String

The operation conditions of every panels are set as Table B.8(A). The string currents  $I_{Str}^1 = 2.7914A$ ,  $I_{Str}^2 = 0.9867A$  and following panel voltages ( $V_P^{i,j}(V)$ ,  $i, j$  correspond to string number and panel number in the PV system, shown in Table B.8(B) are used for calculation.

TABLE B.8: The operating conditions and measured panel's voltage.

(A) The operating conditions of 2x3 PV system.

		String 1	String 2
Panel 1	$I_r(W/m^2)$	800	400
	$T_P(^{\circ}C)$	56	52
	$T_d(^{\circ}C)$	44	47
Panel 2	$I_r(W/m^2)$	900	600
	$T_P(^{\circ}C)$	58	56
	$T_d(^{\circ}C)$	42	45
Panel 3	$I_r(W/m^2)$	1000	1000
	$T_P(^{\circ}C)$	60	62
	$T_d(^{\circ}C)$	40	40

(B) The measured panel voltages are applied in calculation by proposed method for of 2x3 PV system.

$V_P^{i,j}(V)$	String 1	String 2
Panel 1	31.2121	30.4901
Panel 2	31.5055	31.4835
Panel 3	31.7171	32.4610

Table B.9(A) shows the peak voltages of two string by calculation and simulation.

The estimated system power at five determined local peaks are shown in Table B.9(B).

According to calculated results, the PV system yields the GMPP at  $V_{Mcal}^{11} = 79.5320V$  while the simulation gives the voltage at GMPP is  $V_{Msys} = 80.3994V$ . Without the estimation, the voltage error at GMPP is  $0.8674V \approx 1.08\%$ .

TABLE B.9: Voltage at local peaks (A) and estimated peak power (B).

(A) The local peak voltage and voltage error at these points of two strings.

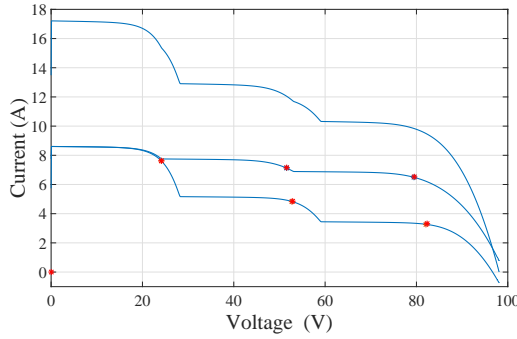
		String 1	String 2
Peak 1	$V_{Mcal}(V)$	79.5320	82.2979
	$V_{Msim}(V)$	79.4220	82.0803
	$ Err.V (\%)$	0.139	0.265
Peak 2	$V_{Mcal}(V)$	51.6130	52.8640
	$V_{Msim}(V)$	51.5680	52.7567
	$ Err.V (\%)$	0.087	0.203
Peak 3	$V_{Mcal}(V)$	n/a	24.1664
	$V_{Msim}(V)$	n/a	24.1465
	$ Err.V (\%)$	n/a	0.082

(B) The estimated power of system at determined local peaks.

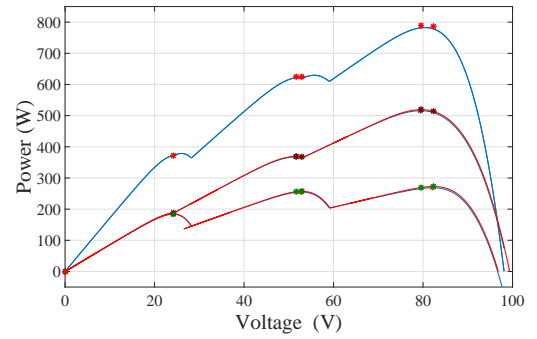
$P_s(W)$ at $V_P^{ij}$	$i=1$	$i=2$
$j=1$	788.60	786.38
$j=2$	625.23	625.15
$j=3$	n/a	372.31

Using the formula (4.36) to estimate the voltage at GMPP as follow:

$$\hat{V}_G = \frac{79.5320 \times 788.60 + 82.2979 \times 786.38}{788.60 + 786.38} = 80.913(V)$$

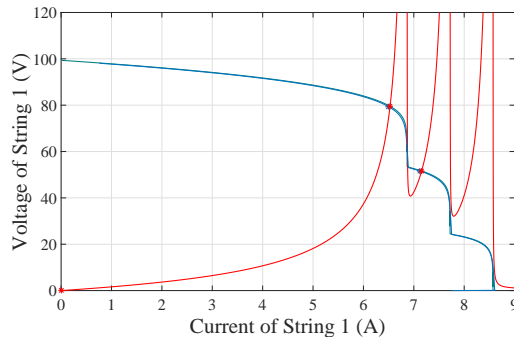
The voltage error is  $\Delta V_G = 0.514V \approx 0.639\%$ .

(A) I-V curves of PV system 2x3.

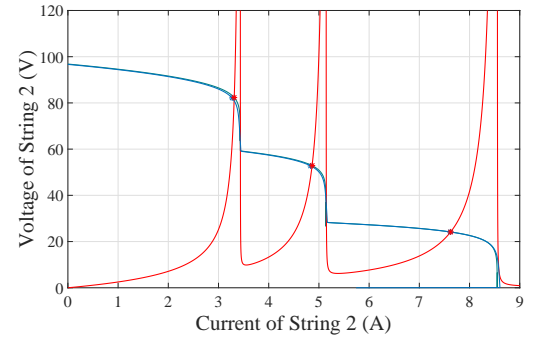


(B) P-V curves of PV system 2x3.

FIGURE B.19: I-V curves (left), P-V curves (right) and local MPP.



(A) Intersections of string 1.



(B) Intersections of string 2.

FIGURE B.21: Intersections correspond to local MPPs in every segment of two strings.

### B.3.2 Case 2: Ten Panels per String

The operation conditions of every panels are set as in Table B.10(A). The string currents  $I_{Str}^1 = 3.8702\text{A}$ ,  $I_{Str}^2 = 5.9154\text{A}$  and following panel voltages ( $V_P^{ij}(\text{V})$ ,  $i, j$  correspond to string number and panel number in the PV system, shown in Table B.11(A) are used for calculation.

TABLE B.10: Operating condition of panels (left) and measured values for calculation (right).

(A) The operating conditions of 2x10 PV system.				(B) The local peak voltage and voltage error at these points of two strings.			
		String 1	String 2		String 1	String 2	
Panel 1	$I_r(\text{W/m}^2)$	450	680	Peak 1	$V_{Mcal}(\text{V})$	272.7213	272.6539
	$T_P(^{\circ}\text{C})$	48	53		$V_{Msim}(\text{V})$	271.8918	272.1510
	$T_d(^{\circ}\text{C})$	50	47		$ Err_V (\%)$	0.305	0.185
Panel 2	$I_r(\text{W/m}^2)$	460	720	Peak 2	$V_{Mcal}(\text{V})$	n/a	241.9950
	$T_P(^{\circ}\text{C})$	48	53		$V_{Msim}(\text{V})$	n/a	241.5609
	$T_d(^{\circ}\text{C})$	50	47		$ Err_V (\%)$	n/a	0.180
Panel 3	$I_r(\text{W/m}^2)$	480	750	Peak 3	$V_{Mcal}(\text{V})$	n/a	n/a
	$T_P(^{\circ}\text{C})$	48	55		$V_{Msim}(\text{V})$	217.0865	212.9785
	$T_d(^{\circ}\text{C})$	51	46		$ Err_V (\%)$	n/a	n/a
Panel 4	$I_r(\text{W/m}^2)$	510	790	Peak 4	$V_{Mcal}(\text{V})$	188.2276	183.8240
	$T_P(^{\circ}\text{C})$	49	56		$V_{Msim}(\text{V})$	187.7915	183.6046
	$T_d(^{\circ}\text{C})$	48	46		$ Err_V (\%)$	0.232	0.119
Panel 5	$I_r(\text{W/m}^2)$	530	850	Peak 5	$V_{Mcal}(\text{V})$	n/a	n/a
	$T_P(^{\circ}\text{C})$	49	57		$V_{Msim}(\text{V})$	n/a	n/a
	$T_d(^{\circ}\text{C})$	48	45		$ Err_V (\%)$	n/a	n/a
Panel 6	$I_r(\text{W/m}^2)$	600	860	Peak 6	$V_{Mcal}(\text{V})$	129.7109	n/a
	$T_P(^{\circ}\text{C})$	52	57		$V_{Msim}(\text{V})$	129.4434	n/a
	$T_d(^{\circ}\text{C})$	46	45		$ Err_V (\%)$	0.207	n/a
Panel 7	$I_r(\text{W/m}^2)$	610	890	Peak 7	$V_{Mcal}(\text{V})$	n/a	n/a
	$T_P(^{\circ}\text{C})$	52	58		$V_{Msim}(\text{V})$	n/a	n/a
	$T_d(^{\circ}\text{C})$	46	45		$ Err_V (\%)$	n/a	n/a
Panel 8	$I_r(\text{W/m}^2)$	620	930	Peak 8	$V_{Mcal}(\text{V})$	n/a	n/a
	$T_P(^{\circ}\text{C})$	52	58		$V_{Msim}(\text{V})$	n/a	n/a
	$T_d(^{\circ}\text{C})$	46	44		$ Err_V (\%)$	n/a	n/a
Panel 9	$I_r(\text{W/m}^2)$	800	960	Peak 9	$V_{Mcal}(\text{V})$	46.8275	n/a
	$T_P(^{\circ}\text{C})$	57	59		$V_{Msim}(\text{V})$	46.7298	n/a
	$T_d(^{\circ}\text{C})$	45	44		$ Err_V (\%)$	0.209	n/a
Panel 10	$I_r(\text{W/m}^2)$	950	1000	Peak 10	$V_{Mcal}(\text{V})$	n/a	n/a
	$T_P(^{\circ}\text{C})$	59	60		$V_{Msim}(\text{V})$	n/a	n/a
	$T_d(^{\circ}\text{C})$	45	44		$ Err_V (\%)$	n/a	n/a

Table B.10(B) shows the peak voltages of two string by calculation and simulation.



TABLE B.11: Voltage at local MPPs (left) and estimated powers at these voltages (right).

(A) The measured panel voltages are applied in calculation by proposed method for of 2x10 PV system.

$V_P^{ij}$ (V)	String 1	String 2
Panel 1	1.5829	-0.6847
Panel 2	19.5587	23.3075
Panel 3	23.9851	25.1062
Panel 4	26.0504	26.4539
Panel 5	26.9111	27.6655
Panel 6	28.3340	27.8378
Panel 7	28.5184	28.1695
Panel 8	28.6911	28.6861
Panel 9	30.0991	28.8921
Panel 10	30.8601	29.1571

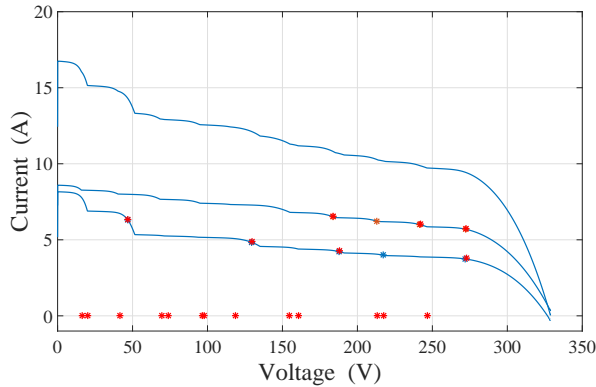
(B) The estimated power of system at determined local peaks.

$P_S$ (W) at $V_P^{ij}$	$i=1$	$i=2$
$j=1$	2601.2	2601.2
$j=2$	n/a	2415.6
$j=3$	n/a	n/a
$j=4$	2020	2007.3
$j=5$	n/a	n/a
$j=6$	1581.5	n/a
$j=7$	n/a	n/a
$j=8$	n/a	n/a
$j=9$	671.9	n/a
$j=10$	n/a	n/a

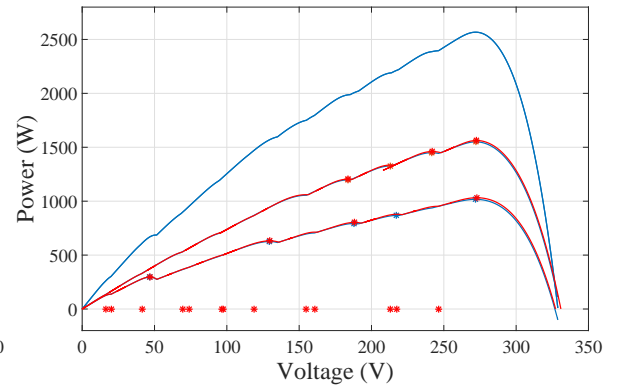
The estimated system power at five determined local peaks are shown in Table B.11(B). In this case, the power at peak voltages of both String 1 and String 2 are high. Using the formula (4.36) to estimate the voltage at GMPP as follow:

$$\widehat{V}_G = \frac{272.7213 \times 1034.08 + 272.6539 \times 1567.08}{1034.08 + 1567.18} = 272.6807(V)$$

The simulation shows  $V_{Gsim} = 271.8918$ . The voltage error is  $\Delta V_G = 0.7889V \approx 0.29\%$ .



(A) I-V curves of PV system 2x10.



(B) P-V curves and local peaks.

FIGURE B.23: I-V curves (left) and P-V curves (right) of strings and whole PV system.

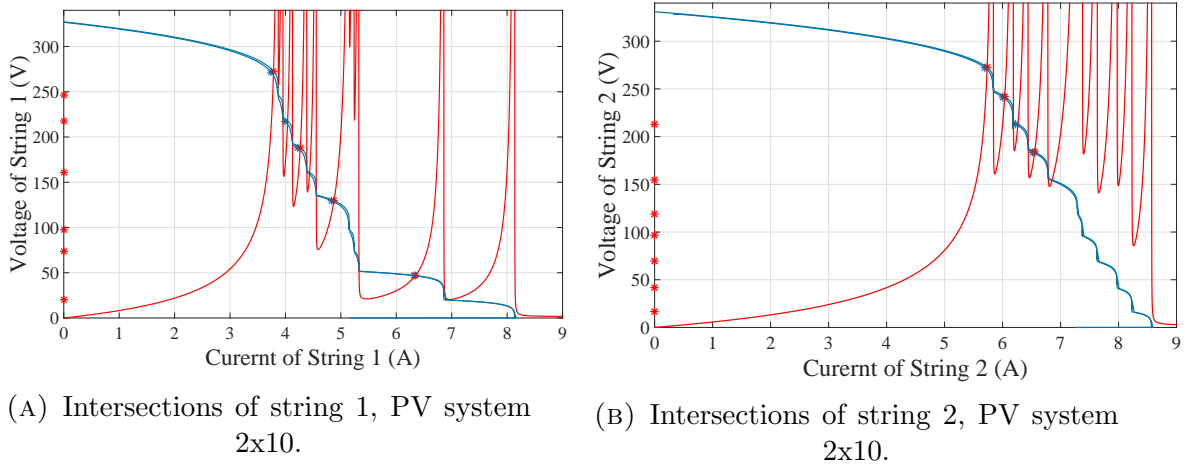


FIGURE B.25: The intersections in segments of two strings.

## B.4 Calculation and Simulation for Three Strings in Parallel

### *Case: Ten Panels per String*

The operation conditions of every panels are set as follows:

Together with data in Table B.12, the string currents  $I_{Str}^1 = 2.2171\text{A}$ ,  $I_{Str}^2 = 3.6085\text{A}$ ,  $I_{Str}^3 = 4.6960\text{A}$  and following panel voltages ( $V_P^{i,j}$  (V),  $i, j$  correspond to string number and panel number in the PV system, shown in Table B.13) are used for calculation.

Table B.14 shows that the number and order of calculated peaks and simulated peaks are the same for all strings. That mean the GMPP of string can be determined exactly by the proposed method.

TABLE B.12: The operating conditions of 3x10 PV system.

		String 1	String 2	String 3
Panel 1	$Ir(\text{W/m}^2)$	250	420	550
	$T_P(^{\circ}\text{C})$	44	48	51
	$T_d(^{\circ}\text{C})$	54	46	48
Panel 2	$Ir(\text{W/m}^2)$	280	450	560
	$T_P(^{\circ}\text{C})$	46	48	52
	$T_d(^{\circ}\text{C})$	54	46	48
Panel 3	$Ir(\text{W/m}^2)$	300	460	580
	$T_P(^{\circ}\text{C})$	48	49	53
	$T_d(^{\circ}\text{C})$	53	46	47
Panel 4	$Ir(\text{W/m}^2)$	350	550	650
	$T_P(^{\circ}\text{C})$	49	51	52
	$T_d(^{\circ}\text{C})$	53	45	47
Panel 5	$Ir(\text{W/m}^2)$	400	600	700
	$T_P(^{\circ}\text{C})$	50	54	53
	$T_d(^{\circ}\text{C})$	52	45	46
Panel 6	$Ir(\text{W/m}^2)$	800	950	960
	$T_P(^{\circ}\text{C})$	56	60	59
	$T_d(^{\circ}\text{C})$	48	54	45
Panel 7	$Ir(\text{W/m}^2)$	950	960	965
	$T_P(^{\circ}\text{C})$	60	61	60
	$T_d(^{\circ}\text{C})$	47	44	54
Panel 8	$Ir(\text{W/m}^2)$	975	970	970
	$T_P(^{\circ}\text{C})$	62	61	62
	$T_d(^{\circ}\text{C})$	46	44	44
Panel 9	$Ir(\text{W/m}^2)$	980	980	975
	$T_P(^{\circ}\text{C})$	61	63	62
	$T_d(^{\circ}\text{C})$	46	44	43
Panel 10	$Ir(\text{W/m}^2)$	1000	990	995
	$T_P(^{\circ}\text{C})$	62	61	62
	$T_d(^{\circ}\text{C})$	45	44	43

TABLE B.13: The measured panel voltages are applied in calculation by proposed method for of 3x10 PV system.

$V_P^{ij}(\text{V})$	String 1	String 2	String 2
Panel 1	-0.702	2.872	13.167
Panel 2	23.370	24.060	20.504
Panel 3	25.276	24.851	23.610
Panel 4	27.516	28.095	27.181
Panel 5	28.636	28.632	28.182
Panel 6	31.648	30.937	30.228
Panel 7	31.855	30.869	30.139
Panel 8	31.717	30.921	29.926
Panel 9	31.856	30.730	29.960
Panel 10	31.815	31.022	30.090

TABLE B.14: The local peak powers by calculation ( $P_{Mcal}^{ij}$ ) and simulation ( $P_{Msim}^{ij}$ ) of strings.

		String 1	String 2	String 3
Peak 1	$P_{Mcal}^{i1}(W)$	612.6 (3 <sup>rd</sup> )	1010.6 (1 <sup>st</sup> )	1281.7 (1 <sup>st</sup> )
	$P_{Msim}^{i1}(W)$	596.6 (4 <sup>th</sup> )	994.2 (1 <sup>st</sup> )	1264.7 (1 <sup>st</sup> )
Peak 2	$P_{Mcal}^{i2}(W)$	611.8 (4 <sup>th</sup> )	965.5 (2 <sup>nd</sup> )	n/a
	$P_{Msim}^{i2}(W)$	597.9 (3 <sup>rd</sup> )	950.7 (2 <sup>nd</sup> )	n/a
Peak 3	$P_{Mcal}^{i3}(W)$	586.5 (6 <sup>th</sup> )	n/a	1097.3 (2 <sup>nd</sup> )
	$P_{Msim}^{i3}(W)$	574.6 (6 <sup>th</sup> )	n/a	1084.7 (2 <sup>nd</sup> )
Peak 4	$P_{Mcal}^{i4}(W)$	594.7 (5 <sup>th</sup> )	906.4 (4 <sup>th</sup> )	1052.2 (3 <sup>rd</sup> )
	$P_{Msim}^{i4}(W)$	584.3 (5 <sup>th</sup> )	896.0 (4 <sup>th</sup> )	1041.4 (3 <sup>rd</sup> )
Peak 5	$P_{Mcal}^{i5}(W)$	583.5 (7 <sup>th</sup> )	843.3 (5 <sup>th</sup> )	961.4 (4 <sup>th</sup> )
	$P_{Msim}^{i5}(W)$	574.9 (7 <sup>th</sup> )	835.1 (5 <sup>th</sup> )	952.6 (4 <sup>th</sup> )
Peak 6	$P_{Mcal}^{i1}(W)$	860.0 (1 <sup>st</sup> )	927.7 (3 <sup>rd</sup> )	933.6 (5 <sup>th</sup> )
	$P_{Msim}^{i1}(W)$	855.3 (1 <sup>st</sup> )	922.9 (3 <sup>rd</sup> )	927.9 (5 <sup>th</sup> )
Peak 7	$P_{Mcal}^{i2}(W)$	732.1 (2 <sup>nd</sup> )	n/a	n/a
	$P_{Msim}^{i2}(W)$	729.4 (2 <sup>nd</sup> )	n/a	n/a
Peak 8	$P_{Mcal}^{i3}(W)$	n/a	n/a	n/a
	$P_{Msim}^{i3}(W)$	n/a	n/a	n/a
Peak 9	$P_{Mcal}^{i4}(W)$	n/a	n/a	n/a
	$P_{Msim}^{i4}(W)$	n/a	n/a	n/a
Peak 10	$P_{Mcal}^{i5}(W)$	n/a	n/a	n/a
	$P_{Msim}^{i5}(W)$	n/a	n/a	n/a

TABLE B.15: The estimated power of system at determined local peaks.

$P_S(W)$ at $V_P^{ij}$	$i=1$	$i=2$	$i=3$
$j=1$	2861.8	2887.7	2875.0
$j=2$	2791.0	2775.3	n/a
$j=3$	2588.7	n/a	2555.3
$j=4$	2492.0	2539.4	2531.6
$j=5$	2365.0	2368.0	2358.6
$j=6$	2706.8	2709.8	2710.7
$j=7$	2335.8	n/a	n/a
$j=8,9,10$	n/a	n/a	n/a

Table B.16 shows the peak voltages of two string by calculation and simulation. The estimated system power at five determined local peaks are shown in Table B.15.

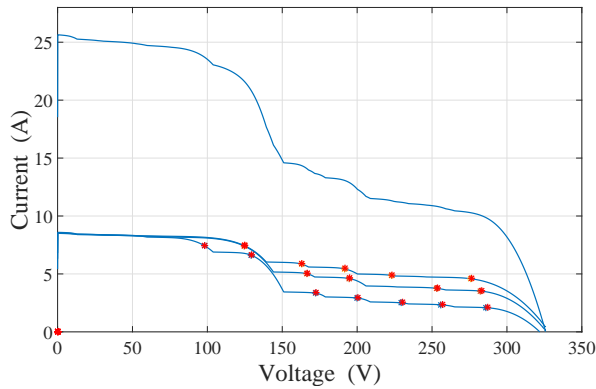
Basing on results in Table B.15, predicting that the GMPP is dropped in peaks 1 of all strings. Using formula (4.36) to determine the voltage at GMPP as follow:

$$\widehat{V}_G = \frac{287.3055 \times 612.6 + 283.1483 \times 1010.6 + 276.3433 \times 1281.7}{612.6 + 1010.6 + 1281.7} = 281.025(V)$$

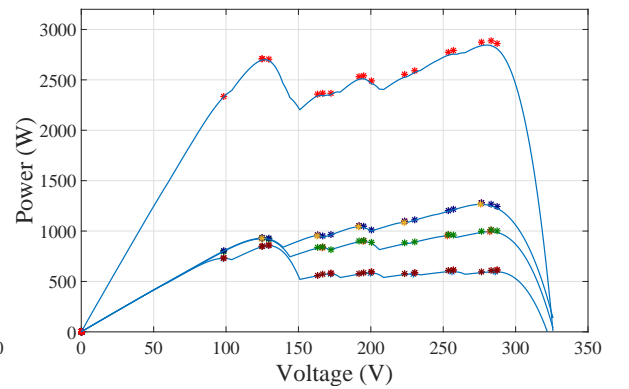
TABLE B.16: The local peak voltage and voltage error at these points of two strings.

		String 1	String 2	String 3
Peak 1	$V_{Mcal}(V)$	287.3055	283.1483	276.3433
	$V_{Msim}(V)$	285.8446	282.2117	275.7819
	$ Err_V (\%)$	0.511	0.332	0.204
Peak 2	$V_{Mcal}(V)$	257.1347	253.5811	n/a
	$V_{Msim}(V)$	255.9611	252.9243	n/a
	$ Err_V (\%)$	0.459	0.260	n/a
Peak 3	$V_{Mcal}(V)$	230.1922	n/a	223.3643
	$V_{Msim}(V)$	229.2884	n/a	222.9668
	$ Err_V (\%)$	0.394	n/a	0.178
Peak 4	$V_{Mcal}(V)$	200.5542	195.0544	191.9599
	$V_{Msim}(V)$	199.9182	194.6546	191.6112
	$ Err_V (\%)$	0.318	0.205	0.182
Peak 5	$V_{Mcal}(V)$	172.4911	166.6442	163.1445
	$V_{Msim}(V)$	172.0878	166.3457	162.8848
	$ Err_V (\%)$	0.234	0.179	0.159
Peak 6	$V_{Mcal}(V)$	129.5360	124.7965	124.9932
	$V_{Msim}(V)$	129.3367	124.5973	124.7767
	$ Err_V (\%)$	0.171	0.160	0.174
Peak 7	$V_{Mcal}(V)$	98.3159	n/a	n/a
	$V_{Msim}(V)$	98.1415	n/a	n/a
	$ Err_V (\%)$	0.178	n/a	n/a
Peak 8,9,10	$V_{Mcal}(V)$	n/a	n/a	n/a
	$V_{Msim}(V)$	n/a	n/a	n/a
	$ Err_V (\%)$	n/a	n/a	n/a

The voltage at GMPP by simulation is  $V_G = 280.1337V$ , so the voltage error is  $\Delta V_G \approx 0.8888V \approx 0.317\%$ .

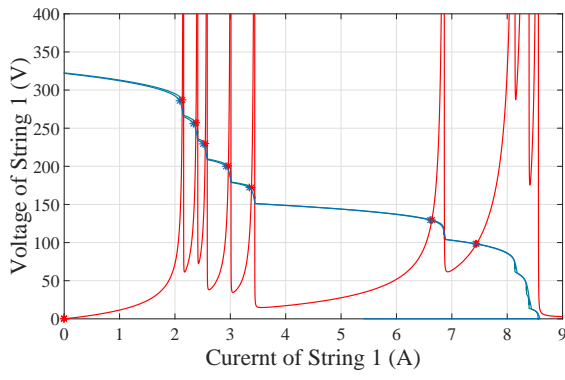


(A) I-V curves of PV system 3x10.

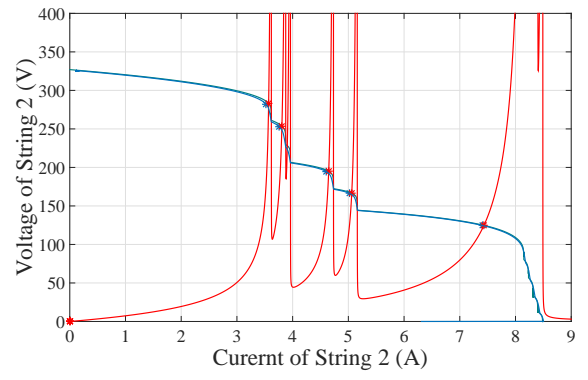


(B) P-V curves of PV system 3x10.

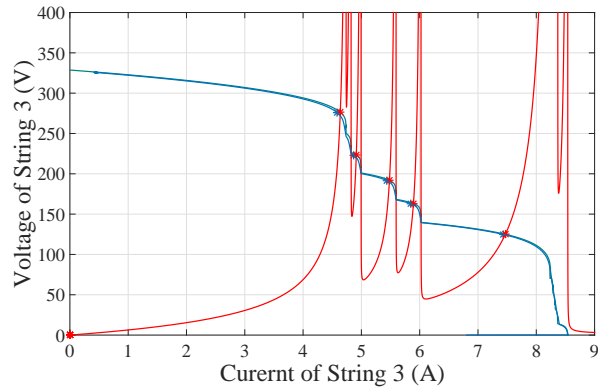
FIGURE B.27: I-V curves (A), P-V curves (B) of strings and whole PV system



(A) Intersections of string 1, PV system  
3x10.



(B) Intersections of string 2, PV system  
3x10.



(C) Intersections of string 3, PV system  
3x10.

FIGURE B.29: Intersections in every segment of three strings.

## Biography

**Name:** Nhan Tong Thanh

**Gender:** Male

**Date of birth:** 05-June-1979

**Place of birth:** Tay Ninh province, Viet Nam

**Nationality:** Vietnamese

**Educational:**

Bachelor of Engineering (Electrical-Electronics Engineering), Ho Chi Minh City University of Technology, 2002.

Master of Engineering (Electronics Engineering), Ho Chi Minh City University of Technology, 2004.

**Work experience::**

2002-2004: Assistant lecturer at Cao Thang Technical College, Ho Chi Minh City, Vietnam.

2004-2013: Lecturer at Cao Thang Technical College, Ho Chi Minh City, Vietnam.

**Academic publications:**

1. *A Maximum Power Point Fast Tracking*, 11th International Conference on Electrical Engineering, Electronics, Computer, Telecommunications and Information Technology (ECTI-CON2014)

2. *A Deterministic Method for Searching the Maximum Power Point of a PV Panel*, ECTI-CON2015, Huahin, Thailand.

3. *Parameter Extraction for a Solar Cell Model with Three Measured Points only*, International Conference on Electronics, Information and Communication (ICEIC 2016), Da Nang, Vietnam.

**Current work position:** Lecturer and Head of Industrial-Electronics Department, Cao Thang Technical College.

**Office:** Industrial Electronics Department (Building F), Cao Thang Technical College, 65 Huynh Thuc Khang Street, District 1, Ho Chi Minh City, Vietnam.